IOCCG Protocol Series

Ocean Optics & Biogeochemistry Protocols for Satellite Ocean Colour Sensor Validation

Volume 7: Aquatic Primary Productivity Field Protocols for SatelliteValidation and Model Synthesis (v7.0)

Editors
Ryan A. Vandermeulen and Joaquín E. Chaves

Authors
Balch, W.M., Carranza, M., Cetinić, I., Chaves, J.E., Duhamel, S., Fassbender, A., Fernandez-Carrera, A., Ferrón, S., García-Martín, E., Goes, J., Gomes, H., Gundersen, K., Halsey, K., Hirawake, T., Isada, T., Juranek, L., Kulk, G., Langdon, C., Letelier, R., López-Sandoval, D., Mannino, A., Marra, J.F., Neale, P., Nicholson, D., Silsbe, G., Stanley, R.H., Vandermeulen, R.A

International Ocean Colour Coordinating Group (IOCCG) in collaboration with National Aeronautics and Space Administration (NASA)

IOCCG, Dartmouth, Canada

September 2022

Ocean Optics & Biogeochemistry Protocols for Satellite Ocean Colour Sensor Validation

IOCCG Protocol Series Volume 7.0, 2022

Aquatic Primary Productivity Field Protocols for Satellite Validation and Model Synthesis

Report of a NASA-sponsored workshop with contributions (alphabetical) from:

William M. Balch	**Bigelow Laboratory for Ocean Sciences, Maine, USA**
Magdalena M. Carranza	**Monterey Bay Aquarium Research Institute, California, USA**
Ivona Cetinić	**Morgan State University, NASA Goddard Space Flight Center, Maryland, USA**
Joaquín E. Chaves	**Science Systems and Applications, Inc., NASA Goddard Space Flight Center, Maryland, USA**
Solange Duhamel	**Department of Molecular and Cellular Biology, University of Arizona, Arizona, USA**
Andrea J. Fassbender	**NOAA Pacific Marine Environmental Laboratory, Washington, USA**
Ana Fernández-Carrera	**Leibniz Institute for Baltic Sea Research Warnemünde, Rostock, Germany**
Sara Ferrón	**University of Hawai'i at Mānoa, Hawaii, USA**
E. Elena García-Martín	**National Oceanography Centre, Southampton, UK**
Joaquim Goes	**Lamont-Doherty Earth Observatory at Columbia University, New York, USA**
Helga do Rosario Gomes	**Lamont-Doherty Earth Observatory at Columbia University, New York, USA**
Kjell Gundersen	**Plankton Research Group, Institute of Marine Research, Bergen, Norway**
Kimberly Halsey	**Department of Microbiology, Oregon State University, Oregon, USA**
Toru Hirawake	**National Institute of Polar Research, Tokyo, Japan**
Tomonori Isada	**Akkeshi Marine Station, Field Science Center for Northern Biosphere, Hokkaido University, Hokkaido, Japan**
Lauren W. Juranek	**College of Earth, Ocean, and Atmospheric Sciences, Oregon State University, Oregon USA**
Gemma Kulk	**Earth Observation Science and Applications, Plymouth Marine Laboratory, Plymouth UK**
Chris Langdon	**Rosenstiel School of Marine, Atmospheric and Earth Science, University of Miami, Florida, USA**
Ricardo Letelier	**College of Earth, Ocean and Atmospheric Sciences, Oregon State University, Oregon, USA**

Daffne C. López-Sandoval	**Coastal and Marine Resources Core Lab, King Abdullah University of Science and Technology, Thuwal, Saudi Arabia**
Antonio Mannino	**National Aeronautics and Space Administration, NASA Goddard Space Flight Center, Maryland, USA**
John F. Marra	**Earth and Environmental Sciences, Brooklyn College, New York, USA**
Patrick Neale	**Smithsonian Environmental Research Center, Maryland, USA**
David. P. Nicholson	**Marine Chemistry and Geochemistry Department, Woods Hole Oceanographic Institution, Massachusetts, USA**
Greg Silsbe	**University of Maryland Center for Environmental Science, Maryland, USA**
Rachel H.R. Stanley	**Department of Chemistry, Wellesley College, Massachusetts, USA**
Ryan A. Vandermeulen	**Science Systems and Applications, Inc., NASA Goddard Space Flight Center, Maryland, USA**

Edited by:
Ryan A. Vandermeulen and Joaquín E. Chaves

Correct citation for this volume:

IOCCG Protocol Series (2022). Aquatic Primary Productivity Field Protocols for Satellite Validation and Model Synthesis. Balch, W.M., Carranza, M., Cetinić, I., Chaves, J.E., Duhamel, S., Fassbender, A., Fernandez-Carrera, A., Ferrón, S., García-Martín, E., Goes, J., Gomes, H., Gundersen, K., Halsey, K., Hirawake, T., Isada, T., Juranek, L., Kulk, G., Langdon, C., Letelier, R., López-Sandoval, D., Mannino, A., Marra, J.F., Neale, P., Nicholson, D., Silsbe, G., Stanley, R.H., Vandermeulen, R.A. IOCCG Ocean Optics and Biogeochemistry Protocols for Satellite Ocean Colour Sensor Validation, Volume 7.0, edited by R.A. Vandermeulen, J. E. Chaves, IOCCG, Dartmouth, NS, Canada. doi:http://dx.doi.org/10.25607/OBP-1835

Acknowledgements: We are grateful to the numerous reviewers that offered helpful feedback during the public comment period, these efforts are not possible without your contributions. We also thank the Associate Editor Peer Review (AEPR) members for their constructive reviews and editorial responsibilities on this document:

Takashi Yoshikawa	**School of Marine Science and Technology, Tokai University, Shizuoka, Japan**
Roberta Hamme	**School of Earth and Ocean Sciences, University of Victoria, Victoria, BC, Canada**
Natalia González-Benítez	**Area of Biodiversity and Conservation, Universidad Rey Juan Carlos, Madrid, Spain**
G. Jason Smith	**Moss Landing Marine Laboratories, California, USA**
Isabel Seguro	**Centre for Ocean and Atmospheric Sciences, School of Environmental Sciences, University of East Anglia, Norwich, UK**
Sandy Thomalla	**Southern Ocean Carbon-Climate Observatory, CSIR, Cape Town, South Africa**
Yibin Huang	**National Oceanic and Atmospheric Administration, Pacific Marine Environmental Laboratory, Washington, USA**

http://www.ioccg.org

Published by the International Ocean Colour Coordinating Group (IOCCG), Dartmouth, NS, Canada, in conjunction with the National Aeronautics and Space Administration (NASA).

doi: http://dx.doi.org/10.25607/OBP-1835

PREFACE

In 2018, a working group sponsored by the NASA Plankton, Aerosol, Cloud, and ocean Ecosystem (PACE) project, in conjunction with the International Ocean Colour Coordinating Group (IOCCG), European Organization for the Exploitation of Meteorological Satellites (EUMETSAT), and Japan Aerospace Exploration Agency (JAXA), was assembled with the aim to develop community consensus on multiple methods for measuring aquatic primary productivity used for satellite validation and model synthesis. A workshop to commence the working group efforts was held December 5–7, 2018, at the University Space Research Association headquarters in Columbia, MD, USA, bringing together 26 active researchers from 16 institutions. In this document, we discuss and develop the workshop findings as they pertain to primary productivity measurements, including the essential issues, nuances, definitions, scales, uncertainties, and ultimately best practices for data collection across multiple methodologies.

Top row, left to right: Solange Duhamel, Mary Jane Perry, Helga Gomes, Maxim Gorbunov, Gemma Kulk, Greg Silsbe, Roo Nicholson, Rachel Stanley, Patrick Neale, John Marra, Mark Brzezinski, Barney Balch, Tomonori Isada, Laurie Juranek, SeungHyun Son, Toru Hirawake. Bottom row, left to right: Joaquim Goes, Ana Fernandez Carrera, Antonio Mannino, Ryan Vandermeulen, Ricardo Letelier, Kimberly Halsey, Priscila Kienteca Lange, Joaquín Chaves. Workshop participants not pictured: Joe Salisbury, Susanne Craig, Jeremy Werdell, Paula Bontempi.

Table of Contents

1. Reconciling Estimates of Oceanic Primary Productivity from Cells to Satellites

Ryan A. Vandermeulen[1,2], Joaquín E. Chaves[1,2], Antonio Mannino[2]
[1]*Science Systems and Applications, Inc., Maryland, USA*
[2]*NASA Goddard Space Flight Center, Maryland, USA*

1.1. Why Are We Doing This?

The measurement of aquatic primary productivity (PP) is central to the quantitative understanding of the global biosphere, yielding critical insights into the role and magnitude of carbon, oxygen, and other bioactive element fluxes between the ocean, the geosphere, and the atmosphere. The accumulation of theoretical, methodological, and technological advances from this endeavor has led to the development of numerous approaches to measure oceanic PP, all with the common objective of quantifying the fluxes of reduced carbon into aquatic ecosystems. While these advances have furthered the understanding of carbon dynamics, from intracellular to global scales, it is notable that perhaps no single measurement in the suite of significant oceanographic observations exhibits as much methodological diversity and interpretive ambiguity (Marra, 2002; del Giorgio and Williams, 2005).

Methods to derive estimates of PP include, but are not limited to, incubations to measure oxygen gas accumulation/consumption (Riley, 1939; Collins et al., 2018), uptake of radioactive ^{14}C (Steeman Nielsen, 1952), stable ^{13}C (Slawyk et al., 1977; Slawyk, 1979; Hama et al., 1993; López-Sandoval, 2019), and ^{18}O (Grande et al., 1989), the isotopic composition of atmospheric and dissolved oxygen (^{16}O,^{17}O, and ^{18}O; Luz and Barkan, 2009), dilution growth and grazing incubation experiments (Calbet and Landry, 2004; Landry et al., 2000), underway measurements of O_2/Ar ratios (Cassar et al., 2009), the use of temporally and spatially integrated time series from gliders or buoys (Claustre et al., 1999; Nicholson et al., 2008; Alkire et al., 2014), and *in situ* methods that use instantaneous kinetic measurements of active fluorescence to derive primary productivity estimates from electron transport rates (Kolber et al., 1998; Gorbunov and Falkowski, 2021).

An assessment of the oceanic carbon flux can be attained by the power of the discrete PP measurements accumulated over years. Still, the capacity afforded by satellite observations of ocean biomass and its physical environment enable the scaling up of those data into a comprehensive, global picture (National Research Council, 2008). Notably, no matter how well characterized, ocean color remote sensing (i.e., measurements of passive water-leaving reflectance) can only elucidate a limited portion of the multitude of degrees of freedom that impact daily water column-integrated rates of primary productivity. The combination of field measurements, modeling efforts, and satellite observations, even if not explicit, is the only viable path to gauge the rate of marine carbon fixation at a global scale (Brewin et al., 2021). Thus, it is critical to evaluate model outputs against accurate *in situ* measurements from diverse regions (Saba et al., 2011). Though PP measurements are ubiquitous within oceanographic research, an unfortunate impact of the variability in methodological approaches is that it can hinder the interoperability and scalability of existing measurements into synthesis efforts aimed at carbon cycle modeling and satellite algorithm development.

The various techniques and approaches used for measuring PP depend on multiple assumptions and are prone to artifacts that can introduce significant biases between measurements (Peterson, 1980; Marra, 2002; Regaudie-de-Gioux et al., 2014). Moreover, variations in results extend beyond the specific parameter used to estimate the rates of carbon fixation and can often arise from environmental or experimental variability due to temperature (Eppley, 1972), source and quality of light (Kirk, 2011), filtration (Sharp, 1977), bottle effects (Worrest et al., 1980), length and type of incubations (Lohrenz et al., 1992), inherent assumptions about respiration and dissolved losses, the depth of the photic zone (Geider and Osborne, 1992; Marra 2015), grazing (Laws et al., 2000), regenerated production (Harrison, 1980), quantum yield (Morel et al., 1996), and mixing and air-sea exchange (Duarte et al., 2013), among a multitude of other factors. Awareness of these uncertainties makes it unsurprising that results from identical samples analyzed at different laboratories have shown an average coefficient of variation of 25–40% (Richardson, 1991).

When these uncertainties are not fully quantified or understood, the result is ambiguity in the interpretation and applicability of data for subsequent global PP model validation. However, establishing a set of best practices and a better understanding of the assumptions and limitations of each measurement approach can minimize systematic and random biases. The reasons above highlight the motivation to develop community consensus on protocols for various PP measurement approaches and define the uncertainty associated with each type of measurement. Accurate determination of carbon cycle parameters is central to priorities set by international space agencies and required for the success of current and future programs producing climate-quality data from sea-going platforms and spaceborne sensors.

1.2. One Step Beyond

Notably, the diverse range of measurements covered in this document are resolving an equally diverse spectrum of specific metabolic processes (see Chapter 2), which can become uncoupled from one another because environmental factors and taxonomic diversity directly impact the efficiency with which carbon is fixed and respired, as well as the intermediate pathways therewithin. These behaviors present formidable challenges when attempting to intercompare derived rates, as any discrepancies observed between two or more measurements may be real, methodological, or simply a result of inherent biases associated with the temporal and spatial scales of measurement (Regaudie-de-Gioux et al., 2014). Differing methods of assessing primary productivity are rarely, if ever, simultaneously measuring the same quantity or process at the same spatial-temporal scales (Fig. 1.1), thereby propagating the impacts of the metabolic disparities and prompting the question: Why issue protocols for a broad set of rate measurements that represent varying metabolic processes, instead of focusing on one “gold standard” measurement for validation of models? Is more always better?

In short, each method or approach presented in this volume elucidates distinct processes that contribute to a holistic and integrated characterization of aquatic microbial energy and carbon dynamics on Earth. Our primary goal in presenting these protocols is to normalize a variety of emerging technologies, thus improving our simultaneous understanding of larger-scale spatial-temporal dynamics and smaller-scale cell physiology, which are intrinsically linked.

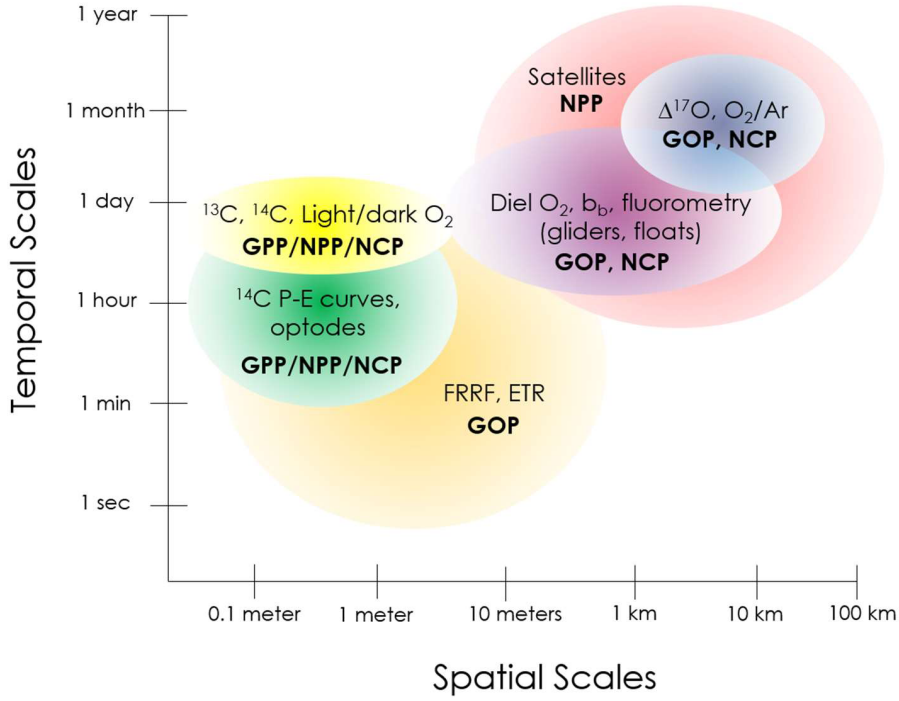

Fig. 1.1. Different methods of assessing primary productivity rates in the ocean examine widely varying spatial-temporal scales and (potentially decoupled) metabolic processes. While integrating across scales can lead to ambiguity in absolute comparisons between methods and ecosystem processes, each approach yields valid information that contributes to a comprehensive understanding of microbial energetics and carbon dynamics.

We intend for these protocols to be complementary, not competitive, to this understanding; by establishing best practices, we may leverage the assets and liabilities of each method. Thus, beyond establishing standardized best practices, we make every effort to be fully transparent about the capabilities, limitations, and impacts of the underlying assumptions inherent to each measurement.

An overarching goal of this effort is to encourage practitioners to consider their measurements in the context of recent and future advances in ocean color remote sensing technologies and their subsequent impact on the understanding of primary production and associated ecosystem modeling efforts. With enhanced observational power gained from emerging sophistication in the capabilities of these technologies, there will be opportunities to directly validate what we only now empirically assume. Future geostationary orbits will make possible the measurement of diurnal changes in standing stocks of chlorophyll *a* and phytoplankton carbon via backscatter, as well as changes in absorption efficiency throughout the day (Fishman et al., 2012). Globally gridded hyperspectral data can yield a better understanding of the distribution of phytoplankton community composition (Werdell et al., 2019), and thus how taxonomically dependent physiological variables are parameterized. Multi-angle polarimetry will allow the resolution of optical and microphysical properties of suspended oceanic particles in a way that may help better determine the phytoplankton size spectra and particle composition and morphology (Jamet et al.,

2019). Sensors built with enhanced signal across the electromagnetic spectrum may enable greater practical use of natural fluorescence line height to help characterize phytoplankton physiology and nutrient stress (Behrenfeld et al., 2009), and elucidate global estimates of ultraviolet stress (Lee et al., 2013). Space-borne active remote sensing via Light Detection and Ranging (LIDAR) can be optimized in such a way to help resolve the three-dimensional vertical structure of particles within the ocean (Lu et al., 2014) and vertical migration patterns (Behrenfeld et al., 2019). Future fleets of Bio-Argo floats and other autonomous platforms can provide greater *in situ* resolution of bio-optical parameters all around the globe (Johnson et al., 2009). The growing sophistication of machine learning, genetic programming, and neural networks can be robustly parameterized and tested as precisely as a laboratory experiment to help learn about subtle processes and trends in the ocean (D'Alelio, 2020). It is imperative to examine and incorporate multiple dimensions of field data into the validation stream to maximize the utility of current and future sensor technologies and computing power. We are hopeful that these protocols will prove useful in advancing our conceptual understanding of global carbon dynamics in the ocean.

1.3. References

Alkire, M., Lee, C., D'Asaro, E., Perry, M., Briggs, N., Cetinić, I., & Gray, A. (2014). Net community production and export from Seaglider measurements in the North Atlantic after the spring bloom. *Journal Of Geophysical Research: Oceans*, *119*(9), 6121–6139. https://doi.org/10.1002/2014jc010105

Behrenfeld, M., Westberry, T., Boss, E., O'Malley, R., Siegel, D., & Wiggert, J. et al. (2009). Satellite-detected fluorescence reveals global physiology of ocean phytoplankton. *Biogeosciences*, *6*(5), 779–794. https://doi.org/10.5194/bg-6-779-2009

Behrenfeld, M., Gaube, P., Della Penna, A., O'Malley, R., Burt, W., & Hu, Y. et al. (2019). Global satellite-observed daily vertical migrations of ocean animals. *Nature*, *576*(7786), 257–261. https://doi.org/10.1038/s41586-019-1796-9

Brewin, R., Sathyendranath, S., Platt, T., Bouman, H., Ciavatta, S., & Dall'Olmo, G. et al. (2021). Sensing the ocean biological carbon pump from space: A review of capabilities, concepts, research gaps and future developments. *Earth-Science Reviews*, *217*, 103604. https://doi.org/10.1016/j.earscirev.2021.103604

Calbet, A., & Landry, M. (2004). Phytoplankton growth, microzooplankton grazing, and carbon cycling in marine systems. *Limnology And Oceanography*, *49*(1), 51–57. https://doi.org/10.4319/lo.2004.49.1.0051

Cassar, N., Barnett, B., Bender, M., Kaiser, J., Hamme, R., & Tilbrook, B. (2009). Continuous High-Frequency Dissolved O2/Ar Measurements by Equilibrator Inlet Mass Spectrometry. *Analytical Chemistry*, *81*(5), 1855–1864. https://doi.org/10.1021/ac802300u

Claustre, H., Morel, A., Babin, M., Cailliau, C., Marie, D., & Marty, J. et al. (1999). Variability in particle attenuation and chlorophyll fluorescence in the tropical Pacific: Scales, patterns, and biogeochemical implications. *Journal Of Geophysical Research: Oceans*, *104*(C2), 3401–3422. https://doi.org/10.1029/98jc01334

Collins, J., Fucile, P., McDonald, G., Ossolinski, J., Keil, R., & Valdes, J. et al. (2018). An autonomous, in situ light-dark bottle device for determining community respiration and net community production. *Limnology And Oceanography: Methods*, *16*(6), 323–338. https://doi.org/10.1002/lom3.10247

Del Giorgio, P., & Williams, P. (2008). *Respiration in aquatic ecosystems*. Oxford University Press.

D'Alelio, D., Rampone, S., Cusano, L., Morfino, V., Russo, L., & Sanseverino, N. et al. (2020). Machine learning identifies a strong association between warming and reduced primary productivity in an oligotrophic ocean gyre. *Scientific Reports*, *10*(1). https://doi.org/10.1038/s41598-020-59989-y

Duarte, C., Regaudie-de-Gioux, A., Arrieta, J., Delgado-Huertas, A., & Agustí, S. (2013). The Oligotrophic Ocean Is Heterotrophic. *Annual Review of Marine Science*, *5*(1), 551–569. https://doi.org/10.1146/annurev-marine-121211-172337

Eppley, R.W. (1972). Temperature and phytoplankton growth in the sea. *Fish Bull*, *70*(4), 1063–1085.

Fishman, J., Iraci, L., Al–Saadi, J., Chance, K., Chavez, F., & Chin, M. et al. (2012). The United States' Next Generation of Atmospheric Composition and Coastal Ecosystem Measurements: NASA's Geostationary Coastal and Air Pollution Events (GEO-CAPE) Mission. *Bulletin Of the American Meteorological Society*, *93*(10), 1547–1566. https://doi.org/10.1175/bams-d-11-00201.1

Geider, R. & Osborne, B. (1992). Algal Photosynthesis: The Measurement of Algal Gas Exchange. Chapman and Hall.

Gorbunov, M. Y., & Falkowski, P. G. (2021). Using chlorophyll fluorescence kinetics to determine photosynthesis in aquatic ecosystems. Limnology and Oceanography, *66*(1), 1–13.

Grande, K., Williams, P., Marra, J., Purdie, D., Heinemann, K., Eppley, R., & Bender, M. (1989). Primary production in the North Pacific gyre: a comparison of rates determined by the 14C, O2 concentration and 18O methods. Deep Sea Research Part A. Oceanographic Research Papers, *36*(11), 1621–1634. https://doi.org/10.1016/0198-0149(89)90063-0

Hama, T., Hama, J., Handa, N. (1993). 13C Tracer Methodology in Microbial Ecology with Special Reference to Primary Production Processes in Aquatic Environments. In: Jones, J.G. (eds) Advances in Microbial Ecology. Advances in Microbial Ecology, vol 13. Springer, Boston, MA. https://doi.org/10.1007/978-1-4615-2858-6_2

Harrison, W. G. (1980). Nutrient Regeneration and Primary Production in the Sea. In Falkowski, P. G. (ed) Primary Productivity in the Sea. Springer US, Boston, MA, 433–460.

Jamet, C., Ibrahim, A., Ahmad, Z., Angelini, F., Babin, M., Behrenfeld, M. J., Boss, E., Cairns, B., Churnside, J., Chowdhary, J., Davis, A. B., Dionisi, D., Duforêt-Gaurier, L., Franz, B., Frouin, R., Gao, M., Gray, D., Hasekamp, O., He, X., … Zhai, P.-W. (2019). Going beyond standard ocean color observations: Lidar and polarimetry. Frontiers in Marine Science, *6*, 251. https://doi.org/10.3389/fmars.2019.00251

Johnson, K. S., Berelson, W. M., Boss, E. S., Chase, Z., Claustre, H., Emerson, S. R., ... & Riser, S. C. (2009). Observing biogeochemical cycles at global scales with profiling floats and gliders: prospects for a global array. *Oceanography*, *22*(3), 216–225.

Kirk, J.T.O. (2011) Light and Photosynthesis in Aquatic Ecosystems. 3rd Edition, Cambridge University Press, Cambridge, England.

Kolber, Z. S., Prášil, O., & Falkowski, P. G. (1998). Measurements of variable chlorophyll fluorescence using fast repetition rate techniques: Defining methodology and experimental protocols. *Biochimica et Biophysica Acta (BBA) - Bioenergetics*, *1367*(1–3), 88–106. https://doi.org/10.1016/S0005-2728(98)00135-2

Landry, M. R., Constantinou J., Latasa M., Brown S. L, Bidigare R. R. & Ondrusek, M. E.. (2000). Biological response to iron fertilization in the eastern equatorial Pacific (IronEx II) III. Dynamics of phytoplankton growth and microzooplankton grazing. *Marine Ecology Progress Series*, *201*, 57–72.

Laws, E. A., Landry, M. R., Barber, R. T., Campbell, L., Dickson, M. L., & Marra, J. (2000). Carbon cycling in primary production bottle incubations: inferences from grazing experiments and photosynthetic studies using 14C and 18O in the Arabian Sea. *Deep Sea Research Part II: Topical Studies in Oceanography*, *47*(7–8), 1339–1352.

Lee, Z., Hu, C., Shang, S., Du, K., Lewis, M., Arnone, R., & Brewin, R. (2013). Penetration of UV-visible solar radiation in the global oceans: Insights from ocean color remote sensing. *Journal of Geophysical Research: Oceans*, *118*(9), 4241–4255.

Lohrenz, S. E., Wiesenburg, D. A., Rein, C. R., Arnone, R. A., Taylor, C. D., Knauer, G. A., & Knap, A. H. (1992). A comparison of in situ and simulated in situ methods for estimating oceanic primary production. *Journal of Plankton Research*, *14*(2), 201–221. https://doi.org/:10.1093/plankt/14.2.201

Lu, X., Hu, Y., Trepte, C., Zeng, S., & Churnside, J. H. (2014). Ocean subsurface studies with the CALIPSO spaceborne lidar. *Journal of Geophysical Research: Oceans*, *119*(7), 4305–4317.

Luz, B., & Barkan, E. (2009). Net and gross oxygen production from O2/Ar, 17O/16O and 18O/16O ratios. *Aquatic Microbial Ecology*, *56*(2–3), 133–145.

Marra, J. (2002). Approaches to the measurement of plankton production. Phytoplankton productivity: Carbon assimilation in marine and freshwater ecosystems, 78–108.

Marra, J. (2015). Ocean productivity: A personal perspective since the first Liege Colloquium. *Journal of Marine Systems*, *147*, 3–8. https://doi.org/10.1016/j.jmarsys.2014.01.012

Morel, A., Antoine, D., Babin, M., & Dandonneau, Y. (1996). Measured and modeled primary production in the northeast Atlantic (EUMELI JGOFS program): the impact of natural variations in photosynthetic parameters on model predictive skill. *Deep Sea Research Part I: Oceanographic Research Papers*, *43*(8), 1273–1304. https://doi.org/10.1016/0967-0637(96)00059-3

National Research Council. (2008). *Earth Observations from Space: The First 50 Years of Scientific Achievements*. National Academies Press, Washington, DC.

Neale, P. J., Cullen, J. J., Lesser, M. P., & Melis, A. (1993). Physiological bases for detecting and predicting photoinhibition of aquatic photosynthesis by PAR and UV radiation. *Photosynthetic responses to the environment*, *33*, 61–77.

Nicholson, D., Emerson, S., & Eriksen, C. C. (2008). Net community production in the deep euphotic zone of the subtropical North Pacific gyre from glider surveys. *Limnology and Oceanography*, *53*(5part2), 2226–2236. https://doi.org/10.4319/lo.2008.53.5_part_2.2226

Peterson, B. J. (1980). Aquatic primary productivity and the 14 C-CO 2 method: a history of the productivity problem. *Annual Review of Ecology and Systematics*, *11*, 359–385.

Regaudie-de-Gioux, A., Lasternas, S., Agustí, S., & Duarte, C. M. (2014). Comparing marine primary production estimates through different methods and development of conversion equations. *Frontiers in Marine Science*, *1*, 19.

Richardson, K. (1991). Comparison of 14C primary production determinations made by different laboratories. *Mar. Ecol. Prog. Ser.*, *72*(1–2), 189–201.

Riley, G. A. (1939). Plankton studies. II. The western North Atlantic, May-June. *J. Mar. Res*, *2*, 145–162.

Saba, V. S., Friedrichs, M. A., Antoine, D., Armstrong, R. A., Asanuma, I., Behrenfeld, M. J., ... & Westberry, T. K. (2011). An evaluation of ocean color model estimates of marine primary productivity in coastal and pelagic regions across the globe. *Biogeosciences*, *8*(2), 489–503.

Sharp, J. H. (1977). Excretion of organic matter by marine phytoplankton: Do healthy cells do it? 1. *Limnology and Oceanography*, *22*(3), 381–399. https://doi.org/10.4319/lo.1977.22.3.0381

Slawyk, G. (1979). 13C and 15N uptake by phytoplankton in the Antarctic upwelling area: Results from the Antiprod I cruise in the Indian Ocean sector. *Marine and Freshwater Research*, *30*(4), 431–448.

Slawyk, G., Collos, Y., & Auclair, J. C. (1977). The use of the 13C and 15N isotopes for the simultaneous measurement of carbon and nitrogen turnover rates in marine phytoplankton 1. *Limnology and Oceanography*, *22*(5), 925–932. https://doi.org/10.4319/lo.1977.22.5.0925

Steeman Nielsen, E. (1952) The use of radioactive carbon (C^14) for measuring organic production in the sea. *J. Con.s Int. Explor. Mer.*, *18*: 117–140.

Werdell, P. J., Behrenfeld, M. J., Bontempi, P. S., Boss, E., Cairns, B., Davis, G. T., ... & Knobelspiesse, K. D. (2019). The Plankton, Aerosol, Cloud, ocean Ecosystem mission: status, science, advances. *Bulletin of the American Meteorological Society*, *100*(9), 1775–1794.

Worrest, R. C., Brooker, D. L., & Van Dyke, H. (1980). Results of a primary productivity study as affected by the type of glass in the culture bottles 1. *Limnology and Oceanography*, *25*(2), 360–364.

2. The Metabolic Continuum of Primary Productivity

Kimberly Halsey[1], Ricardo Letelier[2], Ryan A. Vandermeulen[3,4]
[1]*Department of Microbiology, Oregon State University, Oregon, USA*
[2]*College of Earth, Ocean, and Atmospheric Sciences, Oregon State University, Oregon, USA*
[3]*Science Systems and Applications, Inc., Maryland, USA*
[4]*NASA Goddard Space Flight Center, Maryland, USA*

2.1. Overview of Components of Photosynthesis

The marine ecosystem is wholly dependent on the activity of photosynthetic algae. Within each algal cell, most of the energy derived from light is subsequently used to convert carbon dioxide into the organic material needed to build cell components (e.g., lipids, proteins, nucleic acids). Thus, photosynthetic processes are fundamental drivers of the marine carbon cycle. Furthermore, approximately half of the organic matter produced each day through photosynthesis is consumed by microzooplankton and other herbivorous grazers, initiating the complex marine food web. The global impacts of algae make measuring and monitoring their photosynthetic processes a vital undertaking.

Photosynthesis refers to the biological conversion of light energy into chemical energy, which fuels cell growth and division. There is no single metabolic step that defines photosynthesis. Rather, photosynthesis encompasses a range of processes initiated by light absorption by pigment complexes and the transfer of energy to photosynthetic reaction centers, the site of electron excitation. In algae, the collection of photosynthetic processes includes light energy transfer from pigments to the photosynthetic reaction centers, photosynthetic electron transport, carbon fixation via the Calvin-Benson cycle, nitrogen reduction, subcellular carbon catabolism, and macromolecular anabolism leading to cell division. Many of the fundamental biochemical processes and the connectivity of these processes are shared across algae, making it possible to characterize photosynthetic activities at the community scale.

Note that studies to dissect the tremendous diversity of bacterial and eukaryotic phytoplankton have revealed that photosynthetic activity is rarely confined to strict photoautotrophs. This means that although some photosynthetic algae can use light energy to fuel their growth processes (photoautotrophy), most algae are mixoplankton that can use dissolved organic carbon or phagocytize microbial prey in addition to photosynthesis. The ability to consume preformed organic matter 'subsidizes' the metabolic needs of mixoplankton. An extreme example of mixoplankton is kleptoplastidic protists, which lack the genetic capacity to produce chloroplasts and photosynthetic electron transport chains. Instead, these organisms steal chloroplasts from their prey and use the stolen machinery for chemical energy generation. In addition, many photosynthetic algae depend on the uptake of specific organic compounds, such as vitamins they cannot synthesize (auxotrophy). The spectrum of photosynthetic activities in aquatic microbes challenges interpretations of primary production because the relative reliance on photosynthesis vs. heterotrophy varies depending on species and environment (i.e., light or nutrient availability). Unraveling these various activities is especially important for understanding how planktonic systems and the broader food web will respond to climate change.

2.2. Primary Production: GPP to NCP

Because algae are the base of the marine food web, they are known as the primary producers of the marine ecosystem. Thus, **primary production** *broadly* describes the photosynthetic activity of algae. Primary production measurements aim to assess the rate at which energy or carbon is captured in the aquatic system. Akin to monetary accounting, the rate of light energy absorption by the algal community can be viewed as the gross energy budget that becomes available for algal growth and division over a period. This valuable ecosystem descriptor is called **gross primary production (GPP)**. Energy expenditures to carbon metabolism and respiration cause the remaining energy budget to be less than GPP. The extent to which energy expenditures deplete GPP in an ecosystem depends on algal physiology and the activity of the heterotrophic microbial community. The rate of carbon production after accounting for energy losses and carbon respiration by the entire microbial community is called **net community production (NCP)**. GPP and NCP describe the two endpoints of the primary production continuum (Fig. 2.1).

Understanding the approaches used to assess primary production requires a basic knowledge of the processes by which absorbed light energy becomes chemical energy and is then used by the cell to fuel growth and division. Here, we define the most used descriptors of primary production. Different experimental approaches are needed to assess primary production in the ocean because the methods capture processes that occur across varying spatial and temporal scales (Fig. 1.1). Method comparisons can reveal a broader understanding of ecosystem function but need to be interpreted considering time and space integration. Each method and additional associated considerations such as cost, isotope use regulations, and complementary data needs are discussed in subsequent chapters (Table 2.1). However, these descriptors are not always clearly defined in the literature, challenging the interpretation of results. Thus, we hope this document will assist in the adoption of a common vocabulary for aquatic ecosystem scientists.

The average algal cell in the global ocean funnels about 35% of absorbed light energy to the photosystem II (PSII) reaction centers where the water-splitting reaction occurs. The remaining ~65% of absorbed light energy is lost as heat or fluorescence (Kirk, 1994; Lin et al., 2016). The canonical step in photosynthesis uses light energy to extract electrons from water and simultaneously releases oxygen. The rate of oxygen evolution is thus a measure of the rate of energy (electrons) captured through the light-harvesting reactions of photosynthesis and is called **Gross Oxygen Production (GOP)**. It can be expressed as

$$GOP = GPP - NPQ - F, \tag{2.1}$$

where NPQ is non-photochemical quenching (NPQ) and F is fluorescence, the two pathways by which absorbed energy is lost from the cell (see Chapter 9).

The energized electrons are spontaneously passed through a series of electron carriers with decreasing electrochemical potentials within a membrane, terminating at photosystem I (PSI). This process of photosynthetic electron transport generates a cross membrane proton and electrochemical gradient that supports the conversion of electrochemical potential energy into chemical energy (ATP) through photophosphorylation.

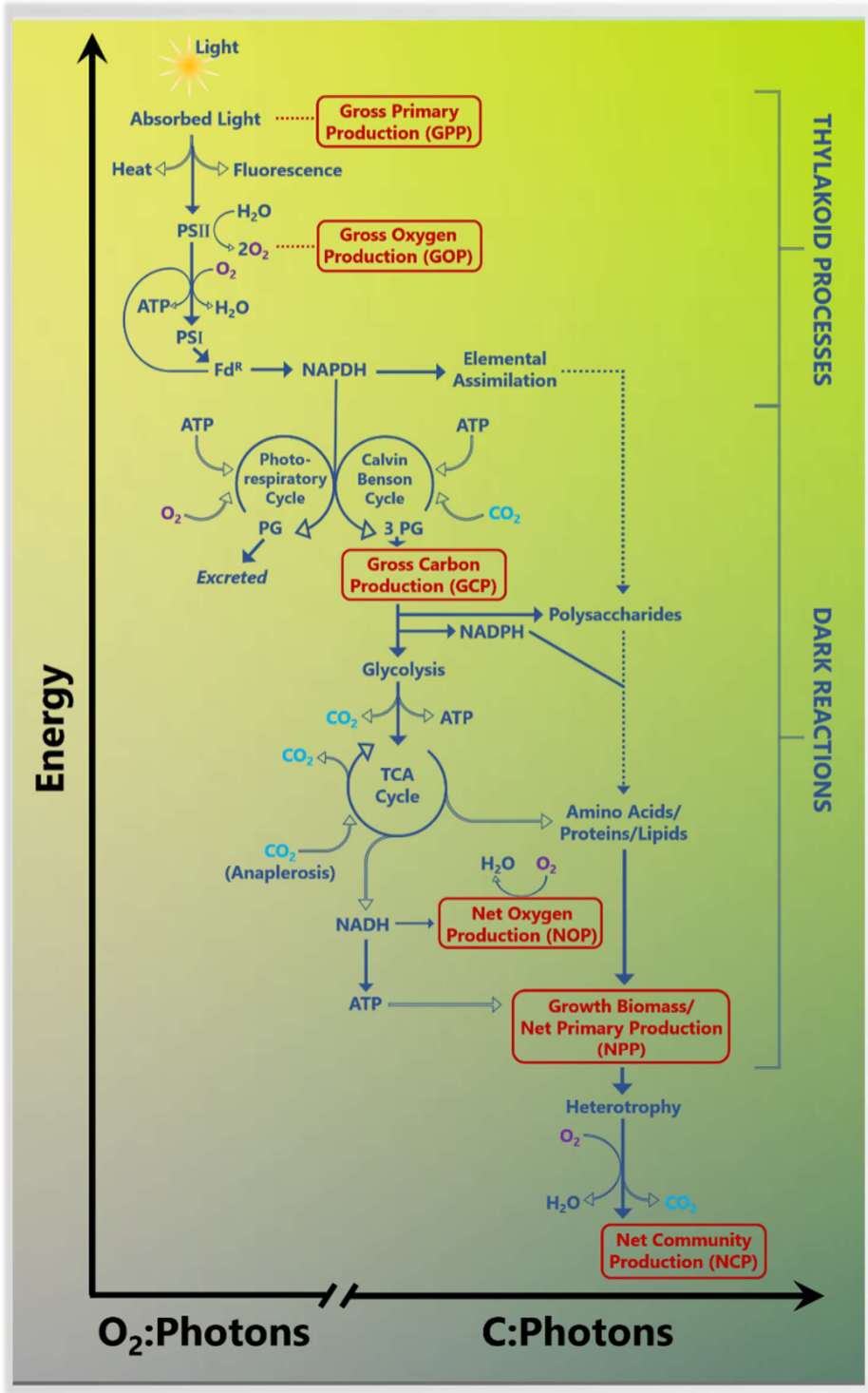

Fig. 2.1. The metabolic processes contributing to the continuum of primary production outlined as a function of solar energy use. The budgetary constraints on the two endpoints of this continuum, gross primary production, and net community production, depend on varying factors influencing algal physiology and microbial heterotrophic activity.

Like PSII, PSI is surrounded by light-absorbing pigments, which concentrate light energy at the PSI reaction center, causing electrons to be re-energized to facilitate the reduction of ferredoxin, the key electron carrier. There are three fates for reduced ferredoxin: (1) it is used to reduce NADP+ to form NADPH, (2) it returns electrons to the photosynthetic electron transport chain, leading to continued ATP production, a process called cyclic electron transport, or (3) it can reduce O_2, which effectively promotes the proton motive force through light-dependent respiration. For biochemical and biophysical details on photosynthetic electron transport, we refer the reader to *Molecular Mechanisms of Photosynthesis* by Robert E. Blankenship (2014). Most of the chemical energy (ATP and NADPH) derived from photosynthetic electron transport is used for carbon fixation (CO_2 reduction into organic molecules).

Gross carbon production (GCP) is the rate at which CO_2 is converted into organic carbon by the Calvin–Benson cycle. GCP is generally about 70–75% of GOP, with the difference between GOP and GCP reflecting losses of energy to rapid O_2 reduction, a process sometimes called water-water cycles because water was the source of the electrons delivered to the photosynthetic electron transport chain and the return of electrons to O_2 produces water. These rapid cycles provide some cell protection from photoinhibition caused by absorption of light in excess of GCP by allowing for the consumption of excess electrons. Water-water cycles are also important in maintaining proper balance in the cell's basic energetic currencies, ATP, and NADPH. Water-water cycles are also known as light-dependent respiration (LDR) because they only occur in the light and cause O_2 to be consumed.

Part of the difference between GOP and GCP is due to the use of NADPH and ATP in the reduction of elements other than carbon, such as the reduction of nitrate to ammonia or sulfate to sulfur (N/S_{red}); this energy sink is generally ~5% of GPP (Halsey et al., 2010). Thus, GCP is expressed as

$$GCP = GPP - NPQ - LDR - N/S_{red}, \tag{2.2}$$

$$GCP = GOP - LDR - N/S_{red}. \tag{2.3}$$

Some of the organic carbon produced by the Calvin-Benson cycle is broken down to produce more chemical energy via glycolysis, the TCA cycle, and respiratory electron transport. **Net oxygen production (NOP)** is the amount of O_2 produced after accounting for all O_2 reduced by respiration,

$$NOP = GPP - NPQ - LDR - N/S_{red} - DR, \tag{2.4}$$

$$NOP = GCP - DR. \tag{2.5}$$

The last expression shows NOP as the difference between GCP and respiration fueled by glycolysis (DR). The presence of heterotrophic microbes will further draw down the O_2 concentration, and NOP is commonly the measure used to obtain NCP (see below). Another fraction of the total organic carbon pool is catabolized to fuel the biosynthesis of cell

components or energy-demanding processes such as DNA replication and cell division. **Net primary production (NPP)** is the rate of organic carbon production after accounting for subcellular carbon catabolism and respiration. By definition,

$$NPP = POC\ x\ \mu, \tag{2.6}$$

where POC is particulate organic carbon, or cell carbon content, and μ is cell growth rate, yielding carbon production per unit time (e.g., C d^{-1}). Both terms are challenging to measure *in situ*; Chapter 3 focuses on NPP capturing approaches. In addition, the relationships between GPP, GOP, GCP, NOP, and NPP can vary depending on the environment and species.

The preceding discussion largely centered on the algal cell and key descriptors of the starting points to aquatic carbon cycling. Of course, algae coexist in nature with a complex microbial community, with each member taking up and respiring carbon that almost entirely originated from algal photosynthesis. Thus, in natural aquatic ecosystems, **net community production (NCP)** is a valuable descriptor of the carbon production rate that escapes degradation by the surface microbial community and is thus available for export into the twilight zone. NCP is commonly estimated by converting NOP determined from oxygen sensors into carbon units using an empirically derived constant. While simple in concept, the complex milieu of dissolved organic carbon substrates and the range of bacterial mechanisms employed to interact and metabolize with these substrates make accurate estimates of NCP a significant challenge in aquatic ecosystem research. Although not discussed in this volume, net ecosystem production (NEP) is a descriptor commonly used in terrestrial research, but rarely in oceanography. NEP was originally defined as the difference between GPP and the sum of autotrophic and heterotrophic respiration (Woodwell and Whittaker, 1968; Lovett et al., 2006). However, it has often been used to describe the net accumulation of organic carbon in an ecosystem, accounting for the abiotic processes that limit or increase the retention of organic carbon in the ecosystem (Raderson et al., 2002). For example, photodegradation, sea-air emission, and cross-ecosystem transfers all impact the net accumulation of organic carbon in the ecosystem.

2.3. Interconversions: $O_2 \rightarrow C$ via PQ and RQ

A suite of measurements is commonly used to assess primary production. Their value depends on understanding what step in the primary production continuum is being targeted and how cell physiology influences energy conservation. Theoretical considerations facilitate conversions between different measures of primary production. One of the most applied conversions is the **photosynthetic quotient (PQ),** which refers to the molar ratio of oxygen produced to CO_2 assimilated into biomass. Thus, PQ can be used to convert oxygen production measurements to carbon production (i.e., the conversion of NOP to NPP). PQ values ranging from 1.0 to 2.25 have been reported (reviewed in Williams and Robertson, 1991; Laws, 1991). A value of 1.4 is commonly applied when nitrate is the primary source of nitrogen, while ammonia assimilation will lower the PQ due to the lower oxidation state of N in NH_4+. A range of environmental, taxonomic, and metabolic factors interact to cause PQ to vary, even within a single species. For example, algae rich in lipids will have higher PQ values than those that are lipid-depleted, and carbon composition depends on growth rate. Environments that cause growth to become imbalanced, such as rapid changes in light intensity, CO_2 or oxygen limitation, and iron

limitation, may also decouple oxygen production from growth, increasing PQ beyond the canonical value of 1.4.

Another conversion factor to consider is the **respiratory quotient (RQ)**, which refers to the molar ratio of CO_2 produced per mole of oxygen consumed. Notably, the RQ varies depending on metabolic pathways involved and the stoichiometric composition of the primary product. The RQ value is frequently assumed to be 1.0 (the theoretical value for complete oxidation of a simple carbohydrate). However, different organic substrates can yield RQ values ranging from 0.13–4, based on their composition (Berggren et al., 2011). For example, substrates rich in lipid composition undergo both glycolysis and β-oxidation; since the latter process does not yield CO_2, lipid metabolization tends to yield a substantially lower RQ (del Giorgio and Williams, 2005). If we consider a 'typical' algal cell containing 40% protein, 40% carbohydrate, 15% lipid, and 5% nucleic acid ($C_1H_{1.7}O_{0.43}N_{0.12}P_{0.0046}$), it will yield a theoretical RQ of 0.89 based on stoichiometry alone (Williams and Robertson, 1991; Hedges et al., 2002); individual contributions from the above substrates would yield an RQ in the range of 0.71–1.23 (Rodrigues and Williams, 2001). Of course, natural waters provide a more complicated reality, in which RQ values measured *in situ* can fall well below traditional bounds (0.2–0.6; Münzner and Berggren, 2019), perhaps due to additional complex biochemical processes such as nitrification or methane oxidation. In addition, not all oxygen-consuming processes are directly linked with organic production/consumption (such as photorespiration or the Mehler Reaction, one of the water-water cycles described earlier) (del Giorgio and Williams, 2005). Thus, the RQ will ultimately vary as a function of cell physiology and environmental factors. Given the relative difficulty in executing a proper measurement of this value, researchers tend to settle on a constant RQ value and accept a 20% margin of error (Robinson, 2019).

Finally, myriad methodological considerations can impact primary production and PQ measurements. It appears that most artifacts are introduced during incubation-based techniques (e.g., bottle effects, intracellular and intercellular C and N recycling), and some of these are discussed with mitigating approaches later in this document. Future approaches that take advantage of incubation-independent measurements (e.g., optics, next-generation 'omics, dyes and imaging, growth rate-dependent metabolite pools) will greatly benefit constraining carbon fluxes on our changing planet.

Table 2.1

Methods used to measure primary production. For methods not described in this protocol document, the reader is referred to the literature suggested in column four.

Ecosystem descriptor	Abbreviation	Methods	Chapter, Section, Reference
Gross primary production	GPP	Fluorescence	Chapter 9
		Chlorophyll	Chapter 10
Gross oxygen production	GOP	Triple oxygen isotopes	Chapter 7
		$^{18}O_2$ tracer addition; $^{18}O_2$ detected by membrane inlet mass spectrometry (MIMS)	Chapter 4, Milligan et al., 2007 Halsey et al., 2010
		$H_2{}^{18}O$ bottle incubations; ^{18}O detected by isotope ratio mass spectrometer or MIMS	Chapter 4, Bender et al., 1987 Ferron et al., 2016
		Fluorescence flash yields	Chapter 9
Gross carbon production	GCP	C-uptake (short incubation duration; 10–60 min for high biomass regions or ~2 hours for oligotrophic regions)	Chapter 3
		By difference (GOP - light dependent respiration)	Chapters 5, 6
Net oxygen production	NOP	Light-dark bottle incubations ($^{16}O_2$)	Chapter 5
		Oxygen electrodes/optodes	Chapter 6
Net primary production	NPP	C-uptake (24-hour incubation, dawn-dawn)	Chapter 3
		Product of cell carbon (C_{phyto}) and growth rate (μ)	C_{phyto}: Graff et al., 2012 m: Landry et al., 1995
		N-assimilation rate	Eppley et al., 1977
		Satellite and optics-derived models	Behrenfeld and Falkowski, 1997 Westberry et al., 2008 Silsbe et al., 2016 Fox et al., 2020
Net community production	NCP	O_2/Ar ratios	Chapter 8
		Optics or biogeochemical sensor derived estimates	Chapter 10

2.4. References

Behrenfeld, M. J., & Falkowski, P. G. (1997). Photosynthetic rates derived from satellite-based chlorophyll concentration. *Limnology and Oceanography*, *42*(1), 1–20.

Bender, M., Grande, K., Johnson, K., Marra, J., Williams, P. J. L., Sieburth, J., ... & Heinemann, K. (1987). A comparison of four methods for determining planktonic community production. 1. *Limnology and Oceanography*, *32*(5), 1085–1098.

Berggren, M., Lapierre, J. F., & Del Giorgio, P. A. (2011). Magnitude and regulation of bacterioplankton respiratory quotient across freshwater environmental gradients. *The ISME Journal*, *6*(5), 984–993.

Blankenship, R. E. (2014). Molecular mechanisms of photosynthesis. John Wiley & Sons.

del Giorgio, P., & Williams, P. (Eds.). (2005). Respiration in aquatic ecosystems: history and background. *Respiration in aquatic ecosystems*, 1–17.

Eppley, R. W., Sharp, J. H., Renger, E. H., Perry, M. J., & Harrison, W. G. (1977). Nitrogen assimilation by phytoplankton and other microorganisms in the surface waters of the central North Pacific Ocean. *Marine Biology*, *39*(2), 111–120.

Ferrón, S., del Valle, D. A., Björkman, K. M., Quay, P. D., Church, M. J., & Karl, D. M. (2016). Application of membrane inlet mass spectrometry to measure aquatic gross primary production by the 18O in vitro method. *Limnology and Oceanography: Methods*, *14*(9), 610–622.

Fox, J., Behrenfeld, M. J., Haëntjens, N., Chase, A., Kramer, S. J., Boss, E., ... & Halsey, K. H. (2020). Phytoplankton growth and productivity in the Western North Atlantic: Observations of regional variability from the NAAMES field campaigns. *Frontiers in Marine Science*, *7,* 24.

Graff, J. R., Milligan, A. J., & Behrenfeld, M. J. (2012). The measurement of phytoplankton biomass using flow-cytometric sorting and elemental analysis of carbon. *Limnology and Oceanography: Methods*, *10*(11), 910–920.

Halsey, K. H., Milligan, A. J., & Behrenfeld, M. J. (2010). Physiological optimization underlies growth rate-independent chlorophyll-specific gross and net primary production. *Photosynthesis Research*, *103*, 125–137.

Hedges, J. I., Baldock, J. A., Gélinas, Y., Lee, C., Peterson, M. L., & Wakeham, S. G. (2002). The biochemical and elemental compositions of marine plankton: A NMR perspective. *Marine Chemistry, 78*(1), 47–63.

Kana, T. M., Darkangelo, C., Hunt, M. D., Oldham, J. B., Bennett, G. E., & Cornwell, J. C. (1994). Membrane inlet mass spectrometer for rapid high-precision determination of N2, O2, and Ar in environmental water samples. *Analytical Chemistry*, *66*(23), 4166–4170.

Kirk, J.T.O. (1994). Light and Photosynthesis in Aquatic Ecosystems. 2nd Edition, Cambridge University Press, Cambridge, England.

Landry, M. R., Kirshtein, J., & Constantinou, J. (1995). A refined dilution technique for measuring the community grazing impact of microzooplankton, with experimental tests in the central equatorial Pacific. *Marine Ecology Progress Series*. Oldendorf, *120*(1), 53–63.

Lin, H., Kuzminov, F.I., Park, J., Lee, S., Falkowski, P.G., & Gorbunov, M.Y. (2016). The fate of photons absorbed by phytoplankton in the global ocean. *Science*, *351*(6270), 264–267.

Lovett, G. M., Cole, J. J., & Pace, M. J. (2006). Is net ecosystem production equal to ecosystem carbon accumulation? *Ecosystems*, *9*, 1–4.

Milligan, A. J., Berman-Frank, I., Gerchman, Y., Dismukes, G. C., & Falkowski, P. G. (2007). Light-dependent oxygen consumption in nitrogen-fixing cyanobacteria plays a key role in nitrogenase protection. *Journal of Phycology*, *43*, 845–852.

Münzner, K., & Berggren, M. (2019). In situ plankton community respiration measurements show low respiratory quotients in a eutrophic lake. *Environmental Microbiology*, *21*(4), 1425–1435.

Randerson, J. T., Chapin, F. S., Harden, J. W., Neff, J. C., & Harmon, M. E. (2002) Net ecosystem production: a comprehensive measure of net carbon accumulation in ecosystems. *Ecological Applications*, *12*, 937–947.

Robinson, C. (2019). Microbial respiration, the engine of ocean deoxygenation. *Frontiers in Marine Science*, *5*, 533.

Rodrigues, R. M., & Williams, P. J. L. B. (2001). Heterotrophic bacterial utilization of nitrogenous and nonnitrogenous substrates, determined from ammonia and oxygen fluxes. *Limnology and Oceanography*, *46*(7), 1675–1683.

Silsbe, G. M., Behrenfeld, M. J., Halsey, K. H., Milligan, A. J., & Westberry, T. K. (2016). The CAFE model: A net production model for global ocean phytoplankton. *Global Biogeochemical Cycles*, *30*(12), 1756–1777.

Westberry, T., Behrenfeld, M. J., Siegel, D. A., & Boss, E. (2008). Carbon-based primary productivity modeling with vertically resolved photoacclimation. *Global Biogeochemical Cycles*, *22*(2).

Williams, P. I., & Robertson, J. E. (1991). Overall planktonic oxygen and carbon dioxide metabolisms: The problem of reconciling observations and calculations of photosynthetic quotients. *Journal of Plankton Research*, *13*(supp1), 153–169.

Woodwell, G.M., & Whittaker, R.H. (1968). Primary production in terrestrial ecosystems. *American Zoologist*, *8*, 19–30.

3. Carbon-Based Incubations

^{14}C Section:

Gemma Kulk[1], Ana Fernández Carrera[2], William M. Balch[3], John F. Marra[4], Patrick Neale[5], and Solange Duhamel[6]

[1]*Earth Observation Science and Applications, Plymouth Marine Laboratory, Plymouth, UK*
[2]*Leibniz Institute for Baltic Sea Research Warnemünde, Rostock, Germany*
[3]*Bigelow Laboratory for Ocean Sciences, Maine, USA*
[4]*Earth and Environmental Sciences, Brooklyn College, New York, USA*
[5]*Smithsonian Environmental Research Center, Maryland USA*
[6]*Department of Molecular and Cellular Biology, University of Arizona, Arizona, USA*

^{13}C Section:

Tomonori Isada[1], Ana Fernández Carrera[2], Toru Hirawake[3], Joaquim Goes[4], Daffne C. López-Sandoval[5], Solange Duhamel[6]

[1]*Akkeshi Marine Station, Field Science Center for Northern Biosphere, Hokkaido University, Hokkaido, Japan*
[2]*Leibniz Institute for Baltic Sea Research Warnemünde, Rostock, Germany*
[3]*National Institute of Polar Research, Tokyo, Japan*
[4]*Lamont-Doherty Earth Observatory at Columbia University, New York, USA*
[5]*Coastal and Marine Resources CL, King Abdullah University of Science and Technology, Thuwal, Saudi Arabia*
[6] *Department of Molecular and Cellular Biology, University of Arizona, Arizona, USA*

3.1. Introduction

This chapter deals with carbon-based primary production measurements using various incubation methods with the radioisotope ^{14}C and the stable isotope ^{13}C. First, a short history of the two tracer techniques is provided (Section 3.1.1 and 3.1.2). Supplies and reagents are then discussed in separate Sections for ^{14}C (Section 3.2.1) and ^{13}C (Section 3.2.2) measurements. Next is a detailed explanation of shipboard sampling procedures (Section 3.3.1) and the three different incubation methods that can be used for both ^{14}C and ^{13}C measurements, i.e., *in situ* incubations (Section 3.3.2), on-deck, simulated *in situ* incubations (Section 3.3.3), and photosynthesis-irradiance incubations (Section 3.3.4). Sample processing and analysis are discussed in separate Sections for ^{14}C (Section 3.4.1) and ^{13}C (Section 3.4.2) measurements; these Sections also provide information on the calculation of photosynthetic rates and the advantages, disadvantages, and caveats of both carbon tracer methods. Section 3.5 discusses the post-processing of carbon-based measurements, including photosynthesis-irradiance models and depth-integrated primary production calculations. Additional methods for carbon-based measurements, including dissolved organic carbon (DOC) production, cell-specific techniques, and the ^{14}C-microdiffusion technique for simultaneous measurement of calcification and primary production are provided toward the end of this chapter (Section 3.6). Finally, ancillary measurements that should be collected in addition to ^{14}C and ^{13}C measurements are discussed in Section 3.7.

3.1.1. History of ^{14}C methods

E. Steemann Nielsen published his "^{14}C technique" in 1952 (Steemann Nielsen, 1952). He submitted a first manuscript while conducting measurements aboard the 1950–1952 Galathea

expedition to illustrate its efficacy, thereby introducing a new means to understand ocean productivity. ^{14}C had only been discovered about ten years earlier. In the late 1940s, Calvin used it in his classic experiments on carbon pathways in photosynthesis (Barber and Hilting, 2002). Steemann Nielsen's method was to add ^{14}C as labeled sodium bicarbonate to a seawater sample and, after an incubation period in the light, assay the amount of ^{14}C appearing in particulate matter filtered out of the sample. The rate of photosynthesis was defined as the proportion of ^{14}C in the organic matter relative to the amount of inorganic ^{14}C added, times the concentration of dissolved inorganic carbon in the seawater.

The advantage of the ^{14}C method for measuring photosynthetic carbon assimilation in the ocean is its extreme sensitivity. Earlier methods, notably the analysis of oxygen changes in incubated samples, cannot discriminate the small changes in O_2 characteristic of many ocean regions. The second advantage is the method's relative facility. It requires, in addition to the isotope, only a means to separate the particulate matter from the seawater and a means to assay the radioactivity. Handling ^{14}C at the activities used is safe, requiring no special equipment. Although on a ship, precautions for all radioisotopes must be taken to ensure the ship itself does not become contaminated.

The "Carbon-14 method," as it came to be known, heralded a new era in the study of ocean productivity. The measurement got to the source of primary productivity in the ocean: the rate of photosynthesis in phytoplankton. After some early controversy in the 1950s (Peterson, 1980), the Carbon-14 method became widely adopted; by the 1960s, global maps of primary productivity based on ^{14}C were being produced for publication (Koblentz-Mishke et al., 1970). One of the corollaries to the extreme sensitivity to the Carbon-14 method is that it could not be validated or compared with other measurements. Perhaps that, and the ease with which the measurements could be made, is why it took a while to recognize significant concerns (Marra, 2002). However, in the late 1970s, criticisms were being made regarding the effects of incubation, respiration, the activities of heterotrophs, etc. Some of these concerns persist to this day.

Nevertheless, much progress has been made using the ^{14}C method for determining oceanic primary production. We have identified a series of milestones in its use after its introduction by Steemann Nielsen (1952):

- 1957: The International Council for the Exploration of the Sea meeting produces the first map of the productivity of the ocean.
- 1970: Wide publication of the 'Koblentz-Mishke' map of ocean productivity (Koblentz-Mishke et al., 1970).
- 1979–1982: The VERTEX program establishes trace metal clean methods for the measurement of plankton rate processes in the ocean (Fitzwater et al., 1982).
- 1982–1985: The program Planktonic Rate Processes in the Ocean (PRPOOS) establishes methodological comparisons among various measures of primary production and identifies errors associated with other than clean methods.
- 1989–1999: The Joint Global Ocean Flux Study (JGOFS) establishes international methodological protocols for measuring primary production.

- 2002: The Plankton Production in Aquatic Environments conference (and book by Williams et al., 2002) commemorates the 50th anniversary of the introduction of the ^{14}C technique.

It is important to note the contribution of JGOFS. The program established international protocols and produced a body of data that used a consistent method over a range of oceanic conditions (JGOFS 1992).

The ^{14}C method remains the preeminent technique for measuring oceanic productivity. However, there are now other means of estimating productivity, for example, through measurements of fluorescence kinetics or the isotopic composition of surface waters.

3.1.2. History of ^{13}C methods

The ^{13}C tracer method, initially developed for phytoplankton cultures by Slawyk et al. (1977) and later modified by Hama et al. (1983) for natural seawater samples, has been employed to determine primary production rates of natural phytoplankton communities in a wide range of environments, including oligotrophic open ocean waters. The ^{13}C tracer method is based on the same principle as the radioactive carbon (^{14}C) labeling method (Steemann Nielsen, 1952), where the sample is enriched (with $NaH^{13}CO_3$), and the uptake of CO_2 into particulate organic matter (POC) is followed, in this case, by tracking changes of the ^{13}C:^{12}C ratio of POC relative to the total inorganic carbon pool (Cullen, 2001).

The main difference between both tracer techniques is that we measure a ratio of isotopic abundances in the sample with the ^{13}C tracer method, while we estimate an absolute amount of isotope with the ^{14}C tracer method (Collos and Slawyk, 1985). Thus, the ^{13}C tracer technique requires information on the ^{13}C:^{12}C of POC before and after the incubation to estimate phytoplankton photosynthetic rates. Additionally, because mass-spectrometric methods used for quantifying stable isotopes are generally less sensitive than scintillation counters for radioactive compounds, the ^{13}C tracer method requires larger sample volumes and incubation times greater than an hour. Yet, despite the inherent methodological differences, several studies demonstrate a good agreement between ^{13}C- and ^{14}C-sodium bicarbonate uptake rates (Slawyk et al., 1977, 1979, 1984; Hama et al., 1983; Sakamoto et al., 1984; Collos and Slawyk, 1985; Mousseau et al., 1995; Regaudie-de-Gioux et al., 2014; López-Sandoval et al. 2018).

The recent introduction of the continuous-flow system of flash combustion for elemental analysis, coupled with a stable isotope ratio mass spectrometer (EA-IRMS) and the advent of new laser absorption techniques (e.g., cavity ring-down spectroscopy), make it possible to measure the isotope ratio of a sample with a small amount of POC (Brenna et al., 1998) and accurately quantify aquatic primary production by using ^{13}C (López-Sandoval et al., 2019). With these advances in mass spectrometric methods, the ^{13}C labeling method is gaining importance as a reliable alternative to the ^{14}C method for measuring phytoplankton photosynthetic rates. Furthermore, because the ^{13}C tracer method does not involve handling radioactive substances, it is not impacted by the restrictive regulations that are becoming a significant impediment to radioactive compound use in some countries. Another consideration are the prices of the different methods. The costs of reagents and consumables for primary production measurements using ^{13}C is estimated at 270 USD per incubation, assuming that all equipment is available, compared to 140 USD for ^{14}C based incubations (cost estimates are based on price lists from main suppliers at the time of writing).

3.2. Supplies and Reagents

Trace metal clean techniques should be used for primary production measurements wherever possible (JGOFS, 1996; Cutter et al., 2010). This includes following a rigorous protocol for the cleaning of sampling and incubation bottles (see Section 3.2.1 and 3.2.2) and the use of ultrapure water (e.g., 18.2 MΩ cm, low Total Organic Carbon (TOC)), such as Milli-Q for the preparation of any reagents. Polyethylene gloves are recommended at all times, from the time of sample collection to sample preparation prior to incubation and filtration (JGOFS, 1996; Cutter et al., 2010). Powder-free latex or vinyl gloves can also be used (Cutter et al., 2010, Becker et al., 2020). The use of a specific glove type should be tested for contamination prior to the measurements.

3.2.1. ^{14}C measurements

3.2.1.1. Sampling and incubation bottles

The generally accepted containers for collecting water subsamples before ^{14}C incubation are 10 L opaque polycarbonate (PC) bottles, for example, Nalgene round or rectangular PC Clearboy bottles with a closure or spigot (2251-0020, 2317-0020; 2322-0020, DS2213-0020; Thermo Scientific). To prevent any contamination by trace metals that could enhance or diminish phytoplankton growth (Fitzwater et al., 1982), all sampling bottles are washed with a dilute solution of trace metal-free non-ionic detergent, followed by thorough rinsing with ultrapure water, and then soaking in 5–10% HCl solution for more than 24 hours. After that, the bottles are rinsed at least 3 times with Milli-Q water. Different types of incubation bottles can be used for ^{14}C measurements, depending on the bottle characteristics and the study goals. An overview of the different incubation bottles is in Table 3.1. Incubation bottle volumes generally range from 10–250 mL, depending on the incubation method (*in situ*, on-deck, simulated *in situ,* or photosynthesis-irradiance curves), available phytoplankton biomass, and expected productivity. Trace metal clean techniques should also be followed in the use of incubation bottles, i.e., (new and re-used) bottles are soaked overnight in 5–10% HCl and thoroughly rinsed 3 times with Milli-Q water before use.

Table 3.1

Overview of incubation bottles and their characteristics available for the use of ^{14}C primary production measurements. Volumes generally range from 10–250 mL.

Type of bottle or flask	UV transparency [1]	Price ($-$$$)	Non-contaminating for trace-metals	Comments
Polycarbonate bottles	Partial	$$	Yes, if cleaned properly with 5–10% HCl	Contamination with DOC possible
Polystyrene cell-culture flasks	Partial	$	Yes	Can be discarded after use
Polysulfone tissue-culture flasks	Partial	$	Yes	Can be discarded after use
Borosilicate glass bottles	Partial	$$$	Yes, if cleaned properly with 5–10% HCl	Contamination with Si possible
Quartz bottles	Full	$$$	Yes	
Teflon[2] bottles	Full	$$$	Yes	

[1] Full transparency typically means > 90% transmission relative to PAR for the UV wavelength range of 280–400 nm. Partial transparency means there can be some transmission over part or all this range depending on manufacturer formulation and material thickness, which can vary widely. Percent transmission typically declines going from long to short wavelengths. If the degree of UV transmission is critical, users are advised to spectrophotometrically scan the actual material under consideration for use.
[2] Teflon is a trademark of the DuPont de Nemours Co.

3.2.1.2. Filters

The selection of filter material, diameter, and pore size used for ^{14}C measurements depends on the study aim and practicalities, such as the size of the filtration setup. Options include Glass Fiber Filters (GF/F; ~0.7 µm pore size), polycarbonate or cellulose filters (from 0.2 µm pore size), with 25 and 47 mm being the most-used diameter for filtration funnels. Traditionally, ^{14}C samples would be filtered onto GF/F (JGOFS 1996) to conform to other methods, but two drawbacks should prevent the use of this type of filter:

- Retention of autotrophic biomass may be lower than other filters due to the relatively large pore size of traditional GF/F (~0.7 µm, Whatman) and GF-75 (0.3 µm, Advantec). This is especially relevant in oligotrophic regions.
- An unknown amount of dissolved organic carbon, likely produced during the incubation and labeled with ^{14}C, can adsorb to the GF/F (Maske and Garcia-Mendoza, 1994), which makes even GF-75 not suitable for ^{14}C measurements.

Instead, polycarbonate or cellulose filters with small pore sizes (from 0.2 µm) are recommended. The filter diameter depends on the size of the filtration setup, the incubation volume, and phytoplankton biomass in the sample, with the idea that 25 mm filters will require less scintillation cocktail (and therefore produce less waste).

3.2.1.3. Reagents

The following reagents and chemicals are required for ^{14}C-based primary production measurements:

- *^{14}C Sodium-bicarbonate ($NaH^{14}CO_3$)*: Available in sealed glass ampoules containing 1 mCi (37 MBq) or 5 mCi (185 MBq) in aqueous solution from several vendors (including product NEC086H001MC from Perkin Elmer).
- *A high-capacity radioactive CO_2 absorber*: Ethanolamine, Phenethylamine, or Carbosorb is used to trap ^{14}C labeled CO_2 for measuring activity in the working (stock) solution (product 6013721 is available from Perkin Elmer).
- *Scintillation cocktail*: Different types of scintillation cocktails can be used, including those that accommodate aqueous solutions (e.g., Ultima Gold XR, Perkin Elmer; Eco-Lume, MP Biomedicals) or dissolve membrane filters (Ultima Gold MV, Perkin Elmer). Other scintillation cocktails are suitable for long-term storage (1–2 months) of samples (e.g., InstaGel Plus, Perking Elmer). Each scintillation cocktail has different counting efficiencies and quench characteristics, which must be corrected during scintillation counting (see Section 3.4.1.2).
- *Hydrochloric acid (HCl)*: Fuming 37% or 1 M is used for trace metal clean working and to vent excess $NaH^{14}CO_3$ after incubation of the samples.
- *Sodium hydroxide (NaOH)*: 1 M is used to control the pH in the working solution and (optionally) adjust the pH of the incubation samples after acidification.

3.2.1.4. ^{14}C working solution

The specific activity of the ^{14}C bicarbonate working (stock) solution depends on the desired final activity during incubation, which is related to phytoplankton biomass and environmental conditions (Table 3.2). The $NaH^{14}CO_3$ ampoule content can be directly (undiluted) transferred to a non-contaminating, screw-cap Teflon bottle or diluted with Milli-Q water (adjusting the pH to 8–9 with NaOH) and then transferred to a non-contaminating screw-cap Teflon bottle. An activity of 100 µCi mL^{-1} is usually a good working solution for various oceanic environments. The ^{14}C working solution should be stored at 4ºC. Note that opening the glass ampoule on ice (i.e., low temperatures) will prevent excess loss of radioactivity.

Total activity in the working solution is measured each time an experiment is performed. Approximately 1 µCi of the working solution (10 µL for a working solution of 100 µCi mL^{-1}) is added to a pre-prepared scintillation vial with 100 µL of a high-capacity radioactive CO_2 absorber. Scintillation cocktail is added (in the same volume of the incubation samples; Section 3.4.1.1), and the vials are vigorously shaken to mix all reagents. Alternatively, to determine the total added activity in the incubation samples, a subsample from selected incubation samples could be collected and added to scintillation vials that contain an empty filter and a high-capacity radioactive CO_2 absorber, after which scintillation cocktail is added. Samples can be assayed by liquid scintillation counting after chemo-luminescence subsides (1–2 hours).

3.2.1.5. Sample enrichment

The seawater sample is transferred to the incubation bottles in the desired volume (2–250 mL), each incubation sample and the dark samples are then enriched with ^{14}C bicarbonate (final

Table 3.2

Information is provided to determine the final concentration of ^{14}C for in situ, on-deck, simulated *in situ,* or photosynthesis-irradiance incubations. As general guidance, the final concentration of ^{14}C in the incubation sample is increased at low phytoplankton biomass when low photosynthetic rates are expected (for example, due to nutrient limitation or low temperatures) or when measuring calcification in parallel.

Oceanic region	Phytoplankton biomass	Final concentration ^{14}C	
		µCi mL^{-1}	kBq mL^{-1}
Coastal, upwelling	High	0.05–0.3	1.85–11.1
Oligotrophic	Low	0.1–0.4	3.7–14.8
Polar Regions	Variable	0.5–0.6	18.5–22.2

concentration 0.05–0.6 µCi mL $^{-1}$ or 1.85-22.2 kBq mL^{-1}; Table 3.2). Alternatively, the total volume for the incubation (including dark samples) can be enriched with ^{14}C bicarbonate and the enriched seawater samples transferred to incubation bottles afterward. The latter method is more practical for low incubation volumes (< 10 mL). Monochannel or repeating pipettes with sterile tips are recommended for enriching samples. After enrichment, samples are gently mixed. All handling of samples is performed under *in situ* temperatures (±2ºC) and low light conditions.

3.2.2. ^{13}C measurements

3.2.2.1. Sampling and incubation bottles

The generally accepted containers for collecting water subsamples before ^{13}C incubation are 10 L opaque polycarbonate (PC) bottles, for example Nalgene round or rectangular PC Clearboy bottles with closure or spigot (2251-0020, 2317-0020; 2322-0020, DS2213-0020; Thermo Scientific). To prevent any contamination by trace metals that could enhance or diminish phytoplankton growth (Fitzwater et al., 1982), all sampling bottles are washed with a dilute solution of trace metal-free, non-ionic detergent, then thoroughly rinsed with ultrapure water, and finally soaked in 5–10% HCl solution for more than 24 hours. After that, the bottles are rinsed at least three times with Milli-Q water.

For ^{13}C *in situ* and on-deck, simulated *in situ* incubations, we recommend acid-washed PC bottles, for example, the Nalgene Narrow-Mouth Square Bottle (2015-series) or Large Narrow-Mouth Round Bottle (2205-series). Larger volumes (> 1 L) are preferred, but if there are water budgeting issues, we recommend a volume of at least 0.5 L for shelf waters, 2 L for oligotrophic waters, and 4 L for ultra-oligotrophic ecosystems. Smaller incubation volumes (e.g., 0.25 L) may be considered during bloom conditions in coastal eutrophic waters when it is challenging to filter larger volumes. For ^{13}C photosynthesis-irradiance incubations, non-treated polystyrene culture flasks and PC bottles are the preferred incubation containers, but tissue polystyrene cell culture flasks are also acceptable. The volume of the flasks and bottles is typically 250 mL and can vary depending on the design of the incubator (Section 3.3.4.3). All incubation bottles should be acid washed and rinsed with Milli-Q water, similar to the procedure described for the sampling bottles.

3.2.2.2. Filters

Glass Fiber Filters (Whatman GF/F with ~0.7 pore size) with a 25 or 47 mm diameter are recommended for all ^{13}C measurements. Advantec^{TM} GF-75 (~0.3 μm pore size) is also acceptable. All filters should be pre-combusted at 450ºC for 4 hours before use (following IOCCG standard protocols).

3.2.2.3. Reagents

Sodium bicarbonate enriched to more than 98% with the stable isotope ^{13}C ($NaH^{13}CO_3$) is available from a variety of vendors, including Cambridge Isotope Laboratories Inc. (product CLM-441) and Sigma-Aldrich C. LLC (product 372382). Hydrochloric acid (HCl, fuming 37% or 1 M) is used for trace-metal clean working and to vent excess $NaH^{13}CO_3$ after sample incubation.

3.2.2.4. ^{13}C working solution

The recommended working solution is prepared by dissolving 0.1 g of ^{13}C-sodium bicarbonate in 25 mL of Milli-Q water in a 25 mL acid-clean volumetric flask for a final concentration of 0.047 M. The solution is then transferred to a 50 mL centrifuge tube (e.g., 62.547.254; SARSTEDT) and kept refrigerated at 4ºC (do not freeze) until use.

3.2.2.5. Sample enrichment

A solution of ^{13}C-sodium bicarbonate roughly equivalent to ca. 5–10% of the total dissolved inorganic carbon (DIC) in the seawater is added to each incubation light and dark bottle. The amount of ^{13}C-sodium bicarbonate to measure depends on the concentration in the working solution and the incubation volume. For example, assuming the DIC concentration of a sample is 2081 μM (~25,000 mg C m^{-3}), if 1 mL of the ^{13}C working solution described above is added to a 0.5 L of seawater by pipette (e.g., Eppendorf, Sartorius, etc.), the atom percentage of ^{13}C in the total DIC is ca. 5.24% (see the Supporting Information for further details on the calculation procedure).

3.3. Incubation methods

3.3.1. Shipboard sampling procedure

Following trace metal clean sampling techniques, Niskin-X bottles and silicone tubing should be cleaned with a 5–10% HCl solution before the cruise or field campaign.. Toxic rubber (nitrile rubber for O-rings) and metals should not be attached to the Niskin-X bottles to prevent inhibition of phytoplankton activity during sampling. Viton O-rings generally have less effect on phytoplankton than nitrile O-rings (Price et al., 1986; Williams and Robertson, 1989; Matsumoto et al., 2012).

At each station, seawater samples are collected from selected depths using Niskin-X bottles attached to a CTD rosette. For *in situ* and on-deck simulated *in situ* incubations, we recommend sampling 8 depths distributed through the entire euphotic zone from the surface to ca. 0.2–1% of incident light at the surface (JGOFS, 1996). For *in situ* incubations, the sampling and incubation depths can be evenly distributed or selected according to the profiles provided by the CTD (density, temperature, fluorescence, and oxygen).

Before sampling for the primary production incubation, separate samples for dissolved inorganic carbon (DIC) analysis should be carefully collected directly from the Niskin-X bottles with a clean silicon tube into 250 mL acid-cleaned and combusted borosilicate bottles (see Section 3.2.1.1 and 3.2.2.1), leaving a headspace of 1% of the bottle volume to allow for water expansion. DIC samples are then poisoned with 50–100 µL of saturated mercuric chloride ($HgCl_2$) solution. Glass or quartz bottles are sealed with lightly silicone greased glass stoppers or some alternate gas-tight fashion and stored in a cool, dark location until analysis. Further details of the sampling and analytical procedure are described by Dickson et al. (2007). DIC measurements are particularly important in coastal ecosystems under the influence of river discharge or by melting sea ice in high-latitude ocean ecosystems like the Arctic and Antarctic Oceans. If a CO_2 coulometer system or a closed-cell potentiometric titrator with a pH meter is unavailable, the less sensitive TOC/TC/TIC analyzer (often used in inland water quality surveys) could provide a sufficiently accurate estimate of the DIC concentration needed to calculate primary production. Alternatively, DIC concentration could be empirically calculated by salinity (Magalhães et al., 2008), but validation of this approach is essential, especially in low-salinity coastal and polar waters.

After collecting the DIC samples, collect seawater for the primary production incubation by gently draining the contents of the Niskin-X bottles into 10 L acid-clean PC carboys after triple rinsing them. Alternatively, the incubation bottles can be filled directly from the Niskin-X bottles using acid-washed non-contaminating silicone tubing. If using samples from depth, it is important to adequately shield the samples from the high irradiance and higher temperatures at the surface. This can be done by wrapping the 10 L PC carboys with black plastic bags and transferring the samples into coolers. Sample transfer from the 10 L PC carboys into the incubation bottles followed by the addition of the ^{14}C or ^{13}C labeled $NaHCO_3$ solution is done in the dark at *in situ* temperatures (±2ºC).

Additionally, triplicate samples for time zero activity should be collected immediately after the sampling at the station. Details on filtration methods are provided in Section 3.4.1.1 for ^{14}C and Section 3.4.2.1 for ^{13}C methods. It is important to note the exact volume of water filtered for time zero activity in the ^{13}C method; this will depend on the system studied, but for guidance, a distinctly-colored filter should contain enough biomass of seston to define the ^{13}C:^{12}C ratio accurately. Any ancillary measurements (Section 3.7) should also be collected at this time.

3.3.2. In situ incubations

In situ incubations with ^{14}C and ^{13}C are the closest representation of what happens in the ocean's euphotic zone and are recommended in the JGOFS protocol (JGOFS 1996). The advantages of the *in situ* incubation method are clear, with temperature structure and light quality being adequately matched during the incubation. As is the case for on-deck, simulated *in situ* incubations, there is no need to obtain information on light or temperature at depth. Yet, care must be taken in the interpretation of results if the physicochemical structure of the water column changes throughout the day. Similarly, the effect on the photophysiology of incubating phytoplankton cells at fixed depths should be considered as cells would not naturally remain static throughout the incubation period. The need for station-keeping near a drifting buoy must be weighed against other shipboard activities. However, such provisions should be made if productivity is a major objective for the field campaign.

3.3.2.1. Time of sampling

Water sampling should be carried out before sunrise if the incubation is conducted from dawn to dusk (~12–14 hours). If ship operations are not flexible, water sampling can be done at any time of day and enriched samples can be incubated for 24 hours. In the latter case, it is also possible to incubate from the sampling time until dusk, assuming linearity in photosynthetic rates throughout the day, allowing for the calculation of a daily rate. This assumption was tested in some ocean regions (Marañón et al., 2005), but it should not be considered a universal rule, and test experiments in specific regions are strongly recommended. A correction factor can be applied as an alternative (Moutin et al., 1999; Duhamel et al., 2007).

3.3.2.2. Incubation duration

Incubation duration is critical in determining primary production with or without autotrophic respiration. JGOFS protocols (JGOFS, 1996) initially recommended 24-hour dawn to dawn incubations, whereas later protocols advised ~12–14 hour dawn to dusk incubations to estimate net primary production (Marra 2009). Both incubation periods can provide useful information; comparing the two methods allows for an estimate of autotrophic respiration (Marra and Barber, 2004), which might otherwise not be amenable to direct measurement.

3.3.2.3. Sample incubation

Three light and 1–2 dark bottles are recommended for the incubation at each depth. It is crucial to fill the bottles with the same volume of water, and the presence of a headspace does not affect bicarbonate uptake. There are several options for creating dark bottles, including wrapping bottles in several layers of black electrical tape, duct tape, or aluminum foil or using a thick, black cloth to prevent light penetration. If aluminum foil is used, bottles should be checked regularly for damage to the foil since the reflection of light inside the bottles can sustain relevant primary production.

Once samples have been enriched with ^{14}C- or ^{13}C-bicarbonate, the incubation bottles are securely hooked by plastic cable ties to the appropriate position of the mooring system in a coordinated fashion to match each sampling depth. The floats and strobe flash are attached to the top of the mooring system and weights to the bottom. If the incubation is conducted from dawn to dusk, the system should be deployed before sunrise and recovered after sunset.

3.3.2.4. *On-deck, simulated in situ incubations*

On-deck, simulated *in situ* incubations with ^{14}C and ^{13}C are an alternative to *in situ* incubations when, for example, it is not possible to keep near-drifting buoys due to other shipboard activities (Figure 3.1). On-deck, simulated *in situ* incubations require information on light and temperature throughout the water column prior to the start of the incubation, which is often collected the day before the incubation to allow enough time to adjust the incubator settings. As with *in situ* incubations, care must be taken when interpreting the results if the physicochemical structure of the water column changes throughout the day.

Fig. 3.1. An example of an on-deck, simulated in situ incubator with re-circulating water baths (left) and the incubator covered with blue tarp during the night (right).

3.3.2.5. Time of sampling

Water sampling should be carried out before sunrise if the incubation is conducted from dawn to dusk (~12–14 hours). If ship operations are not flexible, water sampling can be done at any time of day and incubated for 24 hours (see Section 3.3.2.1 for more details).

3.3.2.6. Incubation duration

Samples are typically incubated for ~12–14 hours from dawn to dusk or for 24 hours from the sampling time. The same considerations discussed for *in situ* incubations (Section 3.3.2.2) apply to on-deck, simulated *in situ* incubations.

3.3.2.7. On-deck incubator design

Incubator designs for on-deck, simulated *in situ* incubations can vary, but incubations are generally carried out in plexiglass containers that represent the water column conditions at each sampling depth (Fig. 3.1). Temperature in the incubator is regulated by running surface seawater through the incubator for surface samples and adjusted using recirculating water baths for the other sampling depths. Light levels reaching the incubation bottles can be adjusted by covering the incubation containers with a combination of blue and neutral photographic filters (Table 3.3 and Fig. 3.1) or by covering the incubation bottles with neutral density bags (no spectral correction for lower depths). If bottles are stacked in the incubator, the low irradiances bottles (1–5% of surface irradiance) are placed on the bottom and the high irradiance bottles (50–100% of surface irradiance) are placed on the top. During 24-hour incubations, covering the plexiglass incubators with a heavy-duty thick black cloth or a plastic tarp overnight is recommended to keep samples shaded, regardless of ship operations and light pollution throughout the night. Additionally, photosynthetically active radiation (PAR, 400–700 nm) above the surface in the incubator should be regularly checked—and preferably measured continuously—using a quantum sensor connected to a data logger (e.g., the LI-190R/LI-1500 system, LI-COR). The achieved proportion of surface irradiance in the incubator should be checked during the system setup by comparing incident PAR with the same inside the various incubation containers, which can be measured using a scalar PAR sensor (for example, a QSL-2100 from Biospherical

instruments or a US-SQS/L from Walz). This enables adjustment for the effects of reflection from surfaces near the incubator and refraction through the incubator walls.

Table 3.3

Combination of Lee filters* for simulating the intensity (in percentage of surface irradiance) and spectral quality of light in an on-deck, simulated *in situ* incubator. Note that Lee HT061 Mist Blue filters have high transmission in the red spectrum, and Lee 724 Ocean Blue filters may be more suitable for use in open ocean conditions.

% Irradiance	# Layers of filter	
	Lee HT061 Mist Blue	Lee 210 Neutral density
100	0	0
55	1	0
33	2	0
20	3	0
14	4	0
7	2	1
4.5	3	1
3	4	1
2	2	2
1	3	2
0.5	4	2

* For more details on Lee filters, see http://www.leefilters.com/lighting/colour-list.html

3.3.2.8. Sample incubation

For each sampling depth, 3 light and 1–2 dark bottles are recommended for the incubation. It is important to fill the bottles with the same volume of water. A headspace in the bottles does not affect bicarbonate uptake. Still, the incubation bottles will float if the headspace is large, and the bottles should be ballasted to stay underwater in the incubator. There are several options for creating dark bottles, including wrapping bottles in several layers of black electrical tape, duct tape, or aluminum foil or using a thick, black cloth to prevent light penetration. If aluminum foil is used, bottles should be checked regularly for damage to the foil since reflection of light inside the bottles can sustain relevant primary production. Once the samples have been enriched with ^{14}C- or ^{13}C-bicarbonate, the incubation bottles can be placed in the on-deck incubator for the chosen incubation time.

3.3.3. Photosynthesis-irradiance incubations

Photosynthesis–irradiance (PE) incubations can provide a means of comparing the photosynthetic characteristics of marine phytoplankton across different natural populations and cultured isolates (Bouman et al., 2018). The relationship between photosynthesis and light can be fitted to different mathematical equations and described by just two parameters, while a third

parameter is needed if photoinhibition is present (see Section 3.5.1.2) (Jassby and Platt, 1976; Platt et al., 1980; Sakshaug et al., 1997). The chlorophyll-normalized PE parameters may be applied to estimate primary production over large scales by using ocean-color remote-sensing derived maps of chlorophyll *a* (Sathyendranath et al., 1995; Antoine and Morel, 1996).

3.3.3.1. Time of sampling

It is recommended to collect samples before noon because photosynthetic parameters may vary significantly throughout the day, with a maximum at around noon (Babin et al., 1995; Anning et al., 2000; Behrenfeld et al., 2008). Sample collection later in the day is also possible, but care must be taken in the interpretation of results and the use of PE parameters in further analysis as variations in PE parameter estimates could affect the calculation of daily primary productivity (Isada et al., 2013; Kulk et al., 2020).

3.3.3.2. Incubation duration

Short incubations are preferred, with times ranging from 0.5–1 hour for high biomass regions and 2–3 hours for oligotrophic regions. Photosynthesis versus irradiance incubations should be less than 4 hours to prevent the effects of photoacclimation processes (Lewis and Smith, 1983).

3.3.3.3. Photosynthesis-irradiance incubator design

Photosynthesis-irradiance incubations are performed in a photosynthetron, where seawater samples are incubated against a light gradient. Photosynthetron designs vary to accommodate different incubation bottle volumes, but all have a light source and a recirculating water bath to control temperature. Temperatures should be kept within ±2ºC of *in situ* temperatures. Different photosynthetron designs are available in Lewis and Smith (1983), Babin et al. (1994), and Kyewalyanga et al. (1997). A common incubator design has entirely black Plexiglass walls, except for the wall facing the light source (Fig. 3.2).

3.3.3.4. Incubator lamp and light gradient

Light sources that provide photosynthetically active radiation (PAR, 400–700 nm) in high intensities (> 2,000 µmol photons m^{-2} s^{-1}; the equivalent to solar irradiance at the sea surface on a bright sunny day; Mobley 1994) and have a spectrum close to solar irradiance are preferred. A range of light sources may be used, including tungsten halogen, halogen, metal halide, and fluorescent lamps (brands include Philips, OSRAM, and ILT; see Bouman et al. 2018 for an overview). Tungsten halogen lamps are commonly used because they can provide high light intensities, but their spectrum is heavily weighted toward red and infrared and requires spectral correction (see Section 3.5.1.1).

A light gradient can be created using neutral density filters (i.e., Lee and Rosco filters, metal screen, black cheesecloth), either in the incubator or by covering the incubation bottles. The PAR gradient within the incubators is generally adjusted to range between 1–2,500 µmol photons m^{-2} s^{-1} for surface samples and between 1–500 µmol photons m^{-2} s^{-1} for subsurface chlorophyll maximum samples, depending on the oceanic region. The light gradient should contain at least 20 different light levels, with sufficiently low light levels (1/3 of the total) to correctly estimate α^B (Section 3.5.1.2). Three additional places should be available for dark incubations. PAR reaching the incubation bottles should be measured and regularly checked using a scalar PAR sensor (for example, a QSL-2100 from Biospherical instruments or a US-SQS/L from Walz).

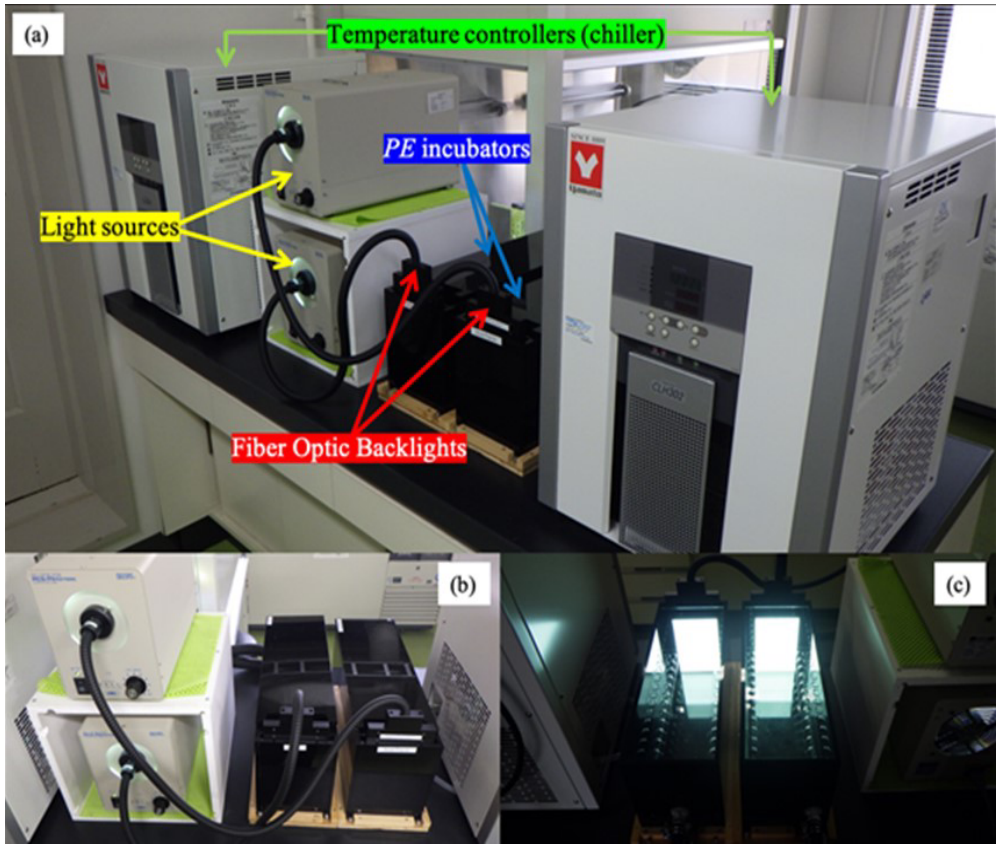

Fig. 3.2. An example of photosynthetron used for photosynthesis-irradiance (PE) incubations with two incubators connected to a light source and temperature controller; a) shows the complete setup, b) shows the front of the PE incubators, and c) shows the inside of the PE incubators.

A further refinement in incubator design is the use of one or more types of spectral filters. Similar to on-deck, simulated *in situ* incubations, broad-band blue filters like the Lee and Rosco gel filters are sometimes used to better approximate *in situ* irradiance (e.g., Bouman et al., 2018). Despite their appearance, these filters still have high transmission in the red. A more spectrally-specific approach is to define different regions of the PAR spectrum with interference filters placed between the lamp and incubation containers, which is most practical when done for small-volume incubations. Lewis et al. (1985) used a photosynthetron with twelve 25 nm bandpass filters to define an action spectrum of photosynthesis for open ocean assemblages. On the other hand, long-pass cut-off filters combined with a full spectrum light source (e.g., xenon bulb) are used to resolve the spectral dependence of UV inhibition (Cullen et al., 1992; Neale et al., 2014). Long-pass filters better replicate the spectral variation of UV in the ocean, which should always be added to a background of high PAR.

3.3.3.5. Sample incubation

Once samples have been enriched with ^{14}C- or ^{13}C-bicarbonate, the light and dark incubation bottles are placed in the photosynthetron for the chosen incubation time. Turning the

photosynthetron on approximately 30–60 minutes prior to the incubation is important so the appropriate temperature and light settings are reached by the start of the incubation.

3.4. Sample Processing and Analysis

3.4.1. ^{14}C measurements

3.4.1.1. Filtration and pretreatment of samples for analysis

After *in situ*, on-deck, simulated *in situ* or photosynthesis-irradiance incubations, the ^{14}C enriched samples (including dark samples) are filtered and further processed. The selection of the material, diameters, and pore size of the filters depends on the study aim and practicalities, such as the size of the filtration setup (details in Section 3.2.1.5). Options include GF/F, polycarbonate, or cellulose filters, with 25 and 47 mm being the most used diameter for filtration funnels. Samples can be filtered on standard vacuum filtration rigs (dedicated to radioactive work only) using low vacuum pressure (< 50 mm Hg or < 0.006 MPa). The entire volume of the incubation bottles is filtered to measure total or size-fractionated particulate organic carbon (POC) production. The filtration procedure for measuring dissolved organic carbon (DOC) along with POC is detailed in Section 3.6.1, with more details in IOCCG (2021).

After filtration, filters are acidified for 24 hours to remove excess ^{14}C-bicarbonate and ^{14}C-calcium carbonate. To this end, filters can be placed on a tray in open Eppendorf vials or directly on a tray placed in an enclosed container (for example, a glass desiccator), fuming HCl (1–2 mL, 37%) or 100 µL HCl (1 M) can be added to the filters directly in a scintillation vial. If not acidified in a scintillation vial, filters are then placed in a plastic or glass scintillation vial (6 or 20 mL, depending on the filter diameter and scintillation counter), and scintillation cocktail is added. Enough scintillation cocktail should be added to cover the filter (3.5–10 mL). Vials are vigorously shaken and stored in the dark for an additional 24 hours before counting.

3.4.1.2. Sample analysis

It is recommended to count samples as soon as possible, at sea or in the field. The activity of ^{14}C is measured using a liquid scintillation counter. Different types of liquid scintillation counters are available that may have preselected programs for counting ^{14}C in Disintegrations Per Minute (DPM). Generating a ^{14}C quenching curve is recommended for the specific scintillation vial, scintillation cocktail, and filter used in the incubation (for example, using the Perkin Elmer "Internal Standard Kit for Liquid Scintillation Counting"). Samples should be counted using a dual-ending mode based on time (> 180 seconds) or precision (1% threshold error).

3.4.1.3. Storage recommendations

Once scintillation cocktail is added, filtered, and acidified, samples can be stored for several weeks before activity decreases due to the loss of performance of the scintillation cocktail. Samples can be stored for longer periods (1–2 months) if a scintillation cocktail suitable for long storage is used (for example, InstaGel Plus, Perking Elmer). Samples should be stored in the dark and preferably at a low temperature (i.e., 4ºC; check specifications of the scintillation cocktail) to prevent degradation, evaporation, and ^{14}C leakage.

3.4.1.4. Calculation of photosynthetic rates

Measured ^{14}C activity (in DPM) in all samples of the *in situ* and on-deck, simulated *in situ* incubations are converted to daily rates of primary production (P in mg C m^{-3} d^{-1}) following JGOFS protocol (1996)

$$P = \frac{DPM_S \times 1.05 \times DIC \times V_T}{V_S \times t \times DPM_T}, \quad (3.1)$$

where DPM_S is the activity in the incubation sample (in DPM), V_S is the volume of the incubation sample (in L), 1.05 is a correction factor for the lower uptake of ^{14}C compared with ^{12}C, *DIC* is the concentration of dissolved inorganic carbon (in mg C m^{-3}, approximately 25,000 mg C m^{-3} for oceanic regions), V_T is the volume of the total activity (working solution) sample (in L), V_S is the volume of the incubation sample (in L), t is time (in d), and DPM_T is the total activity in the working solution sample. For final primary production rates, triplicate values of P are averaged for each sampling depth and (mean) P values in the dark incubation are subtracted. The separate reporting of daily primary production rates in the light and dark incubations is often required by data repositories such as SeaBASS, BCO-DMO, and PANGAEA (see Section 3.8). If this is not the case, final daily primary production rates at each depth can also be calculated directly using Eq. 3.1 by replacing DPM_S by [DPM_S - DPM_D] with DPM_D as the (mean) activity in the dark incubations (in DPM) (Banse, 1993). Daily depth-integrated primary production (mg C m^{-2} d^{-1}) can be calculated using the trapezoidal rule (see Section 3.5.2).

For photosynthesis-irradiance incubations, measured ^{14}C activity (in DPM) in each incubation bottle are converted to chlorophyll *a* normalized photosynthetic rates (P^B in mg C mg Chl-a^{-1} h^{-1}) following

$$P^B = \frac{(DPM_S - DPM_D) \times 1.05 \times DIC \times V_T}{V_S \times t \times Chl \times DPM_T}, \quad (3.2)$$

where DPM_S is the activity of the incubation sample (in DPM), DPM_D is the (mean) activity of the dark samples (in DPM), 1.05 is a correction factor for the lower uptake of ^{14}C compared with ^{12}C, *DIC* is the concentration of dissolved inorganic carbon (in mg C m^{-3}, approximately 25,000 mg C m^{-3} for oceanic regions), V_T is the volume of the total activity (working solution) sample (in mL), V_S is the volume of the incubation sample (in mL), t is time of the incubation (in hours) , *Chl* is the chlorophyll *a* concentration of the incubation samples (in mg m^{-3}), and DPM_T is the total activity in the working solution sample (in DPM).

3.4.1.5. Calibration, uncertainties, and accuracy

Calibration of ^{14}C measurements is impossible, but they can be compared with results from other methods, such as O_2 fluxes. There are a few limits on carbon assimilation based on physiology (Platt and Jassby, 1976; Platt et al., 1980; Sakshaug et al., 1997). For example, it has been determined that the assimilation number P^B_m cannot exceed 25 mg C mg Chl-a^{-1} h^{-1} (Falkowski 1981), and higher values should be viewed with suspicion. Another physiological

limit is provided by the maximum quantum yield of carbon fixation (Φ_m), which theoretically cannot exceed 0.125 mol C mol quanta^{-1} (Platt and Jassby, 1976; Sakshaug et al., 1997). This value is based on the long-standing quantum requirement for the evolution of oxygen, where it takes 8 quanta to evolve 1 molecule of O_2.

Scintillation counters have advanced to the stage where their results can be easily accepted. Standard procedures should be followed to convert counts per minute to disintegrations per minute and correct for quenching (Section 3.4.1.2).

3.4.1.6. Advantages, disadvantages, and caveats

The advantage of the ^{14}C method is its extreme sensitivity. There are no ocean environments where the method fails in its usage. The high specific activity of ^{14}C-bicarbonate and the relatively high concentration of unlabeled bicarbonate in seawater (2.2 mM) allow ^{14}C-bicarbonate to be added to seawater samples at true tracer concentrations. The high specific activity also means that ^{14}C incubations can be performed in small-volume samples, allowing many samples to be processed and treated at once, such as in photosynthesis-irradiance experiments. Moreover, the specific activity of ^{14}C is high enough that single-cell experiments can be performed with reasonable signal-to-noise, especially when cells can be sorted with flow cytometers (see Section 3.6.2). The ^{14}C method can also be combined with the radioactive isotope of phosphorus (^{33}P) (Duhamel et al., 2006), making it possible to measure the carbon and phosphate uptake by phytoplankton simultaneously. Finally, the ^{14}C method is relatively easy, and the activity of ^{14}C used in the incubations is safe.

Yet, ^{14}C is a radioactive isotope and employed at orders of magnitude greater than natural abundances. Therefore, shipboard use requires isolation and care in handling to avoid contaminating a ship for other natural abundance uses such as radiocarbon dating, circulation studies, and other geochemical research. The high sensitivity of the ^{14}C technique also translates to more regulations, difficulties, and costs in the safe handling of radioisotopes in experiments performed in the natural environment and in waste management. This is particularly true when shipping radioisotopes and waste across international borders. Research institutes may have a dedicated health and safety department that can assist in training and handling radioisotopes on expeditions, with established protocols for monitoring contamination. However, some countries prohibit or restrict the use of radioisotopes, limiting the use of the ^{14}C method in some coastal and oceanic regions.

There is also the question of what the ^{14}C method measures along the scale running from gross primary production to net community production (Marra, 2002). The ^{14}C method measures assimilation into particulate matter. Depending on how long the phytoplankton population is exposed to the isotope, the ^{14}C method will estimate gross (~minutes), net primary (minutes to hours), or net community production (24 hours). At longer times and at isotope equilibrium, the ^{14}C method can provide an estimate of carbon biomass.

3.4.2. ^{13}C measurements

3.4.2.1. Filtration and pre-treatment of samples for analysis

At the end of the incubation, samples are gently vacuum filtered (< 0.013 MPa) onto pre-combusted (450ºC for 4 hours) GF/F using a set of laboratory-grade glass filter-holder assemblies following the filtration procedure of the IOCCG protocol series (2021). The glass

filtration cups are carefully rinsed with filtered seawater to collect all particles in the walls and rid the sample of excess ^{13}C labeled $NaHCO_3$. The filters are placed in Petri dishes or 2 mL cryovials and stored at -80°C in a deep freezer or in liquid nitrogen until analysis on land. The filters are then exposed to fuming HCl in a fume hood for removing unincorporated ^{13}C-bicarbonate or incorporated ^{13}C-calcium carbonate, then transferred into pre-combusted (450°C for 4 hours) glass Petri dishes. Alternatively, ca.100 µL of 10% or less HCl can be added directly to the filters. The filters are dried for at least 24 hours in a desiccator following this process (Fig. 3.3).

Finally, the filters should be pelletized prior to analysis in the mass spectrometer (Fig. 3.4). The filter is pelletized in pressed tin capsules (10x10 mm). In this method, a tin capsule is placed on the sealing device and spread out. Next, the filter is folded in half or three and placed onto the tin capsule. The filter is then wrapped in the tin capsule using the sealing device. Trimming the particle-free edge of the filter (non-filtering white area) is also helpful to avoid accumulating residues on the swarf crucible of the elemental analyzer. The final pellet should be as small as possible and cylindrical; there should be no holes or breakages in the capsule after pelletizing. As a rule of thumb, if the pellet fits loosely into a 48 wells plate, it is properly done.

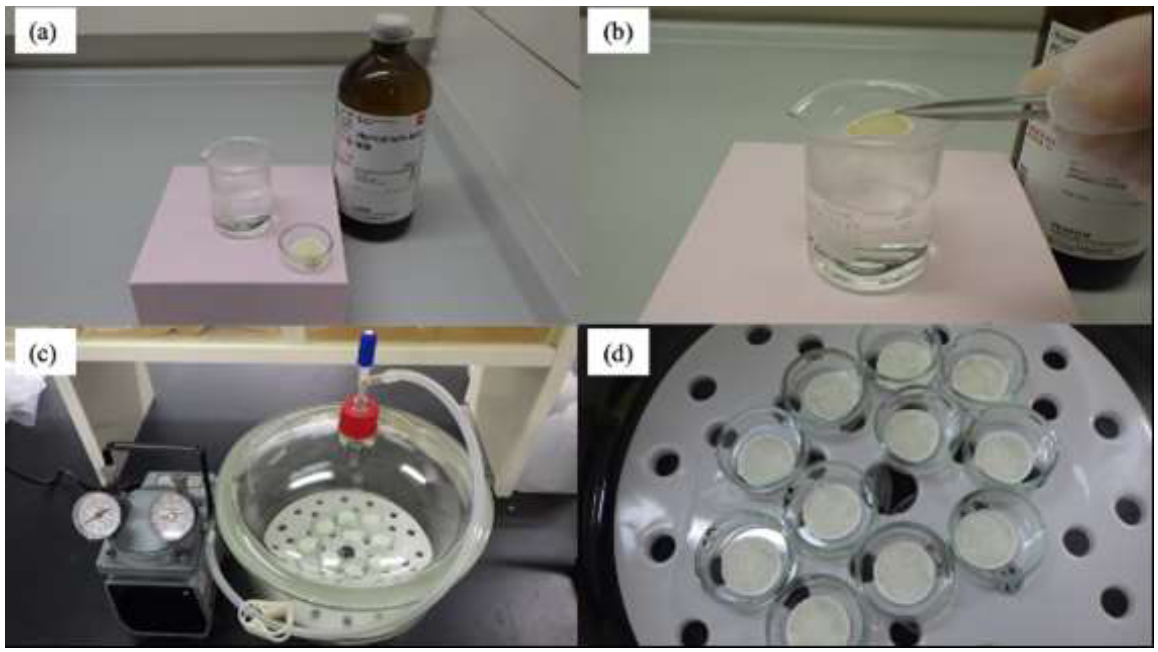

Fig. 3.3. Examples of the pre-treatment of ^{13}C samples with (a) the preparation of HCl in a draft chamber, (b) the exposure of filter to HCl fume, (c) the DURAN desiccator with Millipore Vacuum/Pressure Pump for desiccating the filters, and (d) the HCl exposed and dried samples on the pre-combusted glass Petri dishes.

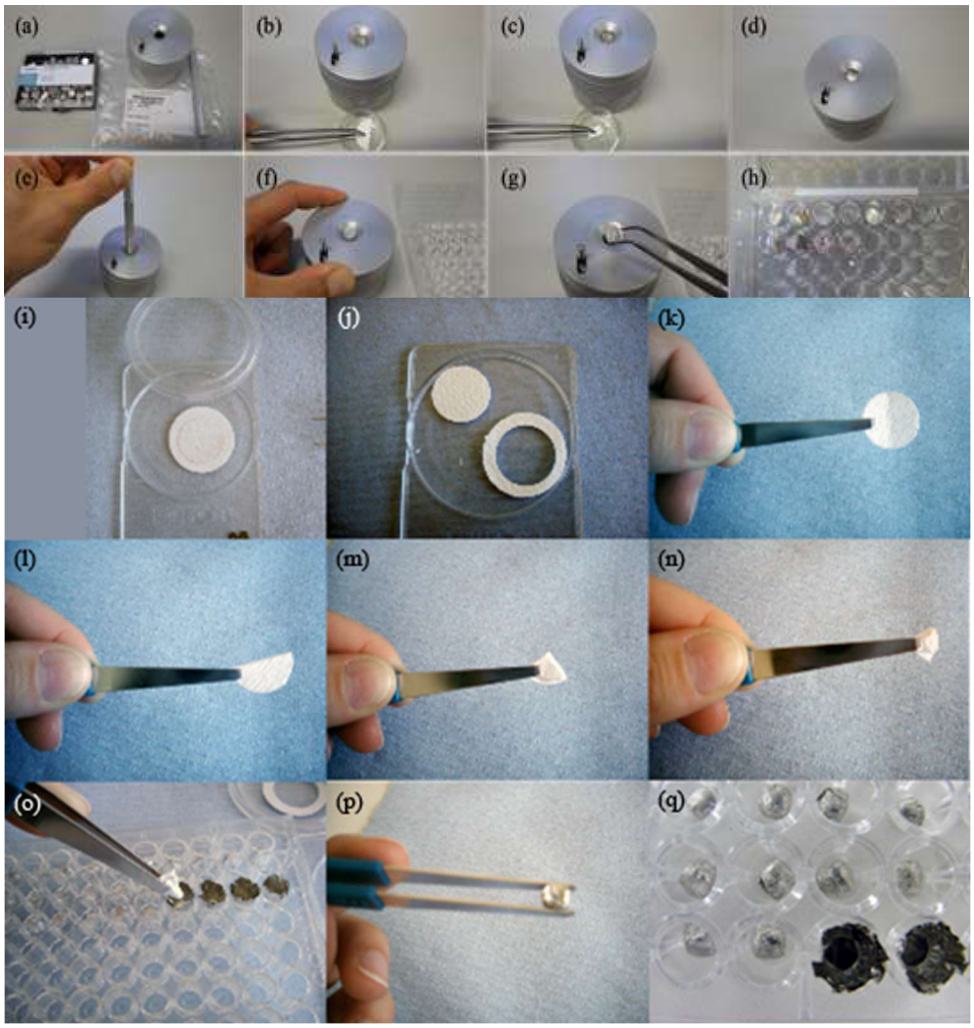

Fig. 3.4. An example (a-h) for pelletizing filters from ^{13}C incubations with the sealing device (Thermo Fisher Scientific, product 25209010) and (i-q) trimming the particle-free edge of the filter before pelletizing the filters.

3.4.2.2. Sample Analysis

Samples can be processed with an elemental analyzer coupled with a stable isotope ratio mass spectrometer (EA-IRMS) or by using laser absorption spectroscopic techniques (Cavity Ring-Down Spectroscopy, CRDS). Measuring the particulate organic matter and the ^{13}C:^{12}C ratio of the samples can be conducted by both systems, i.e., EA-IRMS or CRDS. There are several instruments available, including the ANCA-GSL elemental analyzer (Sercon), the Delta V with Flash2000 and the ConFlo IV (Thermo Scientific), and the CM-CRDS (Picarro, Inc.). We recommend measuring the carbon content of pre-combusted GF/F (at least three filters) as a blank.

The CM-CRDS consists of three components: The combustion module (Costech Analytical Technologies Inc., California, USA), the interface, and the Cavity Ring-Down Spectrometer

analyzer (CM-CRDS G2201-i, Picarro, Inc., Santa Clara CA, USA). After loading the samples into the auto-sampler attached to the combustion module, it is important to specify the time that each sample will be processed. Although the time must be assessed according to the origin of the samples, 600 seconds is a good starting point (further details in López-Sandoval et al., 2019).

3.4.2.3. Storage recommendations

After filtration, filters can be placed in Petri dishes or 2 mL cryovials and stored at -80ºC or liquid nitrogen until further analysis.

3.4.2.4. Calculation of photosynthetic rates

Photosynthetic rates based on the ^{13}C tracer technique for all incubation methods are determined using the method of Hama et al., (1983). The isotopic balance of ^{13}C and ^{12}C in the enriched sample and the ^{13}C in the sample after incubation are as follows

$$a_{is} \times POC = a_{ns} \times (POC - \Delta POC) + a_{ic} \times \Delta POC, \quad (3.3)$$

where a_{is} is the atom percentage of ^{13}C in the incubated light or dark sample, a_{ns} is the atom percentage of ^{13}C in the natural sample, a_{ic} is the atom percentage of ^{13}C in the total inorganic carbon (see Supporting Information for calculating the sample enrichment with ^{13}C), *POC* (in mg C) is particulate organic carbon in the incubated sample, and ΔPOC (in mg C) is the increase in *POC* during the incubation. The a_{is}, a_{ns}, and *POC* were measured by EA-IRMS. The ΔPOC is then calculated by rearranging Eq. 3.3 for ΔPOC

$$\Delta POC = POC \times \frac{(a_{is} - a_{ns})}{(a_{ic} - a_{ns})}. \quad (3.4)$$

The photosynthetic rate (P in mg C m^{-3} h^{-L} or mg C m^{-3} d^{-1}) can be obtained following

$$P = \frac{\Delta POC}{t \times V} \times f, \quad (3.5)$$

where t (in hours or days) is the incubation time, V is the volume filtered (in L or m^{-3}), and f is the discrimination factor of ^{13}C, of which the value is a debated point (see Section 3.4.2.5). This calculation is made for each incubation bottle and then the triplicate light bottles are averaged. The mean production values in the light bottles are subtracted by the production value of the dark bottle (or mean if multiple dark bottles) for each depth. Depth-integrated primary production within the euphotic layer (mg C m^{-2} d^{-1}) is calculated by the trapezoidal rule (see Section 3.5.2).

3.4.2.5. Calibration, uncertainties, and accuracy

Equation 3.5 assumes that the changes in a_{is} by non-algae carbon during the incubation period are minimal. However, bacterial uptake and zooplankton grazing during the incubation period may alter the atom percentage of ^{13}C in the sample, which could affect the calculation of photosynthetic rates measured with either carbon protocols (Karl et al., 1998; Teira et al., 2001; Collos et al., 2014). The adsorption effect becomes negligible as sample sizes increase (> 1 L

samples) (López-Sandoval et al., 2018). Although the enrichment of ^{13}C within the range from 5–15% of total DIC has little effect on the photosynthetic rate (Hama et al., 1983), the fixed values of discrimination factors (1.02 or 1.025 for the ^{13}C method) could bias the photosynthetic rate estimate because the carbon isotopic fractionation varies among species and groups of phytoplankton, cell geometry, and growth condition (Fry, 1996; Popp et al., 1998; Close, 2019). In practice, the correction factor is usually not applied (i.e., $f = 1$) because the correction has little significant effect on the uptake rate compared with ^{14}C methods (Slawyk et al., 1979; Hama et al., 1993).

3.4.2.6. Advantages, disadvantages, and caveats

A main advantage of the ^{13}C method is that it does not pose potential radioactive contamination and health safety concerns as opposed to the ^{14}C method. Moreover, the ^{13}C tracer techniques can be combined with other stable isotopes typically used for phytoplankton physiological rate measurements, for example, with ^{15}N labeled solutions of nitrogenous nutrients or nitrogen gas (NO_3^-, NO_2^-, NH_4^+, Urea, and N_2). The dual stable isotope method thus permits measurement of not only carbon, but also nitrogenous nutrient uptake rates. Care must be taken when applying the ^{13}C protocol for dual stable isotope measurements because the acidification method might affect the analysis of the stable isotope ratios of nitrogen ($\delta^{15}N$) (Brodie et al., 2011a; b). Finally, the larger bottles used in the ^{13}C method reduce "bottle effect" problems associated with smaller size incubation bottles typically used in the ^{14}C method.

A disadvantage of using ^{13}C tracer techniques lies in the method's sensitivity. Since mass spectrometric measurements of ^{13}C are less sensitive than scintillation counting of ^{14}C, the stable isotope technique requires larger sample volumes and longer incubation times than the latter. It is important to note that this is changing as mass spectrometers are becoming more sensitive. Additional disadvantages are that the consumable supplies for the EA-IRMS are expensive, and it require more user training. However, CRDS could overcome these problems (López-Sandoval et al., 2019).

3.5. Post-Processing

3.5.1. Photosynthesis-irradiance models

3.5.1.1. Spectral correction of incubator light source

The spectral distribution of the incubation light source affects the value of the initial slope of the photosynthesis-irradiance curve (α^B), and a correction for the spectral quality is required to compare results from incubations using different types of light sources (Dubinsky et al., 1986; Kyewalyanga et al., 1997; Bouman et al., 2018). A correction factor (X) can be used to calculate α^B under a spectrally neutral ("white") light environment and can be determined by using the following equation

$$X = \frac{\bar{a}_P}{\bar{a}_L}, \tag{3.6}$$

where $\bar{a}_P$ is the unweighted mean absorption coefficient of phytoplankton and $\bar{a}_L$ is mean absorption coefficient weighted by the shape of the emission spectrum of the light source

$$\bar{a}_P = \frac{\int_{400}^{700} a_P(\lambda) d\lambda}{\int_{400}^{700} d\lambda} \quad (3.7)$$

and

$$\bar{a}_L = \frac{\int_{400}^{700} a_P(\lambda) E_L(\lambda) d\lambda}{\int_{400}^{700} E_L(\lambda) d\lambda}, \quad (3.8)$$

where E_L is the normalized lamp irradiance spectrum. To obtain spectrally corrected irradiance levels for each incubation bottle, the irradiance intensity in the photosynthetron is multiplied by the correction factor *X*. Further spectral corrections may be necessary to estimate *in situ* photosynthesis at depths for which the ambient light spectrum deviates substantially from white light (Cullen et al., 2012).

3.5.1.2. Estimation of photosynthesis-irradiance parameters

Photosynthesis-irradiance (PE) measurements can be fitted to a variety of mathematical equations in which the PE parameters are estimated (Fig. 3.5) (Jassby and Platt, 1976; Platt et al., 1980). The three-parameter function of Platt et al. (1980) is the most commonly used equation in the presence of photoinhibition

$$P^B(E) = P_s^B \left(1 - \exp\left(-\frac{\alpha^B E}{P_s^B}\right)\right) exp\left(-\frac{\beta^B E}{P_s^B}\right), \quad (3.9)$$

where P^B (in mg C mg Chl-a^{-1} h^{-1}) is the chlorophyll *a* normalized photosynthetic rate, *E* (in µmol photons m^{-2} s^{-1}) is the scalar irradiance, $P^B{}_s$ (in mg C mg Chl-a^{-1} h^{-1}) is the hypothetical maximum photosynthetic rate in the absence of photoinhibition, α^B (in mg C mg Chl-a^{-1} h^{-1} [µmol photons m^{-2} s^{-1}]$^{-1}$) is the initial slope of the PE curve, and β^B (in mg C mg Chl-a^{-1} h^{-1} [µmol photons m^{-2} s^{-1}]$^{-1}$) is the photoinhibition parameter describing the decrease in the photosynthetic rate at high irradiance. In the presence of photoinhibition, values of the maximum photosynthetic rate ($P^B{}_m$ in mg C mg Chl-a^{-1} h^{-1}) can be derived using the following equation

$$P_m^B = P_s^B \left(\frac{\alpha^B}{\alpha^B + \beta^B}\right)\left(\frac{\beta^B}{\alpha^B + \beta^B}\right)^{\frac{\beta^B}{\alpha^B}}. \quad (3.10)$$

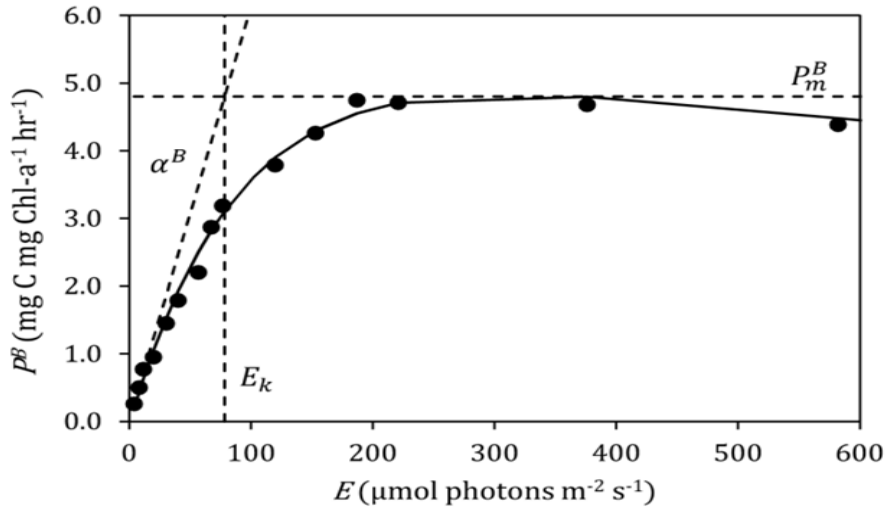

Fig. 3.5. Photosynthesis-irradiance (PE) curve showing the two biomass-normalized photo-physiological parameters, the initial slope (α^B) and the assimilation number (P^B_m) of the PE curve.

In the absence of photoinhibition (i.e., $\beta^B = 0$), the maximum photosynthetic rate is equal to P^B_s. Alternatively, a two-parameter hyperbolic tangent function (Fig. 3.5; Jassby and Platt, 1976) can be used in the absence of photoinhibition

$$P^B(E) = P_m^B tanh\left(\frac{\alpha^B E}{P_m^B}\right). \quad (3.11)$$

For both functions, the photoacclimation parameter (E_K in µmol photons m^{-2} s^{-1}) can be calculated as

$$E_K = \frac{P_m^B}{\alpha^B}. \quad (3.12)$$

The maximum quantum yield of carbon fixation (Φ_m in mol C mol quanta^{-1}), which gives the efficiency of the conversion of light energy into carbon fixation, is derived by dividing α^B by the spectrally weighted mean chlorophyll *a*-specific absorption coefficient of phytoplankton ($\bar{a}^*_{ph}$) (see the IOCCG Protocol Series (2018) for more details on $\bar{a}^*_{ph}$ measurements) and multiplying by a factor of 0.0231 to convert units. Different software packages can be used to perform the curve fit, including curve fitting modules in Python, R, and Matlab. The R package Phytotools (Silsbe and Kromkamp 2012; Silsbe and Malkin, 2015) is recommended to calculate PE parameters (available via www.rdocumentation.org/packages/phytotools/versions/1.0) (Fig. 3.6).

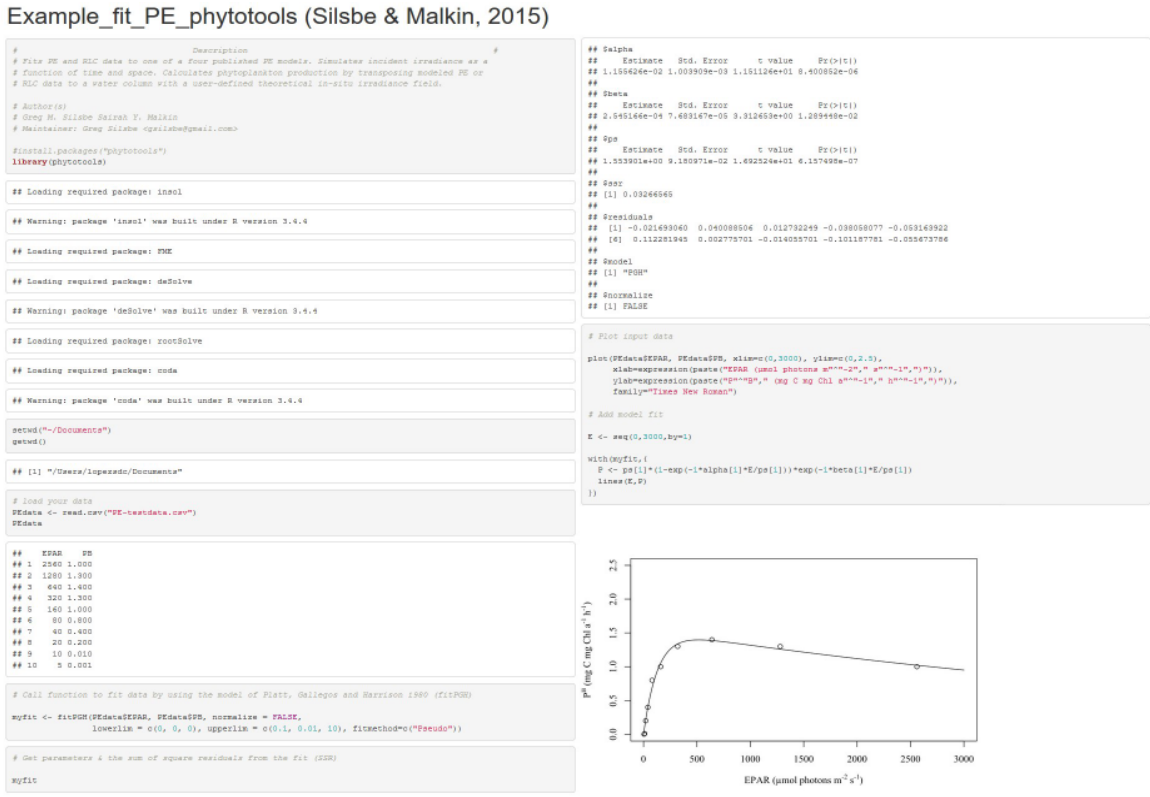

Fig. 3.6. Example of curve fitting of photosynthesis-irradiance measurements using the R package Phytotools (Silsbe and Malkin, 2015), available at https://www.rdocumentation.org/packages/phyto-tools/versions/1.0.

3.5.1.3. Calculation of daily depth-integrated primary production

Primary production measurements using the *in situ* and on-deck, simulated *in situ* incubation methods can be used to calculate daily depth-integrated primary production (P in mg C m^{-2} d^{-1}) by trapezoidal integration (Fig. 3.7) (JGOFS, 1996). To obtain total production within a depth interval, the measured primary production for each pair of depths is averaged and multiplied by the difference between the two depths. The measurement near the surface is assumed to be constant up to the surface (0 m), and primary production is integrated to the deepest incubation depth used (for example, 175 m in Fig. 3.7). The total production within each depth interval is then summed to obtain the integrated primary production for the entire depth range.

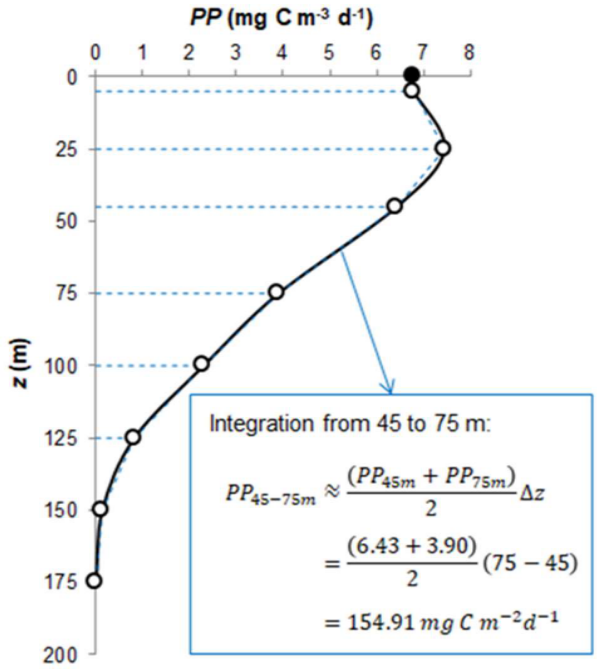

Fig. 3.7. Example of the trapezoidal integration for estimating daily depth-integrated primary production for *in situ* or on-deck, simulated *in situ* incubations. Primary production (PP) is estimated for each depth (z) interval, with an example given for 45–75 m, and then summed to obtain primary production for the entire depth range. PP0-175m for this example is 600 mg C m^{-2} d^{-1}. Data from the Hawaii-Ocean Time series (March 1, 2000: hahana.soest.hawaii.edu/hot/.

3.6. Additional Approaches

3.6.1. Dissolved organic carbon production

Dissolved organic carbon (DOC) production by phytoplankton can also be measured with ^{14}C. Mague et al. (1980) developed the original technique, which has been applied to many systems since (Karl et al., 1998; Marañón et al., 2004; Viviani et al., 2015; Balch et al., 2016). Essentially, a subsample of the filtrate from a normal ^{14}C-bicarbonate incubation is further filtered through a 0.2 µm polycarbonate filter, and the activity of the ^{14}C-DOC filtrate is measured following the removal of all remaining ^{14}C-dissolved inorganic carbon by acidification to a pH of 2–3 with 1 N H_2SO_4 and venting the samples for 24 hours (Mague et al., 1980). What remains is the non-acid-labile ^{14}C-DOC that passed a 0.2 µm filter. This activity is then quantified using liquid scintillation counting. Note, however, that the scintillation cocktail must remain functional with high efficiency following ~50% dilution with acidified seawater. One cocktail that works well for this application is EcoLume liquid scintillation cocktail (MP Biomedicals). Polycarbonate membrane filters (0.2 µm pore-size) are preferred for this technique due to the low levels of adsorption of DOC to these types of filters during the filtration process as opposed to GF/F that adsorb significant quantities of DOC, subsequently causing

underestimates in the DOC production (Maske and Garcia-Mendoza, 1994; Karl et al., 1998; Morán et al., 1999).

3.6.1.1. Cell-specific techniques

The most abundant marine organisms, especially in oceanic gyres and oligotrophic seas, are small phytoplankton cells (< 5 μm, but essentially < 2 μm): *Prochlorococcus*, *Synechoccocus*, pico- and nanophytoeukaryotes. These phytoplankton groups cannot be accurately separated using membrane filters of different porosities, because their respective size range overlaps. Therefore, the classical size fractionation approach does not allow resolving primary production by the dominant marine phytoplankters.

Chisholm et al. (1988) first estimated primary production by the newly discovered *Prochlorococcus* by "sorting the cells in question after incubation with ^{14}C-labeled bicarbonate, using the cell-sorting capability of the flow cytometer," while Balch and Kilpatrick (1993) used a flow cytometer to sort ^{14}C labeled coccolithophores to measure the rate of coccolith formation (calcification) and coccolith detachment. However, it was not until the pioneering work of Li (1994) that a new avenue opened to resolve primary production by the smallest but most abundant groups of marine phytoplankton. Li (1994) used a flow cytometer sorter (FACSort, Becton Dickinson) to separate groups of phytoplankton labeled with ^{14}C by fluorescence-activated cell sorting (FACS). Quantification of high ^{14}C specific activity per sample (1.85 or 3.7 MBq mL-^{1}; Table 3.4) enabled the author to detect radioactivity in sorted cells based on a signal of 50 disintegrations per minute (DPM) above background, which was defined as values of the *y*-intercept in regressions slope of DPM vs. number of sorted cells. The author concluded, "It is a significant step toward an important goal in biological oceanography: Namely, the recovery of the bulk properties of phytoplankton from the details of the properties of the constituents."

Table 3.4

Protocols used to measure cell-specific primary production by fluorescence-activated cell sorting (FACS): Seawater volume and final 14C activity per incubation, sample fixation with paraformaldehyde (PFA, final concentration), cell concentration before cell sorting, post-sorting filtration, and volume and concentration of hydrochloric acid (HCl) used to remove unincorporated ^{14}C after sorting. Pro = *Prochlorococcus*, Syn = *Synechococcus*, Peuk = picophytoeukaryotes, N.D. = Not Determined, N.A. = Not Available.

Reference	Sample volume, mL	Total activity, MBq mL^{-1}	Final PFA (%)	Cell concentration for Pro and Syn sorting	Cell concentration for Peuk sorting	Post-sorting filtration	HCl
Björkman et al. (2015)	15 or 40	0.137	0.24	None. Preserved 2 to 4 mL	N.D.	None	500-µL, 2 M
Duhamel et al. (2018)	60	0.122	0.5	30 to 50 mL concentrated onto 0.2-µm to 4 mL	N.D.	None	500-µL, 1 M
Duhamel et al. (2019)	70	0.243	2	20 mL concentrated onto 0.2-µm to 2 mL	~47 mL concentrated onto 0.8-µm to 4-mL	None	500-µL, 1 M
Grob et al. (2011)	120	0.123	1	N.D.	60 mL concentrated onto 0.8-µm to 1.8 mL	0.8-µm	N.A., 10%
Hartmann et al. (2014)	60	0.246	1	20 mL concentrated onto 0.6-µm	40 mL concentrated onto 0.8-µm	0.2-µm for Pro and Syn, 0.8-µm for Peuk	1 mL, 10%
Jardillier et al. (2010)	7.8	0.95	1	N.D.	None	0.2-µm	1 mL, 1%
Li 1994	20	1.85 or 3.7	None	None. 3 mL	None. 3 mL	Yes	N.A., concentrated
Rii et al. (2016a)	75	0.09	0.24	None. Preserved 5 mL	None. Preserved 5 mL	None	150-µL, 1 M
Rii et al. (2016b)	30	0.14	0.24	None. Preserved 5 mL	None. Preserved 5 mL	None	200-µL, 2 M

Despite the initially successful application of flow cytometric sorting of wild cells labeled with ^{14}C, little work has been done since Li (1994) to quantify cell-specific primary production using this technique. This is likely due to the requirement of combining high-end instrumentation (e.g., most benchtop flow cytometers cannot distinguish surface *Prochlorococcus* from the background noise) with the use of radioactive material. Additionally, the method requires specialized user training and the use of expensive isotopes, which are needed to incubate under a high ^{14}C concentration compared to incubations for bulk or size-fractionated measurements. Nonetheless, recent advances in flow cytometry sorting offer greater detection sensitivity, sort purity, and speed (e.g., the BD Influx). Since 2010, the improved instrumentation allowed for new studies to emerge (Jardillier et al., 2010; Grob et al., 2011; Hartmann et al., 2014; Björkman et al., 2015; Rii et al., 2016a; b; Duhamel et al., 2018, 2019), proving it to be a powerful approach to characterize the contribution of specific groups of phytoplankton to primary production and study their growth and metabolism in the wild.

3.6.1.2. Incubation and sample preparation for FACS

This method requires high ^{14}C concentrations, so the incubation volume should be kept as low as possible. However, the choice of volume must also be large enough to account for expected cell abundances and activities. For example, while Li (1994) used 1.85 or 3.7 MBq mL^{-1} per 20 mL incubation, ~3 mL was sufficient to sort enough cells to detect radioactivity above background. Recent studies typically added ^{14}C at a final concentration of ~0.12 to ~0.24 MBq mL^{-1} (Table 3.4). Using a ^{14}C concentration in the higher range is helpful in environments where growth rates are expected to be low because per-cell radioactivity is expected to be lower.

Another way to obtain radioactivity above background in the sorted cells is to sort a larger number of cells (Table 3.5). Authors typically sort at least three numbers of cells for a given phytoplankton group per sample (e.g., 50,000, 75,000, and 100,000 *Prochlorococcus*; 5,000, 10,000, and 15,000 *Synechococcus*; and 800, 1,600, and 3,200 picophytoeukaryotes) and use the regressions slope of DPM vs. number of sorted cells to calculate per cell radioactivity (DPM $cell^{1}$). It is recommended to select the highest sorting purity mode available on the flow cytometer (e.g., "1.0 drop single" on the BD Influx or "single-cell" sort mode on the BD FACSort). However, using stringent sorting parameters to maintain high sorting performance (Riddell et al., 2015) such as purity (defined as the quality of the sorted sample: Are we recovering the targeted cells only?) and recovery (defined as the number of particles sorted relative to the number of original particles to be sorted: Are we recovering the number of cells targeted?) slows sorting rates.

For instance, it is not unusual to spend at least 30 minutes processing a single sample acquired from an oligotrophic environment. Consequently, a sample volume larger than 3 mL is typically needed to sort at least three numbers of cells for several phytoplankton groups from one sample. This is especially critical for less abundant phytoplankton groups, such as pico- and nanophytoeukaryotes. Therefore, some authors incubate a larger seawater volume and then

Table 3.5

Number of cells sorted to measure cell-specific primary production by fluorescence-activated cell sorting. Pro = *Prochlorococcus*, Syn = *Synechococcus*, Peuk = picophytoeukaryotes, N.D. = Not Determined, N.A. = Not Available.

Reference	# sorted Pro	# sorted Syn	# sorted PPE
Björkman et al. (2015)	25,000 to 200,000	N.D.	N.D.
Duhamel et al. (2018)	10,000 to 300,000	10,000 to 300,000	N.D.
Duhamel et al. (2019)	25,000 to 100,000	5,000 to 15,000	400 to 3,200
Grob et al. (2011)	N.D.	N.D.	8,000 to 35,000
Hartmann et al. (2014)	unspecified	N.D.	N.D.
Jardillier et al. (2010)	3,000 to 18,000	1,000 to 6,000	200 to 1,000
Li (1994)	~50,000	~10,000	N.A.
Rii et al. (2016a)	30,000 to 200,000	2,000 to 75,000	2,700 to 20,000
Rii et al. (2016b)	25,000	100 to 10,000	360 to 35,000

concentrate the sample before cell sorting (Table 3.4). Cell concentration is typically carried out by gentle vacuum filtration (< 100 mm Hg) or using a syringe pump onto a polycarbonate membrane filter. Filtration is stopped before the filter goes dry, and the filter is transferred to a cryovial containing a volume of either pre-filtered (0.2 µm polycarbonate filter) seawater (Fawcett et al., 2011) or the corresponding radiolabeled sample (Duhamel et al., 2018, 2019). Cryovials are vortexed to dislodge cells from the filter before cryopreservation. It is recommended to fix the cells using an electron microscopy grade aqueous solution of paraformaldehyde (PFA) or glutaraldehyde (e.g., Electron Microscopy Sciences) before concentrating the samples to preserve cell integrity.

When sorting cells, it is essential to monitor the event rate, which is dependent on cell concentration, to ensure high sorts purity and recovery (Kormelink et al., 2016). The maximum event rate that a flow cytometer can handle while maintaining high purity and recovery depends on the instrument nozzle size, sheath fluid, and sample pressure. For example, using the Influx with a 70-µm nozzle, sheath fluid and sample pressure at 30 and 31 Psi, respectively, and the 1.0 drop single sorting mode, an event rate of < 5,000 per second works well to sort *Prochlorococcus* and *Synechococcus* (with the sheath fluid < 10 events per second) (Bock et al., 2018), although higher event rates can be used to sort less abundant groups, such as picophytoeukaryotes (Fawcett et al., 2011). While correctly setting up a flow cytometer for cell sorting is critical, a detailed description of the processes is beyond the scope of this protocol and can be found in the literature (Shapiro, 2003; Arnold and Lannigan, 2010; Cossarizza et al., 2017).

3.6.1.3. Post-sorting sample processing

Sorted cells are either collected onto a polycarbonate membrane through gentle filtration and transferred into a scintillation vial or collected directly into a scintillation vial (Table 3.4). If the sorted cells are collected in a scintillation vial, they will be diluted in sheath fluid, the volume of which varies according to the choice of nozzle size and the number of sorted cells. In any case, the maximum volume in the tube after sorting a population should be kept low, preferably less than a quarter of the tube volume to allow the addition of hydrochloric acid (HCl) and scintillation cocktail. Typically, 150 µL to 1 mL HCl 1 M or 2 M are added to the sorted cells to remove unincorporated ^{14}C (Table 3.4). It is recommended to leave the tubes uncapped under the fume hood for 24 to 48 hours before adding the scintillation cocktail.

Considering the relatively low activities expected per sorted cells, it is important to use a scintillation cocktail with very low background levels and high counting efficiency. Moreover, if the sorted cells are not filtered, they will be diluted in sheath fluid plus HCl. Therefore, selecting a scintillation cocktail with high water capacity is critical. One cocktail that works well for this application is Ultima Gold LLT (Perkin Elmer, up to 54% water capacity). Radio-assaying of samples should be carried out using an ultra-low-level liquid scintillation counter, such as the TriCarb 2910TR or 3110 TR (Perkin Elmer) or the 1220 Quantulus (Wallac).

3.6.1.4. Controls

Killed controls can be prepared to determine unspecific radioactivity. Typically, a sample is fixed with PFA at least 15 minutes before adding the radiotracer and then treated as the other samples. Radioactivity measured in the sorted population is then deduced from radioactivity in the respective sample (Duhamel et al., 2018, 2019). Some authors omit the preparation of killed

controls and instead sort calibration beads to estimate unspecific radioactivity. This is especially handy when sorting cells directly into a scintillation vial to account for radioactivity in the small volume of seawater associated with the sorted cells (Björkman et al., 2015). Fluorescent reference beads (typically 1-µm diameter, Fluoresbrite, Polyscience) are added to each sample before sorting. Two to four sort streams are collected simultaneously, directly into individual scintillation vials to separate the microbial cells selected and the fluorescent reference beads. The radioactivity measured in the sorted beads (DPM $bead^{-1}$) is then subtracted from the radioactivity obtained from the cells (DPM $cell^{-1}$). However, the radioactivity measured in sorted killed controls or beads is typically small and, by nature of measuring low DPM per cell or beads, generally leads to an overestimation of unspecific radioactivity. Considering that unincorporated ^{14}C-sodium bicarbonate can be removed by acidification, such control can be omitted for the measurement of cell-specific primary production by FACS (as opposed to the measurement of cell-specific uptake rates of other molecules). However, it is good practice to prepare such controls to verify that unspecific radioactivity is negligible.

A set of samples should be incubated in the dark to estimate the contribution of dark CO_2 fixation. Although the dark-fixation values are typically close to background, values should be subtracted from light-mediated fixation rates (Jardillier et al., 2010).

It is recommended to verify sort purity and mean recovery from sorts regularly. Sort purity is typically calculated as the proportion of sorted events falling into the prescribed gate as a percentage of the total event rate. In contrast, sort recovery is calculated as the number of target events recovered as a percentage of the number of positive sort decisions recorded by the acquisition software (Fawcett et al., 2011; Duhamel et al., 2018). For example, with their FACS configuration (Influx flow cytometer, 70 µm nozzle, sample and sheath pressure of 28.5 Psi and 27.5 Psi, respectively, event rate < 20,000 s^{-1}, coincident event detection of ±1 droplet), Fawcett et al. (2011) obtained sort purity > 95%, and 98.1±1.1% mean recovery from sorts. Alternatively, sorting recovery has been assessed by filtering subsamples (100, 150, 200, 300, 300, and 450 mL) onto 0.2 µm pore size polycarbonate filters, washed twice with ultrapure water and radio-assayed by liquid scintillation counting and comparing with the sum of activity in the sorted populations (Jardillier et al., 2010). Preparing spare samples to determine sort purity and recovery is recommended, but a mixture of calibration beads can also be used. For example, Zubkov and Tarran (2008) used a mixture of two 0.5 µm beads with different yellow-green fluorescence to sort one type of beads; the investigators determined that with their FACS configuration, the sorted material was 99.8% enriched with the target beads and the sorted bead recovery was 98.8±0.9% (n = 7).

3.6.1.5. Calculation

The activity per liter for different groups of phytoplankton can be calculated as the mean per cell radioactivity (DPM $cell^{-1}$) multiplied by the total number of cells in the respective group (cell L^{-1}) and converted to fixation rates as nmol C L^{-1} h^{-1} by their respective specific activities (DPM mol^{-1}) (Björkman et al., 2015). The average per cell rate can also be determined (amol C $cell^{-1}$ h^{-1}). Alternatively, the cell-specific fixation rate (nmol C $cell^{-1}$ h^{-1}) can be calculated by dividing the radioactivity per cell (DPM $cell^{-1}$) by the total (bulk > 0.2 µm) activity (DPM L^{-1}) measured in the same sample and then multiplied by the total fixation rate at ambient DIC concentration (nmol C L^{-1} h^{-1}) (Duhamel et al., 2018, 2019).

It is important to note that the sum of ^{14}C fixation measured per phytoplankton group separated by FACS does not necessarily equal the total amount of primary production by the entire phytoplankton community. Indeed, it would not account for phytoplankton larger than 2 to 5 µm. Moreover, as underlined by Li (1994), only small volumes are analyzed, which would likely not include a proportional representation of the less abundant cells: Typically, larger cells would be underrepresented. Considering the isometric scaling of phytoplankton photosynthesis with cell size, despite being less abundant, larger cells tend to contribute more substantially to primary production on a per cell level, even after normalizing to their biovolume (Duhamel et al., 2019).

3.6.1.6. Alternative using ^{13}C-sodium bicarbonate

In theory, a similar approach can be taken using incubation with ^{13}C-sodium bicarbonate. For example, to study group-specific marine nitrogen cycling, authors have incubated seawater with ^{15}N labeled compounds, separated phytoplankton groups by FACS and analyzed the isotopic composition by mass spectrometry (Casey et al., 2007; Fawcett et al., 2015). Because ^{13}C detection by mass spectrometry is much less sensitive than ^{14}C detection by liquid scintillation counting, a greater isotopic enrichment would be necessary, and a prohibitively large number of cells would need to be sorted (Berthelot et al., 2019). More recently, authors have taken advantage of the sensitivity of nano-scale secondary ion mass spectrometers (nanoSIMS) to measure cell-specific incorporation of stable-isotope-labeled substrates (for review, see Mayali 2020), including ^{13}C-sodium bicarbonate (Zimmermann et al., 2015; Berthelot et al., 2019). A major drawback remains the cost associated with the NanoSIMS instrument (~6 million USD; Mayali, 2020), which cascades into steep user fees, limiting the number of samples that can be processed within a reasonable budget.

3.6.1.7. Other methods to measure cell-specific primary production

Photopigment radiolabeling has been used to measure carbon-specific growth rates among phytoplankton taxa (Redalje and Laws, 1981; Goericke and Welschmeyer, 1993). The method relies on coupling the ^{14}C technique to the separation of diagnostic photopigments by High-Performance Liquid Chromatography (HPLC; for review, see Paerl, 2007). The method is tedious and may not be as specific as needed (e.g., co-elution of ^{14}C-labeled colorless compounds with photopigments; Pinckney et al., 1996). Despite advances in column and instrumentation technology and improvements in software applicable to data interpretation and synthesis (Pinckney et al., 2001), this technique has not been broadly applied.

Microautoradiography can also be used to analyze samples incubated with ^{l4}C to determine photosynthetic capabilities and rates at the single-cell level (Paerl, 2007). Microautoradiography has been used in microbial ecology for years (Brock and Brock, 1966). The technique relies on the detection and microscopic visualization of radiation-sensitive silver halide emulsions reacting with radioactive organisms that are subsequently processed by standard photographic techniques. Microautoradiography has been used to quantify primary productivity on a cell-specific basis (Watt, 1971; Stull et al., 1973; Douglas, 1984). Conveniently, this technique can be combined with fluorescent *in situ* hybridization (FISH) to identify target organisms to link the structural and functional aspects of microbes (Lee et al., 1999; Nielsen and Nielsen, 2005). However, microautoradiography is time-consuming, requires experience (e.g., detection of false positives),

is limited by microscopic resolution, and can be prone to interpretational differences among investigators (Paerl, 2007).

3.6.1.8. Phytoplankton calcification rates

Isotope tracers are useful to directly measure calcification rates in phytoplankton. Typically, these methods involve adding trace quantities of ^{14}C (as $NaH^{14}CO_3$) or ^{45}Ca (as $^{45}CaCl_2$) to bottle samples that are incubated, and the subsequent incorporation of the isotope into biogenic $CaCO_3$ is then quantified. This approach provides a measure of net calcification over the incubation period, resulting from biomineralization subtracting dissolution. Radioisotope methods are highly sensitive and, if used appropriately, can measure extremely low rates of calcification. This allows relatively short incubation times (hours to days), which is a distinct advantage when working at sea.

Coccolithophore calcification rates in cultures, mesocosms, and field populations have been reported using ^{14}C uptake methods in a multitude of studies (Paasche, 1963; Paasche and Brubak, 1994; Balch and Kilpatrick, 1996; Paasche et al., 1996; Balch et al., 2000, 2007; Buitenhuis et al., 2001; Delille et al., 2005; Poulton et al., 2007, 2013, 2014; Charalampopoulou et al., 2016; Daniels et al., 2016; Marañón et al., 2016; White et al., 2018) and less frequently using ^{45}Ca uptake (Van der Wal et al., 1987; van der Wal et al., 1994; Kayano and Shiraiwa, 2009; Fukuda et al., 2014). Generally, ^{14}C is easier to use than ^{45}Ca in coccolithophore calcification rate experiments because the unincorporated isotope Is more readily rinsed from samples than is ^{45}Ca. A commonly used (but older) technique is to filter two samples that have been incubated with ^{14}C, carefully rinse both filters, fume one filter with acid (as described in Section 3.4.1.1), and measure the ^{14}C activity of each filter. The fumed filter provides the photosynthetic fixation of ^{14}C, while the difference between the two filters is the acid-labile component of ^{14}C fixation, assumed to be calcification. However, the problem with this approach is that calcification is calculated as the small difference between two large numbers, each with significant error. Moreover, these errors compound.

3.6.1.9. Microdiffusion method

The microdiffusion method (Paasche and Brubak, 1994) is a highly-sensitive method that allows the direct measurement of ^{14}C fixation into both particulate organic carbon (POC) and coccolith particulate inorganic carbon (PIC; aka calcite) in the same sample. Briefly, this method entails filtration and rinsing of the incubated sample onto a 0.4 μm pore size polycarbonate filter. The filter is placed on the side of a scintillation vial, a small volume of 1% phosphoric acid is pipetted to the bottom of the vial, and a small Glass Fiber Filter (GF/F) containing a CO_2-absorbent (KOH or phenethylamine) is placed on the inside of the cap of the vial. The capped vial is placed on its side and rotated such that the acid covers the polycarbonate filter, dissolving any labeled particulate inorganic carbon, and the resultant $^{14}CO_2$ is absorbed onto the GF/F with CO_2 absorbent. The cap with the glass-fiber filter and CO_2 absorbent is transferred to a new scintillation vial, scintillation cocktail is added, and the activity in both filters is counted for ^{14}C activity. Routine checks with filter efficiency tests and total isotope recovery tests (Paasche and Brubak, 1994) are critical to ensure proper application of this method. Incubation times of coccolithophore calcification experiments that have used radioisotopes typically range from minutes to a day. Balch et al. (2000) adapted the method further for work on ships by fitting scintillation vials with rubber septa with hanging buckets. The filter with CO_2-absorbent is then

placed in the bucket, septum mounted on the scintillation vial where the cap would usually be, and the 1% phosphoric acid injected through the rubber septum, past the bucket, onto the sample filter on the bottom of the vial. The resultant ^{14}C-CO_2 emitted from the sample filter is then captured by the absorbent-soaked filter suspended in the bucket.

Blank filter runs are also suggested in calcification experiments using ^{14}C to correct for non-biological adsorption of radiolabel. Buffered-formalin-killed blanks are most commonly used. Paasche (1962) reported that such blanks corresponded to < 1% of the calcification in living cells under conditions of maximum photosynthesis. Further, Paasche (1963) found that the non-biological isotope exchange measured by buffered-formalin-killed samples accounted for 0.5–4% of the coccolith calcification at light-saturated photosynthesis, and this blank was consistently higher in artificial medium than in natural seawater. This finding supports the notion that the chemistry of $CaCO_3$ surfaces is complex, and that formalin may alter this chemistry, at least under some conditions. However, buffered-formalin-killed blanks provide reproducible estimates of passive exchange of ^{14}C onto calcite coccoliths. Under conditions of reduced light, low coccolithophore abundance, or other factors that can result in low values of coccolithophore calcification rates, care must be taken with processing both blank and treatment filters, owing to the reduced ratio of sample-to-background signals. Calcification rates determined with isotopes typically are recorded as mass or moles of C or $CaCO_3$ per cell or individual organism, per unit time (e.g., μmol C $cell^{-1}$ d^{-1}). Isotope-derived calcification rates also have been normalized to chlorophyll in coccolithophore cultures (Balch et al., 2007). The reader is also referred to Fabry and Balch (2010) for more details on measuring carbon fixation through calcification in marine phytoplankton.

3.7. Ancillary Measurements

For photosynthesis-irradiance (PE) incubations, the location (latitude, longitude, depth) and sampling time should be noted along with *in situ* and incubation temperatures. To calculate photosynthetic rates from PE measurements, knowledge of the following variables is required: Chlorophyll *a* concentration, dissolved inorganic carbon concentration (Section 3.3.1), Chlorophyll *a* specific absorption spectra, and the irradiance spectrum of the light source of the photosynthetron. Additional measurements, including PAR, salinity, micro- and macronutrient concentrations, and taxonomic composition and size structure of the phytoplankton community, could provide valuable information in comparing photosynthetic characteristics of marine phytoplankton across different natural populations.

3.8. SeaBASS Standardized Fields and Units

Most online repositories require the use of standardized field names and associated units for submitting data. The NASA Ocean Biology Processing Group (OBPG) maintains a publicly shared archive of *in situ* oceanographic and atmospheric data in the SeaWiFS Bio-optical Archive and Storage System (SeaBASS). Naming conventions for carbon-based primary production for this repository are available in Table 3.6. Naming conventions for other variables can be found at https://seabass.gsfc.nasa.gov/wiki/stdfields. Note that different field names and associated units may be used as standard in other databases.

Table 3.6

Standardized field names and associated units for carbon-based primary production data currently available in the SeaWiFS Bio-optical Archive and Storage System (SeaBASS). The field names are not case sensitive.

Field name	Units	Description
GPP	mg/m^3/d	Gross Primary Productivity
NPP	mg/m^3/d	Net Primary Productivity
PP	mgC/mgchla/hr	Primary productivity
rate_13C_uptake_bottle	mol/L/d, mol_L^-1_d^-1	Primary productivity determined using ^{13}C. This field should include the experiment time (incubation time) "_###hr".
rate_14C_uptake_bottle	mol/L/d, mol_L^-1_d^-1	Primary productivity determined using ^{14}C. This field should include the experiment time (incubation time) "_###hr".

3.9. References

Anning, T., MacIntyre, H. L., Pratt, S. M., Sammes, P. J., Gibb, S., & Geider, R. J. (2000). Photoacclimation in the marine diatom Skeletonema costatum. *Limnology and Oceanography*, *45*(8), 1807-1817. https://doi.org/10.4319/lo.2000.45.8.1807

Antoine, D., & Morel, A. (1996). Oceanic primary production: 1. Adaptation of a spectral light-photosynthesis model in view of application to satellite chlorophyll observations. *Global biogeochemical cycles*, *10*(1), 43–55. https://doi.org/10.1029/95GB02831

Arnold, L. W., & Lannigan, J. (2010). Practical issues in high-speed cell sorting. *Current protocols in cytometry*, *51*(1), 1–24. https://doi.org/10.1002/0471142956.cy0124s51

Marcel, B., Morel, A., & Gagnon, R. (1994). An incubator designed for extensive and sensitive measurements of phytoplankton photosynthetic parameters. *Limnology and Oceanography*, *39*(3), 694–702. https://doi.org/10.4319/lo.1994.39.3.0694

Babin, M., Therriault, J. C., Legendre, L., Nieke, B., Reuter, R., & Condal, A. (1995). Relationship between the maximum quantum yield of carbon fixation and the minimum quantum yield of chlorophyll *a in vivo* fluorescence in the Gulf of St. Lawrence. *Limnology and Oceanography*, *40*(5), 956–968. https://doi.org/10.4319/lo.1995.40.5.0956

Balch, W. M., Kilpatrick, K., Holligan, P. M., & Cucci, T. (1993). COCCOLITH PRODUCTION AND DETACHMENT BY EMILIANIA HUXLEYI (PRYMNESIOPHYCEAE) 1. *Journal of Phycology*, *29*(5), 566-575. https://doi.org/10.1111/j.0022-3646.1993.00566.x

Balch, W., Drapeau, D., Bowler, B., & Booth, E. (2007). Prediction of pelagic calcification rates using satellite measurements. *Deep Sea Research Part II: Topical Studies in Oceanography*, *54*(5–7), 478–495. https://doi.org/10.1016/j.dsr2.2006.12.006

Balch, W. M., Drapeau, D. T., & Fritz, J. J. (2000). Monsoonal forcing of calcification in the Arabian Sea. *Deep Sea Research Part II: Topical Studies in Oceanography*, *47*(7–8), 1301–1337. https://doi.org/10.1016/S0967-0645(99)00145-9

Balch, W., Huntington, T., Aiken, G., Drapeau, D., Bowler, B., Lubelczyk, L., & Butler, K. (2016). Toward a quantitative and empirical dissolved organic carbon budget for the Gulf of Maine, a semi-enclosed shelf sea. *Global Biogeochemical Cycles*, *30*(2), 268–292. https://doi.org/10.1002/2015GB005332

Balch, W. M., & Kilpatrick, K. (1996). Calcification rates in the equatorial Pacific along 140 W. *Deep Sea Research Part II: Topical Studies in Oceanography*, *43*(4–6), 971–993. https://doi.org/10.1016/0967-0645(96)00032-X

Banse, K. (1993). On the dark bottle in the 14C method for measuring marine phytoplankton production. In *ICES Mar. Sci. Symp*. *197*, 132–140.

Barber, R. T., & Hilting, A. K. (2002). History of the study of plankton productivity. *Phytoplankton Productivity: Carbon assimilation in marine and freshwater ecosystems*, 16–43.

Becker, S., Aoyama, M., Woodward, E. M. S., Bakker, K., Coverly, S., Mahaffey, C., & Tanhua, T. (2020). GO-SHIP repeat hydrography nutrient manual: the precise and accurate determination of dissolved inorganic nutrients in seawater, using continuous flow analysis methods. *Frontiers in Marine Science*, *7*, 581790. https://doi.org/10.3389/fmars.2020.581790

Behrenfeld, M. J., Halsey, K. H., & Milligan, A. J. (2008). Evolved physiological responses of phytoplankton to their integrated growth environment. *Philosophical Transactions of the Royal Society B: Biological Sciences*, *363*(1504), 2687–2703. https://10.1098/rstb.2008.0019

Berthelot, H., Duhamel, S., L'helguen, S., Maguer, J. F., Wang, S., Cetinić, I., & Cassar, N. (2019). NanoSIMS single cell analyses reveal the contrasting nitrogen sources for small phytoplankton. *The ISME Journal*, *13*(3), 651–662. https://doi.org/10.1038/s41396-018-0285-8

Björkman, K. M., Church, M. J., Doggett, J. K., & Karl, D. M. (2015). Differential assimilation of inorganic carbon and leucine by Prochlorococcus in the oligotrophic North Pacific subtropical gyre. *Frontiers in Microbiology*, *6*, 1401. https://doi.org/10.3389/fmicb.2015.01401

Bock, N., Van Wambeke, F., Dion, M., & Duhamel, S. (2018). Microbial community structure in the western tropical South Pacific. *Biogeosciences*, 15(12), 3909‑3925. https://doi.org/10.5194/bg-15-3909-2018

Bouman, H. A., Platt, T., Doblin, M., Figueiras, F. G., Gudmudsson, K., Gudfinnsson, H. G., Huang, B., Hickman, A., Hiscock, M., Jackson, T., Lutz, V. A., Mélin, F., Rey, F., Pepin, P., Segura, V., Tilstone, G. H., van Dongen-Vogels, V., & Sathyendranath, S. (2017). Photosynthesis-irradiance parameters of marine phytoplankton: Synthesis of a global data set [Preprint]. *Oceanography – Biological*. https://doi.org/10.5194/essd-2017-40

Brenna, J. T., Corso, T. N., Tobias, H. J., & Caimi, R. J. (1997). High-precision continuous-flow isotope ratio mass spectrometry. *Mass Spectrometry Reviews*, *16*(5), 227–258. https://doi.org/10.1002/(SICI)1098-2787(1997)16:5<227::AID-MAS1>3.0.CO;2-J

Brock, T. D., & Brock, M. L. (1966). Autoradiography as a tool in microbial ecology. *Nature*, *209*(5024), 734–736. https://doi.org/10.1038/209734a0

Brodie, C. R., Heaton, T. H. E., Leng, M. J., Kendrick, C. P., Casford, J. S. L., & Lloyd, J. M. (2011). Evidence for bias in measured δ15N values of terrestrial and aquatic organic materials due to pre-analysis acid treatment methods: Bias in δ15N values of terrestrial and aquatic organic materials. *Rapid Communications in Mass Spectrometry*, *25*(8), 1089–1099. https://doi.org/10.1002/rcm.4970

Brodie, C. R., Leng, M. J., Casford, J. S., Kendrick, C. P., Lloyd, J. M., Yongqiang, Z., & Bird, M. I. (2011). Evidence for bias in C and N concentrations and δ13C composition of terrestrial and aquatic organic materials due to pre-analysis acid preparation methods. *Chemical Geology*, *282*(3–4), 67–83. https://doi.org/10.1016/j.chemgeo.2011.01.007

Buitenhuis, E. T., van der Wal, P., & de Baar, H. J. W. (2001). Blooms of *Emiliania huxleyi* are sinks of atmospheric carbon dioxide: A field and mesocosm study derived simulation. *Global Biogeochemical Cycles*, *15*(3), 577–587. https://doi.org/10.1029/2000GB001292

Casey, J. R., Lomas, M. W., Mandecki, J., & Walker, D. E. (2007). *Prochlorococcus* contributes to new production in the sargasso sea deep chlorophyll maximum. *Geophysical Research Letters*, *34*(10), L10604. https://doi.org/10.1029/2006GL028725

Charalampopoulou, A., Poulton, A. J., Bakker, D. C. E., Lucas, M. I., Stinchcombe, M. C., & Tyrrell, T. (2016). *Environmental drivers of coccolithophore abundance and calcification across Drake Passage (Southern Ocean)* [Preprint]. Biogeochemistry: Open Ocean. https://doi.org/10.5194/bg-2016-139

Chisholm, S. W., Olson, R. J., Zettler, E. R., Goericke, R., Waterbury, J. B., & Welschmeyer, N. A. (1988). A novel free-living prochlorophyte abundant in the oceanic euphotic zone. *Nature*, *334*(6180), 340–343. https://doi.org/10.1038/334340a0

Close, H. G. (2019). Compound-specific isotope geochemistry in the ocean. *Annual Review of Marine Science*, *11*(1), 27–56. https://doi.org/10.1146/annurev-marine-121916-063634

Collos, Y., Jauzein, C., & Hatey, E. (2014). Particulate carbon and nitrogen determinations in tracer studies: The neglected variables. *Applied Radiation and Isotopes*, *94*, 14–22. https://doi.org/10.1016/j.apradiso.2014.06.015

Collos, Y., & Slawyk, G. (1985). On the compatibility of carbon uptake rates calculated from stable and radioactive isotope data: implications for the design of experimental protocols in aquatic primary productivity. *Journal of plankton research*, *7*(5), 595–603. https://doi.org/10.1093/plankt/7.5.595

Cossarizza, A., Chang, H., Radbruch, A., Abrignani, S., Addo, R., Akdis, M., Andrä, I., Andreata, F., Annunziato, F., Arranz, E., Bacher, P., Bari, S., Barnaba, V., Barros-Martins, J., Baumjohann, D., Beccaria, C. G., Bernardo, D., Boardman, D. A., Borger, J., … Yang, J. (2021). Guidelines for the use of flow cytometry and cell sorting in immunological studies (Third edition). *European Journal of Immunology*, *51*(12), 2708–3145. https://doi.org/10.1002/eji.202170126

Cullen, J. J. (2001). Primary production methods. In *Encyclopedia of Ocean Sciences* (pp. 2277–2284). Elsevier. https://doi.org/10.1006/rwos.2001.0203

Cullen, J. J., Neale, P. J., & Lesser, M. P. (1992). Biological weighting function for the inhibition of phytoplankton photosynthesis by ultraviolet radiation. *Science*, *258*(5082), 646–650. https://doi.org/10.1126/science.258.5082.646

Cullen, J. J., Davis, R. F., & Huot, Y. (2012). Spectral model of depth-integrated water column photosynthesis and its inhibition by ultraviolet radiation: WATER COLUMN PHOTOSYNTHESIS. *Global Biogeochemical Cycles*, *26*(1), n/a-n/a. https://doi.org/10.1029/2010GB003914

Cutter, G., Andersson, P., Codispoti, L., Croot, P., Francois, R., Lohan, M. C., ... & Rutgers vd Loeff, M. (2010). Sampling and sample-handling protocols for GEOTRACES cruises.

Daniels, C., Poulton, A., Young, J., Esposito, M., Humphreys, M., Ribas-Ribas, M., Tynan, E., & Tyrrell, T. (2016). Species-specific calcite production reveals Coccolithus pelagicus as the key calcifier in the Arctic Ocean. *Marine Ecology Progress Series*, *555*, 29–47. https://doi.org/10.3354/meps11820

Delille, B., Harlay, J., Zondervan, I., Jacquet, S., Chou, L., Wollast, R., Bellerby, R. G. J., Frankignoulle, M., Borges, A. V., Riebesell, U., & Gattuso, J.-P. (2005). Response of primary production and calcification to changes of p CO 2 during experimental blooms of the coccolithophorid Emiliania huxleyi. Global Biogeochemical Cycles, 19(2), n/a-n/a. https://doi.org/10.1029/2004GB00231

Dickson, A. G., Sabine, C. L., & Christian, J. R. (2007). Guide to best practices for ocean CO2 measurements. North Pacific Marine Science Organization.

Douglas, D. (1984). Microautoradiography-based enumeration of photosynthetic picoplankton with estimates of carbon-specific growth rates. *Marine Ecology Progress Series*, *14*, 223–228. https://doi.org/10.3354/meps014223

Dubinsky, Z., Falkowski, P. G., & Wyman, K. (1986). Light harvesting and utilization by phytoplankton. *Plant and Cell Physiology*, *27*(7), 1335–1349. https://doi.org/10.1093/oxfordjournals.pcp.a077232

Duhamel, S., Zeman, F., & Moutin, T. (2006). A dual-labeling method for the simultaneous measurement of dissolved inorganic carbon and phosphate uptake by marine planktonic species: Simultaneous DIC and DIP uptake measurement. *Limnology and Oceanography: Methods*, *4*(11), 416–425. https://doi.org/10.4319/lom.2006.4.416

Duhamel, S., Moutin, T., Van Wambeke, F., Van Mooy, B., Rimmelin, P., Raimbault, P., & Claustre, H. (2007). Growth and specific P-uptake rates of bacterial and phytoplanktonic communities in the Southeast Pacific (BIOSOPE cruise). *Biogeosciences*, *4*(6), 941–956. https://doi.org/10.5194/bg-4-941-2007

Duhamel, S., Van Wambeke, F., Lefevre, D., Benavides, M., & Bonnet, S. (2018). Mixotrophic metabolism by natural communities of unicellular cyanobacteria in the western tropical South Pacific Ocean. *Environmental Microbiology*, *20*(8), 2743–2756. https://doi.org/10.1111/1462-2920.14111

Duhamel, S., Kim, E., Sprung, B., & Anderson, O. R. (2019). Small pigmented eukaryotes play a major role in carbon cycling in the P-depleted western subtropical North Atlantic, which may be supported by mixotrophy. *Limnology and Oceanography*, *64*(6), 2424–2440. https://doi.org/10.1002/lno.11193

Fabry, V. J., & Balch, W. M. (2010). Direct measurements of calcification rates in planktonic organisms. *Guide to best practices for ocean acidification research and data reporting.* Luxembourg, 201–212.

Falkowski, P. G. (1981). Light-shade adaptation and assimilation numbers. Journal of Plankton Research, 3(2), 203–216. https://doi.org/10.1093/plankt/3.2.203

Fawcett, S. E., Lomas, M. W., Casey, J. R., Ward, B. B., & Sigman, D. M. (2011). Assimilation of upwelled nitrate by small eukaryotes in the Sargasso Sea. Nature Geoscience, *4*(10), 717–722. https://doi.org/10.1038/ngeo1265

Fawcett, S. E., Ward, B. B., Lomas, M. W., & Sigman, D. M. (2015). Vertical decoupling of nitrate assimilation and nitrification in the Sargasso Sea. *Deep Sea Research Part I: Oceanographic Research Papers*, *103*, 64–72. https://doi.org/10.1016/j.dsr.2015.05.004

Fitzwater, S. E., Knauer, G. A., & Martin, J. H. (1982). Metal contamination and its effect on primary production measurements1: Metal effects and productivity. *Limnology and Oceanography*, *27*(3), 544–551. https://doi.org/10.4319/lo.1982.27.3.0544

Fry, B. (1996). 13C/12C fractionation by marine diatoms. *Marine Ecology Progress Series*, *134*, 283–294. https://doi.org/10.3354/meps134283

Fukuda, S., Suzuki, Y., & Shiraiwa, Y. (2014). Difference in physiological responses of growth, photosynthesis and calcification of the coccolithophore Emiliania huxleyi to acidification by acid and CO2 enrichment. *Photosynthesis Research*, *121*(2–3), 299–309. https://doi.org/10.1007/s11120-014-9976-9

Goericke, R., & Welschmeyer, N. A. (1993). The chlorophyll-labeling method: Measuring specific rates of chlorophyll a synthesis in cultures and in the open ocean. *Limnology and Oceanography*, *38*(1), 80–95. https://doi.org/10.4319/lo.1993.38.1.0080

Grob, C., Hartmann, M., Zubkov, M. V., & Scanlan, D. J. (2011). Invariable biomass-specific primary production of taxonomically discrete picoeukaryote groups across the Atlantic Ocean: Invariable primary production of picoeukaryotes. *Environmental Microbiology*, *13*(12), 3266–3274. https://doi.org/10.1111/j.1462-2920.2011.02586.x

Hama, T. A. K. E. O., Hama, J. U. N. K. O., & Handa, N. O. B. U. H. I. K. O. (1993). 13C tracer methodology in microbial ecology with special reference to primary production.

Hama, T., Miyazaki, T., Ogawa, Y., Iwakuma, T., Takahashi, M., Otsuki, A., & Ichimura, S. (1983). Measurement of photosynthetic production of a marine phytoplankton population using a stable 13C isotope. *Marine Biology*, *73*(1), 31–36.

Hartmann, M., Gomez-Pereira, P., Grob, C., Ostrowski, M., Scanlan, D. J., & Zubkov, M. V. (2014). Efficient co2 fixation by surface prochlorococcus in the Atlantic Ocean. *The ISME Journal*, *8*(11), 2280–2289. https://doi.org/10.1038/ismej.2014.56

IOCCG Protocol Series. 2018. Inherent optical property measurements and protocols: absorption coefficient, In A.R. Neeley and A. Mannino [eds.], IOCCG Ocean optics and biogeochemistry protocols for satellite ocean colour sensor validation. IOCCG.

IOCCG Protocol Series. 2021. Particulate Organic Matter Sampling and Measurement Protocols: Consensus Towards Future Ocean Color Missions. J.E. Chaves, I. Cetinić, G. Dall'Olmo, M. Estapa, W. Gardner, M. Goñi, J. R. Graff, P. Hernes, P. J. Lam, Z. Liu, M. W. Lomas, A. Mannino, M. G. Novak, R. Turnewitsch, P. J. Werdell, T. K. Westberry. IOCCG Ocean Optics and Biogeochemistry Protocols for Satellite Ocean Colour Sensor Validation, Volume 6, In review, IOCCG, Dartmouth, NS, Canada.

Isada, T., Iida, T., Liu, H., Saitoh, S.-I., Nishioka, J., Nakatsuka, T., & Suzuki, K. (2013). Influence of amur river discharge on phytoplankton photophysiology in the Sea of Okhotsk during late summer: Algal photophysiology in the Okhotsk Sea. *Journal of Geophysical Research: Oceans*, *118*(4), 1995–2013. https://doi.org/10.1002/jgrc.20159

Jardillier, L., Zubkov, M. V., Pearman, J., & Scanlan, D. J. (2010). Significant CO2 fixation by small prymnesiophytes in the subtropical and tropical northeast Atlantic Ocean. *The ISME Journal*, *4*(9), 1180–1192. https://doi.org/10.1038/ismej.2010.36

Jassby, A. D., & Platt, T. (1976). Mathematical formulation of the relationship between photosynthesis and light for phytoplankton: Photosynthesis-light equation. *Limnology and Oceanography*, *21*(4), 540–547. https://doi.org/10.4319/lo.1976.21.4.0540

JGOFS. 1992. Joint Global Ocean Flux Study: Implementation Plan. IGBP Report No 23, IGBP Secretariat, Stockholm

JGOFS. 1996. Protocols for the Joint Global Ocean Flux Study (JGOFS) core measurements, p. 170. In A. Knap [ed.], Report No. 19 of the Joint Global Ocean Flux Study.

Karl, D. M., Hebel, D. V., Björkman, K., & Letelier, R. M. (1998). The role of dissolved organic matter release in the productivity of the oligotrophic North Pacific Ocean. *Limnology and Oceanography*, *43*(6), 1270–1286. https://doi.org/10.4319/lo.1998.43.6.1270

Kayano, K., & Shiraiwa, Y. (2009). Physiological regulation of coccolith polysaccharide production by phosphate availability in the coccolithophorid Emiliania huxleyi. *Plant and cell physiology*, *50*(8), 1522–1531. https://doi.org/10.1093/pcp/pcp097

Koblentz-Mishke, O. J. (1970). Plankton primary production of the world ocean. *Scientific exploration of the South Pacific*, 183–193.

Groot Kormelink, T., Arkesteijn, G. J. A., Nauwelaers, F. A., Van Den Engh, G., Nolte-'t Hoen, E. N., & Wauben, M. H. (2016). Prerequisites for the analysis and sorting of extracellular vesicle subpopulations by high-resolution flow cytometry. *Cytometry A*, *89*(2), 135–147. https://doi.org/10.1002/cyto.a.22644

Kulk, G., Platt, T., Dingle, J., Jackson, T., Jönsson, B., Bouman, H., Babin, M., Brewin, R., Doblin, M., Estrada, M., Figueiras, F., Furuya, K., González-Benítez, N., Gudfinnsson, H., Gudmundsson, K., Huang, B., Isada, T., Kovač, Ž., Lutz, V., … Sathyendranath, S. (2020). Primary production, an index of climate change in the ocean: Satellite-based estimates over two decades. *Remote Sensing*, *12*(5), 826. https://doi.org/10.3390/rs12050826

Kyewalyanga, M. N., Platt, T., & Sathyendranath, S. (1997). Estimation of the photosynthetic action spectrum: implication for primary production models. *Marine Ecology Progress Series*, *146*, 207–223. https://doi.org/10.3354/meps146207

Lee, N., Nielsen, P. H., Andreasen, K. H., Juretschko, S., Nielsen, J. L., Schleifer, K. H., & Wagner, M. (1999). Combination of fluorescent in situ hybridization and microautoradiography—a new tool for structure-function analyses in microbial ecology. *Applied and environmental microbiology*, *65*(3), 1289–1297. https://doi.org/10.1128/AEM.65.3.1289-1297.1999

Lewis, M. R., Warnock, R. E., & Platt, T. (1985). Absorption and photosynthetic action spectra for natural phytoplankton populations: Implications for production in the open ocean1. *Limnology and Oceanography*, *30*(4), 794–806. https://doi.org/10.4319/lo.1985.30.4.0794

Lewis, M., & Smith, J. (1983). A small volume, short-incubation-time method for measurement of photosynthesis as a function of incident irradiance. *Marine Ecology Progress Series*, *13*, 99–102. https://doi.org/10.3354/meps013099

Li, W. K. W. (1994). Primary production of prochlorophytes, cyanobacteria, and eucaryotic ultraphytoplankton: Measurements from flow cytometric sorting. *Limnology and Oceanography*, *39*(1), 169–175. https://doi.org/10.4319/lo.1994.39.1.0169

López-Sandoval, D. C., Delgado-Huertas, A., & Agustí, S. (2018). The 13C method as a robust alternative to 14C-based measurements of primary productivity in the Mediterranean Sea. *Journal of Plankton Research*, *40*(5), 544–554. https://doi.org/10.1093/plankt/fby031

López-Sandoval, D. C., Delgado-Huertas, A., Carrillo-de-Albornoz, P., Duarte, C. M., & Agustí, S. (2019). Use of cavity ring-down spectrometry to quantify 13 C-primary productivity in oligotrophic waters. *Limnology and Oceanography: Methods*, *17*(2), 137–144. https://doi.org/10.1002/lom3.10305

Magalhaes, C. (2008). Dissolved organic carbon and nitrogen dynamics in the Douro River estuary, Portugal. *Ciencias Marinas*, *34*(3), 271–282. https://doi.org/10.7773/cm.v34i3.1393

Mague, T. H., Friberg, E., Hughes, D. J., & Morris, I. (1980). Extracellular release of carbon by marine phytoplankton; a physiological approach1. *Limnology and Oceanography*, *25*(2), 262–279. https://doi.org/10.4319/lo.1980.25.2.0262

Marañón, E., Balch, W. M., Cermeño, P., González, N., Sobrino, C., Fernández, A., Huete-Ortega, M., López-Sandoval, D. C., Delgado, M., Estrada, M., Álvarez, M., Fernández-Guallart, E., & Pelejero, C. (2016). Coccolithophore calcification is independent of carbonate chemistry in the tropical ocean. *Limnology and Oceanography*, *61*(4), 1345–1357. https://doi.org/10.1002/lno.10295

Marañón, E., Cermeño, P., Fernández, E., Rodríguez, J., & Zabala, L. (2004). Significance and mechanisms of photosynthetic production of dissolved organic carbon in a coastal eutrophic ecosystem. *Limnology and Oceanography*, *49*(5), 1652–1666. https://doi.org/10.4319/lo.2004.49.5.1652

Marañón, E., Cermeño, P., & Pérez, V. (2005). Continuity in the photosynthetic production of dissolved organic carbon from eutrophic to oligotrophic waters. *Marine Ecology Progress Series*, *299*, 7–17. https://doi.org/10.3354/meps299007

Marra, J. 2002. Approaches to the measurement of plankton production, p. 78–108. In P.J. L. B. Williams, D.N. Thomas, and C.S. Reynolds [eds.], Phytoplankton Productivity: Carbon Assimilation in Marine and Freshwater Ecosystems. Blackwell Science Ltd. https://doi.org/10.1086/382430

Marra, J. (2009). Net and gross productivity: weighing in with 14C. *Aquatic Microbial Ecology*, *56*, 123–131. https://doi.org/10.3354/ame01306

Marra, J., & Barber, R. T. (2004). Phytoplankton and heterotrophic respiration in the surface layer of the ocean. *Geophysical Research Letters*, *31*(9), n/a-n/a. https://doi.org/10.1029/2004gl019664

Maske, H., & Garcia-Mendoza, E. (1994). Adsorption of Dissolved Organic Matter to the Inorganic Filter Substrate and Its Implications for ^{14}C Uptake Measurements. *Applied and Environmental Microbiology*, *60*(10), 3887–3889. https://doi.org/10.1128/aem.60.10.3887-3889.1994

Matsumoto, K., Fujiki, T., Honda, M. C., Wakita, M., Kawakami, H., Kitamura, M., & Saino, T. (2012). Inhibition of primary production by nitrile rubber O-rings in Niskin sampler. *JAMSTEC Report of Research and Development*, *14*, 17–25. https://doi.org/10.5918/jamstecr.14.17

Mayali, X. (2020). NanoSIMS: Microscale Quantification of Biogeochemical Activity with Large-Scale Impacts. *Annual Review of Marine Science*, *12*(1), 449–467. https://doi.org/10.1146/annurev-marine-010419-010714

Mobley, C. D., & Mobley, C. D. (1994). *Light and water: radiative transfer in natural waters*. Academic Press.

Morán, X., Gasol, J., Arin, L., & Estrada, M. (1999). A comparison between glass fiber and membrane filters for the estimation of phytoplankton POC and DOC production. *Marine Ecology Progress Series*, *187*, 31–41. https://doi.org/10.3354/meps187031

Mousseau, L., Dauchez, S., Legendre, L., & Fortier, L. (1995). Photosynthetic carbon uptake by marine phytoplankton: comparison of the stable (13C) and radioactive (14C) isotope methods. *Journal of Plankton Research*, *17*(7), 1449–1460. https://doi.org/10.1093/plankt/17.7.1449

Moutin, T., Raimbault, P., & Poggiale, J. C. (1999). Production primaire dans les eaux de surface de la Mediterranee occidentale. Calcul de la production journaliere. *Comptes Rendus de l'Académie des Sciences-Series III-Sciences de la Vie*, *322*(8), 651–655.

Neale, P. J., Pritchard, A. L., & Ihnacik, R. (2014). UV effects on the primary productivity of picophytoplankton: biological weighting functions and exposure response curves of *Synechococcus*. *Biogeosciences*, *11*(10), 2883–2895. https://doi.org/10.5194/bg-11-2883-2014

Nielsen, J., & Halkjær Nielsen, P. (2005). Advances in Microscopy: Microautoradiography of Single Cells. *Methods in Enzymology*, 237–256. https://doi.org/10.1016/s0076-6879(05)97014-6

Paasche, E. (1962). Coccolith Formation. *Nature*, *193*(4820), 1094–1095. https://doi.org/10.1038/1931094b0

Paasche, E. (1963). The adaptation of the carbon-14 method for the measurement of coccolith production in coccolithus huxleyi. *Physiologia Plantarum*, *16*(1), 186–200. https://doi.org/10.1111/j.1399-3054.1963.tb08302.x

Paasche, E., & Brubak, S. (1994). Enhanced calcification in the coccolithophorid Emiliania huxleyi (Haptophyceae) under phosphorus limitation. *Phycologia*, *33*(5), 324–330. https://doi.org/10.2216/i0031-8884-33-5-324.1

Paasche, E., Brubak, S., Skattebøl, S., Young, J. R., & Green, J. C. (1996). Growth and calcification in the coccolithophorid Emiliania huxleyi (Haptophyceae) at low salinities. *Phycologia*, *35*(5), 394–403. https://doi.org/10.2216/i0031-8884-35-5-394.1

Paerl, H. (2007). Primary Productivity and Producers, In C. Hurst, R. Crawford, J. Garland, M. Lipson, A. Mills, and L. Stezenbach [eds.], Manual of Environmental Microbiology. ASM Press.

Peterson, B. J. (1980). Aquatic primary productivity and the 14C-CO2 method: a history of the productivity problem., p. 359–386. In R.F. Johnston, P.W. Frank, and C.D. Michener [eds.], Annual review of ecology and systematics.

Pinckney, J. L., Richardson, T. L., Millie, D. F., & Paerl, H. W. (2001). Application of photopigment biomarkers for quantifying microalgal community composition and in situ growth rates. *Organic Geochemistry*, *32*(4), 585–595. https://doi.org/10.1016/s0146-6380(00)00196-0

Platt, T. G. C. L., Gallegos, C. L., & Harrison, W. G. (1981). Photoinhibition of photosynthesis in natural assemblages of marine phytoplankton. *Journal of Marine Research*, 38, 103–111.

Platt, T., & Jassby, A. D. (1976). The relationship between photosynthesis and light for natural assemblages of coastal marine phytoplankton [1]. *Journal of Phycology*, *12*(4), 421–430. https://doi.org/10.1111/j.1529-8817.1976.tb02866.x

Popp, B. N., Laws, E. A., Bidigare, R. R., Dore, J. E., Hanson, K. L., & Wakeham, S. G. (1998). Effect of phytoplankton cell geometry on carbon isotopic fractionation. *Geochimica et Cosmochimica Acta*, *62*(1), 69–77. https://doi.org/10.1016/S0016-7037(97)00333-5

Poulton, A. J., Adey, T. R., Balch, W. M., & Holligan, P. M. (2007). Relating coccolithophore calcification rates to phytoplankton community dynamics: Regional differences and implications for carbon export. *Deep Sea Research Part II: Topical Studies in Oceanography*, *54*(5–7), 538–557. https://doi.org/10.1016/j.dsr2.2006.12.003

Poulton, A. J., Painter, S. C., Young, J. R., Bates, N. R., Bowler, B., Drapeau, D., Lyczsckowski, E., & Balch, W. M. (2013). The 2008 *Emiliania huxleyi* bloom along the Patagonian Shelf: Ecology, biogeochemistry, and cellular calcification: 2008 PATAGONIAN SHELF *EMILIANIA HUXLEYI* BLOOM. *Global Biogeochemical Cycles*, *27*(4), 1023–1033. https://doi.org/10.1002/2013GB004641

Poulton, A. J., Stinchcombe, M. C., Achterberg, E. P., Bakker, D. C. E., Dumousseaud, C., Lawson, H. E., Lee, G. A., Richier, S., Suggett, D. J., & Young, J. R. (2014). Coccolithophores on the north-west European shelf: Calcification rates and environmental controls. *Biogeosciences*, *11*(14), 3919–3940. https://doi.org/10.5194/bg-11-3919-2014

Price, N., Harrison, P., Landry, M., Azam, F., & Hall, K. (1986). Toxic effects of latex and Tygon tubing on marine phytoplankton, zooplankton and bacteria. *Marine Ecology Progress Series*, *34*, 41–49. https://doi.org/10.3354/meps034041

Redalje, D. G., & Laws, E. A. (1981). A new method for estimating phytoplankton growth rates and carbon biomass. *Marine Biology*, *62*(1), 73–79

Regaudie-de-Gioux, A., Lasternas, S., AgustÃ, S., & Duarte, C. M. (2014). Comparing marine primary production estimates through different methods and development of conversion equations. *Frontiers in Marine Science*, *1*. https://doi.org/10.3389/fmars.2014.00019

Riddell, A., Gardner, R., Perez-Gonzalez, A., Lopes, T., & Martinez, L. (2015). Rmax: A systematic approach to evaluate instrument sort performance using center stream catch. *Methods*, *82*, 64–73. https://doi.org/10.1016/j.ymeth.2015.02.017

Rii, Y. M., Duhamel, S., Bidigare, R. R., Karl, D. M., Repeta, D. J., & Church, M. J. (2016). Diversity and productivity of photosynthetic picoeukaryotes in biogeochemically distinct regions of the Southeast Pacific Ocean. *Limnology and Oceanography*, *61*(3), 806–824. https://doi.org/10.1002/lno.10255

Rii, Y., Karl, D., & Church, M. (2016). Temporal and vertical variability in picophytoplankton primary productivity in the North Pacific Subtropical Gyre. *Marine Ecology Progress Series*, *562*, 1–18. https://doi.org/10.3354/meps11954

Sakamoto, M., Tilzer, M. M., Gächter, R., Rai, H., Collos, Y., Tschumi, P., Berner, P., Zbaren, J., Dokulil, M., Bossard, P., Uehlinger, U., & Nusch, E. A. (1984). Joint field experiments for comparisons of measuring methods of photosynthetic production. *Journal of Plankton Research*, *6*(2), 365–383. https://doi.org/10.1093/plankt/6.2.365

Sakshaug, E., Bricaud, A., Dandonneau, Y., Falkowski, P. G., Kiefer, D. A., Legendre, L., Morel, A., Parslow, J., & Takahashi, M. (1997). Parameters of photosynthesis: Definitions, theory and interpretation of results. *Journal of Plankton Research*, *19*(11), 1637–1670. https://doi.org/10.1093/plankt/19.11.1637

Sathyendranath, S., Longhurst, A., Caverhill, C. M., & Platt, T. (1995). Regionally and seasonally differentiated primary production in the North Atlantic. *Deep Sea Research Part I: Oceanographic Research Papers*, *42*(10), 1773–1802. https://doi.org/10.1016/0967-0637(95)00059-F

Shapiro, H. M. (2003). Flow Sorting, p. 736. In H.M. Shapiro [ed.], Practical Flow Cytometry. John Wiley & Sons.

Silsbe, G. M., & Kromkamp, J. C. (2012). Modeling the irradiance dependency of the quantum efficiency of photosynthesis: Fluorescence light curves. *Limnology and Oceanography: Methods*, *10*(9), 645–652. https://doi.org/10.4319/lom.2012.10.645

Silsbe, G. M., and Y. Malkin. (2015). Phytotools: Phytoplankton production tools. R package Version 1.0. https://CRAN.R-project.org/package=phytotools

Slawyk, G., Collos, Y., & Auclair, C. (1979). Reply to comment by Fisher et al. *Limnology and Oceanography*, *24*(3), 595–597. https://doi.org/10.4319/lo.1979.24.3.0595

Slawyk, G., Collos, Y., & Auclair, J.-C. (1977). The use of the ^{13}C and ^{15}N isotopes for the simultaneous measurement of carbon and nitrogen turnover rates in marine phytoplankton1. *Limnology and Oceanography*, *22*(5), 925–932. https://doi.org/10.4319/lo.1977.22.5.0925

Slawyk, G., Minas, M., Collos, Y., Legendre, L., & Roy, S. (1984). Comparison of radioactive and stable isotope tracer techniques for measuring photosynthesis: ^{13C} and ^{14}C uptake by marine phytoplankton. *Journal of Plankton Research*, *6*(2), 249–257. https://doi.org/10.1093/plankt/6.2.249

Steemann Nielsen, E. (1952). The use of radio-active carbon (C14) for measuring organic production in the sea. *ICES Journal of Marine Science*, *18*(2), 117–140.

Stull, E. A., de Amezaga, E., & Goldman, C. R. (1973). The contribution of individual species of algae to primary productivity of Castle Lake, California. *SIL Proceedings, 1922-2010*, *18*(3), 1776–1783.

Teira, E., José Pazó, M., Serret, P., & Fernández, E. (2001). Dissolved organic carbon production by microbial populations in the Atlantic Ocean. *Limnology and Oceanography*, *46*(6), 1370–1377. https://doi.org/10.4319/lo.2001.46.6.1370

Viviani, D. A., Karl, D. M., & Church, M. J. (2015). Variability in photosynthetic production of dissolved and particulate organic carbon in the North Pacific Subtropical Gyre. *Frontiers in Marine Science*, *2*. https://doi.org/10.3389/fmars.2015.00073

van der Wal, P., van Bleijswijk, J. D. L., & Egge, J. K. (1994). Primary productivity and calcification rate in blooms of the coccolithophorid *Emiliania huxleyi* (Lohmann) Hay et Mohler developing in mesocosms. *Sarsia*, *79*(4), 401–408. https://doi.org/10.1080/00364827.1994.10413571

Wal, P., Vrind, J. P. M., Jong, E. W., & Borman, A. H. (2007). Incompleteness of the coccosphere as a possible stimulus for coccolith formation in pleurochrysis carterae (Prymnesiophyceae)1. *Journal of Phycology*, *23*(2), 218–221. https://doi.org/10.1111/j.1529-8817.1987.tb04447.x

Watt, W. D. (1971). Measuring the primary production rates of individual phytoplankton species in natural mixed populations. *Deep Sea Research and Oceanographic Abstracts*, *18*(3), 329–339. https://doi.org/10.1016/0011-7471(71)90038-6

White, A. E., Watkins-Brandt, K. S., & Church, M. J. (2018). Temporal variability of trichodesmium spp. And diatom-diazotroph assemblages in the north pacific subtropical gyre. *Frontiers in Marine Science*, *5*, 27. https://doi.org/10.3389/fmars.2018.00027

Williams, P. J. leB., & Robertson, J. I. (1989). A serious inhibition problem from a Niskin sampler during plankton productivity studies. *Limnology and Oceanography*, *34*(7), 1300–1305. https://doi.org/10.4319/lo.1989.34.7.1300

Williams, P. J. L. B., Thomas, D. N., & Reynolds, C. S. (Eds.). (2008). *Phytoplankton productivity: carbon assimilation in marine and freshwater ecosystems*. John Wiley & Sons.

Zimmermann, M., Escrig, S., Hübschmann, T., Kirf, M. K., Brand, A., Inglis, R. F., Musat, N., Müller, S., Meibom, A., Ackermann, M., & Schreiber, F. (2015). Phenotypic heterogeneity in metabolic traits among single cells of a rare bacterial species in its natural environment quantified with a combination of flow cell sorting and NanoSIMS. *Frontiers in Microbiology*, *06*. https://doi.org/10.3389/fmicb.2015.00243

Zubkov, M. V., & Tarran, G. A. (2008). High bacterivory by the smallest phytoplankton in the North Atlantic Ocean. *Nature*, *455*(7210), 224–226. https://doi.org/10.1038/nature07236

4. The $H_2{}^{18}O$ incubation Method for the Determination of Gross Oxygen Production

Sara Ferrón[1], Lauren W. Juranek[2]
[1]*Department of Oceanography, University of Hawai'i at Mānoa, Hawaii, USA*
[2]*College of Earth, Ocean, and Atmospheric Sciences, Oregon State University, Oregon, USA*

4.1. Overview and History of the $H_2{}^{18}O$ Incubation Method

The $H_2{}^{18}O$ incubation method involves spiking a discrete water sample with ^{18}O-labeled water and measuring the amount of $^{18}O^{16}O$ that evolves from the splitting of water through photosynthesis, after the sample is incubated in the light (Bender et al., 1987). This method provides a direct measurement of gross O_2 production (GOP) that is not affected by respiratory losses or incubation duration in the open ocean, assuming that the O_2 produced by photosynthesis is well mixed with the dissolved O_2 pool. This is because the dissolved O_2 pool is large compared to O_2 respiration rates. By conducting parallel measurements of net O_2 exchange (e.g., as the net change in O_2 to Ar molar ratios), it is possible to also calculate respiration rates by difference (Bender et al., 1987, 1999; Grande et al., 1989). Daily GOP (mmol O_2 m^{-3} d^{-1}) using the $H_2{}^{18}O$ incubation method (^{18}O-GOP) is typically determined for a photoperiod from the change in the isotope ratio of dissolved O_2 over the incubation period (Bender et al., 1987; Kiddon et al., 1995)]

$$\mathrm{GOP} = \left[\frac{{}^{18}\mathrm{R}(\mathrm{O_2})_{\mathrm{final}} - {}^{18}\mathrm{R}(\mathrm{O_2})_{\mathrm{initial}}}{{}^{18}\mathrm{R}(\mathrm{H_2O}) - {}^{18}\mathrm{R}(\mathrm{O_2})_{\mathrm{initial}}}\right] \times [\mathrm{O_2}]_{\mathrm{initial,}} \tag{4.1}$$

where $^{18}R(O_2)_{initial}$ and $^{18}R(O_2)_{final}$ are the initial and final isotope ratios ($^{18}O/^{16}O$) for dissolved O_2, $[O_2]_{initial}$ is the initial dissolved O_2 concentration, and $^{18}R(H_2O)$ is the isotope ratio of the incubation water. Regardless of whether the incubations are conducted between sunrise and sunset or sunrise to sunrise, Eq. 4.1 provides the daily GOP (as there is no GOP in the dark).

If O_2 to Ar molar ratios are also measured, the net O_2 change (NOC) during the incubation can be simultaneously determined (Bender et al., 1999)

$$\mathrm{NOC} = \left[\frac{(\mathrm{O_2/Ar})_{\mathrm{final}}}{(\mathrm{O_2/Ar})_{\mathrm{initial}}} - 1\right] \times [\mathrm{O_2}]_{\mathrm{initial,}} \tag{4.2}$$

where $(O_2/Ar)_{initial}$ and $(O_2/Ar)_{final}$ are the initial and final O_2/Ar ratios. Respiration can be calculated without the need for a separate bottle incubated in the dark (see Chapter 5 for a description of the O_2 light/dark bottle method) as the difference between GOP and NOC, assuming that photosynthesis and respiration are the only two processes affecting changes in O_2/Ar in the incubation bottle (Ferrón et al., 2016). For incubations conducted between sunrise and sunset, NOC represents GOP minus respiration in the light, allowing an estimate of respiration under light conditions (Bender et al., 1987, 1999; Grande et al., 1989). However, the uncertainty (estimated as the coefficient of variation of replicate samples) of NOC and

respiration values determined this way is typically considerably larger than for ^{18}O-GOP (Ferrón et al., 2016).

The $H_2{}^{18}O$ incubation method was introduced in the 1980s by K. Grande, M. Bender, and colleagues (Grande et al., 1982; Bender et al., 1987). It is important to distinguish the $H_2{}^{18}O$ method from a different O_2 isotopic tracer method introduced earlier by Brown and colleagues (Brown, 1953), in which the O_2 pool, instead of the water, is labeled with ^{18}O. The ^{18}O-O_2 labeling approach allows one to simultaneously determine photosynthesis and respiration in the light in phytoplankton cultures and plant leaf samples, with the rate of photosynthesis determined from the rate of increase in $^{16}O^{16}O$, and the rate of respiration calculated from the decrease in $^{18}O^{16}O$. The introduction of the $H_2{}^{18}O$ incubation method allowed a more sensitive and straightforward implementation of the isotope tracer approach to the study of GOP in natural oceanic waters. But by the time this method was developed, the ^{14}C assimilation method (Steemann Nielsen, 1952; see Chapter 3) had already become widely used as the standard primary production method for the oceanographic community. However, the interpretation of ^{14}C assimilation rates is not straightforward (e.g., Marra, 2002, 2009; Peterson, 1980). In this regard, studies comparing ^{18}O-GOP and ^{14}C assimilation rates (^{14}C-PP) have proven very valuable in helping interpret what ^{14}C assimilation rates measure (Bender et al., 1999; Bender and Grande, 1987; González et al., 2008; Grande et al., 1989; Juranek and Quay, 2005; Kiddon et al., 1995; Laws et al., 2000; Quay et al., 2010; Timmerman et al., 2021). A number of these comparisons were part of major collaborative programs, such as PRPOOS and JGOFS, aimed at comparing and establishing methodological protocols for measuring primary production in the ocean (e.g., Bender et al., 1999; Dickson et al., 2001; Grande et al., 1989; Laws et al., 2000; see Chapter 3). These studies have shown that ^{14}C-PP in 12- to 24-hour incubations typically yields a value between net community and gross C production (Marra, 2009), but where ^{14}C-PP lies in relation to net community and gross C production depends on phytoplankton community structure, among other things (Pei and Laws, 2013), net growth rate (Halsey et al., 2011; Pei and Laws, 2014), incubation time (Halsey et al., 2011), and dissolved organic C production (typically not measured) (Karl et al., 1998). Despite providing a direct measurement of GOP and helping interpret ^{14}C results, the $H_2{}^{18}O$ incubation method has not been used frequently in oceanic studies and accounts for a small fraction of all oceanic primary production measurements (e.g., Regaudie-de-Gioux et al., 2014).

One of the advantages of the $H_2{}^{18}O$ incubation method compared to the ^{14}C method is that it unambiguously measures the gross O_2 production from the photosynthetic splitting of water. In addition, the labeled product remains in a well-defined pool (dissolved O_2), and the measurement is relatively insensitive to recycling. However, as with other *in vitro* approaches, this technique is susceptible to artifacts associated with incubating seawater in a confined bottle, such as grazer exclusion and perturbations of the natural environmental conditions (Robinson and Williams, 2005). Another potential caveat of this method is the need to know the photosynthetic quotient to convert to gross C production. In addition, the $H_2{}^{18}O$ incubation method measures gross O_2 production regardless of the fate of this O_2 and whether it is linked to the fixation of organic C. A fraction of newly produced O_2 may be consumed by light-dependent reactions (e.g., Mehler reaction, photorespiration), which could result in an overestimation of gross C fixation determined from the $H_2{}^{18}O$ incubation method if these processes are ignored (Bender et al., 1999; Bender et al. 2000; Juranek and Quay, 2005).

Some analytical challenges that have historically limited the widespread application of the $H_2{}^{18}O$ technique to studies of marine primary production are 1) the need for a specialized isotope ratio mass spectrometer (IRMS), and 2) the handling and analysis of samples for $^{18}O/^{16}O$ are technically difficult and require highly trained personnel. As stated by Falkowski and Raven (2007) in their book *Aquatic Photosynthesis*: "This technique allows a relatively precise measurement of gross photosynthesis; however, the method is tedious, requires a (bulky and expensive) mass spectrometer, and hence has not been widely used in studies of aquatic photosynthesis in nature." Ferrón et al. (2016) recently demonstrated that GOP can be precisely measured with the $H_2{}^{18}O$ incubation method using membrane inlet mass spectrometry (MIMS), potentially making this method easier to implement and more accessible to the broader oceanographic community. This novel approach has the advantage of only requiring a relatively inexpensive quadrupole mass spectrometer (~30–50K USD), which is a small, easy-to-operate instrument that can be taken to sea. In addition, handling and analyzing samples is technically easy, as the gases are directly diffused from the water sample into the mass spectrometer without the need for a gas extraction step.

4.2. Sample Collection

4.2.1. General precautions

Seawater samples for incubations should be collected to the extent possible using clean techniques (Fitzwater et al., 1982; JGOFS 1996). Gas-tight ground glass stoppered bottles (typically between 100 and 150 mL in volume) are most used for incubation. Borosilicate glass has been widely used for incubations using the light/dark oxygen incubation method (see Chapter 5), whereas quartz glass bottles are more common when using the ^{18}O-H_2O *in vitro* method. When deciding the type of glass used for the incubation bottles a few considerations are important. First, quartz bottles are significantly more expensive than borosilicate bottles and often need to be custom made (quartz boiling flasks with ground glass joints can be an option, but they often are not sold with stoppers and are relatively fragile). Second, silica-glass can potentially release significant amount of trace metals during an incubation, even after being thoroughly cleaned whereas quartz bottles should not release trace metals if properly cleaned (e.g., quartz filters are suitable for most trace metal analyses, see https://www.geotraces.org/methods-cookbook/). In this respect, iron additions do not typically cause changes in productivity during the first 24 hours. Third, quartz glass bottles are more transparent to the full spectrum of environmental light as borosilicate blocks part of the UV radiation. This is only relevant when the incubation occurs in situ, as UV is typically blocked by on-deck incubators. It is important to note that whereas quartz bottles provide a more realistic environmental light field at each depth, in reality, natural plankton communities do not remain at the same depth for an entire day, so keeping the "true natural conditions" with static incubations is not entirely possible, and the phytoplankton communities incubated at the surface might suffer from photoinhibition during the incubation (Marra, 1978). Regardless of the choice, both borosilicate and quartz glass bottles are significantly more transparent to the full spectrum of light than polycarbonate bottles, which are often used when measuring productivity by the ^{14}C or ^{13}C methods.

When selecting the most appropriate sample volume the following should be considered. If a gas extraction step is conducted (as for the IRMS method), one should consider the minimum incubation volume needed to allow for transfer of a ~30–50 mL uncontaminated sample (no

contact with atmosphere) from the bottom of the incubation bottle into the gas sampling flask to yield enough analytical signal for IRMS determination. Based on experience, the minimal incubation volume given these constraints is ~100 mL. This constraint is not relevant when using MIMS (~10 mL would be enough). Another consideration is that small incubation volumes can discriminate against larger, rare planktonic organisms, biasing rates. On the other hand, larger volumes require more labeled water, which can be expensive, and handling larger samples. Previous studies using this method have mostly utilized 100–150 mL sample bottles (e.g., Bender et al., 1999; Ferrón et al., 2016; Grande et al., 1989; Juranek and Quay, 2005; Quay et al., 2010).

In general, powderless polyethylene gloves are the preferred choice when collecting samples for primary production. However, their loose fit in the hands can make the sample collection and preparation cumbersome, in which case powder-free latex gloves are sufficient. Nitrile gloves should be avoided as they likely contaminate with nitrate.

4.2.2. Pre-cruise sample bottle preparation

The preferred cleaning protocol for the incubation bottles is the same as for ^{14}C and ^{13}C incubations (see Chapter 3): 1) washing with a dilute solution of trace metal clean detergent, 2) thorough rinsing with deionized water, 3) soaking in 5–10% HCl solution for over 24 hours, and 4) thorough rinsing with Milli-Q water.

4.2.3. Water sampling

Determining GOP using Eq. 4.1 requires knowing four terms: the initial and final isotopic ratio ($^{18}O/^{16}O$) of dissolved O_2, the initial isotopic ratio of water (after the spike), and the initial concentration of dissolved O_2. The initial isotopic ratio of water is determined from the amount of labeled water added and the calibrated volume of the incubation bottles. It is necessary to collect initial samples in addition to the incubation bottles for initial and final measurements of the isotopic ratio for dissolved O_2. The initial concentration of dissolved O_2 can be determined by the Winkler method (Carpenter, 1965) in a separate sample from the *in situ* dissolved O_2 concentration measured by the CTD O_2 sensor or measured concurrently with the initial isotopic ratio for dissolved O_2 if using MIMS (Ferrón et al., 2016). The samples are typically subsampled from a larger container, such as Niskin-type bottles attached to a CTD rosette (see Chapter 3).

4.2.3.1. Incubation samples

The incubation samples are collected by attaching an acid-washed silicone tubing to the spigot of the Niskin-type bottle and inserting it to the bottom of the glass bottle. Once the water starts flowing, the bottle and stoppers are rinsed with the seawater sample, and then the bottle is filled from bottom to top ensuring no bubbles are trapped in the tubing or bottle, overflowing at least once the volume of the bottle.

Once the incubation samples are collected, these are spiked with ^{18}O-labeled water (e.g., Medical Isotopes, > 97% ^{18}O). It is important to make sure not to introduce contaminants (e.g., trace metals, macronutrients, etc.) to the incubation bottle with the spike. This can be done by measuring the concentrations of metals and macronutrients in the stock solution to ensure that they are below background levels, triple distilling the ^{18}O-labeled water with a sub-boiling Teflon still (Juranek and Quay, 2005), or conducting experiments to make sure the addition of the spike does not significantly alter the production rates (Ferrón et al., 2016).

The final target enrichment of the water depends on the expected productivity and should be calculated during the planning stages of fieldwork. An enrichment of 5–10 ‰ in the dissolved O_2 pool after the incubation is ideal. However, the enrichment may be lower for very low photosynthetic rates (such as at the base of the euphotic zone). Care should be taken to not overdose the incubation samples with ^{18}O-spike, particularly if the analysis is by IRMS, since labs that measure natural abundance oxygen isotopes will be wary of analyzing heavily enriched samples. The isotopic enrichment of the incubated sample relative to the initial sample is calculated as

$$\delta^{18}O(O_2) = \left[\frac{^{18}R(O_2)_{final}}{^{18}R(O_2)_{initial}} - 1\right] \times 1000. \quad (4.3)$$

Because the isotopic ratio of the water after the spike is typically not measured but calculated based on the amount of labeled water added and the calibrated volume of the incubation bottle, it is important to accurately know the volume of the flask and the volume of added ^{18}O-labeled water. The fractional abundance ($^{18}O/^{16}O+^{18}O$) of the water after the spike ($^{18}F_{water}$) is calculated as

$$^{18}F_{water} = \frac{V_{spike}\,^{18}F_{spike} + V_{sample}\,^{18}F_{SMOW}}{V_{sample} + V_{spike}}, \quad (4.4)$$

where V_{spike} and V_{sample} are the volumes of the spike and sample, respectively, $^{18}F_{spike}$ and $^{18}F_{water}$ are the fractional abundances of the spike and the Standard Mean Ocean Water (SMOW), respectively. The isotopic ratio of the water ($^{18}R_{water}$) can be then calculated as $^{18}F_{water}/(1-^{18}F_{water})$.

A pipette with sterile pipette tips is recommended for spiking the sample. The ^{18}O-labeled water is denser than seawater and will sink to the bottom of the bottle. However, it is essential to make sure the pipette tip is placed well below the neck of the bottle when spiking the sample and that the spike is released slowly to avoid creating turbulence in the sample that could bring the labeled water into the neck area where it can be expelled when the bottle is capped with the ground glass stopper. After the spike, the samples are gently mixed and kept in the dark until the incubation starts. A new pipette tip is used for every sample. The handling of the samples is conducted under low light conditions.

4.2.3.2. Initial samples

The collection procedure for the initial (time-zero) samples depends on whether the analysis is to be done by IRMS or MIMS. Samples for IRMS analysis are typically collected in pre-evacuated glass flasks (typically 200–250 mL in volume) with a LouwersHanique valve (with single or double O-ring). The preparation of the flasks is similar to that described for O_2/Ar and triple oxygen isotope gas sampling (see Chapters 7 and 8 for a detailed overview) and includes: 1) dosing flasks with 100 µL of saturated mercuric chloride solution and drying in a vented oven at 50°C, 2) evacuating them using a vacuum pump to < 10^{-2} mTorr, and 3) filling the neck of the

flasks with CO_2 (Emerson et al., 1999) and capping them, to avoid contamination with atmospheric gas through the O-rings during storage before sampling. Extreme care is needed during sampling to avoid contamination with atmospheric gas bubbles. When possible, the neck of the flask is flushed with CO_2 before sampling to dislodge ambient air. While flushing with CO_2, a ~1/8" Nylon tube connected to the spigot of the Niskin-type bottle is inserted into the neck of the flask. When the sample valve from the Niskin-type bottle is open, a water lock is established with a small volume of seawater, making sure all bubbles in the neck are removed by tapping the glass valve. Then the glass valve is opened and, while maintaining the water lock, the flask is filled with a small volume of seawater sample (~50–100 mL). After the valve is closed, the neck of the flask should be rinsed with distilled water (so that salt crystal accumulation on O-rings does not contribute to potential leaks), dried to the extent possible by inserting a Kimwipe and wicking moisture, and the neck filled with CO_2 to avoid air contamination during storage until analysis. Sometimes, provisioning compressed CO_2 gas at very remote ports can be a challenge; if this is the case, an alternate, but less preferable, storage method is to fill the neck with distilled water and cap. Note that the latter method is more susceptible to leaks, and samples should be analyzed as quickly as possible. Leaks across the O-ring would lead to a dilution of ^{18}O label in the flask, hence an underestimate of rates. Initial samples for MIMS analysis are collected in the same way as the incubation sample and poisoned with saturated mercuric chloride solution at the start of the incubation to inhibit microbial activity (see Section 4.3.1).

4.3. Incubation

Typically, the samples are collected before sunrise and incubated from pre-dawn to dusk or for 24 h. In contrast to ^{14}C- and ^{13}C-derived primary production, ^{18}O-GOP is independent of whether the incubation duration is from dawn to dusk or 24 hours, as there is no splitting of water in the dark, and the measurement is not affected by recycling. Once the samples have been spiked, they are incubated, keeping the *in situ* environmental conditions to the extent possible. This can be achieved by incubating the samples *in situ* or simulating the *in situ* conditions (e.g., using on-deck incubators). For a review of incubation methods, refer to Chapter 3. At each station, samples are collected at different depths within the euphotic zone (8 depths are typically recommended JGOFS, 1996). For *in situ* incubations, replicate bottles (at least 3 recommended) from the same depth are attached to a custom-made rack and deployed at the appropriate depth of a free-floating mooring array. Keeping the samples in the dark until deployment and after recovery is important. Therefore, it is recommended that the array deployment and recovery is conducted before sunrise and after sunset, respectively. Alternatively, the samples can be incubated in on-deck incubators that simulate the *in situ* conditions. In this case, information is needed prior to the start of the incubation regarding the temperature and light conditions through the water column (Chapter 3).

4.3.1. Termination of the incubation and sample storage

The incubation can be terminated by transferring a subsample from the incubation bottle into a different gas-tight container and then inhibiting biological activity using a saturated mercuric chloride solution. Due to its toxicity, it is important to use gloves when dealing with mercuric chloride (nitrile gloves are recommended for handling mercuric chloride). Transferring a subsample from the incubation bottle to a different container is done by siphoning from the bottom of the container, ensuring no air bubbles are trapped in the line. The procedure for the subsample collection depends on whether these will be analyzed by IRMS or MIMS.

For IRMS, subsamples are transferred into evacuated pre-poisoned flasks with LouwersHanique valves, as described in Section 4.2.3.2 and Chapters 7 and 8. Samples are stored in the dark until analysis. The maximum recommended storage time for gas samples is < 2 months.

When using MIMS, subsamples can be transferred into any gas-tight bottle, for example, borosilicate crimped-sealed serum bottles (Ferrón et al., 2016) or screw cap vials with butyl rubber septa (e.g., 12 mL Labco Exetainer). The subsample is transferred by siphoning, filling the serum bottle at low flow from bottom to top, allowing it to overflow. Subsequently, saturated mercuric chloride solution can be added using a pipette, inserting the pipette tip well below the neck of the bottle. As the mercuric chloride solution is denser than seawater, it will sink to the bottom and will not be expelled when the bottle or vial is closed. Alternatively, the mercuric chloride spike can be added after closing the bottle or vial using a 1-mL syringe (connected to a needle) loaded with mercuric chloride solution. In this case, a short needle that will act as a vent is first inserted through the septum or rubber stopper; subsequently, a longer needle connected to the syringe is inserted and the correct amount of mercuric chloride solution is added to the vial or bottle before removing both needles. Care must be taken not to inadvertently inject an air bubble while fixing the sample. Using a pipette is recommended as it avoids the risk of working with needles while handling toxic mercuric chloride solution and poking through the septum or stopper, which could potentially become a source of contamination. Once the sample is fixed with mercuric chloride, it should be gently mixed and stored in the dark until analysis. It is recommended that water samples for MIMS analysis are measured as soon as possible, as O_2 is a chemically active gas in seawater, ideally within a week of collection.

Alternatively, if using MIMS, the sample can be terminated directly in the incubation bottle by fixing with mercuric chloride saturated solution. To re-close the bottle with no bubbles, a ground glass stopper that displaces more water than the one used for incubation is needed. Conically tapered ground glass joints have standard sizes, so it is possible to buy different stoppers that match the bottle ground joint neck. For example, a solid or semi-solid stopper with a flat bottom can be used for the incubation, to then be replaced by a hollow ground glass stopper with a rounded or pointy bottom. It is important to keep the ground glass stopper in place (e.g., using tape) and store the samples immersed in water (to keep the glass ground joint gas-tight by keeping it wet). This can be achieved by storing the samples upside down inside a compartmentalized rack with beakers filled with water.

4.4. Isotopic Analysis

The isotopic ratio ($^{18}O/^{16}O$) of dissolved O_2 can be measured by IRMS or MIMS. Both approaches can also measure O_2 to Ar molar ratios.

4.4.1. IRMS

Samples collected into pre-evacuated flasks are returned to a shore-side laboratory where the sample is left to equilibrate with the headspace by continuous agitation for 8–10 hours at a constant, known temperature, which allows 97–98% of the dissolved gases to exsolve (Emerson et al., 1999). The water flask is then inverted, and sample water is removed from the flask using a vacuum pump, leaving less than 1 mL of sample water to maintain the exsolved gases in the headspace. The sidearm of the flask is then rinsed with distilled water, dried, capped with CO_2, and stored until analysis.

Samples are processed using a high-vacuum gas line that allows samples to be transferred from the sample flask through several cryotraps to remove water vapor and CO_2 from the sample, like the O_2/Ar analysis described in Chapter 8. Samples are then admitted to the IRMS, and the mass/charge (m/z) ratio of $^{18}O^{16}O$ (m/z 34) relative to $^{16}O^{16}O$ (m/z 32) is determined for the sample versus an internal working standard. Typically, an average of 6 measurements are used to constrain the $^{18}O/^{16}O$ value. The $^{18}O/^{16}O$ should be corrected for the O_2/Ar of the sample, as gas matrix effects will affect the ionization efficiencies of oxygen isotopologues differently (see Chapter 7).

4.4.2. MIMS

A MIMS analyzer consists of a membrane inlet system (Ferrón et al., 2016; Kana et al., 1994) connected to a quadrupole mass spectrometer (e.g., Pfeiffer HiQuad QMG 700, Pfeiffer PrismaPlus QMG 220). It is recommended to use a secondary electron multiplier when measuring m/z 34 ($^{18}O^{16}O$). When using MIMS, a fraction of the gases is transferred directly from the water sample to the mass spectrometer, so no prep steps are needed. It is recommended to remove water vapor and CO_2 from the gas stream (e.g., using a cryotrap) as these gases can affect the ionization, and to maintain the membrane inlet at a constant temperature (as diffusion across the membrane is temperature-dependent). Calibration can be done by air equilibrating seawater of known salinity at a given temperature (± 0.01°) (Ferrón et al., 2016). To calculate the concentrations of dissolved O_2 and Ar in the standard we recommend using the solubility equations of García and Gordon (1992) and Hamme and Emerson (2004), respectively. The isotopic composition of dissolved O_2 in the standard can be determined using the solubility fractionation reported by Kroopnick & Craig (1972). It is recommended to run a standard periodically while measuring the samples (every ~20–30 min) to account for drift in the signals (Kana et al., 1994, 2006). Further details can be found in Ferrón et al. (2016).

4.5. Accuracy and Uncertainty

As with any other method for measuring primary production, there are no available standards against which to calibrate ^{18}O-GOP, so it is impossible to calculate the accuracy. Instead, comparing primary production measured by different approaches and ensuring that measured rates are physiologically plausible are two common approaches to validate primary production results (see Chapter 3).

The analytical uncertainty in ^{18}O-GOP can be estimated by propagating the errors in the different terms of Eq. 4.1, which are typically assumed to be the standard deviation of replicate samples. The isotopic ratio of the water after the spike generally is not measured, but when measured, predicted values agreed with measured ones within 5% (Juranek and Quay, 2005). The reproducibility of dissolved O_2 measurements by the Winkler method, measured as the coefficient of variation of replicate samples, is typically between ±0.1–0.2%. The precision for the isotopic ratio of O_2 is typically ~ ±0.002% (0.02 per mil) when using IRMS and ~ ±0.05% when using MIMS (Ferrón et al., 2016). The analytical ^{18}O-GOP error (typically between ± 1–5%) is typically considerably smaller than the coefficient of variation from triplicate incubated samples (~10–20%) (Ferrón et al., 2016; Juranek and Quay, 2005).

Daily depth-integrated ^{18}O-GOP (mmol O_2 m^{-2} d^{-1}) for the euphotic zone can be calculated using the trapezoidal rule, and the standard deviation of the integrated values can be determined through error propagation (Karl et al., 2021 and Chapter 3).

4.6. References

Bender, M. L., Grande, K., Johnson, K., Marra, J., Williams, P. J. L. B., Sieburth, J., et al. (1987). A comparison of four methods for determining planktonic community production. *Limnology and Oceanography*, *32*, 1085–1098. https://doi.org/10.4319/lo.1987.32.5.1085

Bender, M. L., Orchardo, J., Dickson, M.-L., Barber, R., & Lindley, S. (1999). In vitro O_2 fluxes compared with ^{14}C production and other rate terms during the JGOFS Equatorial Pacific experiment. *Deep-Sea Research Part I*, *46*, 637–654.

Bender, M. L., Dickson, M., & Orchardo, J. (2000). Net and gross production in the Ross Sea as determined by incubation experiments and dissolved O_2 studies, *Deep-Sea Research Part II*, *47*, 3141–3158. https://doi.org/10.1016/S0967-0645(00)00062-X

Brown, A. H. (1953). The effects of light on respiration using isotopically enriched oxygen. *American Journal of Botany*, *40*, 719–729. https://doi.org/10.2307/2439688

Carpenter, J. H. (1965). The accuracy of the Winkler method for dissolved oxygen analysis. *Limnology and Oceanography*, *10*, 135–140. https://doi.org/10.4319/lo.1965.10.1.0135

Dickson, M. L., Orchardo, J., Barber, R. T., Marra, J., McCarthy, J. J., & Sambrotto, R. N. (2001). Production and respiration rates in the Arabian Sea during the 1995 Northeast and Southwest Monsoons. *Deep-Sea Research Part II, 48*, 1199–1230. https://doi.org/10.1016/S0967-0645(00)00136-3

Emerson, S., Stump, C., Wilbur, D., & Quay, P. D. (1999). Accurate measurement of O_2, N_2, and Ar gases in water and the solubility of N_2. *Marine Chemistry*, *64*, 337–347. https://doi.org/10.1016/S0304-4203(98)00090-5

Ferrón, S., del Valle, D. A., Björkman, K. M., Quay, P. D., Church, M. J., & Karl, D. M. (2016). Application of membrane inlet mass spectrometry to measure aquatic gross primary production by the ^{18}O in vitro method. *Limnology and Oceanography: Methods*, *14*, 610–622. https://doi.org/10.1002/lom3.10116

Fitzwater, S. E., Knauer, G. A., & Martin, J. H. (1982). Metal contamination and its effect on primary production measurements. *Limnology and Oceanography*, *27*, 544–551. https://doi.org/10.4319/lo.1982.27.3.0544

García, H. E., & Gordon, L. I. (1992). Oxygen solubility in seawater: Better fitting equations. *Limnology and Oceanography*, *37*(6), 1307–1312.

González, N., Gattuso, J. P., & Middelburg, J. J. (2008). Oxygen production and carbon fixation in oligotrophic coastal bays and the relationship with gross and net primary production. *Aquatic Microbial Ecology*, *52*, 119–130. https://doi.org/10.3354/ame01208

Grande, K. D., Kroopnick, P., Burns, D., & Bender, M. L. (1982). ^{18}O as a tracer for measuring gross primary productivity in bottle cxpcriments. (Abstr.) *Eos,* 63: 107.

Grande, K. D., Williams, P. J. L. B., Marra, J., Purdie, D. A., Heinemann, K., Eppley, R. W., & Bender, M. L. (1989). Primary production in the North Pacific gyre : a comparison of rates determined by the ^{14}C, O_2 concentration and ^{18}O methods. *Deep Sea Research*, *36*, 1621–1634.

Halsey, K. H., Milligan, A. J., & Behrenfeld, M. J. (2011). Linking time-dependent carbon-fixation efficiencies in Dunaliella Tertiolecta (Chlorophyceae) to underlying metabolic pathways. *Journal of Phycology*, *47*, 66–76. https://doi.org/10.1111/j.1529-8817.2010.00945.x

Hamme, R. C., & Emerson, S. (2004). The solubility of neon, nitrogen and argon in distilled water and seawater. *Deep-Sea Research Part I: Oceanographic Research Papers*, *51*, 1517–1528. https://doi.org/10.1016/j.dsr.2004.06.009

JGOFS. 1996. Protocols for the Joint Global Ocean Flux Study (JGOFS) core measurements, p. 170. In A. Knap (ed.), Report no. 19 of the Joint Global Ocean Flux Study.

Juranek, L. W., & Quay, P. D. (2005). In vitro and *in situ* gross primary and net community production in the North Pacific Subtropical Gyre using labeled and natural abundance isotopes of dissolved O_2. *Global Biogeochemical Cycles*, *19*, 1–15. https://doi.org/10.1029/2004GB002384

Kana, T. M., Darkangelo, C., Hunt, M. D., Oldham, J. B., Bennett, G. E., & Cornwell, J. C. (1994). Membrane inlet mass spectrometer for rapid high-precision determination of N_2, O_2, and Ar in Environmental Water Samples. *Analytical Chemistry*, *66*, 4166–4170.

Kana, T. M., Cornwell, J. C., & Zhong, L. (2006). Determination of denitrification in the Chesapeake Bay from measurements of N2 accumulation in bottom water. *Estuaries and Coasts*, *29*, 222–231. https://doi.org/10.1007/BF02781991

Karl, D. M., Hebel, D. V., Björkman, K., & Letelier. (1998). The role of dissolved organic matter release in the productivity of the oligotrophic North Pacific Ocean. *Limnology and Oceanography*, *43*, 1270–1286. https://doi.org/10.4319/lo.1998.43.6.1270

Kiddon, J., Bender, M. L., & Marra, J. (1995). Production and respiration in the 1989 North Atlantic spring bloom: an analysis of irradiance-dependent changes. *Deep-Sea Research Part I*, *42*, 553–576. https://doi.org/10.1016/0967-0637(95)00008-T

Kroopnick, P., & Craig, H. (1972). Atmospheric oxygen: Isotopic composition and solubility fractionation. *Science*, *175*, 54–55. https://doi.org/10.1126/science.175.4017.54

Laws, E. A., Landry, M. R., Barber, R. T., Campbell, L., Dickson, M. L., & Marra, J. (2000). Carbon cycling in primary production bottle incubations: Inferences from grazing experiments and photosynthetic studies using ^{14}C and ^{18}O in the Arabian Sea. *Deep-Sea Research Part II: Topical Studies in Oceanography*, *47*, 1339–1352. https://doi.org/10.1016/S0967-0645(99)00146-0

Marra, J. (1978). Phytoplankton photosynthetic response to vertical movement in a mixed layer. *Marine Biology*, 46, 203-208.

Marra, J. (2009). Net and gross productivity: Weighing in with ^{14}C. *Aquatic Microbial Ecology*, *56*, 123–131. https://doi.org/10.3354/ame01306

Pei, S., & Laws, E. A. (2013). Does the ^{14}C method estimate net photosynthesis? Implications from batch and continuous culture studies of marine phytoplankton. *Deep-Sea Research Part I: Oceanographic Research Papers*, *82*, 1–9. https://doi.org/10.1016/j.dsr.2013.07.011

Pei, S., & Laws, E. A. (2014). Does the ^{14}C method estimate net photosynthesis? II. Implications from cyclostat studies of marine phytoplankton. *Deep-Sea Research Part I: Oceanographic Research Papers*, *91*, 94–100. https://doi.org/10.1016/j.dsr.2014.05.015

Quay, P. D., Peacock, C., Björkman, K., & Karl, D. M. (2010). Measuring primary production rates in the ocean : Enigmatic results between incubation and non - incubation methods at Station ALOHA. *Global Biogeochemical Cycles*, *24*(GB3014). https://doi.org/10.1029/2009GB003665

Regaudie-de-Gioux, A., Lasternas, S., Agustí, S., & Duarte, C. M. (2014). Comparing marine primary production estimates through different methods and development of conversion equations. *Frontiers in Marine Science*, *1–14*, 135–140. https://doi.org/10.3389/fmars.2014.00019

Robinson, C., & Williams, P. J. L. B. (2005). Respiration and its measurement in surface marine waters. In P. A. del Giorgio & P. J. L. B. Williams (Eds.), *Respiration in Aquatic Ecosystems* (pp. 147–180). New York: Oxford University Press. https://doi.org/10.1093/acprof:oso/9780198527084.003.0009

Steemann Nielsen, E. (1952). The use of radio-active carbon (C^{14}) for measuring organic production in the sea. *ICES Journal of Marine Science*, *18*, 117–140. https://doi.org/10.1093/icesjms/18.2.117

Timmerman, A. H. V., & Hamme, R. C. (2021). Consistent relationships among productivity rate methods in the NE Subartic Pacific. *Global Biogeochemical Cycles*, 35, e2020GB006721, https://doi.org/10.1029/2020GB006721

5. Light and Dark Dissolved Oxygen Rate Measurements Using the Winkler Method

Chris Langdon[1], E. Elena García-Martín[2]
[1]*Rosenstiel School of Marine, Atmospheric and Earth Science, University of Miami, Florida, USA*
[2]*National Oceanography Centre, Southampton, UK*

5.1. Introduction

Changes in oxygen concentration are directly linked to biological processes. Photosynthesis produces oxygen, whereas aerobic respiration consumes oxygen and forms carbon dioxide. Therefore, the quantification of the dissolved oxygen concentration provides us with very useful information about the balance of the metabolic processes in aquatic systems. At the end of the 19th century, Ludwig Winkler developed a technique to indirectly determine the concentration of dissolved oxygen in water using a series of multi-step chemical reactions (Winkler, 1888). Four years later, Natterer applied the technique for the first time to seawater samples (Natterer, 1892). However, it was not until 1927 that Gaarder and Gran (1927) used it to measure biological oxygen fluxes. Combining light and dark bottles, Gaarder and Gran measured the production and consumption of the oxygen dissolved in an enclosed seawater sample with respect to an initial oxygen concentration. The original method was subject to several limitations during the manipulation, and sample analysis introduced errors that affected the precision and replicability between samples—the limitations related to the need to perform the titration on subsamples. The problem was resolved by the introduction of whole bottle titrations (Carritt and Carpenter, 1966; Carpenter, 1965) and with the development of automated titration using potentiometric, amperometric, or photometric end-point detection (Oudot, 1988; Culberson and Huang, 1987; Williams and Jenkinson, 1982).

The method proposed by Winkler is a multi-step process based on the oxidation of Mn(II) to Mn(III) by oxygen in an alkaline solution (made up of sodium iodide and sodium hydroxide), ultimately releasing free diatomic iodine (I_2) into the solution. These reactions are visualized by the formation of a brown-colored precipitate. The I_2 molecules are directly proportional to the molecules of oxygen. Therefore, to know the molecules of dissolved oxygen in water, the I_2 is titrated with thiosulphate. The stoichiometric equations for the reactions are

$$Mn^{+2} + 2OH^- \rightarrow Mn(OH)_2$$

$$2Mn(OH)_2 + \tfrac{1}{2} O_2 + H_2O \rightarrow 2MnO(OH)_3 \quad \text{oxidation of Mn(II) to Mn(III)}$$

$$2MnO(OH)_3 + 2I^- + 6H+ \rightarrow 2Mn^{+2} + I_2 + 6H_2O \quad \text{oxidation of iodide to iodine}$$

$$I_2 + I \rightarrow +I_3^- \quad \text{oxidation of thiosulphate to tetrathionate and}$$

$$I_3^- + 2\ S_2O_3^{-2} \rightarrow 3I^- + S_4O_6^{2-} \quad \text{reduction of iodine complex to iodide ions}$$

Parallel to the development of the light/dark bottle dissolved oxygen method, the use of the radiolabeled ^{14}C method was introduced to estimate photosynthesis (Chapter 3). The popularity of the ^{14}C incorporation method can be observed in the vast amount of photosynthesis measurements collected in a few years, which allowed the construction of detailed maps of photosynthetic activities in the ocean (Koblentz-Mishke, 1967). Despite the current popularity of the ^{14}C incorporation method, its use is limited to estimating gross and net primary production, as plankton community respiration cannot be quantified directly (González et al., 2008). Therefore, estimations of plankton community respiration and net community production can only be made by measuring changes in the dissolved oxygen concentrations of a water sample.

It is important to understand the difference between net primary production and net community production and their ecological implications to decide which method to use. Net primary production refers to the gross primary production minus the respiration of the autotrophs, and therefore represents the rate at which phytoplankton produces biomass. Whilst net community production is the difference between the gross primary production minus the total community respiration (autotrophic and heterotrophic respiration). Knowledge of net community production is necessary to quantify the carbon a system can potentially export. Thus, on an annual basis, net community production corresponds to the organic carbon biologically produced in the euphotic layer that can be exported to the deep ocean, a process known as the "biological carbon pump" (Emerson, 2014).

In this section, we describe the light/dark bottle dissolved oxygen method for measurement of primary production rates using *in situ* or on-deck incubations. The method has been employed to determine the primary production rates of natural phytoplankton communities in a wide range of environments, including some of the most oligotrophic open ocean waters (Williams et al., 1983, Grande et al., 1989, Gonzalez et al., 2008, Serret et al., 2015). The method can also be used to get rates of community respiration below the photic zone (Robinson et al., 2002a, 2002b).

Here we describe how the pre-cruise preparation of chemical solutions needed for the determination of oxygen concentration of the samples, the options for ship-board automated titration analysis of the samples, and the setup for in situ and on-deck incubations. Finally, we give the precision of the rates that can be expected under typical conditions.

5.2. Best Practices for On-Deck/*In Situ* Incubations

5.2.1. Chemical reagents

Five different reagents are required for the sampling and analysis of the dissolved oxygen concentration in seawater. All chemicals should be stored in amber glass bottles once prepared to prevent photooxidation of the reagents. Wear nitrile gloves and safety glasses during the preparation of the reagent solutions and perform them in a fume hood cupboard.

- **Manganous chloride solution ($MnCl_2 \cdot 4H_2O$, 3 M):** Dissolve 600 g of manganous chloride tetrahydrate ($MnCl_2 \cdot 4H_2O$) in a graduated volumetric glass flask containing 500–700 mL of Milli-Q water. Stir until all the crystals have dissolved. The solution may cool during preparation. Allow it to get to room temperature before making the solution up to a final volume of 1 L. Manganous sulfate ($MnSO_4 \cdot 4H_2O$, 3M) may be used instead of the manganous chloride solution. Dissolve 450 g of manganous sulfate tetrahydrate ($MnSO_4 \cdot 4H_2O$) in a graduated volumetric glass flask containing 500–700 mL of Milli-Q

water. Stir until all the crystals have dissolved. Allow the solution to get to room temperature before making the solution up to a final volume of 1 L.

- **Solution of sodium iodide (NaI, 4M) and sodium hydroxide (NaOH, 8M):** Dissolve 320 g of NaOH in a graduated volumetric glass flask containing 500 mL of Milli-Q water. This is an exothermic reaction, so it is recommended to cool down the solution by stirring the volumetric flask inside an ice bath. Once all the compound is dissolved, add slowly 600 g of NaI and stir until it completely dissolves. It can take several hours. Make the solution up to a final volume of 1 L. If the solution is not transparent (there are some tracers of reagents that have not dissolved), filter the solution through a coarse glass fiber filter to remove the non-dissolved material. If the solution presents a yellowish-brownish color, discard it, and prepare it again with fresh reagents.
- **Sulphuric acid (H_2SO_4, 5M):** Slowly add 280 mL of H_2SO_4 to 650 mL of Milli-Q water. This is an exothermic reaction and will generate a lot of heat and corrosive gases. Perform this in a fume hood cupboard and preferably submerge the volumetric glass flask inside an ice bath to cool it down. Once the solution reaches room temperature, make it up to 1 L.
- **Sodium thiosulphate pentahydrate ($Na_2S_2O_3 \cdot 5H_2O$)**: The concentration of the thiosulphate will depend on the volume of the burette of your titration system. The concentration should be one that allows your titration system to dispense around 80–90% of the burette volume. For example, for a titration system with 1 mL burette and oxygen bottles of 125 mL, the typical concentration is 0.2 M. Dissolve 24.821 g of $Na_2S_2O_3 \cdot 5H_2O$ into 900 mL of Milli-Q water. Make the solution up to 1 L.
- **Potassium iodate (KIO_3, 0.0100 N):** It is important to accurately measure this compound as it will be used to standardize the thiosulphate concentration. It can be bought as a prepared solution or be the laboratory. Weigh 0.5 g of KIO_3 and dry it in an oven at 120°C for several hours. Weigh 0.3567 g of the dried KIO_3 to the closest decimal and dissolve it in 1L of Milli-Q water in a volumetric glass. Use a pipette to add drops at the end to properly level the meniscus to the line of the volumetric glass.

5.2.2. Sampling and incubation bottles

The most common and generally accepted containers for collecting water samples to determine dissolved oxygen concentration are 100 mL borosilicate glass bottles. Other volumes (i.e., from 50 to 500 mL) can be used, but smaller volumes could undersample part of the plankton population and larger bottles will need more water to be collected, larger incubator systems, and a larger volume of reagents. Borosilicate glass bottles are not trace metal clean and remove part of the UV radiation, which could affect the primary production rates (Regaudie de-Gioux et al., 2014; García-Corral et al., 2016). Quartz bottles can be used instead if the investigator wants to study the effects of UV radiation on NCP. In this case, the incubator should not be covered by a polycarbonate blue filter. In general, 100 mL borosilicate bottles are the preferred option. Bottles and their corresponding ground joint stoppers should be numbered (engraved numbers or with a water-resistant label). All bottles must be calibrated, and the volume of each bottle known to ±0.06 mL. As a standard procedure, borosilicate bottles are calibrated at 20°C. The volume of the bottles (V_{bottle}) experiment changes with temperature. Therefore, during the analysis of the sample, it is important to correct for the temperature effect on the volume by applying the equation

$$V_{bottle} = V_{bottle}\,[1 - \alpha(t - 20)], \quad (5.1)$$

where α is the volumetric coefficient of expansion of the glass (3.2×10^{-6} K^{-1} for borosilicate glass) and t is the temperature of the seawater sample.

We recommend at least 15 bottles per depth. Five bottles will be fixed before the incubation ("initial"), five bottles will be incubated in dark ("dark"), and the remaining five will be incubated under *in situ* simulated light conditions.

Before sampling, it is a good practice to confirm that all materials needed are in place (bottles, chemical reagents inside their dispenser bottles, a digital thermometer, the sampling sheet with the numbers of the bottles written down, and a pencil).

5.3. Shipboard Sampling Procedure

At each station, seawater samples will be collected from different depths using water samplers (Niskin bottles) mounted on a rosette system. It is recommended to sample a minimum of 6 depths, preferably 8, through the entire euphotic zone (depth at which the incident irradiance is 1% of surface irradiance). The sampling depths should include the surface depth, the euphotic depth, the depth of maximum chlorophyll, the depth at the top of the chlorophyll gradient, and the depth at the bottom of the chlorophyll gradient to properly determine the variability of the primary production rates (Fig. 5.1). Sampling should be done before sunrise.

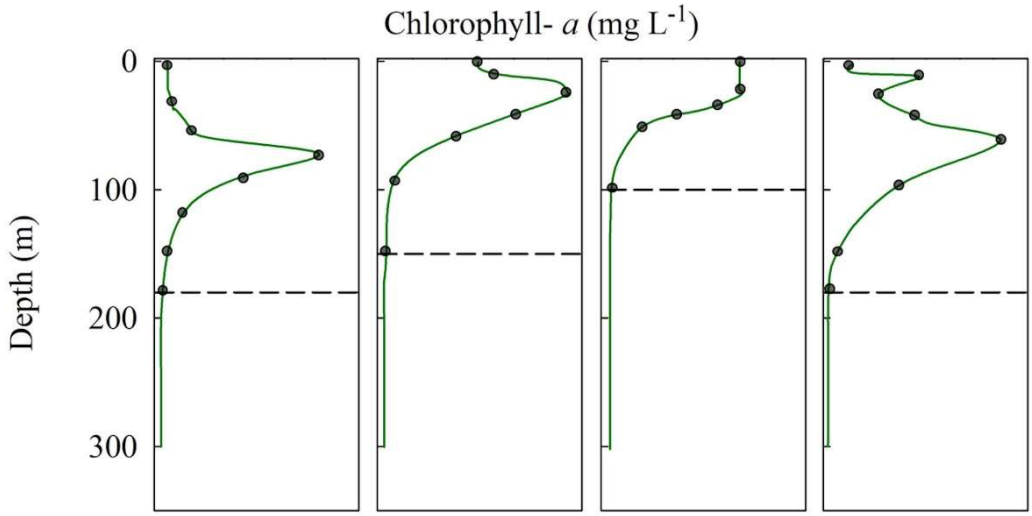

Fig. 5.1. Conceptual diagram showing vertical profiles of chlorophyll *a* fluorescence. In these examples, the grey dots represent the recommended sampling depths, and the dotted line indicates the position of the euphotic depth.

Acid-clean HDPE carboys are needed to transfer the seawater from the Niskin bottles. The carboys should be wrapped in black plastic bags to shield the samples from the boat lights. The transfer of 10 L of seawater from each Niskin to their corresponding acid-clean HDPE carboys is done by a Tygon or silicon tubing, rinsing the carboys at least three times prior to filling. The order for the sampling from the carboys into the dissolved oxygen bottles should be from the

deepest depth to the most surface one. This considers that the water sample from the deepest depth is colder and has lower oxygen concentration than surface waters.

Seawater is gently transferred from each carboy into the dissolved oxygen bottles using a sampling tubing, checking that bubbles are not formed and stuck into the tube. Ideally, bottles should be rinsed by filling them and letting the water overflow for three times the volume of the bottle. This step may seem wasteful, but it is essential to ensure the accuracy of the method. To avoid trapping bubbles in the bottle, fill it to the top of the bottle neck. Stoppers need to be rinsed and carefully placed to their corresponding bottle once all the bottles from the same depth are filled.

When all the carboys are sampled, it is time to fix the "initial" bottles. First, the temperature is measured from each bottle. Then, 1 mL of the $MnCl_2$ solution followed by 1 mL of the NaI/NaOH solution are added to each bottle, and the stoppers are replaced carefully without capturing any bubbles. The bottles are shaken vigorously by inverting them around 30 times. A second round is done to ensure that the reagents have reacted with all the oxygen. It is recommended to hold the stopper and the base of the bottle when shaking the bottles, as the stopper could pop up. The "initial" bottles are stored underwater, whereas the "dark" and "light" bottles are taken to their incubators. As the "dark" and the "light" bottles are incubated in the same incubators, the "dark" bottles must be covered to avoid any light inside the bottles. There are several options to darken them, including taping the bottle with electrical tape, wrapping it in aluminum foil, or using an opaque cloth. We do not recommend wrapping the bottles in tape as it can be difficult to check the appearance of bubbles inside the bottles during the incubation. Aluminum foil can be easily broken, allowing light to bounce inside the bottle. Hence, the preferred option is to use an opaque cloth/plastic bag.

5.4. Sample Incubation and Incubation Time

The incubation duration for estimating primary production (gross and net) with the dissolved oxygen incubation is 24 hours and is therefore considered a daily rate. The sampling is performed pre-dawn, with the incubation set to start during sunrise to contain the light and dark hours of the day. The oxygen consumption measured in the "dark" bottles represents the respiration over 24 hours, and it has the inherent assumption that the oxygen consumption in the light is equivalent to the oxygen consumption in the dark. This assumption was tested with 18O enrichment of dissolved O_2 and oxygen microelectrodes. It was found that oxygen consumption in the light could be greater than in the dark; therefore gross primary production could be underestimated when applying this method (Grande et al., 1989; Luz et al., 2002; Pringault et al., 2007; Robinson et al., 2009).

Incubation lasting 24 hours could introduce some biases associated with "bottle effects" that include changes in the mixing conditions, greater bacterial growth, and increase in grazing, among others (Robinson and Williams, 2005; Vernet and Smith, 2007; Gonzalez-Benitez et al., 2019). These biases could influence the respiration rates and therefore net community production. Yet, despite the potential changes in the community structure of the sample, several studies have shown a linear decrease in oxygen concentration, indicating that the respiration rate does not change during the incubation (Biddanda et al., 1994; Smith and Kemp, 2001; García-Martín et al., 2011).

5.4.1. In situ incubation

In situ incubations perfectly match the light intensity, spectral quality, and temperature during the incubation. The incubation system is usually formed by a buoy or a floating device with weights attached to the bottom and trays with hooks in which to secure the bottles (Fig. 5.2). Trays should be floating at the depths from which the seawater samples were collected. The hooks must be designed to hold the bottle stopper in position so the bottles cannot be accidentally opened during the incubation. It is recommended to lay light bottles on their side so the stoppers do not block the light.

This incubation implies the necessity to be close to the buoy during the 24 hours that the incubation lasts. Therefore, it is not very practical for cruises that cover and extensive sampling area but is ideal for coastal regions and experiments in a small research area.

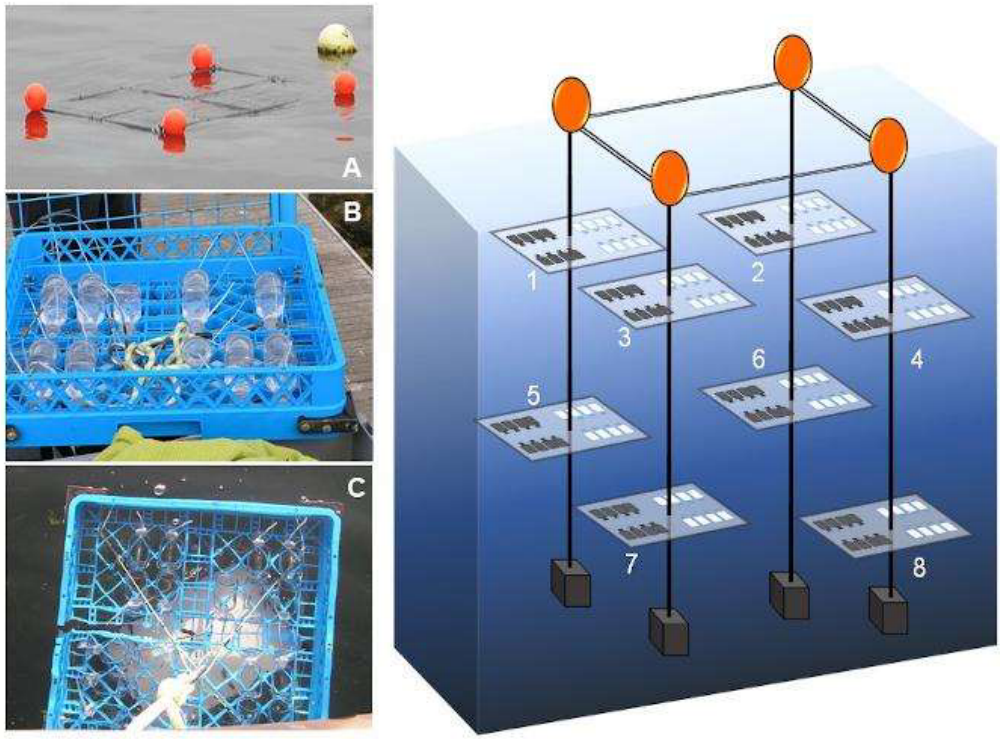

Fig. 5.2. Pictures of *in situ* incubations showing the different parts of the incubation system. (A) Floating buoys, (B-C) Incubation trays with light bottles, (D) schematic diagram of the whole system with 8 trays (numbers indicate 8 different incubation depths).

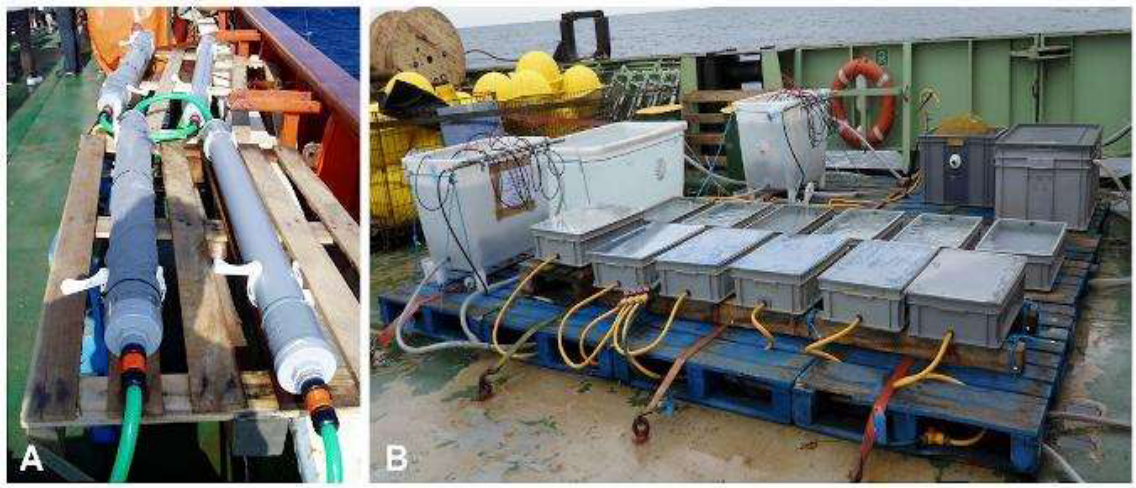

Fig. 5.3 Examples of different on deck incubators (A) cylindrical and (B) plastic boxes with plexiglass lids. Incubators are connected to water baths that supply water at *in situ* temperature.

5.4.2. On-deck incubations

On-deck incubations are an alternative to *in situ* incubations (Fig. 5.3), which require information about *in situ* variables, such as light intensity and temperature, to simulate *in situ* conditions. As the sampling is performed before sunrise, there is no information about the *in situ* light conditions from the sampling day. Therefore, generally, the PAR profile from the previous day is adopted.

Incubators can have different designs, but overall, the system consists of plexiglass containers with two connectors, one to pump water into the incubator and the other to let the water out. The *in situ* light intensities are adjusted with blue and neutral density filters. There should be as many incubators as depths sampled, so all the bottles are incubated approximately at their *in situ* light conditions. Temperature is controlled by running surface water into the system to the incubators containing the bottles from the surface depth or from those depths within the thermocline. For incubators containing bottles from deeper depths, usually at colder temperatures, chilled water is re-circulated from a chiller system. During night hours, it is recommended to cover the incubators with opaque plastic or cloth because the ship's lights could disturb the metabolic processes.

5.5. Sample Processing and Analysis

After the *in situ* or on deck incubations, all bottles ("light" and "dark") are removed from the incubators covered with dark plastic bags and taken to the laboratory. It is important to check for bubbles inside the bottles, as they can introduce biases to the measurements. Fixation is carried out following the same procedure as for the "initial" bottles described above (Section 2.3), recording the temperature just prior to the addition of the reagents. Once that all bottles are shaken, and the solution is uniform, they should be kept underwater in darkness, until the precipitate settles (usually 1–2 hours). Once the precipitate is settled in the bottom, the bottles are ready for analysis. It is convenient to proceed with the analysis straight after the settling

period, which is recommended to be comparable during the different sampling days. However, if a prompt analysis is not possible, bottles can be stored for many days without a detectable change in concentration when water seal is maintained (see GO_SHIP protocols, https://go-ship.org/HydroMan.thtml). However, we recommend minimizing the time they are stored as it is important to avoid temperature changes.

5.5.1. Titration method

There are three titration methods to determine the dissolved oxygen concentration of a water sample: photometric titration, potentiometric titration, and amperometric titration.

5.5.1.1. Photometric titration

The photometric endpoint detection method involves putting the sample bottle in the path of a beam of light and measuring the change in absorbance at 360 nm as I_2 is converted to a colorless form by adding thiosulfate. An automated version suitable for shipboard primary productivity use has been described by Williams and Jenkinson (1982). A typical precision of 0.03–0.1% was claimed.

5.5.1.2. Potentiometric titration

The potentiometric method involves measuring the potential measured across a dual platinum electrode. The endpoint is detected as a maximum in the change in potential per unit addition of thiosulfate. An automated version suitable for shipboard primary productivity use has been described by Oudot et al. (1988). A typical precision of 0.1% was claimed.

5.5.1.3. Amperometric titration

The amperometric method involves applying a potential of 100 mV to a dual platinum electrode placed into the sample bottle. The endpoint is detected as the point at which the current goes to zero. The amperometric method is also known as the “dead stop” method. An automated version suitable for shipboard primary productivity and routine hydrographic work has been described by Langdon (2010). A typical precision of 0.06% was claimed.

5.5.2. Blank determination

Reagents can contain impurities that may interfere with the reduction-oxidation reactions involved in the dissolved oxygen analysis. Therefore, it is essential to perform a reagent blank to quantify the reagents’ contribution to the changes in oxygen concentration. An empty bottle is filled with 100 mL of Milli-Q water and a stir bar. The reagent components are added in inverse order to the sampling procedure, mixing in between the additions. First, 1 mL of the H_2SO_4 is added, then 1 mL of the NaI-NaOH solution, followed by 1 mL of the $MnCl_2$ solution and 1 mL of the KIO_3 standard at the end. Sample titration is carried out until the endpoint is reached. Then another 1 mL of the KIO_3 standard is added and titrated again to find a second end point. The volume of the blank is calculated as V1–V2, where V1 is the volume of thiosulfate used to titrate the first KIO_3 aliquot, and V2 is the volume of thiosulfate used in the titration of the second KIO_3 aliquot. The blank sampling is repeated with ~5 replicates, and the blank value (V_{blk}) is the average of the five independent replicates.

5.5.3. Standardization of the thiosulfate

The thiosulphate concentration can change its molarity because of changes in temperature. Therefore, it is recommended to standardize it frequently, at least once per day of analysis.

Six empty bottles are filled with 100 mL of Milli-Q water and a stir bar. The reagent components are added in inverse order to the sampling procedure, mixing in between the additions. First 1 mL of the H_2SO_4 is added, then 1 mL of the NaI-NaOH solution, followed by 1 mL of the $MnCl_2$ solution and 10 mL of the KIO_3 standard at the end. The sample with reagents is titrated and the endpoint recorded.

The molarity of the thiosulphate solution is calculated as follows

$$M_{thio} = V_{KIO3} * N_{KIO3} /(V_{std} – V_{blk}), \quad (5.2)$$

where V_{KIO3} is the volume of KIO_3 standard added (mL), N_{KIO3} is the molarity of standard KIO_3 (mol/L), V_{std} is the volume of thiosulfate (mL), and V_{blk} is the volume of the blank as measured in the previous section (mL).

The molarity of the thiosulfate solution is determined as the average of the six replicates, and the standard deviation of the replicates should be lower than $1x10^{-6}$ (L). If the standard deviation is higher, additional samples should be considered.

5.5.4. Analysis of the samples

The analysis of the sample can start once the precipitate has settled. It is recommended to analyze the "initial," "dark," and "light" bottles from the same depth in the same batch. In addition, the precipitate is light-sensitive, so it is a good practice to remove only one or two bottles at a time for analysis. Any possible remaining water is wiped, the stopper removed, and a stir bar added into the bottle while taking care that the precipitate is not resuspended. The precipitate is dissolved by adding 1 mL of H_2SO_4 into the bottle and gently mixed. The sample in the bottle is titrated, and the added volume of thiosulfate at the endpoint is recorded. The oxygen concentration of the sample is then calculated by

$$[O2]\ (\mu mol/L) = [(¼) * 10^6 * (V_{sam} – V_{blk}) * M_{thio} – 7.6x10^{-8}] / (V_{bot} – V_{reg}), \quad (5.3)$$

where (¼) converts moles of thiosulfate to moles of O_2, 10^6 converts from moles O_2 to micromoles O_2, V_{sam} is the volume of the thiosulphate used during the titration of the sample (L), V_{blk} is the volume of the blank as measured in the previous Section (L), M_{thio} is the molarity of thiosulphate calculated during the standardization of the thiosulfate (mol/L), V_{bot} is the volume of sample bottle (L), V_{reg} is the volume of the reagents used during the fixation of the sample (0.002 L), and 7.6×10^{-8} is the absolute moles of oxygen added with the reagents (Murray et al., 1968).

If V_{KIO3}=0.010 L, N_{KIO3}=0.010 Equiv/L, V_{std}=0.000700, V_{blk}=0.000001, M_{thio}=0.14306, V_{sam}=0.000800, V_{bot}=0.143, V_{reg}=0.002, O_2=202.67 µmol/L.

Titrated samples should be discarded following the regulation of the country. The bottles are rinsed with deionized water once empty.

5.6. Calculation of Photosynthetic Rates of Phytoplankton

Measuring changes in dissolved oxygen concentration incubated over 24 hours provide two different primary production rates: gross primary production (GPP) and net community production (NCP).

Net community production is estimated as the difference in oxygen concentration between the average of the replicate "light" measurements and the average of the replicate "initial" measurements. Community respiration is estimated as the difference in oxygen concentration between the average of the replicate "dark" measurements and the average of the replicate "initial" measurements. Gross primary production is calculated as the difference between the average of the replicate "light" measurements and the average of the replicate "dark" measurements.

$$\text{NCP} = \text{average } [O_2]_{\text{light}} - \text{average } [O_2]_{\text{initial}} \quad (5.4)$$

$$\text{CR} = \text{average } [O_2]_{\text{dark}} - \text{average } [O_2]_{\text{initial}} \quad (5.5)$$

$$\text{GPP} = \text{NCP} + \text{CR} \quad (5.6)$$

5.7. Uncertainties/Accuracy

The precision of the oxygen method is estimated to be ±10–17 mmol C m^{-2} d^{-1} based on averaging the standard error of the means (SEM) obtained in the studies of Williams et al. 1983, Grande et al. 1989, and Robinson et al. 2009, assuming n=8–10 bottles at each depth. In other units, the average SEM was ±1.4 µg C L^{-1} (12 hours) $^{-1}$ and ±16 µg C (µg Chla)$^{-1}$ (12 hours) $^{-1}$.

Regarding the accuracy of the oxygen method, a previous report indicated that the oxygen method can underestimate NCP by 2–46% in waters where dissolved organic carbon and UV radiation are high due to the process of photochemical oxygen demand (Kitidis et al., 2014). If investigators are interested in quantifying the photochemical oxygen demand, we recommend filtering surface seawater through 0.2 µm filters, collecting the water, and filling quartz bottles using clean silicon tubing. Quartz bottles should be submerged in an irradiated solar simulator incubator with sea surface water running through it.

5.8. Cleaning Procedures

Silicone tubing and glass bottles should be cleaned with a 5–10 % hydrochloric acid solution before the start of the cruise. Glass bottles could be also cleaned with a dilute solution of non-phosphate detergent (i.e., Decon 90) followed by a vigorous rinse with Milli-Q water. Throughout the cruise, it is important that the silicone tubing is rinsed with 5–10 % hydrochloric acid plus Milli-Q water every day after using it. However, Milli-Q water could be used to rinse the glass bottles after the titration if they are going to be used the following day. The regular use of the bottles can lead to the appearance of yellowish/brownish stains on the inside of the neck of the bottle and on the stopper. Staining is caused by the accumulation of tracers of reagents in the grounded areas of the bottle. It is better to remove the stains as soon as they are noticed and not let them dry or accumulate for long periods, as removal could be more difficult. If stains start to appear in the neck of the bottle, we recommend adding a small volume of concentrated

thiosulphate and leaving it for a couple of minutes up to hours. If staining is on the stopper, a small volume of thiosulphate can be added on top of it, or the stopper can be put in a vase covered with thiosulphate. Once the stain disappears, the bottle or/and stopper are rinsed with Milli-Q to remove any remaining thiosulphate, which could bias the measurements.

5.9. Advantages, Disadvantages, and Caveats

All methodologies have strengths and limitations. Therefore it is important to know these and their potential errors to choose the best method for the research interest and study area. The Winkler-based light/dark incubation is a very accessible, inexpensive, and precise method to estimate net community primary production, gross primary production, and community respiration rates. To achieve high precision, it is important to be meticulous and have high numbers of "light," "dark," and "initial" replicates. The large number of bottles needed implies collection of large volumes of seawater and long analytical times, which in some circumstances (i.e., research cruises with a small rosette, high water demands, or low human capability) could be considered a drawback. The equipment required is easily portable and can be mounted in land-based laboratories or research vessels. Furthermore, the reagents needed are not radioactive. Therefore the method can be applied in all laboratories and research vessels and does not require the presence of a certified radioactive responsible person.

The main limitation of the Winkler-based light/dark incubation method is that rates are calculated from two single points measured over 24 hours. As mentioned in Section 5.4, the method assumes linear oxygen consumption in the dark bottles between the two incubation times. However, if the oxygen consumption is not linear (Gattuso et al., 2002; Pomeroy et al., 1994), it could underestimate or overestimate the GPP calculation.

The Winkler-based light/dark incubation method has several limitations that are common to other methodologies. Like any *in vitro* incubation, the method cannot accurately mimic the *in situ* environmental condition. In addition, enclosing a water sample inside bottles could potentially affect the plankton community structure, which may affect the metabolic rates. This is a common drawback for all methods that confine seawater samples in bottles (i.e., oxygen microelectrodes or optodes, ^{14}C tracer method and ^{13}C tracer method) and are not exclusive to this technique. However, the longer incubation time required for the Winkler-based light/dark incubation method (24 hours compared to other methods (12 hours for the ^{14}C tracer method) may amplify the potential biases. Another common caveat is that on-deck incubations may not receive the same irradiance quantity and quality as *in situ* incubations. Thus, the selection of on-deck or *in situ* incubations could provide different primary production rates (Barber et al., 1997). However, there is evidence that primary production rates derived from ^{14}C fixation method in the northeast Atlantic were comparable when incubated on-deck and *in situ* (Joint et al., 1993), suggesting that the choice of the incubation method does not imply a systematic bias.

Despite the method being straightforward, it is important to be meticulous in the procedures as there are several potential sources of error. We will comment on the most common ones.

- All bottles should be carefully calibrated with their respective stoppers. Stoppers may get chipped with use, which could cause changes in the bottle volume. If noticed, bottles should be marked and calibrated again.

- Before starting the titration, it is essential to shake the bottle containing the thiosulphate properly and flush the burette and the connecting tubes to remove any possible remains of thiosulphate leftover from prior analyses. Thiosulphate left from the previous day could have a different concentration than the thiosulphate inside the dispenser bottle and subject the first samples titrated to errors.

- During the flushing process, checking for air bubbles in the burette and in the connecting tubes is recommended. The presence of an air bubble during the titration procedure will affect the precision of the measurement, as the volume of air will be registered as a volume of thiosulphate. This implies that the volume of thiosulphate dispensed by the titrator will not be the amount calculated by the software. There are several ways to remove air bubbles. If the air bubble is in the tip or in the connecting tubes, the easiest way to remove it is to gently tap the burette tip and connecting tubes while the thiosulphate is flushing. An alternative method is more appropriate if the air bubble is in the burette and flows forward and backward through the connecting tubes while flushing and filling the burette. In this case, it will be necessary to unscrew the upper valve of the burette very quickly while the air bubble gets flushed out of the burette through the connecting tubes. It is recommended to do it while wrapping the valve with paper towels, so the thiosulphate drips onto the towel instead of onto the electrical equipment. If the air bubble is not easily removed, for example, it forms on the inside surface of the burette, the easiest approach will be to unscrew the burette from the upper valve and remove the burette from the dispenser unit. After discarding the thiosulphate from inside the burette, it should be filled with thiosulphate manually using a clean glass syringe/pipette. Once filled, it will be connected back to the dispenser unit. In theory, a stuck air bubble that does not get flushed should not bias the readings. However, it is recommended to remove it, as it could be released during the titration process and go unnoticed.

- During sample analysis, we do not recommend acidifying more than two bottles at once as the iodine concentration may decrease due to evaporation and light degradation while waiting to be analyzed. If two bottles are acidified at the same time, the bottle waiting should be covered and kept away from the light. In addition, it is crucial to keep the room temperature as stable as possible, as changes in temperature may facilitate the evaporation of the iodine while being titrated.

5.10. Ancillary Data Collection

Several environmental data, such as temperature, salinity, light attenuation, and fluorescence, are fundamental to the application and interpretation of the results for *in situ* and on-deck incubations, as explained in Gundersen and Vandermeulen (Chapter 6). First, this information is needed to choose the sampling depths. Second, temperature and light irradiance information is essential for the on-deck incubations to select the neutral filters and regulate the temperature of the water bath system. In addition, oxygen saturation can be calculated as a function of temperature and salinity (García and Gordon, 1992). Changes in the oxygen saturation in the initial bottles compared to the *in situ* oxygen saturation may affect the microbial community and interfere with the estimations of the metabolic rates, especially in the undersaturated deep sampling depths.

5.11. References

Barber, R. T., Borden, L., Johnson, Z., Marra, J., Knudson, C., & Trees, C. C. (1997, February). Ground truthing modeled-kPAR and on deck primary productivity incubations with in-situ observations. In *Ocean Optics XIII* (Vol. 2963, pp. 834–839). SPIE.

Biddanda, B., Opsahl, S., & Benner, R. (1994). Plankton respiration and carbon flux through bacterioplankton on the Louisiana shelf. *Limnology and Oceanography*, *39*(6), 1259–1275.

Carpenter, J. H. (1965). The accuracy of the Winkler method for dissolved oxygen analysis 1. *Limnology and Oceanography*, *10*(1), 135–140. https://doi.org/10.4319/lo.1965.10.1.0135

Carrit, D. E. (1966). Comparison and evaluation of currently employed modifications of the Winkler method for determining oxygen in seawater. A NASCO Report. *J. Mar. Res.*, *24*, 286–318.

Culberson, C. H., & Huang, S. (1987). Automated amperometric oxygen titration. *Deep Sea Research Part A. Oceanographic Research Papers*, *34*(5–6), 875–880.

Emerson, S. (2014). Annual net community production and the biological carbon flux in the ocean. Global Biogeochemical Cycles, 28(1), 14–28. https://doi.org/10.1002/2013GB004680

Gaarder, T. (1927). Investigations of the production of plankton in the Oslo Fjord. Rapports et Proces-verbaux des Reunions. *Conseil International pour 1'Exploration de la Mer*, *42*, 1–48.

Garcia, H. E., & Gordon, L. I. (1992). Oxygen solubility in seawater: Better fitting equations. *Limnology and Oceanography*, *37*(6), 1307–1312.

Garcia-Corral, L. S., Holding, J. M., Carrillo-de-Albornoz, P., Steckbauer, A., Pérez-Lorenzo, M., Navarro, N., ... & Agusti, S. (2017). Effects of UVB radiation on net community production in the upper global ocean. *Global Ecology and Biogeography*, *26*(1), 54–64.

García-Martín, E. E., Serret, P., & Pérez-Lorenzo, M. (2011). Testing potential bias in marine plankton respiration rates by dark bottle incubations in the NW Iberian shelf: incubation time and bottle volume. *Continental Shelf Research*, *31*(5), 496–506.

Gattuso, J. P., Peduzzi, S., Pizay, M. D., & Tonolla, M. (2002). Changes in freshwater bacterial community composition during measurements of microbial and community respiration. *Journal of Plankton Research*, *24*(11), 1197–1206.

Gattuso, N. G. J. P., & Middelburg, J. J. (2008). Oxygen production and carbon fixation in oligotrophic coastal bays and the relationship with gross and net primary production. *Aquatic Microbial Ecology*, *52*(2), 119–130.

González-Benítez, N., García-Corral, L. S., Morán, X. A. G., Middelburg, J. J., Pizay, M. D., & Gattuso, J. P. (2019). Drivers of microbial carbon fluxes variability in two oligotrophic Mediterranean coastal systems. *Scientific Reports*, 9(1), 1–13.

Grande, K. D., Marra, J., Langdon, C., Heinemann, K., & Bender, M. L. (1989). Rates of respiration in the light measured in marine phytoplankton using an 18O isotope-labelling technique. *Journal of Experimental Marine Biology and Ecology*, 129(2), 95–120.

Joint, I., Pomroy, A., Savidge, G., & Boyd, P. (1993). Size-fractionated primary productivity in the northeast Atlantic in May–July 1989. *Deep Sea Research Part II: Topical Studies in Oceanography*, 40(1–2), 423–440.

Kitidis, V., Tilstone, G. H., Serret, P., Smyth, T. J., Torres, R., & Robinson, C. (2014). Oxygen photolysis in the Mauritanian upwelling: Implications for net community production. *Limnology and Oceanography*, 59(2), 299–310.

Koblentz-Mishke, O. J. (1967). Primary production. [Russ.] In: The Pacific Ocean; biology of the Pacific Ocean, I. Plankton, pp 86–97. Ed. By V. G. Bogorov. Moscow, Moskva Izdat Nauk.

Langdon, C. (2010). Determination of dissolved oxygen in seawater by Winkler titration using the amperometric technique. In BM Sloyan and C. Sabine, eds. GO-SHIP repeat hydrography manual: a collection of expert reports and guidelines. IOC/IOCCP, Paris.

Luz, B., Barkan, E., Sagi, Y., & Yacobi, Y. Z. (2002). Evaluation of community respiratory mechanisms with oxygen isotopes: A case study in Lake Kinneret. *Limnology and Oceanography*, *47*(1), 33-42.

Murray, C. N., Riley, J. P., & Wilson, T. R. S. (1968). The solubility of oxygen in Winkler reagents used for the determination of dissolved oxygen. *Deep Sea Research A*, *15*(2), 237–238.

Natterer K. (1892). Chemische untersuchungen in östlichen Mittelmeer. Denkschr. Akad. Wiss., Wien, 59, 83–92

Oudot, C., Gerard, R., Morin, P., & Gningue, I. (1988). Precise shipboard determination of dissolved oxygen (Winkler procedure) for productivity studies with a commercial system 1. *Limnology and Oceanography*, *33*(1), 146–150.

Pomeroy, L. R., Sheldon, J. E., & Sheldon Jr, W. M. (1994). Changes in bacterial numbers and leucine assimilation during estimations of microbial respiratory rates in seawater by the precision Winkler method. *Applied and environmental microbiology*, *60*(1), 328–332.

Pringault, O., Tassas, V., & Rochelle-Newall, E. (2007). Consequences of respiration in the light on the determination of production in pelagic systems. *Biogeosciences*, *4*(1), 105–114.

Regaudie-de-Gioux, A., Agustí, S., & Duarte, C. M. (2014). UV sensitivity of planktonic net community production in ocean surface waters. *Journal of Geophysical Research: Biogeosciences*, *119*(5), 929–936.

Robinson, C., Serret, P., Tilstone, G., Teira, E., Zubkov, M. V., Rees, A. P., & Woodward, E. M. S. (2002). Plankton respiration in the eastern Atlantic Ocean. *Deep Sea Research Part I: Oceanographic Research Papers*, *49*(5), 787–813.

Robinson, C., Widdicombe, C. E., Zubkov, M. V., Tarran, G. A., Miller, A. E., & Rees, A. P. (2002). Plankton community respiration during a coccolithophore bloom. *Deep Sea Research Part II: Topical Studies in Oceanography*, *49*(15), 2929–2950.

Robinson, C., Tilstone, G. H., Rees, A. P., Smyth, T. J., Fishwick, J. R., Tarran, G. A., ... & David, E. (2009). Comparison of in vitro and in situ plankton production determinations. *Aquatic Microbial Ecology*, *54*(1), 13–34.

Robinson, C., & Williams, P. L. B. (2005). Respiration and its measurement in surface marine waters. *Respiration in Aquatic Ecosystems*, 147–180.

Serret, P., Robinson, C., Aranguren-Gassis, M., García-Martín, E. E., Gist, N., Kitidis, V., ... & Thomas, R. (2015). Both respiration and photosynthesis determine the scaling of plankton metabolism in the oligotrophic ocean. *Nature Communications*, *6*(1), 1–10.

Smith, E. M., & Kemp, M. W. (2001). Size structure and the production/respiration balance in a coastal plankton community. *Limnology and Oceanography*, *46*(3), 473–485.

Vernet, M., & Smith, R. C. (2007). Measuring and modeling primary production in marine pelagic ecosystems. *Principles and Standards for Measuring Primary Production*, 142–174.

Williams, P. L., & Jenkinson, N. W. (1982). A transportable microprocessor-controlled precise Winkler titration suitable for field station and shipboard use 1. *Limnology and Oceanography*, *27*(3), 576–584.

Williams, P. L. B., Heinemann, K. R., Marra, J., & Purdie, D. A. (1983). Comparison of 14C and O2 measurements of phytoplankton production in oligotrophic waters. *Nature*, *305*(5929), 49–50.

Winkler, L. W. (1888). Die bestimmung des im wasser gelösten sauerstoffes. Berichte der deutschen chemischen Gesellschaft, 21:2843-2854.

6. Calculating Net Community Production and Respiration from Continuous Optode Measurements

Kjell Gundersen[1] and Ryan A. Vandermeulen[2,3]
[1]*Plankton Research Group, Institute of Marine Research, Bergen, Norway*
[2]*Science Systems and Applications, Inc., Maryland, USA*
[3]*NASA Goddard Space Flight Center, Maryland, USA*

6.1. Introduction

In this section, we describe the best practices for estimating gross and net community production (GPP and NCP) and community respiration (CR) rates derived from optode sensors that continuously measure dynamic luminescence quenching of dissolved oxygen (DO) within a controlled volume. Incubation bottles retrofitted with an optode sensor can be deployed *in situ* or used *in vitro* in laboratory experiments or deck-board incubations. The optode technology is relatively new to aquatic sciences and has only recently been used in CR studies (Warkentin et al., 2007; Wikner et al., 2013; Lehner et al., 2015) and combined measurements of NCP and CR (Vandermeulen, 2012; Collins et al., 2018).

Early optode technology in aquatic biology (Klimant et al., 1995) was not commercially available and was primarily aimed at replacing the use of microelectrodes (Revsbech et al., 1980) in benthic sediments. The "microoptrode" (Klimant et al., 1995), later renamed "micro-optode" (Glud et al., 1999a), was essentially a foil matrix attached to the tapered tip of an optical glass fiber cable. The micro-optode was first used to follow oxygen developments in microbial mats and benthic sediments in shallow waters and to create micro-depth profiles of oxygen in deep-water sediments (Glud et al., 1999a, 1999b). So far, the optode sensor foil is only supplied by one manufacturer (PreSens GmbH, Germany). In recent years, the same optode foil has been built into commercially available oxygen sensors, such as "sensor spots" or "planar optodes" from the same manufacturer (Tengberg et al., 2006; Warkentin et al., 2007).

Some of the greatest advantages to the optode technology, are that it does not utilize oxygen molecules (e.g., like the Clark electrode) and that it measures DO continuously. The DO optode sensor consists of a unique hydrophobic silicone foil embedded with a platinum porphyrin compound that illuminates (red fluorescence) when excited by a blue or green LED light. The DO molecules interfere with the fluorescence characteristics of the foil membrane (dynamic luminescence quenching) in proportion to its concentration (and temperature) in water (Tengberg et al., 2006). Thus, DO concentration can be measured non-invasively through internal monitoring of the luminescence in the sensor foil. The foil is sensitive to direct sunlight and is therefore stabilized in an analyte-permeable matrix to shield it from UV light. However, this poses a challenge to gas diffusion and response times since a more effective coating necessarily means less permeability. A lot of effort in recent years has been put into improving the response time in optodes (initially estimated at 15–30 seconds) by improving permeability of the protective coating. Macro-sensors with optode technology today (Table 6.1) have similar response times to conventional DO sensors (e.g., the Clark electrode).

Table 6.1

Reported DO-optode macro-sensors showing type of sensors, precision, accuracy, and response time. Type of sensor calibration and applications are also listed.

Reference	Sensor	Precision (μM)	Accuracy (±μM)	Response time (s)	Calibration	Application
Tengberg et al. 2006	AADI 3830, 3930	0.5–1	< 5 & < 2	45	2-point & n=30	*In situ* measurements
Uchida et al., 2008	AADI 3830	12	10	21	2-point	*In situ* measurements
Vandermeulen, 2012	AADI 3830	0.6	NA	<3 0	2-point	*In situ* NCP, CR incubations
Wikner et al., 2013	AADI 3830	0.3	4.2	25	2-point	*In vitro* CR incubations
Collins et al., 2018	AADI 4531D	< 1	8	< 30	2-point	*In situ* NCP, CR incubations
Vikström et al., 2019	AADI 4330	0.2	5.8	NA	N=12	*In vitro* CR incubations

AADI = Aanderaa Data Instruments; NA = not available

This chapter presents an overview of commercially available, standalone optode sensors (Table 6.2), where only a subset can be reasonably retrofitted to incubation containers. Wikner et al. (2013) and later Vikstrøm et al. (2019) used Aanderaa Data Instruments (AADI) optodes and measured CR in 1 L glass bottles in the dark (Fig. 6.1A). The original micro-optode (see above) has also been retrofitted (Fig. 6.1B) and can now measure CR in the nanomolar range in natural seawater (Lehner et al., 2015). The first light-dark *in situ* incubations were reported by Collins et al. (2018) using AADI optodes retrofitted to large volume polycarbonate chambers (2.6 and 5.7 L) that were lowered and closed at depth (Fig. 6.1C). Vandermeulen (2012) mounted an AADI optode inside a 1 L polycarbonate bottle for *in situ* surface deployments (Fig. 6.1D). Below we discuss the use of two *in situ* optode incubators: One automated system for *in situ* sampling and direct NCP and CR measurements (Collins et al., 2018) and one manually sampled incubator used in daylight surface waters in a turbid estuary in the northern Gulf of Mexico (Vandermeulen, 2012).

Table 6.2

List of commercial vendors (alphabetical order) that offer optode technology.

Vendor	Product
Aanderaa Data Instruments, Norway	Oxygen Optode (3830, 3930, 3975, 4330, 4835, 4831)
Alec Electronics Co., Japan	RINKO series, RINKO-profiler, AAQ-RINKO
Franatech GmbH, Germany	Model D-Opto
HACH, USA	Luminescent Dissolved Oxygen (LDO) sensor
Ocean Optics, USA	FOXY Fiber Optic Oxygen Sensor
PreSens, Germany	Optical O2 sensors
Precision Measurement Engineering Inc., USA	miniDOT Logger, miniDOT Clear Logger
PyroScience GmbH, Germany	FireSting O2 Optical Oxygen Meter
Sea & Sun Technology GmbH, Germany	Fast SST-DO oxygen sensor
SeaBird Scientific, USA	SBE 63 Optical Dissolved Oxygen Sensor
Unisense A/S, Denmark	O_2 Microoptode
YSI-Xylem, USA	YSI 6150 Reliable Oxygen Sensor (ROX)

There are several benefits to optode sensor incubations, such as ease of use, near-continuous, non-intrusive readings of oxygen levels, and the ability to subsample water samples from the incubation bottle (e.g., for microscope counts or biogeochemical parameters) upon termination of the incubation period. Fast repetitive oxygen sensors, such as the DO-optode, are also ideal for kinetic measurements (e.g., light response curves) on a time scale that cannot be reached with other conventional batch incubation methods for NCP and CR measurements (i.e., the light/dark bottle method). Continuous oxygen measurements in natural seawater incubations *in situ* clearly demonstrate that DO-optodes are highly responsive to fast environmental changes such as photosynthetic active radiation (PAR, Fig. 6.2).

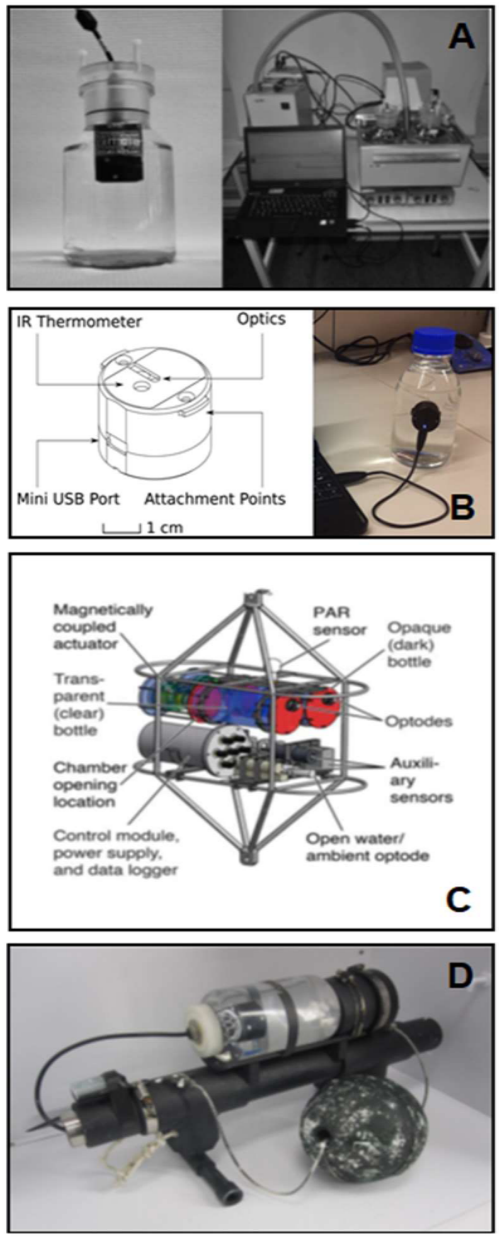

Fig. 6.1. Examples of DO-optodes used in *in vitro* and in field incubations. (A) Wikner et al. (2013) measured CR *in vitro* using an Aanderaa Data Instruments (AADI) 3833 oxygen optode, (B) (Lehner et al., (2015) created a Luminescence Measuring Oxygen Sensor (LUMOS) for *in vitro* CR measurements in the nanomolar range, (C) Collins et al. (2018) retrofitted water samplers with AADI 4531 DO-optodes for *in situ* sampling and NCP and CR measurements, and (D) Vandermeulen (2012) retrofitted an AADI 3835 optode to an incubation bottle for *in situ* NCP and CR measurements. All images are reprinted in accordance with the authors and publisher's terms of use.

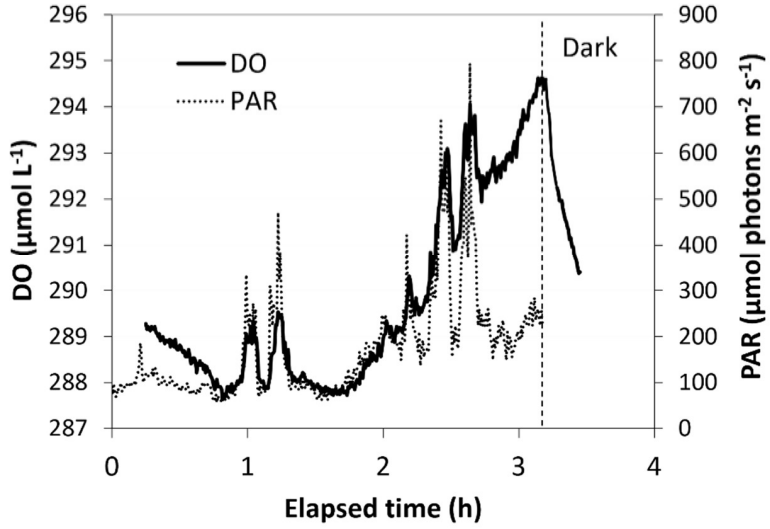

Fig. 6.2. Changes in DO concentration (solid line) and subsurface photosynthetic active radiance (PAR, dotted line) measured in the Mississippi Sound on July 21, 2011 (Vandermeulen and Gundersen, unpubl.). Zooplankton > 200 um was gently removed from a surface water sample and incubated in a polycarbonate bottle retrofitted with an AADI 3835 DO-optode and a gimballed magnet stirrer (see Fig. 6.3 for details). The DO incubation bottle and data logger were mounted on a PVC frame (Fig. 6.1D) and fitted with a HOBO Pendant® sensor (UA-002-08, Onset Computers) that recorded incident PAR at 0.25 m depth during the incubation.

6.2. Best Practices

6.2.1. Sensor accuracy and precision

Most DO-optodes are calibrated from the manufacturer (multiple-point calibrations), but we recommend the user regularly recalibrate the foil membrane sensitivity. The DO-optode is commonly calibrated by exposing the sensor to oxygen-free (anoxic) and completely gas-saturated (100%) conditions in a two-point calibration. Zero DO concentration can be obtained by adding sodium sulfite (5% w/v conc. With trace amounts of cobalt (II) chloride as a catalyst) or sodium dithionite to tap water (e.g., Warkentin et al., 2007, Staudinger et al., 2018). Air-saturated water can be obtained by shaking a bottle of water vigorously (Staudinger et al., 2018), but we prefer to bubble air through the tap water using an aquarium pump for about 1 hour. By then, the tap water is oversaturated and will have to sit for an equal amount of time to equilibrate. Most commercial software used with DO-optodes have a two-point calibration, but some studies (e.g., Tengberg et al., 2006; Vikström et al., 2019) have opted for multiple-point calibrations (n=30 and n=12, respectively) to improve accuracy (Table 1). Tengberg et al. (2006) used a 30-point calibration curve of their DO-optode and managed to improve accuracy from < 5 µmol O_2 L^{-1} to < 2 µmol O_2 L^{-1} deviation. They concluded, however, that most *in situ* applications (e.g., productive coastal waters) show DO gradients on a much larger scale and hence, a two-point batch calibration should be sufficient (Tengberg et al., 2006). In general, low accuracy is not detrimental to DO-optode incubations as we often follow short-term time-course developments of oxygen (relative change over time) in a closed container. The precision of a DO-optode, however (Table 6.2), as demonstrated below, is inherently crucial to short-term NCP and CR determinations. Historically, NCP and CR measurements in low-production environments have been a challenge to conventional sensors.

Table 6.3

A guide to estimating required incubation time to resolve metabolic rates (NCP, CR) based on optode sensor precision. Table shows estimated minimum incubation length needed to gain sufficient signal to noise at different precision levels with the DO-optode. A higher biomass signal relative to sensor noise enables the resolution of shorter-term changes in derived rates.

		Precision (±µmol O_2 $L^{-1}h^{-1}$)			
		0.2	0.5	1	2
	NCP, CR (µmol O_2 $L^{-1}h^{-1}$)	Minimum incubation length (h)			
Oligotrophic waters	0.1	4	10	20	40
Shelf areas	1	0.4	1	2	4
Coastal waters	5	0.08	0.2	0.4	0.8
Eutrophic waters	10	0.04	0.1	0.2	0.4

A significant signal-to-noise ratio would require a large plankton biomass, as is most often the case in highly productive waters (Table 6.3). In open ocean oligotrophic waters, rate extrapolations from long-term incubations are often necessary to get significant NCP or CR rates. Note, as discussed in Section 6.2.8, post-processing binning procedures can be used to reduce the inherent noise of the optode but comes at the cost of reduced confidence in the derived rate (resulting from a lower number of samples) and lower temporal resolution (negating one of the primary advantages of optode technology). The precision of the DO-optode sensor (e.g., the AADI optode at ±0.2 µmol O_2 L^{-1}; Tengberg and Hovdenes, 2014) is in the same order as the precision of widely accepted Winkler titrations (± 0.06–0.12 µmol O_2 L^{-1}; see Langdon and García-Martín, Chapter 5), with the added benefit of continuous measurements. The latter range was estimated by assuming 0.03% precision for photometric titrations, 0.06% precision for amperometric titrations, and a generic DO concentration level of 200 µmol O_2 L^{-1}. In this chapter, we argue that a 2-point batch calibration of the DO-optode (and an accuracy of < 5 µmol O_2 L^{-1}) is sufficient to estimate GPP, NCP, and CR rates in a closed incubator.

DO-optodes appear to be stable (months to years), but after only 2–3 days of continuous deployment, the optode signal may drift due to the appearance of biofouling (Tengberg et al., 2006). Stirring (e.g., by a magnetic stirrer inside an incubation bottle) does not affect the optode sensor itself (Klimant et al., 1995), but a DO-optode used on a profiling platform shows pressure hysteresis (approximately 4% per 100 m) that is fully recoverable at the surface (Tengberg et al., 2006). Temperature and conductivity affect the gas solubility of the foil membrane and hence, measured *in situ* DO concentrations; this should be accounted for in calculations and the expression of results (Uchida et al., 2008). All DO-optodes therefore depend on ambient temperature, conductivity, and depth readings for accurate results. The AADI optode only has a temperature sensor attached to the sensor casing and requires a separate input value for conductivity (salinity) to get accurate DO concentrations. This is not a major issue with *in vitro* incubations, where a separate reading of salinity, using an independent conductivity sensor, can be entered at the beginning of the incubation. In instances that also require *in situ* readings (e.g., the Collins et al. (2018) setup in Fig. 6.1C) in a changing environment where salinities can vary, independent and concurrent conductivity readings are necessary to get accurate AADI DO-optode concentrations. Accuracy of the DO-optode (Table 6.1) is now well documented (Tengberg et al., 2006; Uchida et al., 2008, Wikner et al., 2013; Vikström et al., 2019) and comparable to determinations by the Winkler titration method (Winkler, 1888; Carpenter, 1965; Strickland and Parson, 1972). Since DO-optodes provide stable readings over long periods

(months to years), we consider inaccurate recalibrations and biofouling the two most significant sources of error for these sensors in field applications.

6.2.2. Response time

The optode's ability to respond to abrupt changes in DO concentrations (usually calculated as the time it takes to go from zero oxygen to 65% or 90% of DO saturation) is defined as the response time (t_{65}, t_{90}). Manufacturers are usually reporting the response time in pure oxygen gas solutions and at optimal temperatures (20–25ºC) to claim optimal response for their product (from fractions to 10–15 seconds); these are rarely achieved *in situ* at suboptimal temperatures. Response times reported in the literature (Table 6.1) are therefore often found to be longer since they are estimated in a liquid solution and at lower temperatures. Due to a relatively slower response time than, e.g., the Clark-electrode in water (2–10 seconds), the DO-optode initially appeared less suited for profiling applications. However, the DO-optode has frequently been applied in fixed and moveable buoy platforms where the response time is less critical as DO concentrations are measured continuously on longer time scales. Since the response time depends on temperature and oxygen dissolution over a permeable foil membrane (Bittig et al., 2014), the protective layer of black silicone used to protect against ambient light and optical interference from the surrounding water (Klimant et al., 1995) may slow the response time. A thinner layer would give a faster response time but comes with the risk of making the sensor unstable. Improvements to the oxygen gas diffusion of the silicone coating and, in some cases, combined with the use of a water pump in a closed space void of ambient light, imply that optodes are comparable to other conventional DO sensors in profiling applications.

6.2.3. The incubation bottle

The choice of an incubation chamber is an important consideration when measuring changes in dissolved oxygen concentrations in a controlled volume. Polymer materials are advantageous because they are more robust than glass in standing up to dynamic sea conditions and deployments. However, most available polymers are not transparent to the whole specter of natural sunlight and the ones that are (e.g., acrylic and polycarbonate) may still have PAR attenuation issues (see below). Polymers can also be a source of dissolved organic carbon (DOC) and other volatile compounds that may influence the incubation, and this is best remedied by repeated acid-soaking of the incubation bottle ahead of use. Air-dry polymers are also permeable to gas and, if not preconditioned, they can leak (desorb) dissolved oxygen into the water sample and compromise metabolic rate measurements (Wikner et al., 2013). It is also possible that oxygen may get absorbed by the polymers used inside incubators (e.g., stoppers or the acetal casing of some optode sensors) if the sample is not preconditioned, which may compromise measurements by artificially removing oxygen from the water sample. Stevens (1992) measured desorption of polymer materials and found that nylon, acetal, and polyvinylchloride (PVC) released the least amount of oxygen. Acrylic and high-density polyethylene (HDPE) were more permeable, while polycarbonate and Teflon bottles showed the highest gas permeability. Incubator bottles made of polymers should therefore be "preconditioned" by soaking them in water at a similar DO concentration and temperature to *in situ* conditions (minimum 24 hours) to expel air-saturated oxygen from the dry material. However, the use of these polymers inside incubation bottles should be minimized or completely avoided when assessing extremely low biological rates (e.g., in hypoxic environments or oligotrophic waters). It is also recommended that a test is performed using sterilized (autoclaved) tap water to check for non-biological drift of

the DO-optode (i.e., gas absorption or desorption of dissolved oxygen) over a time course like the one intended for the actual incubation. Glass bottles are less robust but have no gas permeability issues and, for NCP measurements, only quartz glass show minimal attenuation over the entire spectrum of visible light.

Beyond permeability, incubation bottles can also impact the quality of light in optode incubations. Most polymers and borosilicate glass (e.g., Pyrex) are opaque to UVB radiation and may underestimate the impact of UV stress/photoinhibition on metabolic rates (Gala and Giesy, 1991; Regaudie-de-Gioux et al., 2014). Quartz bottles are most transparent to UV radiation, but this may not be so important if neutral density (or blue) filters are used to cause UV attenuation in deck-board incubations (e.g., Robinson et al., 2009). If photoinhibition processes are the focus of your study, quartz bottles should be used without UV-attenuating filters. We find that quartz bottles retrofitted for optodes are hard to come by and most likely will have to be custom-made for this purpose. Therefore, it may be more practical (and inexpensive) to use polymer containers (e.g., PVC or polycarbonate bottles) for *in situ* and deck-board incubations.

Note that the incubation bottle containing the optode must be impermeable to gas/water exchange at the incubation time. When creating a seal between removable parts, avoid using nitrile O-rings or any organic leaching material (e.g., rubber stoppers or rubber cords in Niskin bottles) that can adversely impact biological rates (Williams and Robertson, 1989; Matsumoto et al., 2012). We recommend the use of Viton O-rings and non-toxic stoppers (never silicon stoppers) for incubation bottles. Before use, the incubation bottles and sealing material should be washed with a dilute solution of trace meta–free, non-ionic detergent, followed by thorough rinsing with purified (Milli-Q) water that has been sterilized. Both sensors and bottles should be left soaking in sterile Milli-Q water to desorb for at least 24 hours prior to use.

6.2.4. Sample water collections

Sample water should be collected immediately before the incubation takes place, and great care should be taken to avoid introducing air bubbles when filling the incubation bottle. Collins et al. (2018) collected water directly *in situ* using a timer to close the PHORCYS incubator (Fig. 6.1C). The benefit of direct sampling *in situ*, immediately followed by an *in situ* incubation in the same bottle, is that the body of water is left undisturbed. However, there is no way to prescreen the incubation water to remove larger zooplankton (see details below).

The most common way of collecting sample water is by using a Niskin-type water sampler that can be fired at discrete depths. Non-toxic O-rings should be used in the sealed water samplers (e.g., the original Niskin bottle with stainless steel spring or the relatively new Niskin-X) or other similar equipment used for collecting Winkler titration samples. The benefits of using water samplers are that sample water can be size fractionated. Still, there are challenges to collecting water at depth that is subsequently processed at the surface (e.g., the sudden change in temperature, pressure, and dissolved oxygen concentration) that may inadvertently change the water's physical characteristics.

A third option is to only collect surface water to avoid the sudden change in temperature, pressure, and dissolved oxygen concentrations by using a large volume bucket (Vandermeulen, 2012) or a Niskin-type water sampler. If a large volume bucket is used (10–20 L), the incubation water can be prescreened directly by reverse filtration (Vandermeulen, 2012), and the incubation bottle filled by lowering the entire bottle directly into the sample water (use long gloves). For

diurnal (sunrise to sunset) or 24-hour diel incubations, sample water should be collected before first light (ideally 1 hour before sunrise). For daily NCP and CR estimates, the incubator bottle should be deployed before sunrise and retrieved after sunset. If this is not possible, great care should be taken to avoid abrupt changes in temperature (work fast), and the water sample should not be exposed to direct sunlight prior to *in situ* deployment (use a tent or canopy for dim light conditions).

6.2.5. Sample volume and prescreening

Incubation bottle size has, in principle, no limit for DO-optode incubations. Wikner et al. (2013) opted for no prescreening of their samples, as the literature suggests that most respiration (99–100 %) can be accounted for by cells < 200 µm (Robinson and Williams, 2005 and references therein). However, in coastal waters in spring, when there is a high abundance of mesozooplankton (> 10 individuals L^{-1}), there is a good chance that larger zooplankton can be included in the incubation chamber (Wikner et al., 2013). Therefore, if the study aims to also include mesozooplankton, or even macrozooplankton, we recommend using natural seawater in a large incubation bottle (>> 2 L) and no prescreening of the sample. On the other hand, if you are looking at small-scale processes, including the most abundant micro- and nano-plankton, we suggest a smaller incubation bottle (e.g., 1 L) where individuals > 200 µm (predominantly meso- and macrozooplankton) have been separated by gentle, reverse filtration (see Vandermeulen, 2012 for details).

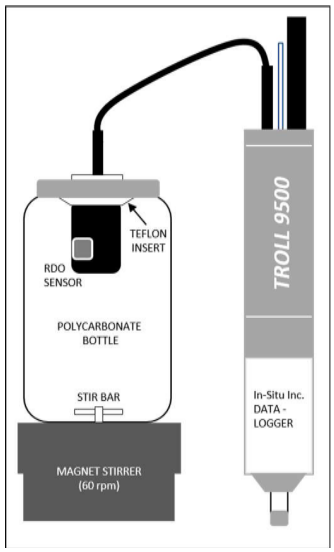

Fig. 6.3. DO-incubator retrofitted with an AADI 3835 oxygen optode mounted inside the lid of a 1L polycarbonate centrifuge bottle. The optode was attached to an In-Situ Instruments Troll 9500 data logger. A magnetic stir bar was mounted in a gimble suspension attached to the bottom of the PC bottle to avoid heterogeneity in the bottle during incubations. The stir bar was rotated by a magnetic stirrer (70 rpm) positioned immediately outside the bottom of the incubation bottle. To avoid contamination from oxygen trapped in the Teflon insert and the PC bottle itself, the unit was soaked in tap water in near-*in situ* temperature for a minimum of 48 hours before incubation. From Gundersen and Vandermeulen (unpubl.).

6.2.6. In situ incubations

Most DO-optodes are standalone units designed for long and short-term *in situ* deployments in the water column, or short-term monitoring of benthic DO profiles in sediments (Table 2). Therefore, most units are not specifically designed for an incubation chamber that requires gas-tight conditions. Some of the available AADI available are relatively small units with a bulkhead mount for the sensor platforms used by the company. So far, they are the design most used in *in situ* incubations (Fig. 6.1C and 6.1D).

An *in situ* DO-incubator can be retrofitted with an optode mounted inside the incubation chamber lid or another point in the chamber that can be sealed (e.g., Fig. 6.3). Collins et al. (2018) opted for a complete *in situ* system (Fig. 6.1C) with polycarbonate incubation bottles (5.7 L usable volume) fitted with DO-optodes. The PHORCYS incubation bottles automatically open and close at designated time intervals. This solution enables undisturbed *in situ* incubations of whole seawater samples, where CR (dark bottle) and NCP (clear bottle) are measured simultaneously. The PHORCYS is also equipped with an array of other sensors keeping track of environmental parameters that may influence measured NCP and CR (CTD, external DO-optode, 2pi PAR sensor, beam transmissometer, chlorophyll fluorometer). Vandermeulen (2012) retrofitted a DO-optode in a polycarbonate bottle (Fig. 6.3) that was mounted on a surface float (Fig. 6.1D). Early *in situ* incubations revealed that more stable, homogenous readings were achieved by a slowly rotating magnet stirrer (Fig. 6.4). The unit was soaked in tap water at room temperature for a minimum of 48 hours prior to each incubation to avoid desorption (Stevens 1992). The surface float, equipped with a HOBO sensor (temperature and PAR), was deployed manually at sunrise (Vandermeulen, 2012).

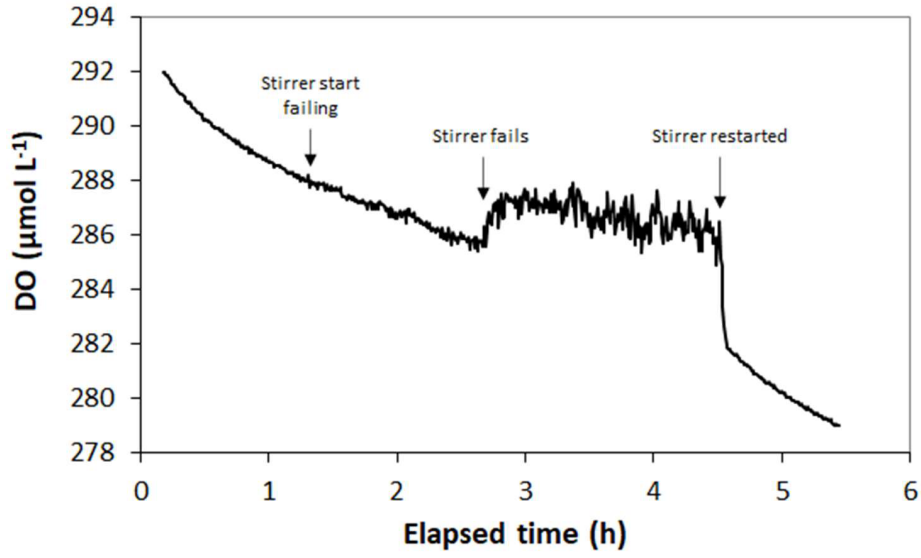

Fig. 6.4. Changes in DO concentration in a PC incubation bottle (see Fig. 6.3 for details) where the magnet stirrer (70 rpm) stopped working. The incubator (Fig. 6.1D) was quickly retrieved, batteries replaced, and the unit was covered in double layers of heavy-duty aluminum foil for the dark incubation (CR) as the stirrer was restarted. From Vandermeulen and Gundersen (unpubl.).

DO-optodes are prohibitively expensive compared to BOD bottles and Winkler titrations. Since we are still in an exploratory phase of *in situ* incubations with DO-optodes, we have no data on replicate *in situ* optode incubations. Collins et al. (2018) solved this by estimating the standard error of the linear regression as a measure of uncertainty, combined with an adjusted degree of freedom. However, as they also point out, this approach does not fully account for biological variance between incubation bottles from *in situ* patchiness (see Appendix in Collins et al., 2018 for details). The variability between replicate incubation bottles may exceed optode accuracy and precision faster, especially in highly productive waters with high biological activity. Therefore, replicate incubation volumes > 1 L that are not prescreened for larger swimmers (mesozooplankton) may have an even greater potential to develop differently and express differing NCP or CR rates than < 200 µm incubations.

6.2.7. Time-course incubations

Collins et al. (2018) measured NCP and CR rates simultaneously in sub-Arctic open ocean waters using the PHORCYS incubator (Fig. 6.1C) over a wide range of incubation times (10–94 hours). Similarly, Gundersen and Vandermeulen (unpubl.) determined NCP from *in situ* light incubations (2–4 hours), immediately followed by a short dark incubation to determine instantaneous CR (0.2–0.3 hour), in a strongly eutrophic estuary in the northern Gulf of Mexico (Fig. 5). The continuous recordings of DO in both these incubations, showed that rates of NCP are typically not linear throughout a day (Fig. 6.5; Collins et al., 2018).

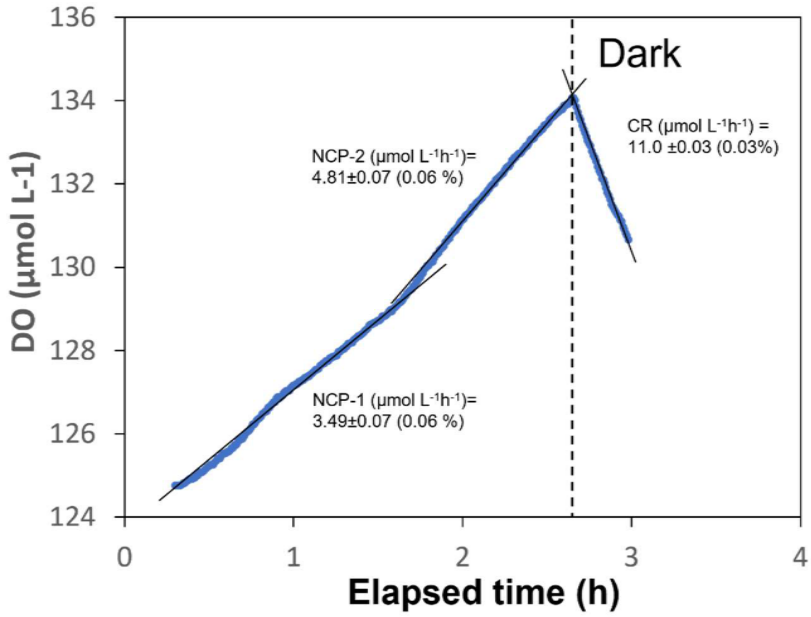

Fig. 6.5. NCP and CR measured in the Mississippi Sound on September 13, 2010. Surface seawater was collected at sunrise using a 20 L bucket, and zooplankton > 200 µm was gently removed by gently lowering another bucket with a 200 µm Nytex screen in the bottom. The < 200 µm incubation water was collected in a PC bottle retrofitted with an AADI 3835 optode and a gimballed magnet stirrer (see Fig. 6.3 for details). The DO incubation bottle was mounted on a PVC frame (Fig. 6.1D) for approximately 2.5 hours at 0.25 m depth (NCP). The unit was quickly retrieved, wrapped with double layers of heavy-duty aluminum foil, and redeployed for a 15 min dark incubation (CR). Sensor sampling frequency was 0.03 Hz (blue markers) two significantly different periods of production were identified (NCP-1, NCP-2), and one rate of dark respiration (CR) was calculated. In a separate test, an incubator was filled with sterilized water (DO blank) but showed no uniform sensor drift (±0.3 µmol L^{-1}).

These changes could result from changes in incident irradiance or *in situ* temperature. DO-optode readings (which are temperature sensitive) can be slightly off with abrupt changes in *in situ* temperature. Also, abrupt response in community photosynthesis to changes in incident irradiance (PAR) is well documented in the literature and previously in this chapter (Fig. 6.2). Therefore, differences in the rate of DO may change rates of NCP and CR throughout a day and hence, should be considered when calculating daily metabolic budgets. Gross primary production (GPP) is calculated from NCP and CR (GPP = NCP + CR). During periods of low photosynthesis (e.g., at low incident irradiance), DO concentrations in the light incubated bottles may show no net changes when GPP equals CR (NCP = 0). Collins et al. (2018) and Fig. 6.4 show that in some cases, the optode signal in the light-incubated bottle may show a decrease in DO concentrations with time (NCP < 0), but as DO consumption in the dark incubated bottle will be equal or greater than in the light bottle, the calculated GPP rate will still be zero or positive. These observations only emphasize the importance of accurate CR (dark bottle) estimates in daily GPP determinations.

6.2.8. Incubation length

Contrary to BOD incubations and Winkler DO-titrations, optodes can measure short-term changes in the DO concentration in the order of minutes to hours (e.g., Fig. 6.5). This is partially a function of a high sampling rate (n) of continuous measurements, which clusters values more around the true population mean compared to incremental values, reducing the standard deviation, and thus enabling an increased capability to resolve subtle rate changes. However, this enhanced utility is highly dependent on the level of ambient biological rates. For example, in oligotrophic waters where GPP often is balanced by daytime CR, longer incubation times may be required to overcome the sensor sensitivity. To illustrate the impacts of this sensitivity, we modeled two constant linear rates of oxygen evolution (0.1 and 2.0 µmol O2 L-1 h-1) and introduced controlled random Gaussian noise bounded by various manufacturer precision levels of 0.2–2.0 µmol O2 L-1 (Fig. 6.6). At low rates of oxygen evolution (Fig. 6.6A) that are indicative of extremely oligotrophic waters (Williams et al., 2004), only the highest precision measurements (< 0.5 µmol O2 L-1) can resolve linear rates over 12 hours. If the preservation of a high sampling rate is not a priority for the incubation, the incremental averaging of output values in post-processing can work to increase the relative precision of the optode, assuming that the noise component of the signal is purely random. However, there are additional limitations and uncertainties to consider when doing this. Using the modeled time series, Fig. 6.7 shows the standard error of several linear regressions as a function of data points averaged for various optode precision levels. This demonstrates how much data must be averaged to achieve various levels of equivalent precision performance. For example, according to Fig. 6.7, a sensor with a precision of ±2.0 µmol O2 L-1 would require averaging of ~128 data points to achieve a precision level adequate to resolve changes on the scale of 0.1 µmol O2 L-1 h-1. How this translates to total incubation length depends on the sampling rate of the sensor, e.g., 128 data points at a sampling rate of 1/30 seconds would represent an averaging of 64 minutes of data to retrieve one “high precision” data point. Depending on the sampling logistics, biological rates, and experimental objectives, this technique could become prohibitive. At lower ambient biological rates, random biases may have a higher impact on the derived slope/rate due to having too few data points to derive a robust regression. In a series of 100 randomized simulations, the binning of lower precision data to dampen noise and estimate a rate of 0.1 µmol O2 L-1 h-1 resulted in an average rate of 0.1 ±0.04 µmol O2 L-1 h-1 (up to 38% difference).

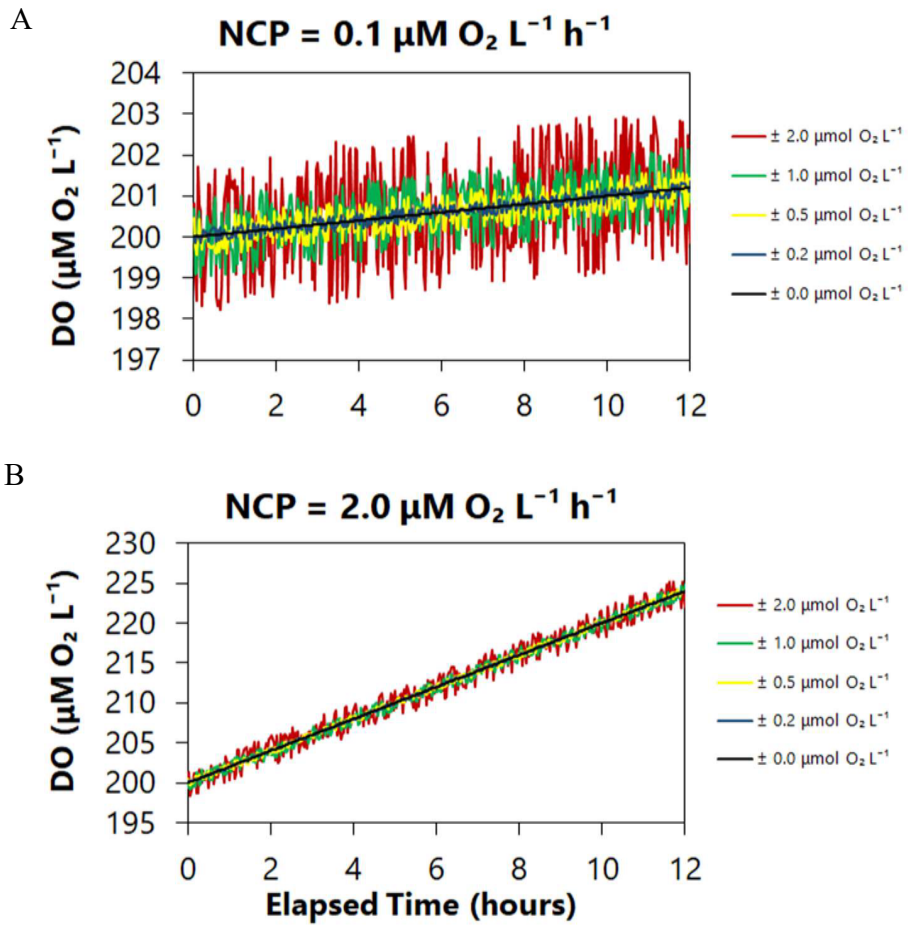

Fig. 6.6. Demonstration of changes in DO concentration in a time course at varying levels of optode sensor precision (±µmol L^{-1} conc. on right side). The simulated time course is shown for (A) low rates of NCP typically encountered in oligotrophic waters, and (B) moderate rates commonly found in coastal/shelf environments.

More moderate oxygen evolution rates (Fig. 6.6B) exhibit more flexibility with regard to overcoming the signal-to-noise ratio at all precision levels, and higher precision sensors offer the ability to make shorter term rate assessments. This analysis can be extended more quantitatively to determine the length of time it takes for a given rate of oxygen evolution to exceed the magnitude of random noise by a factor of two, thus guiding recommendations for minimum incubation duration for various sensor precision levels (Table 6.3). Finally, incubation bottles retrofitted with a slow-moving magnetic stirrer (Fig. 6.3) may also improve the precision of your DO-readings, and this is clearly demonstrated in Fig. 6.4. We also note that the linear extrapolated rates of NCP and CR in the northern Gulf of Mexico (Fig. 6.5) using a slow-moving stirrer had very good precision (0.03–0.07 µmol O_2 L^{-1}).

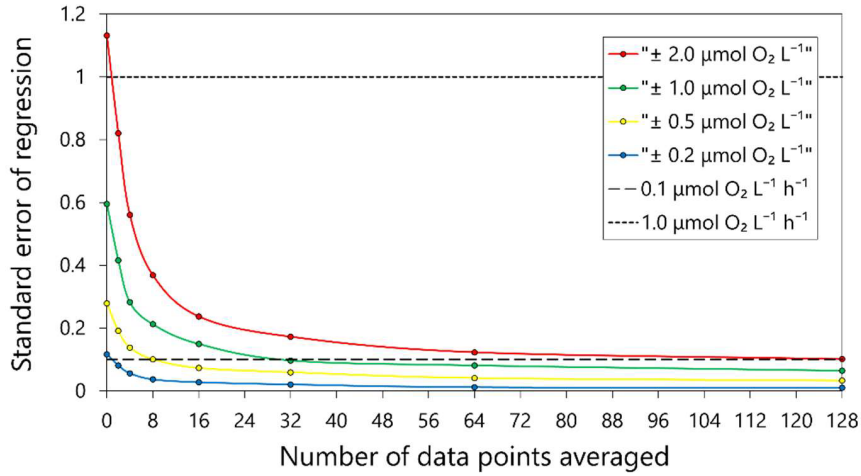

Fig. 6.7. Average data points used to dampen the impact of sensor noise on the derivation of NCP at the expense of resolution of short-term kinetics. The standard error of the least squares linear regression of $\Delta O_2 \Delta t^{-1}$ as a function of data points averaged is shown for various simulated sensor precision levels. For reference, dashed horizontal lines represent low (0.1 µmol O_2 L^{-1} h^{-1}) and moderate (1.0 µmol O_2 L^{-1} h^{-1}) NCP rates. Ideally, the standard error of the regression should approach targeted rate, combined with the maximized collection of individual data points, to increase confidence in the fit. A point of diminishing returns is reached when averaging inhibits the ample collection of data points for the regression.

6.3. Calculations and Expressions of Results

6.3.1. Expression of results

If ambient pressure and temperature readings are available (see Ancillary Data below), you will have several options of available units for your DO readings (mL L^{-1}, mg L^{-1}, µmol L^{-1}). At standard temperature and pressure (STP), it follows that O_2 L^{-1} can be expressed as

1 µmol = 44.6596 mL = 31.2512 mg.

Early reports on DO determinations, such as the descriptions of the Winkler titration method, were in mg-at L^{-1} or mL L^{-1} (Strickland and Parsons, 1972). The v/v unit has been used up until recent years and can still be seen in long-term monitoring data archives going back multiple decades. Currently, the most common denomination for DO is µmol O_2 L^{-1} in oceanography. Accurate DO-optode profile measurements today are commonly compensated for temperature, conductivity, and pressure changes as a function of depth (Uchida et al., 2008).

Rates of net community production (NCP) and community respiration (CR) can be calculated directly from linear regressions (e.g., Fig. 6.5). Gross primary production (GPP) is calculated as the rate of NCP corrected for community respiratory losses (GPP = NCP + CR). NCP and CR rates can also be expressed in carbon units (see PQ and RQ conversion below). Also, NCP is often normalized to autotroph biomass (measured as Chlorophyll *a*) since this, despite its flaws (Ramaraj et al., 2013), is one of the most common biomass estimates of the phototroph community. Detecting dissolved oxygen changes in light and dark bottle incubations is a function of metabolic rates (NCP and CR), sensor precision, and the length of the incubation

(Table 6.3). In low productive regions, changes in the dissolved oxygen concentration, as a function of time, may become increasingly difficult to differentiate isolated segments of NCP and CR within a day as signal-to-noise ratio is low (Fig. 6.6). For an overall long-term estimate, this can to some extent be remedied by extending the incubations period (Table 6.3) in extreme environments. To detect changes in dissolved oxygen concentrations in oligotrophic oceans, i.e., to get an estimate within the confines of a day, we recommend an optode precision < 0.2 µmol O_2 L^{-1} (Table 6.3). Likewise, in all other regions (coastal and shelf areas), you can obtain significant daily rates with an optode precision in the 2–5 µmol O_2 L^{-1} range (Table 6.3). Still, this level of precision may not aid in determining varying NCP and CR rates during the course of a day.

6.4. PQ and RQ Conversion

The photosynthetic quotient (PQ) is the molar ratio of oxygen development to carbon biomass by primary productivity. Autotroph cellular carbohydrate synthesis, and protein synthesis utilizing ammonia as an N-source, have both a PQ approximating 1, while other common cellular products (proteins synthesized from nitrate as an N-source and lipids) are in the range of 1.4–1.6 (Valiela, 1984, and references therein). Robinson and Williams (1999) demonstrated the huge variability in PQ from field studies and associated the estimated lower range (PQ=1.03) with cell synthesis using ammonium as the N-source, while the upper boundary matched theoretical cell synthesis based on nitrate (PQ=1.4). Recommended choice of PQ will depend on *in situ* concentrations of ammonium and nitrate. However, many current PQ estimates are from dawn-to-dusk incubations of BOD bottles (light-and-dark bottles) and CO_2 assimilation by the ^{14}C-bicarbonate method. These two approaches have inherent differences since Winkler BOD is a less sensitive method than ^{14}C-incubations. Hence, these ratios may become highly variable and inaccurate in extreme environments (e.g., at depth, at low light, and with minimal photosynthesis). The wide range in respiration quotients (RQ) reported by Robinson and Williams (1999) can also be ascribed to uncertainty with the methods (Winkler BOD and DIC analysis) in addition to variable substrate compositions. “Typical” plankton material would have a theoretical RQ=0.89 (Williams and Robertson, 1991; Hedges et al., 2002) based on stoichiometry alone (see details in the introduction to this report). We also note that since NCP is a balance between GPP and CR (GPP = NCP + CR), PQ cannot be applied directly to calculate a carbon-based NCP. Instead, selected PQ and RQ should be applied to GPP and CR, respectively, and NCP is calculated as the difference between the two (NCP = GPP – CR).

6.5. Ancillary Data Collection

The changing regime of physical parameters with depth, such as ambient temperature, salinity, and light attenuation, is essential to interpret the results from *in situ* incubations. In addition to the community composition of auto- and heterotrophs inside the incubation bottle, temperature and incident light are perhaps the two parameters with most profound impact on NCP and CR rates throughout an incubation. A number of light irradiance sensors are set up to measure PAR (400–700 nm), but UVA and UVB inhibition (radiation in the 280–400 nm range) is not accounted for in these measurements. Therefore, if light inhibition is an important focus of your study, you may want to consider a full spectral light sensor in addition to PAR determinations. We strongly recommend that, at a bare minimum, *in situ* PAR and temperature are monitored during the course of an incubation. Likewise, Chl-*a* biomass and measurements of dissolved inorganic nutrients are also helpful parameters for interpreting rate measurements from

DO-optode incubations. Ideally, as incubation technology advances, several of these measurements may eventually take place inside the incubation chambers themselves.

Optode incubation chambers are unique in that they can be sampled for ancillary data before and after deployment. Therefore, any remaining sample water not used in the incubator can be analyzed at the start. Due to its non-invasive nature, the sample water inside the incubator can also be sampled after deployment. Of special interest are parameters describing the community composition (abundance estimates of auto- and heterotrophic plankton) and its potential development during the incubation period. A broader characterization of the photoautotrophs (than just Chlorophyll *a* estimates) may also be of interest. A more comprehensive characterization of the multitude of pigments can be obtained from HPLC and the use of CHEMTAX (e.g., Mackay et al., 1996 and others). More advanced instrumentation, such as flow cytometry for bacteria and imaging techniques, such as ZooSCAN (e.g., Grosjean et al., 2004) and FlowCAM (e.g., Le Bourg et al., 2015) for phyto- and zooplankton cell abundance and volume, are now also available. Alternatively, low-cost solutions to microscope imaging (e.g., the PlanktonScope) are now also showing promising results (Pollina et al., 2020). The latter techniques will, perhaps, replace more conventional cellular abundance detection by microscope with time.

Inside the DO-optode incubator, it may also be of interest to monitor environmental parameters that change during the incubation. These are, first and foremost, the macronutrients (dissolved inorganic, dissolved organic, and particulate derivatives), which together with ambient light, are essential for all biological activity inside the incubator. Dissolved inorganic nutrients (nitrate, nitrite, phosphate, silicate, and ammonium) are measured with conventional techniques (e.g., Strickland and Parsons, 1972; Becker et al., 2020) and may become depleted during longer time-course incubations. Available nutrients are also paramount in your choice of photosynthetic and respiratory quotients (see Section 6.4) for your expression of results.

6.6. Summary

6.6.1. Advantages

The main advantage of DO-optodes over Winkler determinations is the capacity to measure continuous changes in oxygen concentrations over time. With careful maintenance and calibrations, the optode is an accurate and precise sensor for oxygen measurements with a reasonable response time that covers changes in DO concentrations for most NCP and CR processes in an incubation bottle. For these reasons, DO-optodes can also be used to calculate NCP and CR rates on shorter timescales and with greater precision than what is possible in a Winkler BOD incubation. Since optodes provide near-continuous measurements of DO in an incubator bottle (with time-resolution as low as 30 seconds), it is possible in regions with high primary productivity to conduct short-term manipulations (e.g., light-dark treatments) to elucidate short-term NCP and CR rates.

To account for the metabolic rates (NCP and CR) associated with most organisms, the volume of the incubator ought to be > 1 L, which this has been a challenge in Winkler BOD incubations. In theory, the volume in optode incubations can be of infinite size. However, it is a logistical challenge to handle large-volume containers and keep the incubation volume homogenous. Abundance estimates indicate that plankton organisms < 200 μm account for 99% of CR and are adequately represented in a 1 L incubator.

6.6.2. Caveats

Compared to expenses associated with Winkler BOD incubations, the cost of an optode is considerably more expensive, which may limit the number of available sensors for an investigator. The expression of results from DO-optodes is highly dependent on concurrent conductivity (salinity) and temperature readings. DO gas dissolution also depends on ambient conductivity and pressure, but in an incubator bottle, this will not change (contrary to temperature) provided that the incubation depth remains constant. On a short-term temporal scale, the optode is also sensitive to diffusion issues and microscale biological activities during an incubation, which may appear as noise in the DO readings. However, if the goal is to measure whole community rates in a given volume of seawater, microscale production and respiration can be avoided by using a slow-moving magnetic stirrer (50–70 rpm) mounted in a gimble.

The optode foil membrane may also experience interference from hydrogen peroxide, gaseous sulfur dioxide, and chlorine (cross-sensitivity), but this is usually not an issue in most natural environments. Incubations at deeper depths will lead to membrane hysteresis, and inaccurate DO readings. If the incubator is kept at the same depth for the longevity of the incubation and precision is maintained, these may not significantly impact NCP and CR rate calculations.

6.7. Acknowledgements

This work was partially supported by Northern Gulf Institute research grant 09-NGI-13 to Kjell Gundersen. The authors would also like to thank Elena García-Martín for comments on an early version of this chapter.

6.8. References

Becker, S., Aoyama, M., Woodward, E.M.S., Bakker, K., Coverly, S., Mahaffrey, C., & Tanhua, T. (2020). GO-SHIP Repeat Hydrography Nutrient Manual: The Precise and Accurate Determination of Dissolved Inorganic Nutrients in Seawater, Using Continuous Flow Analysis Methods. *Frontiers in Marine Science*, *7*, 581790. https://doi.org/10.3389/fmars.2020.581790

Bittig, H. C., Fiedler, B., Scholz, R., Krahmann, G. & Körtzinger, A. (2018) Time response of oxygen optodes on profiling platforms and its dependence on flow speed and temperature. *Limnology & Oceanography: Methods*, *12*, 617–636.

Collins, J. R., Fucile, P. D., McDonald, G., Ossolinski, J. E., Keil, R. G., Valdes, J. R., ... & Van Mooy, B. A. (2018). An autonomous, *in situ* light-dark bottle device for determining community respiration and net community production. *Limnology & Oceanography: Methods*, *16*(6), 323–338.

Gala, W. R., & Giesy, J. P. (1991). Effects of ultraviolet radiation on the primary production of natural phytoplankton assemblages in Lake Michigan. *Ecotoxicology and Environmental Safety*, *22*(3), 345–361.

Glud, R. N., Klimant, I., Holst, G., Kohls, O., Meyer, V., Kühl, M., & Gundersen, J. K. (1999a). Adaptation, test and *in situ* measurements with O2 microoptodes on benthic landers. *Deep-Sea Research Part I: Oceanographic Research Papers*, *46*(1), 171–183.

Glud, R. N., Kühl, M., Kohls, O., & Ramsing, N. B. (1999b). Heterogeneity of oxygen production and consumption in a photosynthetic microbial mat as studied by planar optodes. *Journal of Phycology*, *35*(2), 270–279.

Grosjean, P., Picheral, M., Warembourg, C., & Gorsky, G. (2004). Enumeration, measurement, and identification of net zooplankton samples using the ZOOSCAN digital imaging system. *ICES Journal of Marine Science*, *61*(4), 518–525.

Holtappels, M., Tiano, L., Kalvelage, T., Lavik, G., Revsbech, N. P., & Kuypers, M. M. (2014). Aquatic respiration rate measurements at low oxygen concentrations. *PloS One*, *9*(2), e89369.

Hedges, J. I., Baldock, J. A., Gélinas, Y., Lee, C., Peterson, M. L., & Wakeham, S. G. (2002). The biochemical and elemental compositions of marine plankton: A NMR perspective. *Marine Chemistry*, *78*(1), 47–63.

Klimant, I., Meyer, V., & Kühl, M. (1995). Fiber-optic oxygen microsensors, a new tool in aquatic biology. *Limnology & Oceanography*, *40*(6), 1159–1165.

Le Bourg, B., Cornet-Barthaux, V., Pagano, M., & Blanchot, J. (2015). FlowCAM as a tool for studying small (80–1000 μm) metazooplankton communities. *Journal of Plankton Research*, *37*(4), 666–670.

Lehner, P., Larndorfer, C., Garcia-Robledo, E., Larsen, M., Borisov, S. M., Revsbech, N. P., ... & Klimant, I. (2015). LUMOS-A sensitive and reliable optode system for measuring dissolved oxygen in the nanomolar range. *PloS One*, *10*(6), e0128125.

Mackey, M. D., Mackey, D. J., Higgins, H. W., & Wright, S. W. (1996). CHEMTAX-a program for estimating class abundances from chemical markers: application to HPLC measurements of phytoplankton. *Marine Ecology Progress Series*, *144*, 265–283.

Matsumoto, K., T. Fujiki, M. C. Honda, M. Wakita, H. Kawakami, M. Kitamura, & T. Saino. 2012. Inhibition of primary production by nitrile rubber O-rings in Niskin sampler. *AMSTEC Report of Research and Development*, *14*, 17–25.

Pollina, T., Larson, A. G., Lombard, F., Li, H., Colin, S., de Vargas, C., & Prakash, M. (2020). PlanktonScope: affordable modular imaging platform for citizen oceanography. *BioRxiv*. https://doi.org/10.1101/2020.04.23.056978

Ramaraj, R., Tsai, D. D., & Chen, P. H. (2013). Chlorophyll is not accurate measurement for algal biomass. *Chiang Mai J. Sci*, *40*(4), 547–55.

Regaudie-de-Gioux, A., Lasternas, S., Agustí, S., & Duarte, C. M. (2014). Comparing marine primary production estimates through different methods and development of conversion equations. *Frontiers in Marine Science*, *1*, 19.

Robinson, C., & Williams, P. J. le B. (1999). Plankton net community production and dark respiration in the Arabian Sea during September 1994. *Deep-Sea Research Part II: Topical Studies in Oceanography*, *46*(3–4), 745–765.

Robinson, C., & Williams, P. L. B. (2005). Respiration and its measurement in surface marine waters, pp 147–180. In: del Giorgio, P.A. & Williams, P.J. le B., Respiration in aquatic ecosystems, Oxford University Press.

Robinson, C., Tilstone, G. H., Rees, A. P., Smyth, T. J., Fishwick, J. R., Tarran, G. A., ... & David, E. (2009). Comparison of in vitro and *in situ* plankton production determinations. *Aquatic Microbial Ecology*, *54*(1), 13–34.

Staudinger, C., Strobl, M., Fischer, J. P., Thar, R., Mayr, T., Aigner, D., ... & Fritzsche, E. (2018). A versatile optode system for oxygen, carbon dioxide, and pH measurements in seawater with integrated battery and logger. *Limnology and Oceanography: Methods*, *16*(7), 459–473.

Stevens, E. D. (1992). Use of plastic materials in oxygen-measuring systems. *Journal of Applied Physiology*, *72*(2), 801–804.

Strickland, J.D.H. & Parsons, T.R. (1972) A practical handbook of seawater analysis. *Fisheries Research Board of Canada, Bulletin 167*, pp 310.

Tengberg, A., Hovdenes, J., Andersson, H. J., Brocandel, O., Diaz, R., Hebert, D., ... & Rey, F. (2006). Evaluation of a lifetime-based optode to measure oxygen in aquatic systems. *Limnology & Oceanography: Methods*, *4*(2), 7–17.

Tengberg, A., & Hovdenes, J. (2014). Information on long-term stability and accuracy of Aanderaa oxygen optodes; information about multipoint calibration system and sensor option overview. Aanderaa Data Instruments AS Tech. Note.

Uchida, H., Kawano, T., Kaneko, I., & Fukasawa, M. (2008). *In situ* calibration of optode-based oxygen sensors. *Journal of Atmospheric and Oceanic Technology*, *25*(12), 2271–2281.

Valiela, I. (1984). Producers and processes involved in primary production. In Marine ecological processes (pp. 3–37). Springer, New York, NY.

Vandermeulen, R.A. (2012). Factors influencing the spatial and temporal distribution of primary productivity and community respiration in the Mississippi coastal Estuarine region. The University of Southern Mississippi, MS (thesis), pp 152.

Vikström, K., Tengberg, A., Wikner, J. (2019). Improved accuracy of optode-based oxygen consumption measurements by removal of system drift and non-linear derivations. *Limnology & Oceanography: Methods, 17*, 179–189.

Warkentin, M., Freese, H. M., Karsten, U., & Schumann, R. (2007). New and fast method to quantify respiration rates of bacterial and plankton communities in freshwater ecosystems by using optical oxygen sensor spots. *Applied and Environmental Microbiology*, *73*(21), 6722-6729.

Wikner, J., Panigrahi, S., Nydahl, A., Lundberg, E., Båmstedt, U., & Tengberg, A. (2013). Precise continuous measurements of pelagic respiration in coastal waters with oxygen optodes. *Limnology & Oceanography: Methods*, *11*(1), 1-15.

Williams, P. L., & Robertson, J. I. (1989). A serious inhibition problem from a Niskin sampler during plankton productivity studies. *Limnology and Oceanography*, *34*(7), 1300-1305.

Williams, P. I., & Robertson, J. E. (1991). Overall planktonic oxygen and carbon dioxide metabolisms: the problem of reconciling observations and calculations of photosynthetic quotients. *Journal of Plankton Research*, *13*(supp1), 153–169.

Williams, P. J. L. B., Morris, P. J., & Karl, D. M. (2004). Net community production and metabolic balance at the oligotrophic ocean site, station ALOHA. *Deep-Sea Research Part I: Oceanographic Research Papers*, *51*(11), 1563–1578.

7. *In Situ* Gross Primary Production from Triple Oxygen Isotopes

Rachel H. R. Stanley[1], Laurie W. Juranek[2], and David P. Nicholson[3]
[1]*Department of Chemistry, Wellesley College, Massachusetts, USA*
[2]*College of Earth, Ocean, and Atmospheric Sciences, Oregon State University, Oregon USA*
[3]*Marine Chemistry and Geochemistry Department, Woods Hole Oceanographic Institution, Massachusetts, USA*

7.1. Introduction

Rates of gross primary production (GPP) and net community production (NCP) yield important mechanistic information about the marine carbon cycle. Triple oxygen isotopes (TOI) of dissolved oxygen and the closely related O_2/Ar ratios (see Chapter 8) are gas tracers that can quantify GPP and NCP *in situ*. GPP, the total photosynthetic flux, represents the total amount of carbon processed in a biological system. It reflects the amount of energy coming from the sun and thus the maximal possible photosynthesis. Net primary production (NPP), which is often assessed by ^{14}C or ^{13}C incubations, represents GPP minus autotrophic respiration. NCP represents GPP minus autotrophic and heterotrophic respiration and represents the net amount of carbon that can be exported. Triple oxygen isotopes have been used to quantify GPP in the Atlantic (Howard et al., 2017; Luz and Barkan, 2000; 2009), Pacific (Haskell et al., 2016; Hendricks et al., 2005; Juranek and Quay, 2005; Juranek and Quay, 2010; Juranek et al., 2012; Palevsky et al., 2016; Quay et al., 2010; Stanley et al., 2010), Southern (Cassar et al., 2007; Goldman et al., 2015; Hamme et al., 2012; Hendricks et al., 2004; Reuer et al., 2007), and Arctic Oceans (Ji et al., 2019; Stanley et al., 2015), as well as in coastal environments (Haskell et al., 2017; Manning et al., 2019; Manning et al., 2017b; Munro et al., 2013), and salt marshes (Howard et al., 2020; Stanley and Howard, 2013).

Why care about GPP vs. the more commonly measured NPP? GPP is useful because it reflects the energy at the true base of the ecosystem and thus might be more directly related to environmental variables such as sunlight and chlorophyll than NPP. Hence it might be easier to develop parameterizations of GPP as a function of easily measured variables, either *in situ* or remotely sensed ones. Furthermore, including GPP directly in models allows for mechanistic cell allocation models (Nicholson et al., 2018). The most powerful approach is to measure all three types of production concurrently: GPP, NPP, and NCP. When all three production types are measured together, it is possible to construct energy flow diagrams (Halsey et al., 2010; Manning et al., 2017b) showing the total amount of biological energy/carbon in the system and how it is distributed between different pools (Fig. 7.1).

7.2. Interpreting triple oxygen isotope-derived rates of photosynthetic production

Because the isotopic signature of oxygen produced from photosynthesis is different than the isotopic signature of oxygen derived from the stratosphere and mixed into the ocean through air-sea gas exchange, and because respiration does not impact the triple oxygen isotope signature, TOI allows one to quantify rates of photosynthesis only—no assumptions about respiration need to be made. In contrast, oxygen concentrations, as measured on floats (e.g., Riser and Johnson, 2008), gliders (e.g., Nicholson et al., 2015), or bottles (e.g., Collins et al., 2018; see Chapters 6

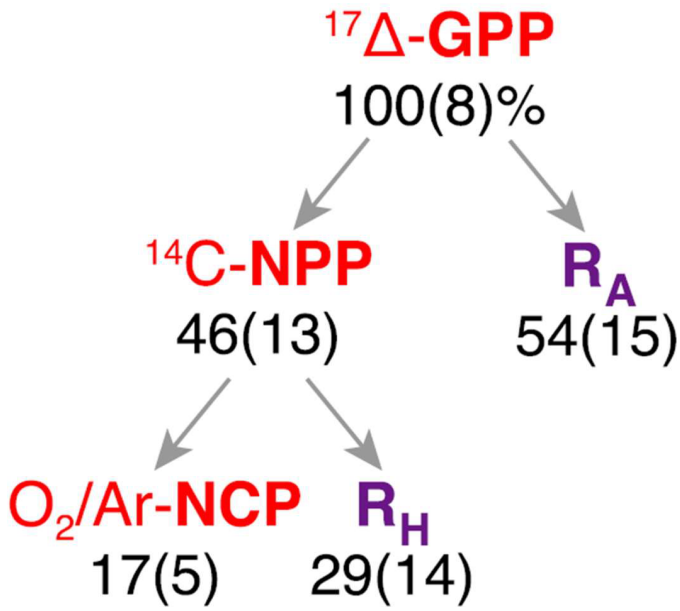

Fig. 7.1. Energy flow diagram from Monterey Bay before an upwelling event. Numbers outside the parentheses represent the percent of energy in each of the productivity pools; numbers inside the parentheses represent the uncertainty associated with the percentage. R_A represents autotrophic respiration and R_H heterotrophic respiration. Figure from Manning et al. (2017b).

and 10 for more information on such methods), are very valuable but constrain the net effect of photosynthesis and respiration, and thus assumptions about respiration are needed (i.e., the equivalence of dark and light respiration) to isolate the photosynthetic signature if GPP is calculated.

Triple oxygen isotopes directly constrain gross oxygen production (GOP), a measure of the oxygen produced during photosynthesis (Juranek and Quay, 2013; Luz and Barkan, 2000). GOP can then be converted to GPP using a photosynthetic quotient to convert from oxygen to carbon units. Typically, the photosynthetic quotient for marine organisms is considered to be 1.4 if nitrate is the dominant nitrogen source and 1.1 if ammonium is the dominant nitrogen source (Laws, 1991). In addition, photorespiration and the Mehler reaction are two processes that result in oxygen production in the photosystem but not direct fixation of carbon. Thus, when converting from GOP to GPP, the combined effect of those two processes must be estimated; typically, they are considered to be 15% to 20% of the total GOP (Bender et al., 1999; Halsey et al., 2010; Halsey et al., 2013; Kana, 1992).

Gross primary production determined from triple oxygen isotopes typically reflects photosynthetic production integrated over the mixed layer over the previous days to several weeks, depending on the depth of the mixed layer and the gas transfer velocity. Shallower mixed layers and larger gas transfer velocities lead to shorter residence times of oxygen and thus a shorter timescale. Spatially, the gases represent processes that occurred as a given water mass traveled during that period and, therefore, can represent production integrated over tens to hundreds of kilometers. However, GPP from triple oxygen isotopes reflects the patchiness of the

water where it was sampled. Water in the surface ocean is often patchy, with different water masses in close proximity (Klein and Lapeyre, 2009); each of these water masses has its own spatial trajectory and biological activity and will therefore show distinctive GPP. Thus, GPP reveals spatial variability in biological production (Juranek and Quay, 2010; Palevsky et al., 2016; Stanley et al., 2017), despite the time integration.

7.2.1. Advantages and disadvantages of triple oxygen isotopes

Like all methods for assessing production, triple oxygen isotopes have advantages and disadvantages. The largest advantage is that triple oxygen isotopes yield *in situ* estimates of GPP; the water does not have to be manipulated, thus avoiding potential biases due to bottle effects. Samples are poisoned as they are drawn into sample bottles, and thus the data reflect the community photosynthesis in its natural environment. Furthermore, no assumptions about light and dark respiration must be made (as is typical in other oxygen studies), removing a significant source of uncertainty. Additionally, since the rates are based on oxygen, and the residence time of oxygen in the upper ocean is typically a few days to a few weeks, TOI-derived GPP rates give a weighted average of production over the previous few residence times, even when the system is not in steady state (Teeter et al., 2018). This can be an advantage since the data reflect a longer production history than the limited temporal and spatial footprint of snapshot approaches such as incubations and thus may yield a truer picture of productivity in that region. However, it also can be a disadvantage when attempts are made to compare TOI-derived rates to other instantaneous measures of production or environmental variables (such as chlorophyll distributions, temperature, etc.) or during times of rapid change when estimates with shorter timescales would more accurately reflect current conditions.

TOI measurements require specialized, high-vacuum sample processing lines that must be custom-made by a laboratory (i.e., no commercial options exist). Samples are negatively impacted by atmospheric contamination and failure to incompletely separate dissolved nitrogen gas from samples, as it negatively impacts isotopic analysis. After preparation, samples must be analyzed on an isotope ratio mass spectrometer with an appropriate cup configuration for amplifying the rare $^{17}O^{16}O$ isotopologue to enable very high precision (5 to 7 per meg) and yield oceanographically relevant results. Each of these factors dictate a significant investment in time, cost, and expertise—setting up a lab to measure triple oxygen isotopes can easily take a year or more. One option for working around this significant time and financial investment is for investigators to collect triple oxygen isotope samples and send them to a lab that routinely measures triple oxygen isotopes for analysis. Once a laboratory invests in the required instruments to measure TOI (or collaborates with a laboratory where such measurements are made), it is relatively easy to collect large sample numbers. On a single cruise, 200 to 300 samples can be taken with relative ease, while achieving this high level of a sampling for incubations on a cruise would not be feasible. Finally, triple oxygen isotopes can be paired easily with O_2/Ar samples (see Chapter 8) since O_2/Ar data is obtained from the same analyses, yielding information on NCP and ratios of NCP/GOP at the same time for no additional effort. The NCP/GOP ratio (Hendricks et al., 2004; Seguro et al., 2019) is particularly valuable for estimating carbon cycle efficiency (akin to the f-ratio).

Other disadvantages are related to the model-based assumptions required to convert TOI observations into GPP rates. TOI only provides estimates of GPP in the mixed layer, unless a time series is possible, where depths below the mixed layer can be sampled in the same water

mass at subsequent times. Mixed layer production is often the bulk of production, but in some locations, significant production can occur below the mixed layer and would be missed by the triple oxygen isotope method. There can also be considerable uncertainty in the rates of GPP estimated from TOI if physical transport (vertical mixing, entrainment, lateral advection, etc.) is not properly considered (Nicholson et al., 2014). In some regions, the transport is not simply known well enough to allow precise corrections to the triple oxygen isotope data to be made. These corrections have varying effects depending on the time of year and location and, thus, depending on the study design, can be of minor to major significance (Howard et al., 2017; Ji et al., 2019; Munro et al., 2013; Nicholson et al., 2014; Palevsky et al., 2016; Seguro et al., 2019).

7.3. Theoretical Underpinnings

For a complete description of the theoretical underpinnings of the triple oxygen isotope method, see Juranek and Quay (2013) or the seminal papers by Luz (Luz and Barkan, 2000, 2005; Luz et al., 1999). A short description is furnished here so interested readers can learn the basic rationale of the method. On the earth's surface, isotopes undergo mass-dependent fractionation. Because ^{18}O (natural abundance 0.20%) has a two atomic mass unit difference from ^{16}O (natural abundance 99.76%), whereas ^{17}O (natural abundance 0.04%) has a one atomic mass unit difference from ^{16}O, most surface earth processes fractionate ^{18}O approximately twice as much as ^{16}O. Thus, for example, during respiration, dissolved oxygen removed from the water is depleted in ^{18}O by twice as much as ^{17}O. Similarly, the remaining O_2 dissolved in the water will be twice as enriched in ^{18}O relative to ^{17}O. In contrast, mass-independent processes in the stratosphere, such as ultraviolet induced interactions between O_2, O_3, and CO_2, lead to mass-independent fractionation (Lammerzahl et al., 2002; Thiemens et al., 1995). The notation $^{17}\Delta$ is used to quantify the triple oxygen isotope signature of dissolved oxygen in a sample

$$^{17}\Delta = 10^6 \times \left[\ln\left(\frac{\delta^{17}O}{1000}+1\right) - \lambda \ln\left(\frac{\delta^{18}O}{1000}+1\right)\right], \quad (7.1)$$

where $\delta^X O$ represents standard isotopic notation ($^X O/^{16}O$-1) x 1000 with ^{X} = 17 or 18, and λ represents the slope of mass-dependent respiration, which equals 0.5179 (Luz and Barkan, 2005; 2009). When defined in this way, $^{17}\Delta$ is insensitive to respiration since respiration is a mass-dependent process that removes oxygen. Note that some papers (e.g., Luz and Barkan 2011) do not explicitly include the factors of 10^6 or 1000 in the printed version of the equation, but they still use those factors when doing the calculations; it is assumed the factors are included in the definition of the per mil and per meg units.

Photosynthetic activity adds oxygen with a $^{17}\Delta$ signature based on the isotopic composition of seawater to the dissolved oxygen "pool." For example, if seawater has the isotopic composition of VSMOW (standard mean ocean water), $^{17}\Delta$ of dissolved oxygen due to photosynthesis is 249 per meg (Luz and Barkan, 2000). Air-sea exchange adds oxygen with an isotopic composition of 8 per meg (Reuer et al., 2007)—the $^{17}\Delta$ of tropospheric air (0 per meg) combined with the solubility effect of dissolving the air in water. Hence, any sample of oxygen dissolved in seawater represents a mixture of air and photosynthetic oxygen and, therefore, lies on an isotopic mixing line between those two extremes (Fig. 7.2). The $^{17}\Delta$ thus can be used to calculate the fraction of dissolved oxygen in the sample that is derived from photosynthesis.

To obtain a rate of photosynthesis and thus GPP, the $^{17}\Delta$ signature is combined with an estimate of gas exchange. A mass balance of oxygen isotopes shows that $^{17}\Delta$ is increased by photosynthesis and eroded by gas exchange. Steady state is commonly assumed; thus, gas exchange balances photosynthesis and provides a "clock" for calculating the rate. In practice, calculations are done with $\delta^{17}O$ and $\delta^{18}O$ (see Calculations, Section 7.3) for a more accurate estimation of GPP (Kaiser 2011; Prokopenko et al., 2011). Additionally, steady state does not have to be assumed; including a time rate of change term (if data exists to constrain this term) can improve GPP estimates in the surface ocean (Manning et al., 2017b) and is essential for constraining GPP below the mixed layer (Quay et al., 2010). Furthermore, corrections must be made if the seawater does not have SMOW isotopic composition, as is typical in the Arctic or some coastal/inland waters (Manning et al., 2017a).

7.4. Calculations

7.4.1. Equations

Triple oxygen isotopes are typically used to calculate GOP integrated over the mixed layer, neglecting horizontal and vertical advection and assuming steady state. In that case, GOP is calculated using Eq. 7 in Prokopenko et al., (2011)

$$\frac{G}{kO_{eq}} = \frac{\frac{X_{dis}^{17} - X_{eq}^{17}}{X_{dis}^{17}} - \lambda \frac{X_{dis}^{18} - X_{eq}^{18}}{X_{dis}^{18}}}{\frac{X_P^{17} - X_{dis}^{17}}{X_{dis}^{17}} - \lambda \frac{X_P^{18} - X_{dis}^{18}}{X_{dis}^{18}}}, \tag{7.2}$$

where G is GOP rate in units of mmol m^{-2} d^{-1}, *k* is the gas transfer velocity in units of m d^{-1}, O_{eq} is the solubility value of oxygen in units of mmol O_2 m^{-3} (i.e., the concentration of O_2 in the water in equilibrium with the atmosphere at a given temperature, salinity, and pressure), X^{17} is the ratio of $^{17}O^{16}O/^{16}O^{16}O$ of the sample (X^{17}_{dis}), equilibrated water (X^{17}_{eq}) or photosynthetic end member (X^{17}_{P}), and the same for $X^{18,}$ but it is the ratio of $^{18}O^{16}O/^{16}O^{16}O$ in those substances. λ =0.5179 and is a constant for mass-dependent fractionation between ^{17}O and ^{18}O during respiration (Kaiser, 2011; Luz and Barkan, 2005, 2009).

In δ notation, Eq. 7.2 equals

$$\frac{G}{kO_{eq}} = \frac{\left(1 - \frac{10^{-3}\delta^{17}O_{eq} + 1}{10^{-3}\delta^{17}O_{dis} + 1}\right) - \lambda\left(1 - \frac{10^{-3}\delta^{18}O_{eq} + 1}{10^{-3}\delta^{18}O_{dis} + 1}\right)}{\left(\frac{10^{-3}\delta^{17}O_P + 1}{10^{-3}\delta^{17}O_{dis} + 1} - 1\right) - \lambda\left(\frac{10^{-3}\delta^{18}O_P + 1}{10^{-3}\delta^{18}O_{dis} + 1} - 1\right)}, \tag{7.3}$$

where $\delta^{17}O_{eq}$ is the $\delta^{17}O$ value of equilibrated water, $\delta^{17}O_{dis}$ is the $\delta^{17}O$ value measured in the sample, and $\delta^{17}O_P$ is the $\delta^{17}O$ value of photosynthetic end member, with similar meaning for the $\delta^{18}O$ values.

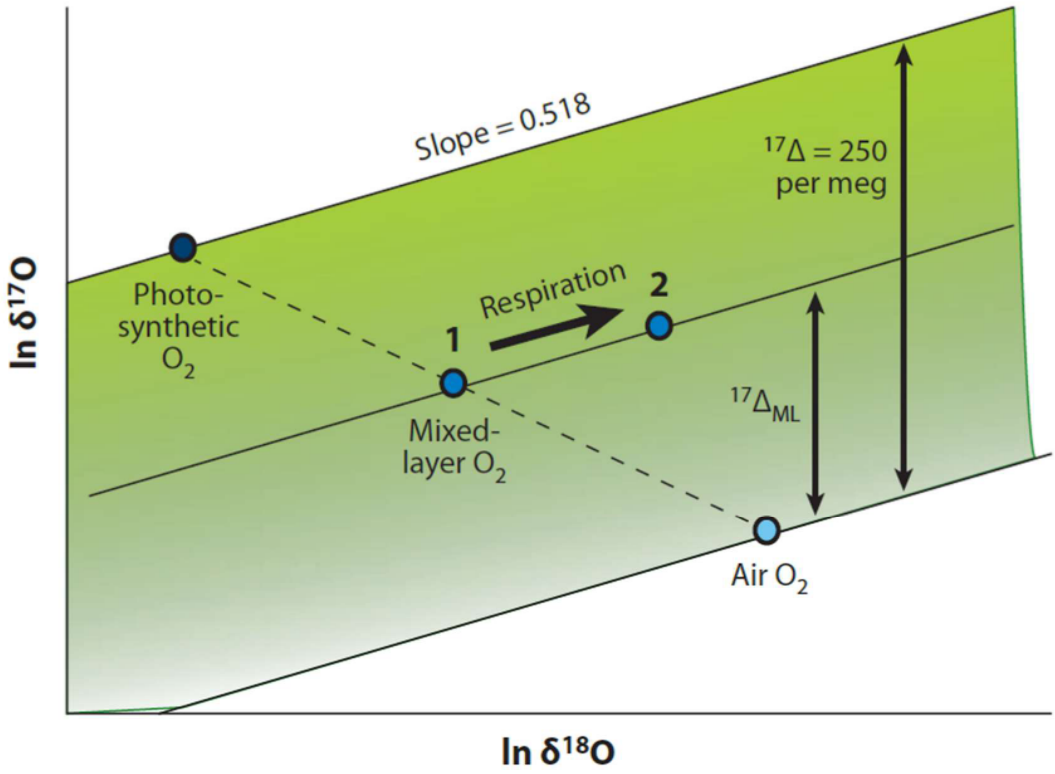

Fig. 7.2. Photosynthetic O_2 represents one end-member with a $^{17}\Delta$ of approximately 250 per meg. Air O_2 represents another, with a $^{17}\Delta$ of 0 per meg. A sample falls within the middle of the two, and the $^{17}\Delta$ of that sample reflects the fraction of dissolved O_2 in that sample, stemming from photosynthesis vs. air-sea exchange. Respiration changes the $\delta^{17}O$ and $\delta^{18}O$ but does not change the $^{17}\Delta$. Figure from Juranek and Quay (2013).

The non-steady state version of this equation (Eq. S8 in Propenko et al., 2011) can be used if the time rate of change is known. It is similar to Eq. 7.2 and 7.3, but includes a term $\partial^{17}\Delta/dt$, which represents the change in $^{17}\Delta$ with time and includes the mixed layer thickness h

$$G = kO_{eq}\left(\frac{\frac{X_{dis}^{17} - X_{eq}^{17}}{X_{dis}^{17}} - \lambda\frac{X_{dis}^{18} - X_{eq}^{18}}{X_{dis}^{18}}}{\frac{X_P^{17} - X_{dis}^{17}}{X_{dis}^{17}} - \lambda\frac{X_P^{18} - X_{dis}^{18}}{X_{dis}^{18}}}\right) + \frac{hO_{dis}\frac{\partial^{17}\Delta}{\partial t}}{\frac{X_P^{17} - X_{dis}^{17}}{X_{dis}^{17}} - \lambda\frac{X_P^{18} - X_{dis}^{18}}{X_{dis}^{18}}} \quad (7.4)$$

and could also be expressed in δ notation if desired. Software for calculating GOP using these equations is available on GitHub http://github.com/caramanning/calcGOP (Manning and Nicholson, 2017).

If samples are collected below the mixed layer and the sampling region is one with active entrainment or vertical diffusion, corrections that take into account vertical mixing and

entrainment can be used, such as the equation below (see the supplemental information in Howard et al. (2017) for the derivation of the equation)

$$C_G = \left(\frac{dz}{dt} + \frac{K_z}{z_d - z}\right) O_{2,d} \left(\left[\frac{X_d^{17}}{X_{dis}^{17}} - 1\right] - \lambda \left[\frac{X_d^{18}}{X_{dis}^{18}} - 1\right]\right) \rho_{sw}, \quad (7.5)$$

where C_G is the correction to GOP due to entrainment and vertical diffusivity, *dz/dt* is the change in mixed layer depth over time (set to 0 for a shoaling mixed layer), K_z is the vertical diffusivity coefficient, z is the mixed layer depth, z_d is the depth at which the sample used for depth correction is taken (often 10 to 20 m below the mixed layer), $O_{2,d}$ is the oxygen concentration at that depth below the mixed layer, X_d^{17} is the ratio of ^{17}O to ^{16}O at that depth below the mixed layer, and X_d^{18} is the ratio of ^{18}O to ^{16}O at that depth below the mixed layer.

7.4.2. Isotopic end members: $\delta^x O_{eq}$ and $\delta^x O_P$

Values must be known for the isotopic ratios of equilibrated water and photosynthetic end members to use these equations. The equilibrated end members can be determined by measuring the isotopic value of water equilibrated with air (see Section 7.6.2).

The photosynthetic end members are more difficult to ascertain since they depend both on the organisms conducting photosynthesis (Luz and Barkan, 2011) and on the isotopic composition of seawater itself (Manning et al., 2017a). The isotopic composition of photosynthetic oxygen is slightly different for diatoms ($\delta^{18}O_P$ = -19.001) vs cyanobacteria ($\delta^{18}O_P$ = -22.868), for example. Complete lists of the isotopic values for different community groups and a seawater average that can be used when community composition is not known can be found in Luz and Barkan (2011). The values above are based on assuming seawater has VSMOW isotopic composition, and indeed most studies assume the seawater isotopic composition is equal to VSMOW. However, certain environments, especially those that contain large amounts of meteoric water, such as waters affected by ice melt in the Arctic or inland/very near coastal environments, have $\delta^{18}O$-H_2O that differ from VSMOW by 6 per mil or greater. Ignoring the isotopic composition of seawater can lead to errors of up to 60%. The GitHub calculation software described above (http://github.com/caramanning/calcGOP) also contains modules for calculating photosynthetic end member based on the measured isotopic composition of seawater at the sample location.

Because the choice of end-member values affects the GOP calculation, and such choices may be revised in the future, data should include the end members used in the calculation when it is reported.

7.4.3. Calculating gas transfer velocity k

Another term in the GOP equations (Eq. 7.2–7.4) that must be carefully considered is *k*, the gas transfer velocity. Numerous parameterizations exist for calculating *k* in open, ice-free marine waters (e.g., Ho et al., 2006; Nightingale et al., 2000; Wanninkhof, 2014), and any of these equations could be used for calculating *k*. Bubbles are not expected to influence triple oxygen isotopes but can be included if desired (Kaiser, 2011). It is important to carefully choose a wind product and an appropriate weighting scheme when calculating *k*. The gas tracers integrate mixed layer productivity over several previous residence times of oxygen in the mixed layer,

with the residence time typically days to weeks. Thus, it would not be appropriate to use the instantaneous wind speed (such as measured on a ship) when calculating *k*. Instead, it is best to use a record of wind speed over the preceding month or two months, such as those from the NCEP/NCAR reanalysis (Kalnay et al., 1996), winds from a buoy within the study region, or from remote sensing data based on scatterometry (i.e., QuikSCAT, ASCAT, or future sensors). Wind data for 30 to 60 days preceding sample collection should be used to calculate k, using the weighting scheme by Reuer et al. (2007) (updated by Teeter et al., (2018) to work for shorter weighing times), which calculates the fraction of oxygen ventilated at point back in time and uses that fraction to calculate a weighted effective gas transfer velocity, can be used to calculate a weighted gas transfer velocity appropriate for each sample.

In ice-covered waters, such as in the Arctic or the Southern Ocean, calculating *k* is more difficult since there is a lot of uncertainty regarding how ice cover affects gas exchange. The most straightforward approach is to scale the gas transfer velocity by the fraction of free water (Butterworth and Miller, 2016; Prytherch et al., 2017). Other parameterizations that consider open water are also being developed (Loose et al., 2014; Loose et al., 2017) and could be used. With partially covered water, it is essential to have an ice history, such as from remote sensing, so the weighting scheme can be applied to the ice and the winds.

7.4.4. Relative sizes of uncertainties in the calculations

The relative amount of uncertainty stemming from the various terms in the equations for GOP depends on the condition. In general, the errors associated with the measurement of $\delta^{17}O$ and $\delta^{18}O$ contribute the largest fraction of error, leading to 10% to 40% uncertainties depending on how productive the region is and how well a particular mass spectrometric system is working (Juranek and Quay, 2013 and references therein). However, in regions of higher productivity, uncertainties in $\delta^{17}O$ and $\delta^{18}O$ matter less than in lower-productivity regions (since a difference between $\delta^{17}O_{dis}$ and $\delta^{17}O_{eq}$ is used in the equations). The next largest error source is the gas transfer velocity; in the ice-free open ocean, errors associated with *k* are likely around 10 to 20% (Ho et al., 2011; Wanninkhof, 2014; Wanninkhof et al., 2009; Woolf et al., 2019). In ice-covered regions or regions with high winds or limited fetch, errors associated with gas transfer are likely higher. Other uncertainties stem from the end members. These uncertainties can be lowered if the isotopic composition of seawater is known and if the community composition is measured so informed choices of photosynthetic end members can be made.

7.5. Study Design Considerations

Several factors must be considered when setting up a sampling plan for triple oxygen isotope samples to quantify GPP. Typically, samples are collected from the underway water on a ship or from Niskin bottles on a CTD rosette triggered within the mixed layer to assess mixed layer GPP. As described above, the most common method is to assume steady state because samples are typically only available from a particular water mass at one point in time. However, if it is possible to collect multiple samples from the same water mass at different times (i.e., sampling at multiple time points in a Lagrangian cruise), the time rate of change term can be calculated, which will increase GPP accuracy (Manning et al., 2017b). In particular, it will allow "instantaneous rates" to be calculated rather than rates that integrate over several residence times of the tracer (as done by Hamme et al. (2012) for O_2/Ar). Note that sampling at the same location (latitude and longitude) a few hours to days later does not mean the same water mass is being

sampled due to horizontal advection; water masses do not stay at a fixed location. Thus, interpreting TOI observations within a time rate-of-change framework requires Lagrangian tracking approaches.

Sampling from the underway system can enable a much higher sampling density than sampling solely from the CTD on many cruises. However, discrepancies between underway and surface water can be observed either due to biofouling causing respiration in the lines (Juranek et al., 2010) or perhaps because of bubbles in the underway line or gas contamination during the process of pumping underway water. Therefore, it is important to always collect a number of comparison samples between underway water and surface CTD bottles by comparing samples collected from the underway system while the surface CTD is fired.

Additionally, depending on the amount of vertical mixing expected, a recommended best practice is to collect TOI samples below the mixed layer at some locations during the cruise, (this necessitates collection from Niskins). A sample from 5 or 10 m below the mixed layer can be used to calculate the effect of vertical diffusion across the base of the mixed layer (Howard et al., 2017; Nicholson et al., 2014). Deeper samples can be used to estimate the effect of sudden changes in mixed layer depth and thus can be used in corrections for entrainment.

Lateral advection and diffusion are usually neglected in the calculations. However, if the sampling area is one with large advection, it should be possible to correct for lateral advection by collecting samples upstream of the main sampling area and estimating the horizontal velocities.

It may not be possible to entirely correct for all physical effects, and thus care should be taken when designing a study. It is best not to try to use triple oxygen isotopes during a time of a lot of entrainment, such as during the fall in the northern subtropical gyres when mixed layers are deepening, or in a region of very strong advection, such as the Gulf Stream or other western boundary currents. Back-of-the-envelope calculations or OSSEs can be used to determine if corrections can be made in a particular environment. Nicholson et al. (2014) also contains maps with expected sizes of various corrections, as estimated by incorporating triple oxygen isotopes in a 3D model. Such a map can be used to guide a study design and the feasibility of using triple oxygen isotopes in a given time and location.

7.6. Sample Collection

7.6.1. Triple oxygen isotope sample collection

Triple oxygen isotope samples are collected in pre-evacuated, custom-made sample bottles (Emerson et al., 1991) (Fig. 7.3). The bottles are typically made by a glassblower from 500 mL bottles that are attached to LouwersHanique (formerly called LouwersHoupert) valves (part number H10402009). Each bottle should be prepared by first adding 100 μg of saturated mercuric chloride solution that is then dried in a 70°C oven. The relatively low temperature of the oven helps the mercuric chloride stay at the bottom of the bottle; when the oven temperature is 100°C, the solution spreads, and mercuric chloride may get into the neck of the bottle where it could interfere with the seal. The bottle "stem" (the glass part with the O-rings) should never go in the oven. O-rings on the bottle valves should be scrutinized before each cruise and greased lightly with TorrLube or Apiezon. Some informal reports suggest Apiezon may interfere with mass spectrometry at later stages of analysis, so TorrLube is preferred. The bottles should then

be evacuated on a vacuum manifold to pressures smaller than 1×10^{-4} torr and sealed under vacuum. These pre-evacuated, poisoned bottles can then be used for samples.

Since gases can diffuse in or out of Niskins after they are opened, triple oxygen isotope samples are usually among the first sampled from a Niskin; they are sampled after CFCs or helium but before DIC, nutrients, salts, etc. Water from the underway system or a Niskin should be gravity fed via silicone tubing into the valve neck with a strong enough flow so the water overflows. Usually, two different tubing sizes are joined with a nylon adaptor. For example, ¼" ID tubing to fit around the nipple of a Niskin is joined with 3/16" ID thin-walled tubing that will fit inside the valve neck. The valve on the sample bottle is slowly opened, allowing some water to enter the sample flask and the rest of the water to overflow the whole time; the water in the valve neck forms a barrier that prevents atmospheric air from entering and contaminating the sample. It is imperative to ensure the water in the tubing and neck of the bottle is bubble-free. It is often necessary to tap the neck before you open the valve to dislodge bubbles to achieve this. When the sample flask is roughly half-full, the valve should be closed. Rather than aiming for half-full, optimal volume of water can be estimated based on the water temperature (Seguro et al., 2019). The neck should be rinsed and then refilled with fresh water and capped to form a diffusion barrier. Keeping water in the neck of the flask enables samples to stay gas-tight for 3 months instead of only days to weeks (Reuer et al., 2007). For detailed instructions on sampling procedures, see Appendix A.

Fig. 7.3. A custom-made triple oxygen isotope sample bottle containing a seawater sample. Note the water in the neck used as a diffusion barrier.

7.6.2. Ancillary data collection

Temperature and salinity data are required for the calculations that convert triple oxygen isotope signatures into rates of GPP since the solubility of oxygen is a function of temperature and salinity (Garcia and Gordon, 1992). Wind speed information is also needed from external databases based on either buoy data, reanalysis fields (e.g., NCEP/NCAR, (Kalnay et al., 1996), or remote sensing products (see Section 7.3.3). Since a wind history is needed, rather than instantaneous wind speed, wind products from specific cruises are usually not helpful.

Nonetheless, when designing a study, ensure wind data will be available (which can be more of a challenge in very near-shore or very remote environments). Other ancillary data that are not required for sample calculations but can aid the interpretation of data and thus are recommended, if possible, are O_2/Ar ratios (which can be measured on the same samples), fluorescence data, and information on community composition. It is important to remember when collecting ancillary data—and when ultimately comparing GPP to this ancillary data—that GPP rates from triple oxygen isotopes have a longer temporal and spatial footprint than many other kinds of data (see Section 7.1.1).

7.7. Sample Analysis

7.7.1. Processing line and isotope ratio mass spectrometry

Before being attached to the processing line, samples must be drained of most of their water. First, the samples should be shaken for at least 6 hours to equilibrate gases between the headspace and the water in the samples—unless it is deemed they have been shaken enough in transport. The samples should then be attached to a vacuum drainage system, inverted, and water drained into an evacuated filter flask, being sure to leave a "plug" of ~1 cm^3 of water in the neck so that the sample gas itself is not pumped away. The samples that now contain all the gas but only a small amount of water are ready for analysis.

Triple oxygen isotope samples are analyzed by first processing the sample on a specialized processing line (Barkan and Luz, 2003) to remove CO_2, water vapor, and N_2 gas, and then analyzing the remaining gas on an isotope ratio mass spectrometer (IRMS) for ^{16}O, ^{17}O, ^{18}O, and Ar. Typically a Thermo Fisher 253 MAT or Delta XP IRMS is used. Different labs have variations of the processing line (Juranek and Quay, 2005; Stanley et al., 2015), but all contain the same essential elements: a water trap that removes water vapor from the system (typically at temperatures < -65°C), two molsieve traps that can be either at liquid nitrogen temperatures or heated in order to trap and release gases both before and after gas chromatography, a gas chromatography column that is used to separate the O_2 and Ar from other gases (primarily nitrogen but also CO_2, methane, etc.), and a cryogenic trap (Lott, 2001) or a tube at liquid helium samples that is used to trap the final gas before release into the IRMS. GC columns range in length from 2 to 5 m (Barkan and Luz, 2003; Stanley et al., 2015) and are held at different temperatures, such as -5°C or 50°C. Each lab determines what timing gives good separation of the gases based on column length and temperature. Such separation should be checked occasionally since the separation timing differs with sample size and may drift over time.

Some labs have tried to omit the final cryogenic trap since liquid helium is hard to obtain and cryogenic traps are expensive. However, an intercalibration assessment between five labs that measured triple oxygen isotopes on the same air and water samples showed that the final cryogenic trap (or liquid helium) was necessary to obtain accurate $\delta^{17}O$ and $\delta^{18}O$ measurements (Stanley unpublished). If samples are from salt marshes or other high methane environments, an additional cold trap may be required to trap out methane before sample analysis (Howard et al., 2020).

Some systems have the processing line attached directly to an IRMS, allowing a sample to be processed and then analyzed on the IRMS immediately with no connections needing to be changed (Stanley et al., 2015) (Fig. 7.4) and allowing for 24-hour operation. Other systems operate by processing a suite of samples (e.g., 6–8) on a dedicated processing line and then

collecting on a sample manifold. This manifold is then moved to the IRMS the subsequent day for analysis (Reuer et al., 2007). When operating correctly, the TOI processing line and associated mass spectrometer should yield uncertainties of 4 to 7 per meg in $^{17}\Delta$, 0.01 to 0.02 per mil for $\delta^{17}O$ and $\delta^{18}O$. Constant vigilance is required to maintain this high level of precision and, in particular, to ensure there are no leaks in any part of the system, degradation of the water traps or GC column, impurities in the helium gas stream, problems with the cryogenics, etc.

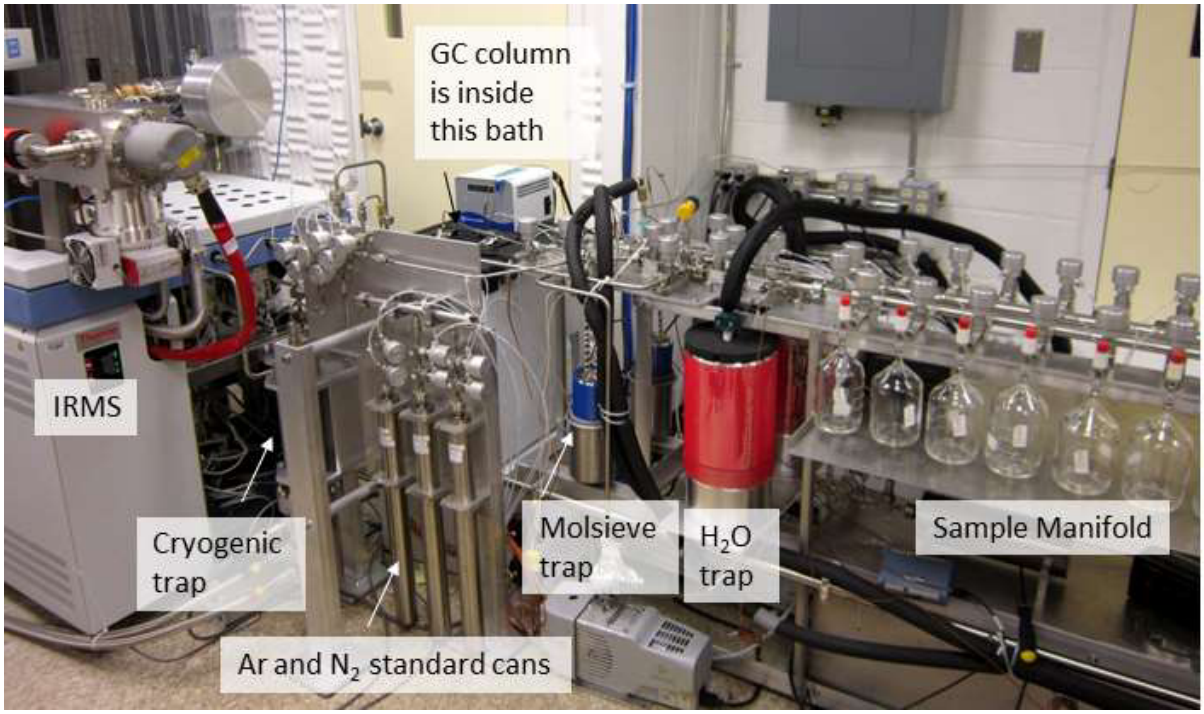

Fig. 7.4. Photograph of a triple oxygen isotope sampling line and the attached Isotope Ratio Mass Spectrometer (IRMS). Samples are attached to a sample manifold so multiple samples can be analyzed in quick succession. One sample at a time is opened, the gas contained in that sample is expanded through an H_2O trap, caught by a molsieve trap, and passed through a gas chromatography (GC) column held in a constant temperature bath (-5°C for this line but temperatures can vary) to separate the oxygen and argon from other gases. The oxygen and argon are caught in a liquid nitrogen-cooled molsieve trap and then on a cryogenic trap held at 12 K. The cryogenic trap is warmed, and the sample is released into the IRMS where it is analyzed for $^{16}O^{16}O$, $^{17}O^{16}O$, and $^{18}O^{16}O$. Often the sample is also analyzed for Ar to quantify NCP and GPP.

7.7.2. Standardization

Standardization of triple oxygen isotope samples occurs on multiple levels. First, samples are directly run on the IRMS in conjunction with a running standard, typically a custom-made gas with O_2 and Ar in similar proportions to seawater (such as 95% O_2, 5% Ar). It is important this running standard is not regular air, which contains large amounts of nitrogen and interferes with the triple oxygen isotopic measurements. Since triple oxygen isotope data needs to be reported compared to real air (rather than the running standard), air standards also need to be run on the line. Thus, approximately every day, a sample of atmospheric air should be measured and the difference between the air and the running standard used to calculate the difference between seawater samples and air. Atmospheric air is typically collected from a "clean air" location, such

as a beach with the wind blowing off the ocean or from a mountain top. It is assumed that tropospheric air around the globe does not have significant natural variations in TOI, i.e., the variations are small enough to be undetectable, given current measurement capabilities.

Additionally, to confirm that the line is working well and to furnish the data required for the calculations, samples of equilibrated water should be measured frequently (daily to weekly, depending on the lab). Dissolved oxygen in water equilibrated with the atmosphere has a known $^{17}\Delta$ value of 8 per meg (Stanley et al., 2010). Initially, the equilibrated water $^{17}\Delta$ value was reported as 8 per meg on larger samples (Reuer et al., 2007) vs. 16 per meg on smaller samples (Juranek and Quay, 2005; Luz and Barkan, 2000) or as being temperature dependent (Luz and Barkan, 2009) but after corrections for the size of the sample were taken into account, labs converged on a value of 8 per meg regardless of size or temperature (Stanley et al., 2010). Equilibrated water can be made by stirring distilled water (not too vigorously—bubbles should not be entrained) previously poisoned with mercuric chloride in a partially covered beaker for several days. Some labs make equilibrated water by bubbling distilled water with atmospheric air, but great care must be taken not to supersaturate the samples. Stirring the water makes it easier to achieve equilibration without supersaturation. Samples from this equilibrated water can then be collected as described in the sample collection section.

7.7.3. Required corrections

Given the high levels of precision required, each sample is typically measured for approximately two hours in the IRMS. The IRMS then directly outputs values for $\delta^{17}O$ and $\delta^{18}O$ for each sample. $^{17}\Delta$ can be calculated based on Eq. 7.1. However, several corrections need to be made to the data before it can be used in calculations. First, the presence of Ar in the mass spectrometer changes the $\delta^{17}O$ and $\delta^{18}O$ via matrix effects. Some labs remove all Ar in the gas chromatography step to avoid this problem (Yeung et al., 2018), but other labs want to measure O_2/Ar to obtain rates of NCP from the same samples and thus cannot remove Ar. Therefore they correct for the presence of Ar. Argon corrections can be made by creating a suite of standards with the same oxygen content and isotopic composition but varying amounts of Ar. These standards can be run regularly (every few weeks), and the response of $\delta^{17}O$, $\delta^{18}O$, and $^{17}\Delta$ to the presence of Ar can be determined and then used to correct natural samples where the $\delta^{17}O$ and $\delta^{18}O$ are not already known. The Ar correction can take the form of plotting $^{17}\Delta$, $\delta^{17}O$, or $\delta^{17}O$ vs. $\delta Ar/O_2$ for all standards (Fig. 7.5a) and then using the resulting slope to correct the seawater samples based on the sample $\delta Ar/O_2$.

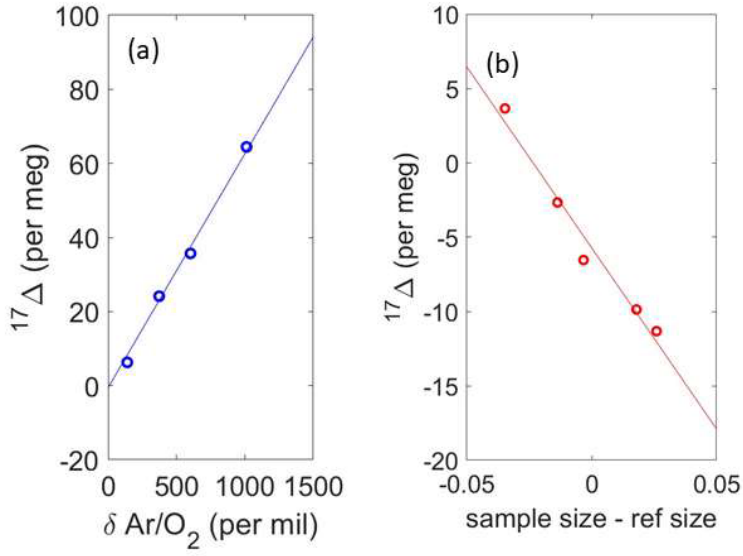

Fig. 7.5. (a) The presence of Ar in the mass spectrometer interferes with the $^{17}\Delta$ measurement so $^{17}\Delta$, $\delta^{17}O$, and $\delta^{18}O$ are all corrected for Ar by running a calibration curve of the same oxygen standard but with varying amounts of Ar. Only the calibration curve for $^{17}\Delta$ is shown here. $\delta\frac{Ar}{O_2} = \left(\frac{\left(\frac{Ar}{O_2}\right)_{std}}{\left(\frac{Ar}{O_2}\right)_R} - 1\right) \times 1000$, where std refers to the given Ar standard and R refers to the reference gas in the IRMS. (b) The difference in sizes of the sample in the standard and reference bellows affects the $^{17}\Delta$, $\delta^{17}O$ and $\delta^{18}O$ measurements so calibrations are also run where the reference gas is in both standard and reference bellows but at different relative sizes. "Sample size – reference size" refers to $\frac{O_{2\ int\ S} - O_{2\ end\ S}}{O_{2\ int\ S}} - \frac{O_{2\ int\ R} - O_{2\ end\ R}}{O_{2\ int\ R}}$, where $O_{2\ int\ S}$ is the integrated ^{32}O in millivolts reported by the IRMS for the sample side bellows, $O_{2\ end\ S}$ is the jump to mass 32 measured in millivolts at the end of the block for the sample side bellows, $O_{2\ int\ R}$ is the integrated ^{32}O in millivolts reported by the IRMS for the reference side bellows, and $O_{2\ end\ R}$ is the jump to mass 32 in millivolts measured at the end of the block for the reference side bellows.

Second, the effect of differing sizes of samples within the sample and the reference bellows needs to be corrected (Stanley et al., 2010). The different sizes may cause problems because larger samples lead to slower pressure changes within the bellows during the sample block. This is because the bellows are pressure-adjusted at the beginning of the block but not during the block itself. The size corrections can be obtained by analyzing "zeros" of differing sizes; reference gas in both standard and reference bellows but with the bellows initially at different volumes (such as 100% standard and 50% reference vs. 50% standard size and 100% reference side). Thus, the gas should have a 0 offset since it is the same gas in each side, but because of the size effect, the offset will be nonzero. The size of the calculated $\delta^{17}O$, $\delta^{18}O$, and $^{17}\Delta$ can be used to calculate a calibration curve (Fig. 7.5b), which is then applied to all samples. This size correction also inherently corrects for any effects due to pressure imbalance, precluding the need for separate pressure imbalance corrections.

The presence of nitrogen in the IRMS interferes with the proper determination of triple oxygen isotope signatures. Typically, the separation with the GC column is good enough that there is practically no nitrogen within the IRMS; correcting for this very small amount of nitrogen is less important than the corrections mentioned above. However, standard curves should be run in much the same way as for Ar (an artificial standard created with the same O_2

content as regular air standard but differing amount of nitrogen), and the resulting calibration curve applied to all samples. For some systems, the corrections due to nitrogen are significant and need to be included, whereas they are less than 0.1 per meg for other systems.

7.8. Databases

When reporting triple oxygen isotope data and GOP rates derived from triple oxygen isotopes to a database, it is important to report the direct oxygen isotopic data, the ancillary data, and other values used required for the calculations. For example, data on $\delta^{17}O$, $\delta^{18}O$, and $^{17}\Delta$ should be reported ($^{17}\Delta$ should be reported separately from $\delta^{17}O$ and $\delta^{18}O$ because even though $^{17}\Delta$ can be calculated from $\delta^{17}O$ and $\delta^{18}O$, mass spectrometric calibrations can be directly done on $^{17}\Delta$ giving more accurate values, see Section 7.6.3). Additionally, O_2/Ar data from the samples should be reported, if measured. If isotopic seawater samples were collected, i.e., if $\delta^{17}O$ -H_2O and $\delta^{18}O$ -H_2O were made, those should be reported too.

Metadata that need to be included are sample depth, temperature, salinity, latitude and longitude, and the time samples were collected. It may be useful to include a value of the weighted gas transfer velocity and the weighted square of the wind speed for each data point, where the weightings are made using the scheme of Reuer et al. (2007) to take into account fraction ventilated (see Section 7.3.3). It could also be helpful to include mixed layer depth, along with an explanation of the criterion used to calculate mixed layer depth. Mixed layer depth is important for anyone wishing to convert the areal productivity rates to volumetric ones, which enables easier comparison with ^{14}C-derived primary productivity.

It is essential in the documentation to explain how GOP was calculated, what assumptions were made (e.g., assumed steady state, neglecting lateral advection, etc.), which equations were used, and which values were used of the photosynthetic and equilibrium end members.

7.9. Appendix A: Detailed Instructions for Collecting a Triple Oxygen Isotope Sample

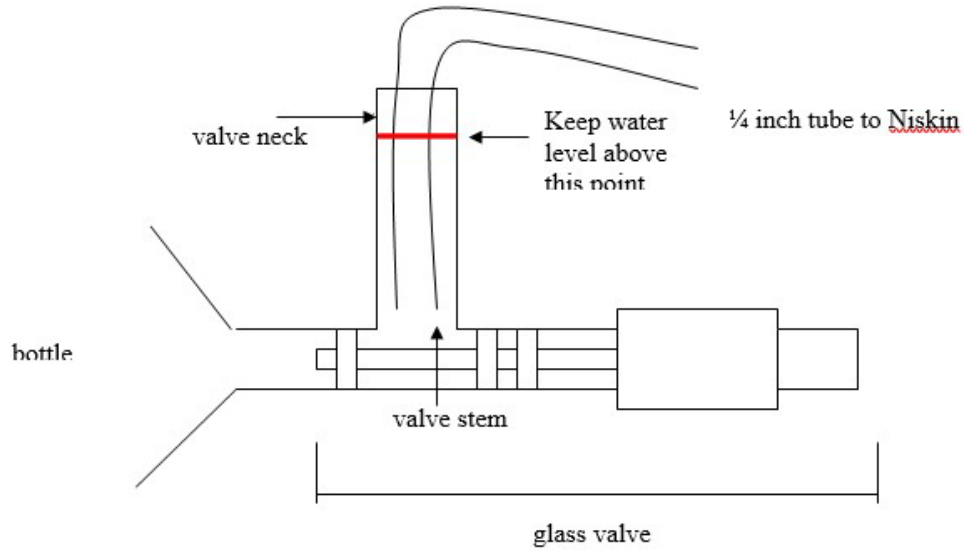

1. Attach larger diameter tubing (~3/8 in) to the Niskin bottle nipple. If using a continuous seawater system, attach tubing to the seawater supply.
2. Remove the black rubber cap and drain deionized water from the neck of triple oxygen isotope bottle. If the cap sticks, wet it with water from the Niskin or a squirt bottle.
3. Place small diameter tubing inside the bottle neck to almost touch the valve stem.
4. Open the Niskin bottle.
5. Open the plastic flow controller and adjust the seawater flow to establish a strong stream (three "clicks" works well). Hold the tubing in a gentle curve, ensuring the tubing isn't kinked.
6. Allow sample seawater to flow for several seconds or until the valve neck has flushed 3–4 times and the water in the neck is bubble-free (tap on the glass gently or mash tubing around to get rid of bubbles).
7. **Slowly open the glass valve while ensuring sufficient flow to keep the bottle neck flush with the sample. This is very important**. If the water level drops below the Louwer's valve stem, the vacuum in the bottle will pull in atmospheric gases and contaminate the sample. A good rule is not to let the water level in the neck drop below the halfway mark and always try to keep the water level at the top.
8. **Fill the bottle ½ to 2/3rds full**, always keeping an eye on the water level in the valve.
9. Close the glass valve.
10. Refill valve neck with sample water, ensuring the water is bubble free. Fill the black cap with sample water.
11. Recap valve neck with the black rubber cap.

7.10. References

Barkan, E., & Luz, B. (2003). High-precision measurements of 17O/16O and 18O/16O of O2 and O2/Ar ratio in air. *Rapid communications in mass spectrometry: RCM*, *17*(24), 2809–2814. https://doi.org/10.1002/rcm.1267

Bender, M., Orchardo, J., Dickson, M. L., Barber, R., & Lindley, S. (1999). In vitro O2 fluxes compared with 14C production and other rate terms during the JGOFS Equatorial Pacific experiment. *Deep Sea Research Part I: Oceanographic Research Papers*, *46*(4), 637–654.

Butterworth, B. J., & Miller, S. D. (2016). Air-sea exchange of carbon dioxide in the Southern Ocean and Antarctic marginal ice zone. *Geophysical Research Letters*, *43*(13), 7223–7230. https://doi.org/10.1002/2016GL069581

Cassar, N., Bender, M. L., Barnett, B. A., Fan, S., Moxim, W. J., Levy, H., & Tilbrook, B. (2007). The Southern Ocean Biological Response to Aeolian Iron Deposition. Science, *317*(5841), 1067–1070. https://doi.org/10.1126/science.1144602

Collins, J. R., Fucile, P. D., McDonald, G., Ossolinski, J. E., Keil, R. G., Valdes, J. R., Doney, S. C., & Van Mooy, B. A. S. (2018). An autonomous, in situ light-dark bottle device for determining community respiration and net community production: Autonomous observations of community metabolism. *Limnology and Oceanography: Methods*, *16*(6), 323‐338. https://doi.org/10.1002/lom3.10247

Emerson, S., Quay, P., Stump, C., Wilbur, D., & Knox, M. (1991). O2, Ar, N2, and 222Rn in surface waters of the subarctic ocean: Net biological O2 production. *Global Biogeochemical Cycles*, *5*(1), 49–69. https://doi.org/10.1029/90GB02656

Garcia, H. E., & Gordon, L. I. (1992). Oxygen solubility in seawater: Better fitting equations. *Limnology and oceanography*, *37*(6), 1307–1312.

Goldman, J. A. L., Kranz, S. A., Young, J. N., Tortell, P. D., Stanley, R. H. R., Bender, M. L., & Morel, F. M. M. (2015). Gross and net production during the spring bloom along the Western Antarctic Peninsula. *New Phytologist*, *205*(1), 182–191. https://doi.org/10.1111/nph.13125

Halsey, K. H., Milligan, A. J., & Behrenfeld, M. J. (2010). Physiological optimization underlies growth rate-independent chlorophyll-specific gross and net primary production. *Photosynthesis Research*, *103*(2), 12–5137. https://doi.org/10.1007/s11120-009-9526-z

Halsey, K. H., O'Malley, R. T., Graff, J. R., Milligan, A. J., & Behrenfeld, M. J. (2013). A common partitioning strategy for photosynthetic products in evolutionarily distinct phytoplankton species. *New Phytologist*, *198*(4), 1030‐1038. https://doi.org/10.1111/nph.12209

Hamme, R. C., Cassar, N., Lance, V. P., Vaillancourt, R. D., Bender, M. L., Strutton, P. G., Moore, T. S., DeGrandpre, M. D., Sabine, C. L., Ho, D. T., & Hargreaves, B. R. (2012). Dissolved O 2 /Ar and other methods reveal rapid changes in productivity during a Lagrangian experiment in the Southern Ocean. *Journal of Geophysical Research: Oceans*, *117*(C4), n/a–n/a. https://doi.org/10.1029/2011JC007046

Haskell, W. Z., Prokopenko, M. G., Stanley, R. H. R., & Knapp, A. N. (2016). Estimates of vertical turbulent mixing used to determine a vertical gradient in net and gross oxygen production in the oligotrophic South Pacific Gyre. *Geophysical Research Letters*, *43*(14), 7590–7599.

Haskell, W. Z., Prokopenko, M. G., Hammond, D. E., Stanley, R. H. R., & Sandwith, Z. O. (2017). Annual cyclicity in export efficiency in the inner Southern California Bight. Global Biogeochemical Cycles, *31*(2), 357–376. https://doi.org/10.1002/2016GB005561

Hendricks, M. B., Bender, M. L., & Barnett, B. A. (2004). Net and gross O2 production in the Southern Ocean from measurements of biological O2 saturation and its triple isotope composition. *Deep Sea Research Part I: Oceanographic Research Papers*, *51*(11), 1541–1561.

Hendricks, M. B., Bender, M. L., Barnett, B. A., Strutton, P., & Chavez, F. P. (2005). Triple oxygen isotope composition of dissolved O 2 in the equatorial Pacific: A tracer of mixing, production, and respiration. *Journal of Geophysical Research, 110*(C12), C12021. https://doi.org/10.1029/2004JC002735

Ho, D. T., Law, C. S., Smith, M. J., Schlosser, P., Harvey, M., & Hill, P. (2006). Measurements of air-sea gas exchange at high wind speeds in the Southern Ocean: Implications for global parameterizations. *Geophysical Research Letters*, *33*(16). https://doi.org/10.1029/2006gl026817

Ho, D. T., Wanninkhof, R., Schlosser, P., Ullman, D. S., Hebert, D., & Sullivan, K. F. (2011). Toward a universal relationship between wind speed and gas exchange: Gas transfer velocities measured with 3 He/SF 6 during the Southern Ocean Gas Exchange Experiment. *Journal of Geophysical Research*, *116*, C00F04. https://doi.org/10.1029/2010JC006854

Howard, E. M., Durkin, C. A., Hennon, G. M. M., Ribalet, F., & Stanley, R. H. R. (2017). Biological production, export efficiency, and phytoplankton communities across 8000 km of the South Atlantic. *Global Biogeochemical Cycles*, *31*(7), 1066–1088. https://doi.org/10.1002/2016GB005488

Howard, E. M., Spivak, A. C., Karolewski, J. S., Gosselin, K. M., Sandwith, Z. O., Manning, C. C., & Stanley, R. H. R. (2020). Oxygen and triple oxygen isotope measurements provide different insights into gross oxygen production in a shallow salt marsh pond. *Estuaries and Coasts*, *43*(8), 1908–1922. https://doi.org/10.1007/s12237-020-00757-6

Ji, B. Y., Sandwith, Z. O., Williams, W. J., Diaconescu, O., Ji, R., Li, Y., Van Scoy, E., Yamamoto-Kawai, M., Zimmermann, S., & Stanley, R. H. R. (2019). Variations in rates of biological production in the Beaufort Gyre as the Arctic changes: Rates from 2011 to 2016. *Journal of Geophysical Research: Oceans*, *124*(6), 3628–3644. https://doi.org/10.1029/2018JC014805

Juranek, L. W., & Quay, P. D. (2005). In vitro and in situ gross primary and net community production in the North Pacific Subtropical Gyre using labeled and natural abundance isotopes of dissolved O 2. *Global Biogeochemical Cycles*, *19*(3). https://doi.org/10.1029/2004GB002384

Juranek, L. W., & Quay, P. D. (2010). Basin-wide photosynthetic production rates in the subtropical and tropical Pacific Ocean determined from dissolved oxygen isotope ratio measurements. *Global Biogeochemical Cycles*, *24*(2), n/a-n/a. https://doi.org/10.1029/2009GB003492

Juranek, L. W., & Quay, P. D. (2013). Using triple isotopes of dissolved oxygen to evaluate global marine productivity. *Annual Review of Marine Science*, *5*, 503–524.

Juranek, L. W., Hamme, R. C., Kaiser, J., Wanninkhof, R., & Quay, P. D. (2010). Evidence of O 2 consumption in underway seawater lines: Implications for air-sea O 2 and CO 2 fluxes. *Geophysical Research Letters*, *37*(1), n/a-n/a. https://doi.org/10.1029/2009GL040423

Juranek, L. W., Quay, P. D., Feely, R. A., Lockwood, D., Karl, D. M., & Church, M. J. (2012). Biological production in the NE Pacific and its influence on air-sea CO 2 flux: Evidence from dissolved oxygen isotopes and O 2 /Ar. *Journal of Geophysical Research: Oceans*, *117*(C5), n/a-n/a. https://doi.org/10.1029/2011JC007450

Kaiser, J. (2011). Technical note: Consistent calculation of aquatic gross production from oxygen triple isotope measurements. *Biogeosciences*, *8*(7), 1793–1811. https://doi.org/10.5194/bg-8-1793-2011

Kalnay, E., Kanamitsu, M., Kistler, R., Collins, W., Deaven, D., Gandin, L., Iredell, M., Saha, S., White, G., Woollen, J., Zhu, Y., Leetmaa, A., Reynolds, R., Chelliah, M., Ebisuzaki, W., Higgins, W., Janowiak, J., Mo, K. C., Ropelewski, C., … Joseph, D. (1996). The ncep/ncar 40-year reanalysis project. *Bulletin of the American Meteorological Society*, *77*(3), 437–471. https://doi.org/10.1175/1520-0477(1996)077<0437:TNYRP>2.0.CO;2

Kana, T. M. (1992). Relationship between photosynthetic oxygen cycling and carbon assimilation in synechococcus wh7803 (Cyanophyta)1. *Journal of Phycology*, *28*(3), 304–308. https://doi.org/10.1111/j.0022-3646.1992.00304.x

Klein, P., & Lapeyre, G. (2009). The Oceanic Vertical Pump Induced by Mesoscale and Submesoscale Turbulence. *Annual Review of Marine Science*, *1*(1), 351–375. https://doi.org/10.1146/annurev.marine.010908.163704

Lämmerzahl, P. (2002). Oxygen isotope composition of stratospheric carbon dioxide. *Geophysical Research Letters*, *29*(12). https://doi.org/10.1029/2001gl014343

Laws, E. A. (1991). Photosynthetic quotients, new production and net community production in the open ocean. *Deep Sea Research Part A. Oceanographic Research Papers*, *38*(1), 143–167.

Loose, B., McGillis, W. R., Perovich, D., Zappa, C. J., & Schlosser, P. (2014). A parameter model of gas exchange for the seasonal sea ice zone. *Ocean Science*, *10*(1), 17–28. https://doi.org/10.5194/os-10-17-2014

Loose, B., Kelly, R. P., Bigdeli, A., Williams, W., Krishfield, R., Rutgers van der Loeff, M., & Moran, S. B. (2017). How well does wind speed predict air-sea gas transfer in the sea ice zone? A synthesis of radon deficit profiles in the upper water column of the Arctic Ocean. *Journal of Geophysical Research: Oceans*, *122*(5), 3696–3714. https://doi.org/10.1002/2016JC012460

Lott, D. E. (2001). Improvements in noble gas separation methodology: a nude cryogenic trap, *Geochemistry, Geophysics, Geosystems*, *2*. https://doi.org/10.129/2001GC000202.

Luz, B. (2000). Assessment of Oceanic Productivity with the Triple-Isotope Composition of Dissolved Oxygen. *Science*, *288*(5473), 2028–2031. https://doi.org/10.1126/science.288.5473.2028

Luz, B., & Barkan, E. (2005). The isotopic ratios 17O/16O and 18O/16O in molecular oxygen and their significance in biogeochemistry. *Geochimica et Cosmochimica Acta*, *69*(5), 1099–1110. https://doi.org/10.1016/j.gca.2004.09.001

Luz, B., & Barkan, E. (2009). Net and gross oxygen production from O2/Ar, 17O/16O and 18O/16O ratios. *Aquatic Microbial Ecology*, *56*, 133–145. https://doi.org/10.3354/ame01296

Luz, B., & Barkan, E. (2011). Proper estimation of marine gross O 2 production with 17 O/ 16 O and 18 O/ 16 O ratios of dissolved O 2: ESTIMATION OF MARINE GROSS O 2 PROD. *Geophysical Research Letters*, *38*(19), n/a-n/a. https://doi.org/10.1029/2011GL049138

Luz, B. (2000). Assessment of Oceanic Productivity with the Triple–Isotope Composition of Dissolved Oxygen. *Science*, *288*(5473), 2028–2031. https://doi.org/10.1126/science.288.5473.2028

Manning, C. C., & Nicholson, D. P. (2017). http://github.com/caramanning/calcGOP, in calcGOP: Functions for calculating gross oxygen production from measurements of the triple oxygen isotopic composition of dissolved O2, edited.

Manning, C. C., Howard, E. M., Nicholson, D. P., Ji, B. Y., Sandwith, Z. O., & Stanley, R. H. R. (2017). Revising estimates of aquatic gross oxygen production by the triple oxygen isotope method to incorporate the local isotopic composition of water: GOP estimates incorporating H2O isotopes. *Geophysical Research Letters*, *44*(20), 10,511–10,519. https://doi.org/10.1002/2017GL074375

Manning, C. C., Stanley, R. H. R., Nicholson, D. P., Loose, B., Lovely, A., Schlosser, P., & Hatcher, B. G. (2019). Changes in gross oxygen production, net oxygen production, and air-water gas exchange during seasonal ice melt in Whycocomagh Bay, a Canadian estuary in the Bras d'Or Lake system. *Biogeosciences*, *16*(17), 3351–3376. https://doi.org/10.5194/bg-16-3351-2019

Manning, C. C., Stanley, R. H. R., Nicholson, D. P., Smith, J. M., Timothy Pennington, J., Fewings, M. R., Squibb, M. E., & Chavez, F. P. (2017). Impact of recently upwelled water on productivity investigated using in situ and incubation-based methods in Monterey Bay. *Journal of Geophysical Research: Oceans*, *122*(3), 1901–1926. https://doi.org/10.1002/2016JC012306

Munro, D. R., Quay, P. D., Juranek, L. W., & Goericke, R. (2013). Biological production rates off the Southern California coast estimated from triple O2 isotopes and O2: Ar gas ratios. *Limnology and Oceanography*, *58*(4), 1312–1328. https://doi.org/10.4319/lo.2013.58.4.1312

Nicholson, D., Stanley, R. H. R., & Doney, S. C. (2014). The triple oxygen isotope tracer of primary productivity in a dynamic ocean model: Triple oxygen isotopes in a global model. *Global Biogeochemical Cycles*, *28*(5), 538–552. https://doi.org/10.1002/2013GB004704

Nicholson, D. P., Stanley, R. H. R., & Doney, S. C. (2018). A phytoplankton model for the allocation of gross photosynthetic energy including the trade-offs of diazotrophy. *Journal of Geophysical Research: Biogeosciences*, *123*(6), 1796–1816. https://doi.org/10.1029/2017JG004263

Nicholson, D. P., Wilson, S. T., Doney, S. C., & Karl, D. M. (2015). Quantifying subtropical North Pacific gyre mixed layer primary productivity from Seaglider observations of diel oxygen cycles. *Geophysical Research Letters*, *42*(10), 4032–4039. https://doi.org/10.1002/2015GL063065

Nightingale, P. D., Malin, G., Law, C. S., Watson, A. J., Liss, P. S., Liddicoat, M. I., Boutin, J., & Upstill-Goddard, R. C. (2000). In situ evaluation of air-sea gas exchange parameterizations using novel conservative and volatile tracers. *Global Biogeochemical Cycles*, *14*(1), 373–387. https://doi.org/10.1029/1999gb900091

Palevsky, H. I., Quay, P. D., Lockwood, D. E., & Nicholson, D. P. (2016). The annual cycle of gross primary production, net community production, and export efficiency across the North Pacific Ocean. *Global Biogeochemical Cycles*, *30*(2), 361–380. https://doi.org/10.1002/2015GB005318

Prokopenko, M. G., Pauluis, O. M., Granger, J., & Yeung, L. Y. (2011). Exact evaluation of gross photosynthetic production from the oxygen triple-isotope composition of O 2: Implications for the net-to-gross primary production ratios. *Geophysical Research Letters*, *38*(14), n/a-n/a. https://doi.org/10.1029/2011GL047652

Prytherch, J., Brooks, I. M., Crill, P. M., Thornton, B. F., Salisbury, D. J., Tjernström, M., Anderson, L. G., Geibel, M. C., & Humborg, C. (2017). Direct determination of the air-sea CO 2 gas transfer velocity in Arctic sea ice regions. *Geophysical Research Letters*, *44*(8), 3770–3778. https://doi.org/10.1002/2017GL073593

Quay, P. D., Peacock, C., Björkman, K., & Karl, D. M. (2010). Measuring primary production rates in the ocean: Enigmatic results between incubation and non-incubation methods at Station ALOHA. *Global Biogeochemical Cycles*, *24*(3), n/a-n/a. https://doi.org/10.1029/2009GB003665

Reuer, M. K., Barnett, B. A., Bender, M. L., Falkowski, P. G., & Hendricks, M. B. (2007). New estimates of Southern Ocean biological production rates from O2/Ar ratios and the triple isotope composition of O2. *Deep Sea Research Part I: Oceanographic Research Papers*, *54*(6), 951–974. https://doi.org/10.1016/j.dsr.2007.02.007

Riser, S. C., & Johnson, K. S. (2008). Net production of oxygen in the subtropical ocean. *Nature*, *451*(7176), 323–325. https://doi.org/10.1038/nature06441

Seguro, I., Marca, A. D., Painting, S. J., Shutler, J. D., Suggett, D. J., & Kaiser, J. (2019). High-resolution net and gross biological production during a Celtic Sea spring bloom. *Progress in Oceanography*, *177*, 101885. https://doi.org/10.1016/j.pocean.2017.12.003

Stanley, R. H. R., & Howard, E. M. (2013). Quantifying photosynthetic rates of microphytobenthos using the triple isotope composition of dissolved oxygen: Quantifying microphytobenthic photosynthesis. *Limnology and Oceanography: Methods*, *11*(7), 360–373. https://doi.org/10.4319/lom.2013.11.360

Stanley, R. H. R., Sandwith, Z. O., & Williams, W. J. (2015). Rates of summertime biological productivity in the Beaufort Gyre: A comparison between the low and record-low ice conditions of August 2011 and 2012. *Journal of Marine Systems*, *147*, 29–44. https://doi.org/10.1016/j.jmarsys.2014.04.006

Stanley, R. H. R., McGillicuddy, D. J., Sandwith, Z. O., & Pleskow, H. M. (2017). Submesoscale hotspots of productivity and respiration: Insights from high-resolution oxygen and fluorescence sections. *Deep Sea Research Part I: Oceanographic Research Papers*, *130*, 1–11. https://doi.org/10.1016/j.dsr.2017.10.005

Stanley, R. H. R., Kirkpatrick, J. B., Cassar, N., Barnett, B. A., & Bender, M. L. (2010). Net community production and gross primary production rates in the western equatorial Pacific. *Global Biogeochemical Cycles*, *24*(4), n/a-n/a. https://doi.org/10.1029/2009gb003651

Teeter, L., Hamme, R. C., Ianson, D., & Bianucci, L. (2018). Accurate Estimation of Net Community Production from O2/Ar Measurements. *Global Biogeochemical Cycles*. https://doi.org/10.1029/2017gb005874

Thiemens, M. H., Jackson, T., Zipf, E. C., Erdman, P. W., & van Egmond, C. (1995). Carbon dioxide and oxygen isotope anomalies in the mesosphere and stratosphere. *Science*, *270*(5238), 969–972.

Wanninkhof, R. (2014). Relationship between wind speed and gas exchange over the ocean revisited: Gas exchange and wind speed over the ocean. *Limnology and Oceanography: Methods*, *12*(6), 351–362. https://doi.org/10.4319/lom.2014.12.351

Wanninkhof, R., Asher, W. E., Ho, D. T., Sweeney, C., & McGillis, W. R. (2009). Advances in Quantifying Air-Sea Gas Exchange and Environmental Forcing. *Annual Review of Marine Science*, *1*(1), 213–244. https://doi.org/10.1146/annurev.marine.010908.163742

Woolf, D. K., Shutler, J. D., Goddijn-Murphy, L., Watson, A. J., Chapron, B., Nightingale, P. D., Donlon, C. J., Piskozub, J., Yelland, M. J., Ashton, I., Holding, T., Schuster, U., Girard-Ardhuin, F., Grouazel, A., Piolle, J. -F., Warren, M., Wrobel-Niedzwiecka, I., Land, P. E., Torres, R., & Prytherch, J. (2019). Key Uncertainties in the Recent Air-Sea Flux of CO 2. *Global Biogeochemical Cycles*, *33*(12), 1548–1563. https://doi.org/10.1029/2018gb006041

Yeung, L. Y., Hayles, J. A., Hu, H., Ash, J. L., & Sun, T. (2018). Scale distortion from pressure baselines as a source of inaccuracy in triple-isotope measurements. *Rapid Communications in Mass Spectrometry*, *32*(20), 1811–1821. https://doi.org/10.1002/rcm.8247

8. *In Situ* Net Community Production with Dissolved O_2/Ar

Laurie W. Juranek[1], Rachel H. R. Stanley[2], David .P. Nicholson[3]
[1]*College of Earth, Ocean, and Atmospheric Sciences, Oregon State University, Oregon USA*
[2]*Department of Chemistry, Wellesley College, Massachusetts, USA*
[3]*Marine Chemistry and Geochemistry Department, Woods Hole Oceanographic Institution, Massachusetts, USA*

8.1. Introduction

This chapter describes methods pertaining to the use of the dissolved ratio of oxygen to argon (O_2/Ar) to constrain net biological oxygen production *in situ*. Net biological oxygen production can be used to evaluate ocean metabolic balance (i.e., autotrophy vs. heterotrophy) and to calculate net community production (NCP) rates at the community level without the need for incubation and associated bottle containment effects. O_2/Ar observations can constrain NCP rates over timescales of days to weeks, and spatial scales of a few hundreds of meters to hundreds of kilometers, depending on how the data are collected and interpreted.

8.2. Method Background

8.2.1. Theoretical underpinnings

Net biological oxygen production, the quantity directly tracked by O_2/Ar observations, is stoichiometrically linked to the net community production of organic carbon and, when averaged over appropriate space and time scales, equal to carbon export from the biological pump. The premise is based on the simple stoichiometric relationship between net O_2 generation and net organic carbon production in the photosynthesis (left to right) and respiration (right to left) equation (summarized in shorthand version as follows)

$$\mathrm{CO_2 + H_2O \leftrightarrow CH_2O + O_2}. \quad (8.1)$$

The net generation of dissolved O_2 is proportional to the net organic carbon (CH_2O) produced by photosynthesis. Any subsequent respiration of organic carbon would also require consumption of O_2, hence the biological O_2 production tracks organic carbon residing in the system and available for export. Importantly, net O_2 tracks the organic carbon export potential of both particulate and dissolved organic carbon phases. Thus, in theory, it should be the sum of vertical sinking flux and physical subduction of dissolved organic carbon contained within water masses. Recent work has shown that the net community production of organic matter inferred from net biological oxygen correlates well to export production over spatial scales on the order of tens of kilometers, although these terms can be decoupled at sub-mesoscales (Estapa et al., 2015). To the extent that respiration of organic matter consumed by vertically migrating zooplankton is not co-located with the region of O_2 generation (i.e., the surface mixed layer), the approach would also capture this mode of vertical transport. Most commonly, dissolved gas observations are used to constrain NCP in the surface mixed layer; however, with information on the time evolution of O_2/Ar at depth, the approach can be extended below the mixed layer throughout the photic zone (e.g., Quay et al., 2010).

Dissolved O_2 concentrations in the surface ocean are set primarily by solubility, which is a function of temperature and salinity (Garcia and Gordon, 1992), and exchange with an overlying atmosphere. In the absence of physical circulation or biological processes, warm and salty waters would contain less O_2 than cold and less saline water masses when the surface ocean O_2 is in equilibrium with the atmosphere for the given temperature and salinity (i.e., at its solubility value). However, both biotic and abiotic processes perturb O_2 concentrations from equilibrium. In some cases, these physical and biological perturbations can be large and drive significant deviations from equilibrium. However, deviations are often small relative to the absolute O_2 concentration range. To understand how far from equilibrium surface O_2 concentration is, an insightful metric is the gas saturation

$$\Delta O_2 = \left(\frac{C_m}{C_{eq}} - 1\right), \tag{8.2}$$

where C_m and C_{eq} refer to the measured and equilibrium concentration of O_2, respectively, and a negative/positive value would imply less/more O_2 is present relative to that expected based on solubility equilibrium. The C_{eq} is calculated using the equations of Garcia and Gordon (1992). Deviations from solubility equilibrium are driven by both biological and non-biological sources. For example, an excess of photosynthesis over respiration would cause ΔO_2 to become positive (supersaturated), but a recent warming of the water mass (without sufficient time for the water to re-equilibrate at the new temperature) would result in a lower C_{eq}, and thus could also result in positive ΔO_2. Air injection by breaking/collapsing bubbles and gas rejection during sea ice formation also lead to a supersaturation of dissolved gases (Hamme and Emerson, 2006; Hamme et al., 2019; Stanley et al., 2009). Cooling, an excess of community respiration over photosynthesis, or a significant contribution of ice melt (because gases are excluded from the ice matrix as it forms) can contribute to negative ΔO_2. Regardless of biological or physical origin, the surface ocean will always be restored toward a solubility equilibrium by air-sea gas exchange given enough time; the characteristic timescale associated with this process depends on several factors, including the gas-transfer rate (k, usually parameterized as a function of wind-speed; Wanninkhof, 2014), the mixed layer depth, and the magnitude of the deviation of gas saturation from equilibrium. An approximation of this timescale is given by MLD/k, where MLD is the mixed layer depth (m), and k is the gas transfer coefficient with units m d^{-1}. For most of the ocean, the timescale of re-equilibration is on the order of a few weeks, but deeper mixed layers and stronger winds will result in slower/faster equilibration, respectively (see Section 7.3.3 for more discussion on this topic).

The tracer gas argon (Ar) is employed because it has very similar solubility and diffusivity characteristics to O_2 but no known biological sources or sinks (Benson and Krause, 1984; Craig and Hayward, 1987; Hamme et al., 2019; Spitzer and Jenkins, 1989). Thus, Ar responds in the same way as O_2 to most physical processes but not to biological ones, which allows a user to isolate the physical processes affecting gas saturations (e.g., recent warming or cooling) from those driven by net biological processes. The use of Ar to separate physical and biological saturation components is particularly important in open ocean settings where total gas saturation deviations are small and biological and physical gas saturations are of the same order of magnitude. The O_2/Ar gas saturation is defined similarly to ΔO_2

$$\Delta O_2/\mathrm{Ar} = \left(\frac{R_m}{R_{eq}} - 1\right), \quad (8.3)$$

where R_m and R_{eq} refer to the measured and equilibrium O_2/Ar, respectively. The $\Delta O_2/\mathrm{Ar}$ is typically multiplied by 100 and expressed as a percentage when it is reported. To compute O_2/Ar solubility, O_2 solubility is calculated from given temperature and salinity using Garcia and Gordon (1992) as before, and Ar solubility is calculated using either Hamme and Emerson (2004) or Jenkins et al. (2019). As described by Kaiser et al. (2005), $\Delta O_2/\mathrm{Ar}$ is equivalent to net biological oxygen saturation, while further calculations and a mass balance approach are required to derive NCP (see Section 8.4).

8.2.2. Historical application and method evolution

The O_2/Ar approach has been applied widely throughout the global oceans. Some of the earliest work focused on time-series measurements in the subtropical Atlantic and Pacific Oceans to evaluate the biological contribution toward a subsurface oxygen saturation maximum that occurs seasonally in these regions (e.g., Craig and Hayward, 1987; Schulenberger and Reid, 1981; Spitzer and Jenkins, 1989). Over the last several decades, a number of studies have used repeated, seasonally-resolved observations of O_2/Ar in the surface ocean at time-series sites (HOT, BATS, Stn P, CalCOFI) to evaluate NCP (e.g., Emerson et al., 1991; Emerson et al., 1997; Luz and Barkan, 2009; Munro et al., 2013; Quay et al., 2010). Importantly, these annually-resolved data have indicated that the annual NCP (ANCP), i.e., NCP integrated over a full annual cycle, implies that oligotrophic oceans export 2–3 mol C m^{-2} yr^{-1} from the surface ocean (Emerson, 2014); this stands in contrast to results of incubation-based approaches for constraining NCP (O_2 light/dark approach, see Chapter 5) which have tended to imply the oligotrophic oceans are heterotrophic and require import of organic carbon (see Williams et al., 2013 for further discussion).

Another salient point that has emerged from the constraint of ANCP with O_2/Ar budgets at both time-series sites (summarized by Emerson, 2014) and annually-resolved regional surveys (Palevsky et al., 2016) is the recognition that studies that do not resolve the full annual cycle in net O_2 production can result in overestimates of ANCP. In many open ocean systems, a fraction of the summer NCP is associated with shallow carbon export. Respiration of this shallow carbon export results in O_2 loss (and CO_2 accumulation) that is later mixed into the surface layer via entrainment in fall or winter and re-equilibrated with the atmosphere (e.g., Emerson, 2014; Palevsky et al., 2016). From a budgeting perspective, this NCP, produced earlier in the year (and registered by short-term observations of O_2/Ar), is temporary and does not contribute to ocean biological pump uptake and storage. However, many field studies are biased toward summer sampling and will measure the net biological O_2 via O_2/Ar at the surface in summer, but not the corresponding deficit in fall when the O_2 deficit from respiration is mixed to the surface. Therefore, it is important to be mindful of the timescales implied by observational data and to distinguish between short-term (sub-seasonal and seasonal) and annual organic carbon storage implied by gas-based approaches.

The O_2/Ar approach has also been used on ship transits to evaluate regional and basin-scale trends in NCP. Initial studies utilized discrete sampling from either the surface seawater pumped from a bow intake of a research or commercial cargo vessel (colloquially known as “surface underway”) or from traditional CTD casts spanning zonal or meridional gradients (e.g.,

Hendricks et al., 2004; Hendricks et al., 2005; Howard et al., 2010; Juranek et al., 2012; Reuer et al. 2007). However, in some cases, biases were observed when sampling dissolved gases from the surface underway due to microbial growth in the plumbing of these systems (Juranek et al., 2010). Therefore, studies that use surface underway for dissolved gas sampling should make efforts to cross-calibrate with samples collected from CTD-based water samplers, if possible.

More recently, the use of sea-going mass spectrometers to measure O_2/Ar with higher spatial- or temporal resolution has become more commonplace (Kaiser et al., 2005; Cassar et al., 2009; Tortell and Long, 2009; Stanley et al., 2010). An advantage of these high-resolution studies is that it allows sufficient data quantity to compare with other easily obtainable sensor-based and discrete observations (temperature, salinity, fluorescence, pCO_2, Fv/Fm, particle size distributions, nutrients, community composition, optical properties) to help diagnose underlying physical and biological drivers of spatial gradients and the relationships between NCP and air-sea CO_2 gas exchange (e.g., Eveleth et al., 2014; Hamme et al., 2012; Izett et al., 2018; Juranek et al., 2019; Lin et al., 2017; Stanley et al., 2010; Seguro et al., 2019).

8.3. O_2/Ar Data Acquisition and Quality Control

8.3.1. Bottle-based sampling

A discrete sampling approach can be used to obtain O_2/Ar data. This discrete-sampling approach is commonly used to obtain depth profiles of O_2/Ar, which are useful in diagnosing potential mixing biases to surface values (as discussed in Section 8.4). Discrete sampling can also be used for resolving O_2/Ar budgets in the surface ocean (Emerson et al., 1997; Hamme et al., 2006; Quay et al., 2010).

8.3.1.1. Preparation of high-vacuum gas sampling bottles

Most commonly, the sampling is achieved using a custom glass bottle with a 200–600 mL volume, equipped with a LouwersHanique high-vacuum stopcock. The sampling bottle specifications are identical to those for triple oxygen isotope sampling, and the same bottle sample can be used to obtain both measurements (see Chapter 7 for further description and pictures). Samples that are collected solely for O_2/Ar determination can be collected in smaller volume flasks, while a larger volume sample is required if analysis of dissolved oxygen triple isotopes and O_2/Ar is desired. Bottles are prepared by dosing with 100 µL of saturated mercuric chloride and drying at 50°C (higher temperatures lead to volatilization of Hg). Bottles must be sealed with high vacuum grease (Apiezon or TorrLube) and evacuated to less than 10^{-2} mTorr. It is good practice to inspect the O-rings on the high vacuum stopcock for damage or debris and replace them as necessary prior to evacuation, as this will improve the high vacuum performance of the bottles. When time and resources allow, a leak test of bottles should be performed one-week post-evacuation to help identify any problems. This leak test entails sequentially opening previously evacuated bottles to an isolated section of a vacuum line and monitoring pressure. Bottles with large leaks will result in a rapid increase in pressure and should not be used. After the leak test, bottles should be pumped to the vacuum baseline, removed from the line, and capped with CO_2 in the sidearm for storage until sampling. Both the evacuation and leak check of bottles require access to a high vacuum line equipped with vacuum pumps, a pressure gauge, and leak-tight seals for attaching sampling bottles (e.g., Swagelok Ultra-Torr fittings).

8.3.1.2. Collecting a water sample using high-vacuum sampling bottles

The approach for obtaining a high-quality dissolved gas sample is similar to that described in the triple oxygen isotope sampling protocol (see Chapter 7); it has also been described by Emerson et al. (1999). Primary concerns are preserving the unique gas signature dissolved in seawater and not contaminating a sample by atmospheric contact. This is achieved by creating and maintaining a water "lock" of several inches between the point where a sample is admitted to the sample bottle and ambient air. To create and maintain the water lock, a thinner diameter tubing containing flow from the sample source (a Niskin bottle or underway seawater supply) is inserted into a larger diameter outer tubing attached to the side arm of the bottle. Before sampling, care must be taken to completely dislodge and eliminate any bubbles in the tubing. When possible, pre-flushing the high vacuum flask side-arm and space above the O-ring with CO_2 gas (to displace air) immediately before establishing the water lock will reduce the potential for atmospheric contamination of the sample. After eliminating bubbles and thoroughly flushing tubing with sample water, the LouwersHanique valve is slowly opened to admit the sample until the sample bottle is roughly half full. The LouwersHanique valve is then re-seated to close, and the space above the valve is flushed with de-ionized water, dried, and then capped with CO_2 or water for storage. If the logistics of procuring compressed gas in remote locations are challenging, an alternate approach is to cap the side-arm with distilled water (Reuer et al., 2007).

8.3.1.3. Analysis of bottle samples

Upon return to a shoreside lab, the bottle sample is equilibrated with the headspace by gently shaking it for several hours at a constant temperature to ensure gases are partitioned between headspace and water under known conditions. Next, the sample bottle is inverted and the sample water contained therein is gently pumped by vacuum suction until only approximately 1 mL of water remains in the neck, isolating the gases that remain in the bottle headspace. After closing the LouwersHanique valve, the bottle side-arm is again flushed with DI water, dried, and capped with CO_2 for storage until analysis.

If the samples will also be analyzed for triple isotopes of dissolved O_2, the samples should be processed to remove CO_2, water vapor, and N_2, as described in Section 7. If measurement of triple isotopes of O_2 is not required, samples are prepared for analysis by passing them through a cryogenic trap to remove water vapor and CO_2 and are then collected into a temporary holding vessel using a cryotrap or liquid helium (Emerson et al., 1999). Samples are then warmed and admitted into an isotope ratio mass spectrometer to analyze the O_2/Ar gas ratio. The O_2/Ar is determined by peak jumping and measurement of mass/charge (m/z) peaks for O_2 (32) and Ar (40). When a sample is also being analyzed for triple oxygen isotopes (see Section 7), the measurement of O_2/Ar is typically obtained at the end of the first block of ~25 measurements for oxygen isotopes. The measured O_2/Ar value is corrected using O_2/Ar from air standards (O_2/Ar = 22.4261241970) as well as the value of an internal reference standard that is typically custom mixed to have an O_2/Ar similar to the value of most surface ocean samples (e.g., O_2/Ar ≈20). As with the triple oxygen isotope analysis, equilibrated water samples are also used as an external check since the solubility of O_2 and Ar for a given temperature are well known (e.g., equilibrium O_2/Ar = 20.37 at 25°C). See the triple isotope method in Section 7 for details on how the equilibrated water standards are made and sampled.

8.3.1.4. Correction of measured O2/Ar for sample size effect

As with $\delta^{17}O$, $\delta^{18}O$, and $^{17}\Delta$ analysis for the triple oxygen isotope method, the effect of differing sample and standard sizes and their impact on O_2/Ar determination in the IRMS must be evaluated. To diagnose these effects, the same reference gas is admitted to both the sample and standard sides with the sample bellows expanded to varying capacities. This results in

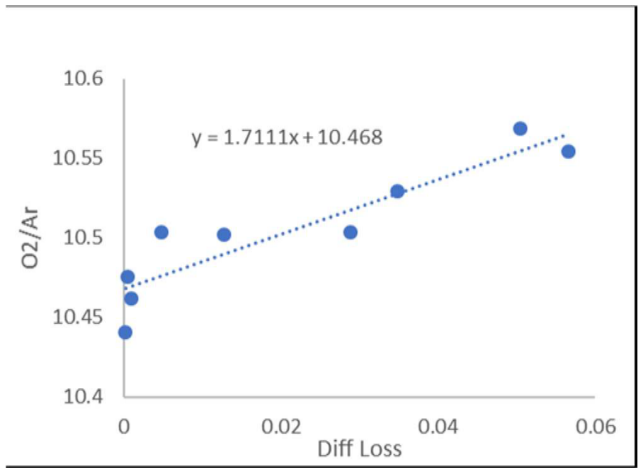

Fig. 8.1. Illustration of the size effect on determination of raw 32/40 ratio measured by a Thermo Fisher IRMS at Oregon State University. The "diff loss" is a measure of relative sample size and is quantified as suggested by Stanley et al. (2010): Diff loss = "Sample size – reference size" or, more specifically, $\frac{V_{samp\_i}-V_{samp\_f}}{V_{samp\_i}} - \frac{V_{ref\_i}-V_{ref\_f}}{V_{ref\_i}}$ where V_{samp_i} is the integrated ^{32}O in millivolts reported by the IRMS for the first measurement of the sample, V_{samp_f} is the ^{32}O measured in millivolts at the end of the measurement block for the sample, V_{ref_i} is the integrated ^{32}O in millivolts reported by the IRMS for the reference side bellows for the first measurement, and V_{ref_f} is the ^{32}O in millivolts measured at the end of the block for the reference side bellows. The O_2/Ar correction is larger for small volume samples.

differing volumes of the same gas at the same pressure. Because the slope of the size effect can change as an IRMS ionization source ages, the effect should be evaluated semi-frequently (i.e., once each month or for each sample "batch"). Figure 8.1 shows an example of the size effect for a reference gas analyzed at different sample volumes on a Thermo Fisher 253 mass spectrometer at Oregon State University.

8.3.1.5. Alternative sampling approaches

Some alternative approaches have been used to collect discrete samples for O_2/Ar. These typically include the admission of a small volume sample to a glass vial that is either crimp-sealed or otherwise closed in an air-tight fashion without headspace. Plastic containers are gas-permeable and should not be used for dissolved gas sampling. These approaches tend to be more suitable for temporary storage of samples that will be analyzed within a few days of collection, but longer-term storage using these approaches has also been reported (Charoenpong et al., 2014; Ferrón et al., 2015). Similar principles of reducing the possibility of atmospheric contamination with thorough flushing of the sample vessel and dislodging of bubbles are followed when these sampling approaches are used. For example, Ferron et al. (2016, 2020) describe sampling into 250 mL borosilicate serum vials, with water overflowing the volume of the vial at least twice.

The samples are immediately sealed with septa while ensuring no bubbles are trapped in the vial and then poisoned by injecting 250 μL of mercuric chloride through the septa. Samples are analyzed by shipboard membrane inlet mass spectrometry within 3–5 days. The shipboard analysis involves passing the sample through a capillary to stabilize the temperature and then to a semi-permeable silicone membrane where gases are partially extracted and admitted to a vacuum inlet system. After passing through a cryotrap to remove CO_2 and water vapor, the sample is analyzed by a quadrupole mass spectrometer. Standardization is achieved by admitting water samples equilibrated with air at a known and constant temperature. For more details on this approach, see Ferron et al. (2016, 2020).

8.3.2 Continuous sampling

In the last several decades, methods to determine O_2/Ar in a continuous or quasi-continuous mode at sea have become more widely used (Cassar et al., 2009; Eveleth et al., 2014; Hamme et al., 2012; Izett et al., 2018; Juranek et al., 2019; Kaiser et al., 2005; Lin et al., 2017; Palevsky et al., 2016; Stanley et al., 2010; Seguro et al., 2019). These approaches allow robust O_2/Ar and NCP estimates every few minutes, equivalent to ~1km-scale sampling while a vessel is transiting at normal speed. These methods, known as membrane inlet mass spectrometry (MIMS) (Kaiser et al., 2005; Tortell, 2005) or equilibrated inlet mass spectrometry (EIMS) (Cassar et al., 2009), share many core respects but have important differences that imbue distinct advantages/disadvantages in certain settings. Both approaches use quadrupole mass spectrometers (QMS) as analyzers; these QMS are relatively compact, cost-effective (~30–50K USD), suitable in precision, and stable in their performance at sea. Because QMS analyzers measure samples in a gas phase, dissolved gases must be extracted from seawater prior to analysis, and this critical step is where MIMS and EIMS approaches diverge. In a MIMS, a gas-permeable membrane held at constant temperature allows gases to diffuse into a vacuum chamber attached to the QMS. In an EIMS, a high surface-area contactor membrane allows gases to equilibrate in a headspace that is subsampled by a capillary connected to the QMS. The best approach in any given study will depend on user requirements, as each approach has distinct advantages and disadvantages. The equilibration approach used in an EIMS cause these systems to have an inherently slower time response to a change in O_2/Ar than a MIMS will. Cassar et al. (2009) calculated a 7-minute response time for their system based on theoretical principles, and this is broadly consistent with response lags calculated in the field (e.g., Juranek et al., 2020). However, the response time can be reduced to 2–3 minutes if counter airflow is added to the equilibrator cartridge (Manning et al., 2016). This dynamic response lag is typically not a hindrance in continuous flow-through applications given normal ship transit speeds and spatial scales over which biogeochemical gradients are observed. A disadvantage to the use of a MIMS is that gas separation is sharply affected by the sample temperature, and therefore a water bath is required to maintain stable temperature control. MIMS are more flexible in terms of easily adapting to measure a diverse array of gas analytes (including N_2O, dimethylsulfide, and CO_2), whereas EIMS tend to be configured specifically for O_2/Ar. MIMS are also better suited for measuring small volume discrete samples (e.g., those collected from CTD rosette sampling), whereas EIMS require much larger colume samples due to the time needed for equilibration. The ease of calibration of QMS data also varies between methods—EIMS data can be adjusted in near-real time using periodic admission of uncontaminated air (e.g., from an atmospheric air intake line) to the QMS using a switching valve controlled by software. However, the air-calibrated values of O_2/Ar should ultimately be compared to a sufficient number of discrete

bottle samples analyzed by a shoreside IRMS, as described in Section 8.3.1. This external check is necessary because slight differences in system total pressure (e.g., from small differences in system configuration) can occur, causing small offsets in O_2/Ar saturation ratios from true values. MIMS data are typically manually calibrated at sea using a suite of equilibrated water standards.

8.3.3 Additional observations required for calculation of NCP

In addition to the O_2/Ar value obtained from bottle samples, EIMS, or MIMS data, additional fields are necessary to interpret observations and compute NCP rates. The most critical observations are *in situ* temperature and salinity of the water sample at the time of collection. Absolute O_2 concentration is also useful for diagnosing differences between biologically-driven and physically-driven gas saturations, i.e., the total gas saturation (ΔO_2) is the sum of net biological ($\Delta O_2/\mathrm{Ar}$) and physical gas saturation (determined by difference). However, for O_2 concentration data to be useful for this purpose, they must be well-calibrated; O_2 sensor data must be frequently calibrated via comparison to Winkler bottle data as accuracy biases on the order of a few percent arising from drift or storage are common.

Wind speed measurements are also necessary to constrain the air-sea gas transfer rate (k), an essential term in the calculation of NCP, as described in Section 8.4. The relevant timescale for these observations depends on the study region and the residence time of O_2 with respect to air-sea gas transfer. To determine the best approach, users might want to conduct simple box model experiments where winds are systematically varied within specified ranges, and the surface O_2 equilibration response is determined for given conditions (temperature, salinity, mixed layer depth). While most open ocean systems can often be appropriately modeled using daily winds that are weighted over the preceding month or two (a function of mixed layer depth) before sampling (Reuer et al., 2007; Teeter et al., 2018), coastal systems might require higher frequency winds modeled over a shorter timescale. Reanalysis fields (i.e., NCEP, NARR, ERA) or nearby buoy winds are the most widely used sources of wind data. Cross-calibrated buoy winds, satellite winds, and models are also useful (Izett et al., 2021). If using shipboard winds, care must be taken to remove the influence of the ship's motion from the measured wind speeds and to be mindful of the need for historical winds that pre-date the start of sample collection. Several parameterizations that relate wind speed to air-sea gas transfer exist (as reviewed by Wanninkhof, 2014). A procedure for computing weighted k for O_2 mass balance studies based on wind-speed history is described by Reuer et al. (2007) with an update by Teeter et al. (2018). As bubble-mediated exchange processes are assumed to have a similar impact for O_2 and Ar, exchange parameterizations that explicitly include bubble dynamics are often not used to calculate NCP.

8.4. Calculation of O_2/Ar Saturation and NCP

The approach for calculating NCP rates from O_2/Ar observations is based on a surface O_2 mass balance. The details of the mass balance approach depend on the physical setting and the spatial and temporal resolution of O_2/Ar data. For example, studies that resolve the diel pattern in O_2/Ar in a given location can use this information to evaluate the net daily O_2 inventory change and estimate community respiration rates from nighttime O_2/Ar change (e.g., Hamme et al., 2012; Ferrón et al., 2015). Lacking this temporal resolution, single-point measurements in a given location (as in sampling during transit) are often interpreted in a steady-state framework

where net biological production is balanced by air-sea gas transfer of O_2, which allows NCP to be calculated as follows

$$NCP = kC_{eq}(\Delta O_2/\mathrm{Ar}). \tag{8.4}$$

The calculation of NCP as in Eq. 8.4 assumes the first order terms determining surface O_2 inventory are production and gas exchange, and that the influence of non-steady state dynamics and physical mixing are small, which is often, but not always, appropriate for open ocean regions. Though autonomous and high-resolution observations have revealed that the ocean is often not in steady state, modeling and observational work suggest that even under these circumstances, $\Delta O_2/\mathrm{Ar}$ tracks a weighted average NCP over the several-week equilibration timescale of O_2 (Ferron et al., 2015; Teeter et al., 2018). However, when processes other than gas exchange and biological production influence surface O_2 balance, Eq. 8.4 will not be appropriate (cf., Cassar et al., 2014; Manning et al., 2017; Izett et al., 2018). For example, during seasonal periods of substantial vertical mixing or entrainment of subsurface waters into the mixed layer, it will be necessary to resolve depth gradients in O_2/Ar and to model physical mixing terms (Cassar et al., 2014; Haskell and Felming, 2018; Hamme and Emerson, 2006; Izett et al., 2018; Manning et al., 2017; Munro et al., 2013; Quay et al., 2010).

A more explicit mass balance expression that includes terms for non-steady state dynamics and physical mixing is as follows

$$NCP = k[O_2]_B + K_z \frac{\partial [O_2]_B}{\partial z} + h \frac{\partial [O_2]_B}{\partial t}, \tag{8.5}$$

where $[O_2]_B$ refers to biological O_2 concentration, a simplification of the product of $C_{eq}(\Delta O_2/\mathrm{Ar})$, which appears in Eq. 8.4. Note that equating biological O_2 with $C_{eq}(\Delta O_2/\mathrm{Ar})$ assumes that [Ar] is at saturation (Kaiser et al., 2005; Cassar et al., 2014). Alternately, $[O_2]_B$ can be calculated with a small correction for the deviation of Ar from equilibrium, as discussed in Manning et al. (2017). The first term on the right side of Eq. 8.5 refers to the net air-sea O_2 flux (as in Eq. 8.4), the second term refers to the net vertical flux of O_2 (with K_z being the apparent vertical mixing coefficient, $m^2\ s^{-1}$, which can include upwelling, diffusion, entrainment, and obduction, depending on the system; Cassar et al., 2014), and the third term refers to non-steady state time variability of $[O_2]_B$in the surface mixed layer of depth h. As is clear from Eq. 8.5, the depth gradient of $[O_2]_B$ must be resolved (usually from discrete samples from the CTD sampler) along with an estimate of the apparent mixing coefficient to account for physical mixing biases, and the time variability in $[O_2]_B$ must be resolved to account for non-steady state dynamics.

In some recent studies, the $K_z \frac{\partial [O_2]_B}{\partial z}$ term has been resolved with the help of observed microstructure turbulence profiles and subsurface gradients of O_2 (Manning et al., 2017; Seguro et al., 2019). However, coincident microstructure profiles and O_2/Ar observations are not commonly available, leading to challenges when trying to explicitly account for the physical mixing effects as in Eq. 8.5. To remedy this, Cassar et al. (2014) proposed a method to use

coupled observations of N_2O and O_2/Ar to account for physical mixing bias. The rationale for this approach is that the concentration of N_2O is often inversely, linearly related to $[O_2]$ below the surface mixed layer; this relationship arises because the production of N_2O is associated with decomposition of organic matter and subsequent nitrification (thought to be photoinhibited, although there is some debate). Therefore, physical mixing will supply excess N_2O to the surface ocean, which can be measured by discrete and continuous sampling approaches. Cassar et al. (2014) showed that by neglecting the non-steady state term (3rd term in Eq. 8.5) and combining the remaining terms in Eq. 8.5 with an equivalent mass balance for N_2O, one could derive the following expression

$$NCP = k_{O2}\left[[O_2]_B + \frac{k_{O2}}{k_{N2O}}\frac{\partial[O_2]_B}{\partial[N_2O]_B}[N_2O]_B\right], \quad (8.6)$$

where k_{O2} and k_{N2O} are gas transfer coefficients for O_2 and N_2O, respectively (m d^{-1}), $[O_2]_B$ is the biological O_2, as described above (mmol m^{-3}), and $[N_2O]_B$is the biological N_2O excess in the surface mixed layer (mmol m^{-3}). The term $\frac{\partial[O_2]_B}{\partial[N_2O]_B}$ refers to the vertical gradient of $[O_2]_B$ and $[N_2O]_B$ (mmol O_2 / mmol N_2O). Izett et al. (2018) conducted a comprehensive study of simultaneous O_2/Ar and N_2O observations in a transect spanning coastal and open ocean waters of the Northeast Pacific. They found that a combined O_2/Ar and N_2O approach allowed them to correct for significant physical biases in a coastal upwelling region where surface O_2/Ar alone would have implied net heterotrophy (NCP < 0). They also found significant corrections were necessary in some open ocean regions. Areas where the vertical gradient $\frac{\partial[O_2]_B}{\partial[N_2O]_B}$ was non-linear (due to subsurface O_2 maxima or N_2O minima) led to biased estimates of physical mixing using the dual gas approach.

When calculating NCP from O_2/Ar observations, it is important to remember that, in all cases, the physical/hydrographic setting should dictate the approach for calculating NCP and not the resolution of available data. In other words, just because one *can* calculate NCP doesn't mean one *should*. In cases where significant physical transports influence the O_2 budget, and these effects are not quantified, NCP should not be reported, or NCP rates should be reported with clear statements regarding the higher uncertainty of estimates and how they are likely to be influenced by known physical biases.

8.5. Reporting O_2/Ar and NCP Data

O_2/Ar data should be reported as either a calibrated measured ratio or $\Delta O_2/Ar$ along with the time (UTC), location (latitude and longitude), *in situ* temperature, and salinity, and, if measured, dissolved O_2 concentration. Metadata should include a description of the method for data acquisition and data quality control for O_2/Ar and O_2 concentration data (if reported). NCP rates should be reported with the weighted gas transfer coefficient k and a description of how this rate was determined. If terms for vertical mixing or advection are employed in the calculation of NCP, these values should also be reported with the data. It is also helpful to report mixed layer depth and local time offset for UTC (e.g., to evaluate potential day/night effects).

Other variables that may be helpful in the interpretation of O_2/Ar and NCP data and that should be reported, if possible, include fluorescence, backscatter, nutrient concentrations, HPLC pigment data, and gross O_2 production from triple oxygen isotopes.

8.5.1 Estimating and reporting uncertainties

It is best practice to report an estimate of uncertainty alongside NCP rate information. This uncertainty should include relative uncertainty in O_2/Ar measurements, the uncertainty in the gas transfer coefficient k (typically taken as between ±15% to ±20%), and the best estimate of the uncertainty in any other modeled terms, depending on the equation used. Generally, this error will increase as signal-to-noise ratio decreases (as O_2/Ar observations get closer to equilibrium). The uncertainty can be calculated using standard error propagation techniques or, in the case of more complex expressions involving physical O_2 flux, can be calculated using a Monte Carlo analysis. The latter approach involves calculating NCP many times with input fields varied in Gaussian random distribution with standard deviation equivalent to uncertainty estimates. The standard deviation of the resulting NCP is then taken as a robust estimate of total uncertainty.

8.6. References

Benson, B.B. and Krause, D. (1984). The concentration and isotopic fractionation of oxygen dissolved in freshwater and seawater in equilibrium with the atmosphere, *Limnol. Oceanogr.*, *29*(3), 620-632.

Cassar, N., Barnett, B. A., Bender, M. L., Kaiser, J., Hamme, R. C., & Tilbrook, B. (2009). Continuous high-frequency dissolved O_2/Ar measurements by equilibrator inlet mass spectrometry. *Analytical Chemistry*, *81*(5), 1855–1864. https://doi.org/10.1021/ac802300u

Cassar, N., C. D. Nevison, and M. Manizza (2014). Correcting oceanic O2/Ar–net community production estimates for vertical mixing using N2O observations, *Geophys. Res. Lett.*, *41*, 8961–8970. https://doi.org/10.1002/2014GL062040

Charoenpong, C. N., Bristow, L. A., & Altabet, M. A. (2014). A continuous flow isotope ratio mass spectrometry method for high precision determination of dissolved gas ratios and isotopic composition: Gas and isotope ratio analysis by CF-IRMS. *Limnology and Oceanography: Methods*, *12*(5), 323–337. https://doi.org/10.4319/lom.2014.12.323

Craig, H., and Hayward, T.L. (1987). Oxygen supersaturation in the ocean: biological vs. physical contributions, *Science*, *235*, 199–202. https://doi.org/10.1126/science.235.4785.199

Emerson, S. (2014). Annual net community production and the biological carbon flux in the ocean. *Global Biogeochemical Cycles*, *28*(1), 14–28. https://doi.org/10.1002/2013GB004680

Emerson, S., P. Quay, C. Stump, D. Wilbur, and M. Knox (1991). O_2, Ar, N_2, and ^{222}Rn in surface waters of the subarctic ocean: Net biological O_2 production, *Global Biogeochem. Cycles*, *5*, 49–69.

Emerson, S., P. Quay, D. Karl, C. Winn, L. Tupas, and M. Landry (1997). Experimental determination of the organic carbon flux from open-ocean surface waters, *Nature*, *389*, 951–954.

Emerson, S., C. Stump, D. Wilbur, and P. Quay (1999). Accurate measurement of O2, N2, and Ar gases in water and the solubility of N2, *Mar. Chem.*, 64, 337–347.

Estapa, M. L., Siegel, D. A., Buesseler, K. O., Stanley, R. H. R., Lomas, M. W., & Nelson, N. B. (2015). Decoupling of net community and export production on submesoscales in the Sargasso Sea. *Global Biogeochemical Cycles, 29*(8), 1266–1282. https://doi.org/10.1002/2014GB004913

Eveleth, R., Timmermans, M.-L., & Cassar, N. (2014). Physical and biological controls on oxygen saturation variability in the upper Arctic Ocean. *Journal of Geophysical Research: Oceans, 119*, 7420–7432. https://doi.org/10.1002/2014JC009816

Ferrón, S., Barone, B., Church, M. J., White, A. E., & Karl, D. M. (2021). Euphotic Zone Metabolism in the North Pacific Subtropical Gyre Based on Oxygen Dynamics. *Global Biogeochemical Cycles*, *35*(3). https://doi.org/10.1029/2020GB006744

Ferrón, S., del Valle, D. A., Björkman, K. M., Quay, P. D., Church, M. J., & Karl, D. M. (2016). Application of membrane inlet mass spectrometry to measure aquatic gross primary production by the ^{18} O in vitro method. *Limnology and Oceanography: Methods*, *14*(9), 610–622. https://doi.org/10.1002/lom3.10116

Ferrón, S., Wilson, S. T., Martínez-García, S., Quay, P. D., & Karl, D. M. (2015). Metabolic balance in the mixed layer of the oligotrophic North Pacific Ocean from diel changes in O 2 /Ar saturation ratios: METABOLIC BALANCE FROM O 2 /AR DIEL CHANGE. *Geophysical Research Letters*, *42*(9), 3421–3430. https://doi.org/10.1002/2015GL063555

Garcia, H.E., & Gordon L.I. (1992). Oxygen solubility in seawater: better fitting equations, *Limnol. Oceanogr.*, *37*, 1307–1312. https://doi.org/10.4319/lo.1992.37.6.1307

Hamme, R. C., Cassar, N., Lance, V. P., Vaillancourt, R. D., Bender, M. L., Strutton, P. G., et al. (2012). Dissolved O2/Ar and other methods reveal rapid changes in productivity during a Lagrangian experiment in the Southern Ocean. *Journal of Geophysical Research*, *117*, C00F12. https://doi.org/10.1029/2011JC007046

Hamme, R., & Emerson, S. E. (2004). The solubility of neon, nitrogen and argon in distilled water and seawater, *Deep Sea Res., Part I*, *51*, 1517–1528.

Hamme, R., & Emerson, S. E. (2006). Constraining bubble dynamics and mixing with dissolved gases: Implications for productivity measurements by oxygen mass balance, *J. Mar. Res.*, *64*(1), p. 73–95.

Hamme, R. C., Nicholson, D. P., Jenkins, W. J., & Emerson, S. R. (2019). Using Noble Gases to Assess the Ocean's Carbon Pumps. *Annual Review of Marine Science*, *11*(1), 75–103. https://doi.org/10.1146/annurev-marine-121916-063604

Haskell, W.Z., & Fleming, J. C. (2018). Concurrent estimates of carbon export reveal physical biases in ΔO 2 /Ar-based net community production estimates in the Southern California Bight. *Journal of Marine Systems*, *183*, 23–31. https://doi.org/10.1016/j.jmarsys.2018.03.008

Hendricks, M. B., Bender, M. L., & Barnett, B. A. (2004). Net and gross O2 production in the Southern Ocean from measurements of biological O2 saturation and its triple isotope composition. *Deep Sea Research Part I: Oceanographic Research Papers*, *51*(11), 1541–1561.

Hendricks, M. B., Bender, M. L., Barnett, B. A., Strutton, P., & Chavez, F. P. (2005). Triple oxygen isotope composition of dissolved O 2 in the equatorial Pacific: A tracer of mixing, production, and respiration. *Journal of Geophysical Research*, 110(C12), C12021. https://doi.org/10.1029/2004JC002735

Howard, E., Emerson, S., Bushinsky, S., & Stump, C. (2010). The role of net community production in air-sea carbon fluxes at the North Pacific subarctic-subtropical boundary region. *Limnology and Oceanography*, *55*(6), 2585–2596. https://doi.org/10.4319/lo.2010.55.6.2585.

Izett, R. W., Hamme, R. C., McNeil, C., Manning, C. C. M., Bourbonnais, A., & Tortell, P. D. (2021). ΔO2/N2′ as a New Tracer of Marine Net Community Production: Application and Evaluation in the Subarctic Northeast Pacific and Canadian Arctic Ocean. *Frontiers in Marine Science*, *8*, 718625. https://doi.org/10.3389/fmars.2021.718625

Izett, R. W., Manning, C. C., Hamme, R. C., & Tortell, P. D. (2018). Refined Estimates of Net Community Production in the Subarctic Northeast Pacific Derived From ΔO_2 /Ar Measurements With N_2 O-Based Corrections for Vertical Mixing. *Global Biogeochemical Cycles*, *32*(3), 326–350. https://doi.org/10.1002/2017GB005792

Jenkins, W.J., & Goldman J. C. (1985). Seasonal oxygen cycling and primary production in the Sargasso Sea, *J. Mar. Res.*, *43*, 465–491.

Jenkins, W. J., Lott, D. E., & Cahill, K. L. (2019). A determination of atmospheric helium, neon, argon, krypton, and xenon solubility concentrations in water and seawater. *Marine Chemistry*, *211*, 94–107. https://doi.org/10.1016/j.marchem.2019.03.007

Juranek, L. W., Hamme, R. C., Kaiser, J., Wanninkhof, R., Quay, P. D. (2010). Evidence of O_2 consumption in underway seawater lines: Implications for air-sea O_2 and CO_2 fluxes, *Geophys. Res. Lett.*, 37, L01601. https://doi.org/1029/2009GL040423

Juranek, L. W., Quay, P. D., Feely, R. A., Lockwood, D., Karl, D. M., & Church, M. J. (2012). Biological production in the NE Pacific and its influence on air-sea CO2 flux: Evidence from dissolved oxygen isotopes and O2/Ar. *Journal of Geophysical Research*, 117, C05022. https://doi.org/10.1029/2011JC007450

Juranek, L., Takahashi, T., Mathis, J., & Pickart, R. (2019). Significant Biologically Mediated CO_2 Uptake in the Pacific Arctic During the Late Open Water Season. *Journal of Geophysical Research: Oceans*. https://doi.org/10.1029/2018JC014568

Kaiser, J., Reuer, M. K., Barnett, B., & Bender, M. L. (2005). Marine productivity estimates from continuous O_2 /Ar ratio measurements by membrane inlet mass spectrometry. *Geophysical Research Letters*, *32*(19), n/a-n/a. https://doi.org/10.1029/2005GL023459

Lin, Y., Cassar, N., Marchetti, A., Moreno, C., Ducklow, H., & Li, Z. (2017). Specific eukaryotic plankton are good predictors of net community production in the Western Antarctic Peninsula. *Scientific Reports*, *7*(1), 14845. https://doi.org/10.1038/s41598-017-14109-1

Luz B., & Barkan E. (2009). Net and gross oxygen production from O_2/Ar, $^{17}O/^{16}O$ and $^{18}O/^{16}O$ ratios. *Aquat Microb Ecol*, *56*, 133–145. https://doi.org/10.3354/ame01296

Manning, C. C., Stanley, R. H. R., & Lott, D. E. (2016). Continuous measurements of dissolved ne, ar, kr, and xe ratios with a field-deployable gas equilibration mass spectrometer. *Analytical Chemistry*, *88*(6), 3040–3048. https://doi.org/10.1021/acs.analchem.5b03102

Manning, C. C., Stanley, R. H. R., Nicholson, D. P., Smith, J. M., Timothy Pennington, J., Fewings, M. R., Squibb, M. E., & Chavez, F. P. (2017). Impact of recently upwelled water on productivity investigated using in situ and incubation-based methods in Monterey Bay: MB PRODUCTIVITY USING MULTIPLE METHODS. *Journal of Geophysical Research: Oceans, 122*(3), 1901–1926. https://doi.org/10.1002/2016JC012306

Munro, D. R., Quay, P. D., Juranek, L. W., & Goericke, R. (2013). Biological production rates off the Southern California coast estimated from triple O 2 isotopes and O 2: Ar gas ratios. *Limnology and Oceanography*, *58*(4), 1312–1328. https://doi.org/10.4319/lo.2013.58.4.1312

Palevsky, H. I., Quay, P. D., Lockwood, D. E., & Nicholson, D. P. (2016). The annual cycle of gross primary production, net community production, and export efficiency across the North Pacific Ocean: North Pacific GOP, NCP, and Export Efficiency. *Global Biogeochemical Cycles*, *30*(2), 361–380. https://doi.org/10.1002/2015GB005318

Quay, P. D., Peacock, C., Björkman, K., & Karl, D. M. (2010). Measuring primary production rates in the ocean: Enigmatic results between incubation and non-incubation methods at Station ALOHA. *Global Biogeochemical Cycles*, *24*, GB3014. https://doi.org/10.1029/2009GB003665

Reuer, M. K., Barnett, B. A., Bender, M. L., Falkowski, P. G., & Hendricks, M. B. (2007). New estimates of Southern Ocean biological production rates from O2/Ar ratios and the triple isotope composition of O2. *Deep Sea Research Part I: Oceanographic Research Papers*, *54*(6), 951–974.

Shulenberger, E., & Reid, J. L. (1981). The Pacific shallow oxygen maximum, deep chlorophyll maximum, and primary productivity, reconsidered. *Deep Sea Research Part A. Oceanographic Research Papers*, *28*(9), 901–919.

Seguro, I., Marca, A. D., Painting, S. J., Shutler, J. D., Suggett, D. J., & Kaiser, J. (2019). High-resolution net and gross biological production during a Celtic Sea spring bloom. *Progress in Oceanography*, *177*, 101885. https://doi.org/10.1016/j.pocean.2017.12.003

Spitzer, W. S., & Jenkins, W. J. (1989). Rates of vertical mixing, gas exchange and new production: Estimates from seasonal gas cycles in the upper ocean near Bermuda. *Journal of Marine Research*, *47*(1), 169–196.

Stanley, R. H. R., Jenkins, W. J., Lott, D. E., & Doney, S. C. (2009). Noble gas constraints on air-sea gas exchange and bubble fluxes. *Journal of Geophysical Research*, *114*, C11020. https://doi.org/10.1029/2009JC005396

Stanley, R.H.R., Kirkpatrick, J.B., Cassar, N., Barnett, B.A., Bender, M.L., 2010. Net community production and gross primary production rates in the western equatorial *Pacific. Glob. Biogeochem. Cycles,* 24.

Teeter, L., Hamme, R. C., Ianson, D., & Bianucci, L. (2018). Accurate estimation of net community production from O2/Ar measurements. *Global Biogeochemical Cycles*, *32*, 1163–1181. https://doi.org/10.1029/2017GB005874

Tortell, P. D. (2005). Dissolved gas measurements in oceanic waters made by membrane inlet mass spectrometry. *Limnol. Oceanogr. Methods*, *3*, 24–37.

Tortell, P. D., & Long, M. C. (2009). Spatial and temporal variability of biogenic gases during the Southern Ocean spring bloom. *Geophysical Research Letters*, *36*(1), L01603. https://doi.org/10.1029/2008GL035819

Wanninkhof, R. (2014). Relationship between wind speed and gas exchange over the ocean revisited: Gas exchange and wind speed over the ocean. *Limnology and Oceanography: Methods*, *12*(6), 351–362. https://doi.org/10.4319/lom.2014.12.351

Williams, P. J. le B., Quay, P. D., Westberry, T. K., & Behrenfeld, M. J. (2013). The Oligotrophic Ocean Is Autotrophic. *Annual Review of Marine Science*, *5*(1), 535–549. https://doi.org/10.1146/annurev-marine-121211-172335

9. The Use of Variable Chlorophyll Fluorescence for Assessment of Phytoplankton Photosynthetic Physiology and Rates of Primary Production

Greg Silsbe[1], Helga do Rosario Gomes[2]
[1]*University of Maryland Center for Environmental Science, Maryland, USA*
[2]*Lamont-Doherty Earth Observatory at Columbia University, New York, USA*

9.1. Introduction

Variable chlorophyll fluorescence (ChlF) is a powerful and widely used photosynthetic measurement technique in terrestrial and aquatic ecosystems. Over the past two decades, variable ChlF, also referred to as active ChlF, has been increasingly used to estimate the physiological status and primary production of phytoplankton and other photosynthetic organisms. Variable fluorometers are fast, sensitive, non-destructive, and can operate autonomously to provide highly resolved productivity measurements in space and time while revealing important physiological characteristics of the underlying phytoplankton community. However, unlike other primary productivity rate measurements, different instrument variants and associated protocols have been advanced in the scientific literature, causing some divergence, debate, and potential confusion over best operational practices (Hughes et al., 2018).

This chapter draws upon a recent community assessment (Schuback et al., 2021) and an under-development user guide (Scientific Committee on Oceanic Research (SCOR) Working Group 156) to summarize the current best practices to assess primary production and photosynthetic physiology using variable fluorescence. This chapter focuses solely on single turnover variable fluorescence (ST-ChlF), the most common variant of variable fluorescence and the best suited for aquatic primary production. Other variable fluorescence variants not addressed here include pulse modulated fluorescence (PAM, Schreiber et al., 1986) and picosecond fluorescence decay kinetics (Lin et al., 2016). Section 9.2 provides a brief theoretical overview of ST-ChlF protocols and the derivation of primary ChlF parameters. During the collection and initial data processing of these data, many of the recommended best practices are implemented, and important considerations arise. Section 9.2, therefore, also discusses the treatment of blank and baseline fluorescence, induction curve optimization and statistical characterization. Section 9.3 describes a set of algorithms that then scale ChlF parameters to photosynthetic electron transport rates and, ultimately, carbon fixation. We specifically focus on the three most common algorithms and briefly discuss their respective operational demands, advantages, assumptions, and requirements for ancillary data. Section 9.4 discusses variable fluorescence measurements in the context of remotely sensed passive chlorophyll fluorescence. Section 9.5 provides more general best practices, including underway measurements, instrument calibration, and data archiving. For further details, readers are referred to documentation of the SCOR Working Group 156, "Active Chlorophyll Fluorescence for Autonomous Measurements of Global Marine Primary Productivity" (SCOR Working Group, 2022).

9.2. Single Turnover Fluorescence Protocols

The degree to which a user can control and modify single turnover fluorescence induction protocols is instrument dependent. Fortunately, most instrument manuals are very detailed and can supplement the generalized description provided here.

9.2.1. Theoretical foundations and concepts

The basic principle underlying ChlF analysis is relatively straightforward. Chlorophyll *a* (Chla) is the primary oxygenic photosynthetic pigment. When Chla is extracted in an organic solvent (*in vitro*), the measured ChlF is directly related to the total Chla concentrations, which is often used as a proxy for phytoplankton biomass (Holm-Hansen and Riemann, 1978). But *in vivo* ChlF measurements are subject to variable amounts of "quenching" that cause changes in the ChlF:Chla ratio (Thomalla et al., 2018). The utility of variable ChlF lies in the physiological processes that govern quenching. Each photon of light absorbed by Chla, or generally any *in vivo* photosynthetic pigment, has one of the three mutually exclusive fates: 1) it can be re-emitted at longer wavelengths as fluorescence (Maxwell and Johnson, 2000), 2) it can be consumed in the photosynthetic generation of reductant and ATP (photochemical quenching), or 3) it can be dissipated as heat (non-photochemical quenching, NPQ). As these three fates are mutually exclusive and sum to unity, quantum yields (ϕ) define the fractional importance of each fate. Phytoplankton actively regulate photochemistry and NPQ, such that measured changes in the quantum yield of ChlF (ϕ_F) are directly linked to changes in the quantum yields of photochemistry (ϕ_P) and NPQ (ϕ_{NPQ}). This general concept has been applied and refined for over a century of photosynthetic research (Govindje, 1995), leading to many important insights (Schuback et al., 2021).

Modern variable fluorometers leverage these competitive fates by directly manipulating the redox state of photosystem II (PSII), the pigment-protein complex that photo-oxidizes water to generate electrons for reductive biosynthesis (Hughes et al., 2018). ST-ChlF delivers rapid bursts of high-energy light that sequentially closes photosystem II (PSII) reaction centers within the turnover timescale of the primary PSII electron acceptor Q_A while simultaneously measuring resultant changes in ChlF. Following this so-called "saturation phase," many instruments then increase the time-step between the delivery of high energy light to track the rate of PSII re-oxidation, the so-called "relaxation phase." The technique was introduced by Kolber et al. (1998) and has been comprehensively reviewed elsewhere (Falkowski et al., 2004; Huot and Babin, 2010; Schuback et al., 2021). The measured ChlF signal is assumed to derive exclusively from PSII, so the technique is most suited to study reactions and processes at or close to PSII reaction centers. But given the tight coupling of reductant and energy fluxes across the entire photosynthetic system and beyond, information well beyond PSII function can be inferred from variable ChlF measurements (Hughes et al., 2018).

9.2.2. Primary and secondary ChlF parameters

Primary ChlF parameters refer to ChlF measurements made during the saturation and relaxation phases. ST-ChlF measurements are often performed both in the absence or presence of actinic light, where a prime symbol $'$ is used to differentiate light from dark regulated states. Figure 9.1 shows fluorescence induction curves in the dark and light. In the absence of actinic light (Fig. 9.1A), all functional PSII reaction centers are open such that photochemical quenching is maximal and ChlF is minimal (F_o). Note that depending on the recent light exposure of a given

sample, non-photochemical pathways may still be engaged in the dark (see Section 9.3.3). As excitation energy provided by variable fluorometers progresses through the saturation phase, the temporary reduction of the primary electron acceptors Q_A stimulates a transient increase in the complementary fluorescence yield until all reaction centers are reduced, photochemical quenching is 0, and ChlF is maximal (F_M). The amplitude of the ChlF transient ($F_m - F_o$) is denoted F_v, whereby F_v/F_m can be interpreted as the maximum photochemical efficiency for a given population of PSII under a given environmental condition (Schuback et al., 2021). In addition to F_o and F_m, the primary parameters derived in the dark regulated state include the absorption cross-Section for PSII photochemistry (σ_{PII}) derived from the slope of the initial ChlF transient rise, the connectivity factor (ρ), defined as the probability of excitation transfer from a closed reaction center to an open one and τ_{Qa}, the time constant(s) for PSII (Q_A) re-oxidation in the dark-regulated state as measured during the relaxation phase and often modeled using four distinct time constants (Gorbunov et al., 2020). In the presence of actinic light (Fig. 9.1B), ChlF at the beginning of the saturation phase is referred to as F' because a fraction of PSII reaction centers are already photochemically reduced. Here, the parameter $F_o{}'$ represents the minimum ChlF measured immediately after the transition from light to dark. Following the excitation pulse(s), ChlF increases to $F_m{}'$, but it is typically less than F_m of the dark-regulated state because of ChlF quenching by NPQ. The amplitude of the ChlF transient ($F_m{}' - F_o{}'$) is denoted $F_q{}'$, whereby $F_q{}'/F_m{}'$ is the realized quantum yield of PSII photochemistry. The light-regulated transient also provides $\sigma_{PII}{}'$, ρ' and $\tau_{Qa}{}'$.

The primary ChlF parameters are retrieved by fitting fluorescence transient data (e.g., Fig. 9.1) to a biophysical model (Section 9.2.4). The secondary ChlF parameters are derived from the primary parameters listed in Table 9.1 that are then scaled to electron transport rates. ST-ChlF induction was introduced by Kolber et al. (1998), and comprehensive reviews are available elsewhere (Falkowski et al., 2004; Huot and Babin, 2010; Hughes et al., 2018; Schuback et al., 2021).

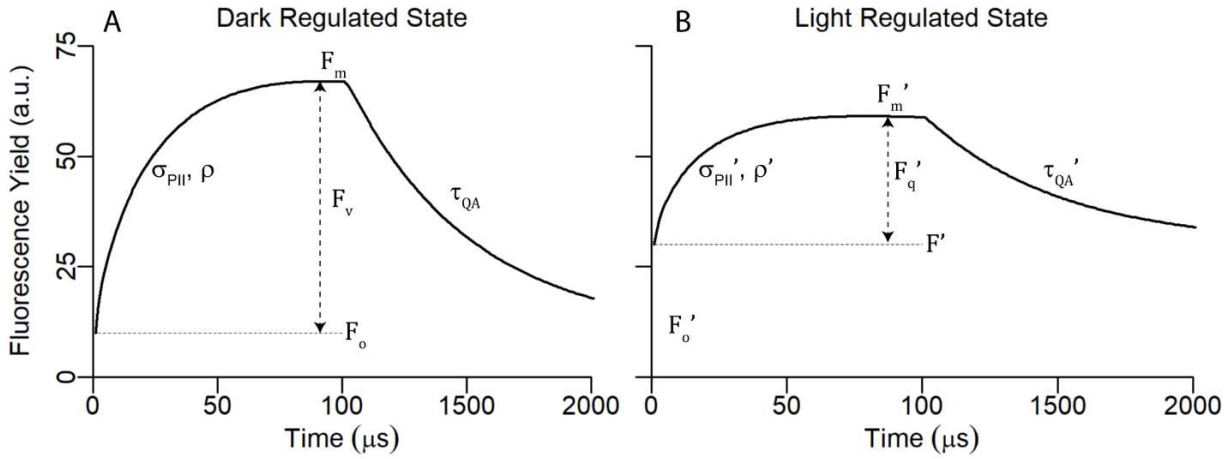

Fig. 9.1. An example of a single turnover variable fluorescence transient and resultant primary ChlF parameters under A) dark- and B) light-regulated states. The time axis is non-linear as sampling frequency changes between saturation and relaxation phases to reflect the changing temporal resolution required to understand the dynamics of fluorescence saturation and relaxation.

9.2.3. Treatment of blank and baseline fluorescence

The biophysical models applied to fluorescence transient data implicitly assume that all measured ChlF originates from functional PSII reaction centers. In practice, however, fluorescence can originate from a variety of other sources that together may constitute a significant fraction of the observed signal (Cullen and Davis, 2003; Moore et al., 2008). Schuback et al. (2021) review and partition non-PSII fluorescence into two categories; the non-physiological analytical blanks and the physiological baseline fluorescence.

Analytical blanks are quantifiable and subtracted from ChlF prior to curve fitting. Software packages associated with specific instrument variants typically allow users to subtract analytical blanks. The reader is also referred to the open-source "Phytoplankton Photophysiology Utilities" Python package developed and described by Ryan-Keogh and Robinson (2021). This package, compatible with data from the most common model variants, is flexible in model selection, and provides useful statistical metrics.

Analytical blanks constitute an instrument blank (B_{inst}) and fluorescence from dissolved substances (F_{diss}) that are independently measured. B_{inst} can vary widely between instrument types, but improved designs have reduced this signal to < 5% in even the most oligotrophic waters (Schuback et al., 2021). B_{inst} is measured using pure water, and regular measurements can identify instrumental drift. B_{inst} can also be used to quantify and mitigate potential biofouling by interpolating measurements at regular intervals (e.g., daily) through time. Simple subtraction of B_{inst} from ChlF is only recommended when it less than 5% of F_m; this number thus serves as an upper limit beyond which biofouling should be mitigated. F_{diss} is quantified following 0.2 μm filtration and measured with a clean optical configuration. As filtration can create micro-bubbles that strongly scatter light, it is recommended to wait 10–15 minutes after filtration before making a measurement. When operating within an underway system or at a fixed location, F_{diss} measurements should be performed regularly or autonomously acquired following best practices for collecting and processing flow-through optical data (IOCCG, 2019). If profiling, then F_{diss} should be measured at different depths. Finally, the user should be aware of instrument-specific settings that affect the magnitude of measurements. These settings include instrument changes in instrument excitation energy (E_{ex}) and/or signal amplification (e.g., photomultiplier settings), although most software automatically normalize measurements to changes in instrument settings. Regardless, analytical blanks should be performed with the same instrument settings as attendant field measurements. By recording measurements over time, the user can gauge analytical blank variance and importance (i.e., % of F_m).

9.2.4. Induction curve optimization and statistical metrics

Most recent variable fluorometers have onboard automated approaches to ensure optimal fluorescence induction, nominally achieved by tuning emitted excitation energy and/or signal amplification. Where real-time data inspection permits, a general rule is that F (F') should approach F_m (F_m') approximately halfway through the saturation phase. Most fluorometers also allow the user to average successive saturation and relaxation phase data into a single dataset, though in principle, this can also be achieved in a post-processing pipeline. While most variable fluorometers can acquire data in even the most oligotrophic regions of the global ocean, measurements taken when a significant fraction of PSII light reaction centers are reduced (i.e., where F′ approaches F_m' in high-light environments) generally have high ChlF parameter

uncertainty. Considerable averaging of repeated ChlF transients helps alleviate this uncertainty (Ryan-Keogh and Robinson, 2021).

Statistical metrics that describe the fit of the biophysical model and the ChlF parameter uncertainty provide the most direct way to assess the efficacy of induction curve fits. Statistical metrics can also be used in a post-processing pipeline, for example, to identify the optimal treatment of ρ (Ryan-Keogh and Robinson, 2021). Variable fluorometer software generally report either the coefficient of determination (r^2) or goodness of fit (χ^2), which may not be suitable for non-linear models (Ryan-Keogh and Robinson, 2021). The community recommendation to both instrument developers and users is to adopt and report normalized root mean square errors and normalized bias of model fit. Normalization will help minimize any instrument-dependent changes in the magnitude of ChlF parameters, allowing easier QA/QC within and across datasets.

Biophysical model differences also arise through the treatment of the dimensionless connectivity coefficient (ρ) that defines the probability of excitation transfer between closed and open reaction centers. Eq. 9.1 assumes no connectivity (ρ is absent), while in Eq. 9.2 and 9.3 ρ is either constant or iteratively solved for. In the absence of energy transfer ($\rho = 0$), fluorescence rises exponentially, but as connectivity increases, fluorescence induction is increasingly sigmoidal (Kolber et al., 1998). In these equations, $C(t)$ is the fraction of open reaction centers at time t and $E_{ex}(t)$ is the known excitation energy delivered at time t. Critically, the numerical treatment of ρ influences both the absorption cross-section for PSII (σ_{PII}) and F_v/F_m (Ryan-Keogh and Robinson, 2021). The shape of the induction curve and the statistical ability to resolve the underlying ChlF parameters should dictate the numerical treatment of ρ (Section 9.1.3).

$$F(t) = F_o + (F_m - F_o) \cdot \left(1 - e^{-\sigma_{PII} \int_0^t E_{ex} dt}\right) \quad (9.1)$$

$$F(t) = F_o + (F_m - F_o) \cdot \left(C(t) \frac{1-\rho}{1-C(t)\cdot\rho}\right) \quad (9.2)$$

$$\frac{dC}{dt} = E_{ex}(t) \cdot \sigma_{PII} \cdot \frac{1-C(t)}{1-C(t)\cdot\rho} \quad (9.3)$$

Eq. 9.4 is an extension of Eq. 9.1 that includes relaxation kinetics of PSII re-oxidation (note the longer timescale in Fig. 9.1 beginning at 100 µs). Relaxation kinetics constitute the sum of distinct components (i), each defined by an amplitude α_i and a time constant τ_i. Description of the Q_a^- relaxation kinetics, with sufficient accuracy, in natural phytoplankton populations requires a 3-component model (Gorbunov and Falkowski, 2020) that represents electron transport from Q_a to Q_B (τ_1 and τ_2, depending on the state of Q_B) and the slow Q_a re-oxidation in inactive reaction centers (τ_3). The average time constant (τ_{Qa}) for the two fastest components (τ_1 and τ_2) reflects the rate of Q_a re-oxidation in active reaction centers (Eq. 9.5; Gorbunov and Falkowski, 2020).

$$F(t) = F_o + (F_m - F_o) \cdot \left(1 - e^{-\sigma_{PII} \int_0^t E_{ex} dt}\right) \cdot \sum_{i=1}^{n} \alpha_i e^{-t/\tau_i} \quad (9.4)$$

$$\tau_{QA} = (\alpha_1 \cdot \tau_1 + \alpha_2 \cdot \tau_2) \times (\alpha_1 + \alpha_2)^{-1} \quad (9.5)$$

9.3. Estimates of Photosynthetic Electron Transport Rates

Several algorithms have been developed to derive ETR (electrons $PSII^{-1}$ s^{-1}) from variable fluorescence measurements (Kolber and Falkowski, 1993; Oxborough et al., 2012; Gorbunov and Falkowski, 2020). The merits, assumptions, and disadvantages of these algorithms and how they are ultimately scaled to carbon fixation have also been reviewed (Suggett et al., 2010; Hughes et al., 2018; Schuback et al., 2021; Gorbunov and Falkowski, 2022). In the following sections, the two main approaches, amplitude-based and kinetic-based ETR algorithms, are discussed alongside model specific caveats, scaling measurements to carbon fixation, photosynthetic irradiance curves, and spectral correction.

9.3.1. Amplitude-based ETR algorithms

The two amplitude-based ETR algorithms discussed below follow the simple rationale that ETR can be calculated from estimates of incident photon irradiance, the fraction of incident photons absorbed by PSII pigments, and the distribution of absorbed photon energy among the three energy dissipation pathways (Schuback et al., 2021).

Thus ETR is a product of spectral PAR (E_{PAR}) with units of mol photons m^{-2} s^{-1}, the spectral absorption coefficient of light-harvesting pigments associated with photosystem II (a_{LHII}) with units m^{-1}, the dimensionless quantum yield of PSII photochemistry ($\phi_{PSII}{}'$) estimated as $\phi_{PSII}{}' = F_q{}'/F_m{}'$ (Table 9.1). Note that this formulation yields ETR units of mol photons m^{-3} s^{-1}, an additional term often not shown in the literature is a quantum yield that assumes one electron from charge separation is produced per photon absorbed for PSII photochemistry. This term is often implicitly used to arrive at ETR units of mol electrons m^{-3} s^{-1}. E_{PAR} is either an ancillary measurement (e.g., alongside an *in situ* profile) or an actinic source provided by the instrument. For simplicity, this section ignores any spectral dependencies, which are discussed in Section 9.3.5. Additional derivation of parameters not shown here are provided in Table 9.1.

Amplitude based variable fluorescence algorithms differ in their derivation of a_{LHII}. As the term a_{LHII} is likely new to non-experts, a brief overview of relevant absorption terms is warranted. The spectral phytoplankton absorption coefficient (a_{ph}; see IOCCG, 2018 for methods) can be partitioned based on the association of pigments with either photosystem I (a_{LHI}) or photosystem II (a_{LHII}) The active fluorescence literature further makes the distinction between a_{LHII} and the spectral absorption coefficient of photosystem II (a_{PII} or a_{PSII}). a_{PII} represents pigment absorption of functional PSII reaction centers with units of m^{-1} such that $a_{LHII} = a_{PII} \cdot (F_v/F_m)^{-1}$. This distinction is important as a_{PII} is equivalent to the product of volumetric concentration of photosystem II reaction centers [RCII] with units of $PSII/m^{-3}$ and the primary ChlF parameter σ_{PII}.

The most widely used algorithm to date is the Sigma algorithm (Eq. 9.6) that calculates ETR as the product of E_{PAR}, [RCII], the product of σ_{PII} normalized to F_v/F that represent the PSII absorption cross-Section ($\sigma_{LHII} = \sigma_{PII} \cdot (F_v/F_m)^{-1}$), and the quantum yield of PSII photochemistry ($F_q{}'/F_m{}'$).

$$ETR = E_{PAR} \cdot [RCII] \cdot \sigma_{PII} \cdot (F_v/F_m)^{-1} \cdot F_q{}'/F_m{}' \quad (9.6)$$

Eq. 9.7 shows an equivalent derivation that does not require dark adapted σ_{PII} and F_v/F_m measurements. These equations are equivalent if light-induced changes in PSII absorption cross-section and quantum yield of PSII photochemistry are equivalent ($\sigma_{PSII}/\sigma_{PSII}{}' = F_v/F_m/F_v{}'/F_m{}'$).

$$ETR = E_{PAR} \cdot [RCII] \cdot \sigma_{PII}{}' \cdot F_q{}'/F_v{}' \quad (9.7)$$

The above two approaches require $[RCII]$. Most commonly, $[RCII]$ is estimated as the product of ancillary measurements of $[chl\ a]$ and the molar ratio of chl a per PSII reaction center (n_{PSII}, Eq. 9.8), where n_{PSII} is typically assumed to be 300 and 500 mol chl a mol RCII^{-1} for prokaryotes and eukaryotes respectively (Suggett et al., 2010).

$$[RCII] = n_{PSII} \cdot [chl\ a] \quad (9.8)$$

Ancillary field measurements of $[RCII]$ can be performed through the oxygen flash yield method (Suggett et al. 2004), but these are laborious and require high sample concentrations (~1 mg chl *a*/L). In the absence of either ancillary measurements of $[chl\ a]$ or $[RCII]$, ETR can be expressed per unit PSII (Eq. 9.9). Though ETR_{PSII} units are less biogeochemically relevant (mol photons m^{-3} s^{-1} PSII^{-1}), they are nonetheless meaningful. Lab-based ETR_{PSII} measurements co-vary with phytoplankton growth rates (Gorbunov and Falkowski, 2020), and the underlying measurements provide important photosynthetic physiological data that can also help inform remotely sensed products (Section 9.4).

$$ETR_{PSII} = E_{PAR} \cdot \sigma_{PII}{}' \cdot F_q{}'/F_v{}' \quad (9.9)$$

The absorption algorithm differs from the Sigma algorithm in that a_{LHII} is directly estimated from ChlF and an instrument specific coefficient K_a (Eq. 9.10). Briefly, K_A is experimentally derived through parallel ChlF and $[RCII]$ measurements and is based on the hypothesis that the quantum yields of fluorescence and photochemistry are equally impacted by changes in the rate constant of non-radiative decay (Oxborough et al., 2012). This experimental approach was refined by Boatman et al. (2019) to include fluorescence emission measurements at 730 nm in order to correct for fluorescence. Eq. 9.11 shows the derivation of ETR via the absorption algorithm; note that both dark and actinic measurements are required.

$$a_{LHII} = K_a \cdot \frac{F_m \cdot F_o}{F_m - F_o} \quad (9.10)$$

$$ETR = E_{PAR} \cdot K_a \cdot \frac{F_m \cdot F_o}{F_m - F_o} \cdot F_q{}'/F_m{}' \quad (9.11)$$

9.3.2. Kinetic-based ETR algorithm

An alternative measurement of ETR_{PSII} relies on the kinetics of the re-oxidation of Q_a during the PSII relaxation phase (Eq. 9.12) and is more thoroughly explained in Gorbunov and Falkowski (2020). This approach relies on measuring the rate of photosynthetic turnover under saturating actinic light ($1/\tau_{QA}'$), which defines maximum ETR_{PSII} achieved under saturating irradiance. The second term in the equation (in square brackets) is from measurements of light-dependent changes in F_q'/F_m'. The optimal level of E_{max} is selected as approximately 3 x E_k, where E_k is the light saturating parameter of the F_q'/F_m' versus E curve.

$$ETR_{PSII} = 1/\tau_{QA}' \cdot \left[(E_{PAR} \cdot F_q'/F_m') \cdot (E_{Max} \cdot F_q'/F_m'_{Emax})^{-1}\right] \quad (9.12)$$

The algorithm and operational protocol for kinetic measurements of ETR have been implemented in mini-FIRe instruments developed and manufactured at Rutgers University (Gorbunov and Falkowski, 2020) and in upgraded Satlantic FIRe fluorometers.

9.3.3. Algorithm selection and caveats

The ability to implement a given ETR algorithm has clear operational considerations. As described above, some algorithms yield volumetric ETR rates while others yield ETR_{PSII}, or ETR normalized to $[RCII]$. If volumetric ETR rates are desired, ancillary data are required to measure or model $[RCII]$, or a K_a calibrated fluorometeris used for the absorption algorithm (Oxborough, 2021).

Another clear operational consideration is whether the algorithm requires both dark and actinic ChlF parameters. While most new instrument variants permit both, dark measurements should correspond to fully dark-regulated phytoplankton where light-induced NPQ processes have been fully reversed. Unfortunately, there is no single ideal timescale that ensures full NPQ relaxation as it varies with environment and community. That said, a recommend a 10–20-minute low light (5–10 μmol m^{-2} s^{-1}) treatment to induce NPQ-relaxation and avoid "dark-quenching" caused by respiratory reduction in prokaryotes or chlororespiration in diatoms (Goss and Lepetit, 2015; Schuback et al., 2021).

An additional caveat is that baseline fluorescence cannot be analytical determined and equally increases F_o and F_m, which results in lowering F_v/F_m and their light-equivalent parameters. The importance of the various sources of baseline fluorescence is environment-dependent and to date largely unknown (Schuback et al., 2021). The impact of baseline fluorescence on algorithm-specific ETR rates can be assessed by subtracting an arbitrary value(s) from F' given some sensical constraints ($F'> 0$, $F_v/F_m < 0.70$, $1 \times 10^{-1} < \sigma_{PII} < 2 \times 10^{-17}$ m^2/RCII) (Ryan-Keogh and Robinson, 2021) and propagating baseline corrected ChlF parameters through each algorithm.

9.4. Electron Requirement for Carbon Fixation

Photosynthetic electron transport fundamentally drives ecosystem productivity and biogeochemistry, and compelling arguments can be made as to why electrons and not carbon should be the *de facto* photosynthetic currency (Hughes et al., 2018). The electron requirement

for carbon fixation ($\Phi_{e,C}$ mol e^- [mol C]$^{-1}$) is an analytical measurement of the stoichiometry between photosynthetic electron transport and carbon fixation rates ($P_C = ETR \cdot \Phi_{e,C}$). Hughes et al. (2018) provide a comprehensive theoretical and experimental overview of the drivers of $\Phi_{e,C}$ variability. Meta-analysis of $\Phi_{e,C}$ in diverse biogeochemical regions suggest that the fraction of photosynthetic energy stored as carbon decreases with increasing nutrient limitation with additional taxonomic variance (Lawrenz et al., 2013; Schuback et al., 2015, 2017; Zhu et al., 2017; Hughes et al., 2018), though with the important caveat that $\Phi_{e,C}$ meta-analysis is susceptible to methodological artifacts in both ETR and C fixation. When phytoplankton productivity is limited by the paucity of major nutrients (such as nitrogen), $\Phi_{e,C}$ has been estimated from the kinetic analysis of fluorescence relaxation and photosynthetic turnover rates (Gorbunov and Falkowski, 2022). The current community recommendation is that future $\Phi_{e,C}$ measurements focus on timescales that approach net primary production (Chapter 3 of this document).

9.5. Photosynthetic Irradiance Curves and Spectral Correction

The traditional photosynthetic light-response (PE) curves, which describe the characteristic dependence of the instantaneous rate of photosynthesis (carbon uptake or O2 evolution), P, on the incident illumination E, serve as a means of comparing the photosynthetic characteristics of marine phytoplankton across natural populations from different environments and of varied taxonomic composition (Platt and Jassby, 1976). ST-ChlF instruments also allow for easy and rapid acquisition of light response curves and the parameters that describe the PE curve, namely α (initial slope of light-dependent increase in photosynthetic rate), P_{max} (the maximum photosynthetic rate), and E_k (the light saturation parameter) (Platt and Gallegos, 1980; Bouman et al., 2018).

Most commercial variable fluorometers are equipped with programmable actinic light sources, which allow users to measure ChlF and ETR parameters across a defined light gradient. Indeed, such measurements are required to calculate the kinetic-based measurement of ETR_{PSII} (Eq. 9.12). Alternatively, light-dependent changes can be acquired through *in situ* deployments (depth profiles or fixed depth deployments through time), provided that ancillary measurements of E_{PAR} are also made. Onboard and programmable actinic light sources typically allow a user to program the length and magnitude of light steps. This flexibility has led to a variety of approaches being adopted, consistent with other photosynthetic rate measurements (Schuback et al., 2021). The current minimum community guideline is that PE parameters (α, P_{max}, and E_k) derived from variable fluorescence measurements report the exact actinic light treatment employed. Like traditional PE curves, a variety of models can be used to the fit data (Chapter 3 of this document). Silsbe and Kromkamp (2012) further show that E-dependency of ETR is best modeled by normalizing a given PE model to E as it preserves the desired PE parameters, removes E as a dependent variable, and critically places less dependency on high light measurements resulting in better fitting of the data. The open-source R package "phytotools" (Silsbe and Malkin, 2015) and the Python package "Phytoplankton Photophysiology Utilities" (Ryan-Keogh and Robinson, 2021) both allow for PE curve fitting.

Like all photosynthetic measurements, variable fluorescence PE curves are sensitive to the spectral quality of actinic irradiance. Spectral correction requires knowledge of the spectral optical environment(s) (instrument actinic sources, *in situ* optical environment) and the spectral

absorption coefficient of phytoplankton ($a_{ph}(\lambda)$). Spectra of instrument-specific actinic sources are normally provided by the manufacturer. Spectral correction procedures are provided in Section 3.5.1 of this IOCCG Volume. As a component of $a_{ph}(\lambda)$, σ_{PII} and σ_{PII}' are also sensitive to spectral quality, therefore measurements should be treated with the same spectral correction formulation. Detailed examples of spectral correction of variable fluorescence data are provided by Silsbe et al. (2015) and Schuback et al. (2021).

9.6. Phytoplankton Physiology from Space: Validation and Calibration of Solar-Induced Chlorophyll Fluorescence Yields

With the launch of the Moderate Resolution Imaging Spectroradiometer (MODIS) and Medium Resolution Imaging Spectrometer (MERIS) satellites, which possess the capability of detecting solar-induced chlorophyll fluorescence (SIF, also called passive fluorescence) in the global ocean, it became theoretically possible to calculate the quantum yield of ChlF (ϕ_{sat}) from space (Abbott and Letelier, 1999; Behrenfeld et al., 2009; Huot et al., 2013). The MODIS/MERIS and now Ocean and Land Colour Instrument (OLCI) analytical algorithms retrieve ϕ_{sat} from the ratio of SIF and the number of photons absorbed by phytoplankton in a defined and discrete near-surface volume of water. SIF is detected as a red peak (centered at ca. 683 nm) in spectra of water-leaving radiance spectra (Neville and Gower, 1977; Gordon et al., 1988; Gower et al., 1999). SIF is the only signal emitted from the ocean and detectable from space that can be unambiguously ascribed to phytoplankton (Behrenfeld et al., 2009).

The improvement of extant remote sensing algorithms that estimate SIF and ϕ_{sat} can benefit from vicarious *in situ* calibration and knowledge of the underlying ChlF parameters. Direct *in situ* measurements of the quantum yield of SIF have been performed using a multi-excitation fluorometer (non-variable) calibrated against a range of fluorophores with known optical properties and fluorescence yield (Griffith et al., 2018). The significant ϕ_{sat} variability in the global ocean (ca. ten-fold) has been broadly correlated to environmental forcings, namely light, temperature, and perhaps most notably iron (Letelier et al., 1997; Juot et al., 2005; Behrenfeld et al., 2009). Behrenfeld et al. (2009) demonstrated that accounting for the impact of non-photochemical quenching on ϕ_{sat} through a simple inverse-light correction term improved the detection of iron-limited regions with some notable exceptions (e.g., Southern Ocean). ChlF measurements through space and time can directly help improve our understanding of ϕ_{sat}, for example, improved characterization of NPQ variability may lead to improved ϕ_{sat} algorithms and ultimately a better understanding of biogeochemical controls on phytoplankton physiology globally.

9.7. Practical Recommendations

9.7.1. Instrument calibration

A comprehensive discussion on instrument calibration is currently being prepared (SCOR Working Group 2022). But the reader is advised that the most important document concerning calibration will be the instrument's user manual. Here, two calibration sources are identified, the excitation light (E_{ex}) used to excite PSII, and the actinic light sources now common to most variable fluorometers. The LEDs used in both light sources are considered very stable, such that factory calibrations can be valid for months to years (Schuback et al., 2021). Nevertheless, users should be aware of the need for routine monitoring and calibration, if necessary. Actinic light

levels can be verified by immersing a 4π sensor in a cuvette filled with pure water. Retrievals of σ_{PSII} in absolute units (m^2 $RCII^{-1}$) require accurate calibration of the average photon flux density in the measuring volume, i.e., the volume from which the signal is recorded. At present, calibration of E_{ex} is largely confined to manufacturers as the measurements may extend beyond the dynamic range of most PAR sensors. Recommendations have been put forth for these companies to provide guidelines and ancillary hardware (e.g., cuvette inserts that hold PAR sensors) for improved calibration going forward.

9.7.2. Underway measurements

Most variable fluorometers are well suited for autonomous deployments as part of an underway system or coastal observatory. The best practices for underway flow-through optical data have recently been documented (IOCCG, 2019) and are applicable to variable fluorometers. Best practices relevant to variable fluorometry include general plumbing, debubbling, geolocation, light contamination, flow rates, and inline optical blanks (i.e., water passed through a 0.2 mm filter). Some variable fluorometers have flow-through cuvettes, while others use programmable peristaltic pumps for sample exchange. The instrument should be set up in a way that minimizes vibration, while stray light can be mitigated by covering the instrument, if needed. If using a flow-through cuvette, a debubbler should be placed immediately in front of the cuvette and routinely checked for leaks. The water flow should be sufficiently slow such that residence time exceeds the length of the saturation and relaxation protocol. A GPS antenna that connects to a USB port can be purchased for ~20 USD and used to automatically synchronize the logging computer time. Inline optical blanks can help measure analytical blanks, though the user should carefully monitor biofouling.

9.7.3. Data archiving

The full potential of variable fluorescence can only be achieved through the compilation of inter-comparable data across the international research community. This requires the specification and adoption of standard reporting procedures and associated metadata for both new observations and, where possible, for archived datasets. Following the data hierarchy established by the satellite remote sensing community, the recommended community standard is to organize variable fluorescence data into the well-defined processing levels detailed below.

Level 0: Each instrument generates raw data (relatively large data files). The raw data format may vary among instruments and sampling protocols used. These data files have no value to a general user without access to instrument characterization records. The raw data files are usually stored, with a backup, on the user's memory resources (for potential re-processing if needed).

Level 1: Calibrated observational data from ChlF transients. L1 data applies instrument-specific calibration coefficients and characterization procedures to L0 data, thus these calibration coefficients are essential metadata. Analytical blanks constitute L1 data, and metadata should indicate their values and whether they have been applied to L1 data. Additional metadata includes instrument serial number, date, and time and location of observations. The community recommends archiving Level 1 data to facilitate and further test extant and future biophysical models.

Level 2: Photosynthetic physiological data derived from Level 1 (e.g., ϕ_{PSII}, τ_{Qa}, σ_{PII}, ETR) including statistical metrics (Section 9.2.3). Metadata should be repeated from Level 1 and

extended to include a complete description of analysis and protocols (e.g., ETR and/or bio-physical model employed, actinic irradiance details) and any ancillary data.

Table 9.1

List of active fluorescence symbols, definitions, and, where appropriate, derivations.

Symbol	Definition (Derivation)	Units
Primary ChlF Parameters		
F_o, F_m	Minimum, maximum ST-ChlF in the dark-adapted state	Relative
F', $F_m{}'$	Steady-state, maximum ST-ChlF in the light-regulated state	
$F_o{}'$	Minimum fluorescence in the light-regulated state. Measured after a brief (~1 s) period of darkness or: $F_o{}' = F_o/(F_v/F_m + F_o/F_m{}')$	Relative
τ_{Qa}, $\tau_{Qa}{}'$	Time constant for Qa re-oxidation in the dark-adapted, light-regulated state	ms
σ_{PII}, $\sigma_{PII}{}'$	Absorption cross section of PSII photochemistry in the dark-adapted, light regulated state	m^2 $RCII^{-1}$
ρ, ρ'	Connectivity factor in the dark-adapted, light-regulated state	Dimensionless
Secondary ChlF Parameters		
F_v	Variable fluorescence in the dark-adapted state $F_v = F_m - F_o$	Relative
$F_v{}'$	Maximum variable fluorescence in the light-regulated state $F_q{}' = F_m{}' - F_o{}'$	Relative
$F_q{}'$	Variable fluorescence in the light-regulated state $F_q{}' = F_m{}' - F'$	Relative
ϕ_{PSII}	The maximum quantum yield of PSII photochemistry $\phi_{PSII} = F_V/F_M$	Dimensionless
$\phi_{PSII}{}'$	The realized quantum yield of PSII photochemistry $\phi_{PSII}{}' = F_q{}'/F_m{}'$	Dimensionless
Rate Measurements and Ancillary Data		
E_{PAR}	Actinic photosynthetic active radiation	photons m^{-2} s^{-1}
ETR	PSII volumetric electron transport rate	photons m^{-3} s^{-1}
ETR_{PSII}	PSII electron transport rate per unit [PSII]	photons $RCII^{-1}$ s^{-1}
[chl *a*]	Volumetric concentration of chlorophyll *a*	mg chl *a* m^{-3}
K_a	Instrument specific calibration coefficient	photons m^{-3} s^{-1}
n_{PSII}	Molar ratio of chl a per PSII reaction center	mol chl a $mol\ PSII^{-1}$
$\Phi_{e,C}$	Photon requirement of carbon fixation	mol photons $mol\ C^{-1}$
[RCII]	Volumetric concentration of PSII reaction centers	RCII m^{-3}

9.8. References

Abbott, M. R., and Letelier, R. M. (1998). Decorrelation scales of chlorophyll as observed from bio-optical drifters in the California Current. *Deep Sea Research Part II: Topical Studies in Oceanography, 45*, 1639–1667.

Abbott, M. R., and Letelier, R. M. (1999). "Algorithm theoretical basis document: chlorophyll fluorescence", in: *MODIS Product Number 20). Ocean Biology Processing Group, NASA's Earth Observing System, 1999*).

Behrenfeld, M. J., Westberry, T. K., Boss, E. S., O'Malley, R. T., Siegel, D. A., Wiggert, J. D., Franz, B. A., Mcclain, C. R., Feldman, G. C., Doney, S. C., Moore, J. K., Dall'olmo, G., Milligan, A. J., Lima, I., and Mahowald, N. (2009). Satellite-detected fluorescence reveals global physiology of ocean phytoplankton. *Biogeosciences*, *6*, 779–794.

Boatman, T. G., Geider, R. J., and Oxborough, K. (2019). Improving the Accuracy of Single Turnover Active Fluorometry (STAF) for the Estimation of Phytoplankton Primary Productivity (PhytoPP). *Frontiers in Marine Science,* 6.

Bouman, H. A., Platt, T., Doblin, M., Figueiras, F. G., Gudmundsson, K., Gudfinnsson, H. G., Huang, B., Hickman, A., Hiscock, M., Jackson, T., Lutz, V. A., Mélin, F., Rey, F., Pepin, P., Segura, V., Tilstone, G. H., Van Dongen-Vogels, V., and Sathyendranath, S. (2018). Photosynthesis–irradiance parameters of marine phytoplankton: synthesis of a global data set. *Earth Syst. Sci. Data, 10*, 251–266.

Cullen, J., Ciotti, A., Davis, R., and Neale, P. (1997). Relationship between near-surface chlorophyll and solar-stimulated fluorescence: biological effects. SPIE.

Cullen, J. J., and Davis, R. F. (2003). The blank can make a big difference in oceanographic measurements. *Limnology and Oceanography Bulletin,* 12.

Esaias, W. E., Abbott, M. R., Barton, I., Brown, O. B., Campbell, J. W., Carder, K. L., Clark, D. K., Evans, R. H., Hoge, F. E., Gordon, H. R., Balch, W. M., Letelier, R., and Minnett, P. J. (1998). An overview of MODIS capabilities for ocean science observations. *IEEE Transactions on Geoscience and Remote Sensing,* 36, 1250–1265.

Falkowski, P. G., Koblfzek, M., Gorbunov, M., and Kolber, Z. (2004). "Development and Application of Variable Chlorophyll Fluorescence Techniques in Marine Ecosystems," in *Chlorophyll a Fluorescence: A Signature of Photosynthesis,* eds. G.C. Papageorgiou & Govindjee. (Dordrecht: Springer Netherlands), 757–778.

Falkowski, P.G., Lin, H., and Gorbunov, M. Y. (2017). What limits photosynthetic energy conversion efficiency in nature? Lessons from the oceans. *Philosophical Transactions of the Royal Society B: Biological Sciences,* 372.

Gorbunov, M. Y., and Falkowski, P. G. (2020). Using chlorophyll fluorescence kinetics to determine photosynthesis in aquatic ecosystems. *Limnology and Oceanography, 66*, 1–13.

Gorbunov, M. Y. & Falkowski P. G. (2022) Using chlorophyll fluorescence to determine the fate of photons absorbed by phytoplankton in the world's oceans. *Annual Reviews in Marine Sciences*, https://doi.org/10.1146/annurev-marine-032621-122346.

Gordon, H.R., Brown, O.B., Evans, R.H., Brown, J.W., Smith, R.C., Baker, K.S., and Clark, D.K. (1988). A semianalytic radiance model of ocean color. *Journal of Geophysical Research: Atmospheres, 93*, 10909–10924.

Gordon, H. R., and Morel, A. Y. (1983). "In-Water Algorithms," in Remote Assessment of Ocean Color for Interpretation of Satellite Visible Imagery, Lecture Notes on Coastal and Estuarine Studies book series (COASTAL, volume 4). Springer-Verlag), 24-67.

Goss, R., and Lepetit, B. (2015). Biodiversity of NPQ. *Journal of Plant Physiology, 172*, 13–32.

Govindje, E. (1995). Sixty-Three Years Since Kautsky: Chlorophyll a Fluorescence. *Functional Plant Biology, 22*, 131–160.

Gower, J. F. R., Doerffer, R., and Borstad, G. A. (1999). Interpretation of the 685nm peak in water-leaving radiance spectra in terms of fluorescence, absorption and scattering, and its observation by MERIS. *International Journal of Remote Sensing, 20*, 1771–1786.

Holm-Hansen, O., and Riemann., B. (1978). Chlorophyll *a* determination: improvements in methodology. *Oikos, 30*, 438–447.

Hughes, D.J., Varkey, D., Doblin, M. A., Ingleton, T., Mcinnes, A., Ralph, P. J., Van Dongen-Vogels, V., and Suggett, D. J. (2018). Impact of nitrogen availability upon the electron requirement for carbon fixation in Australian coastal phytoplankton communities. *Limnology and Oceanography, 63*, 1891–1910.

Huot, Y., and Babin, M. (2010). "Overview of fluorescence protocols: theory, basic concepts, and practice," in *Chlorophyll a Fluorescence in Aquatic Sciences: Methods and Applications in Applied Phycology,* eds. D.J. Suggett, M.A. Borowitzka & O. Prášil. (Netherlands: Springer Science+Business Media B.V).

Huot, Y., Brown, C. A., and Cullen, J. J. (2005). New algorithms for MODIS sun-induced chlorophyll fluorescence and a comparison with present data products. *Limnology and Oceanography-Methods, 3*, 108–130.

Huot, Y., Franz, B. A., and Fradette, M. (2013). Estimating variability in the quantum yield of Sun–induced chlorophyll fluorescence: A global analysis of oceanic waters. *Remote Sensing of Environment, 132*, 238–253.

IOCCG Protocol Series (2018). Inherent Optical Property Measurements and Protocols: Absorption Coefficient, Neeley, A. R. and Mannino, A. (eds.), IOCCG Ocean Optics and Biogeochemistry Protocols for Satellite Ocean Colour Sensor Validation, Volume 1.0, IOCCG, Dartmouth, NS, Canada. http://dx.doi.org/10.25607/OBP-119

IOCCG Protocol Series (2019). "Inherent Optical Property Measurements and Protocols: Best Practices for the Collection and Processing of Ship-Based Underway Flow-Through Optical Data.", in: *Ocean Optics and Biogeochemistry Protocols for Satellite Ocean Colour Sensor Validation.* (eds.) A.R. Neeley & A. Mannino. (Dartmouth, NS, Canada: International Ocean-Colour Coordinating Group (IOCCG)).

Kolber, Z., and Falkowski, P. G. (1993). Use of active fluorescence to estimate phytoplankton photosynthesis i*n situ*. *Limnology Oceanography, 38*, 1646–1665.

Kolber, Z. S., Prášil, O., and Falkowski, P. G. (1998). Measurements of variable chlorophyll fluorescence using fast repetition rate techniques: defining methodology and experimental protocols. *Biochimica et Biophysica Acta (BBA) – Bioenergetics, 1367*, 88–106.

Lawrenz, E., Silsbe, G., Capuzzo, E., Ylöstalo, P., Forster, R. M., Simis, S. G. H., Prášil, O., Kromkamp, J. C., Hickman, A. E., Moore, C. M., Forget, M. -H., Geider, R. J., and Suggett, D. J. (2013). Predicting the Electron Requirement for Carbon Fixation in Seas and Oceans. *PloS One, 8*, e58137.

Letelier, R. M., Abbott, M. R., and Karl, D. M. (1997). Chlorophyll natural fluorescence response to upwelling events in the Southern Ocean. *Geophysical Research Letters, 24*, 409–412.

Lin, H., Kuzminov, F. I., Park, J., Lee, S., Falkowski, P. G., and Gorbunov, M. Y. (2016). The fate of photons absorbed by phytoplankton in the global ocean. *Science, 351*, 264–267.

Maritorena, S., Morel, A., and Gentili, B. (2000). Determination of the fluorescence quantum yield by oceanic phytoplankton in their natural habitat. *Applied Optics, 39*, 6725–6737.

Maxwell, K., and Johnson, G. N. (2000). Chlorophyll fluorescence—a practical guide. *Journal of Experimental Botany, 51*, 659–668.

Moore, C. M., Mills, M. M., Langlois, R., Milne, A., Achterberg, E. P., La Roche, J., and Geider, R. J. (2008). Relative influence of nitrogen and phosphorous availability on phytoplankton physiology and productivity in the oligotrophic sub-tropical North Atlantic Ocean. *Limnology and Oceanography, 53*, 291–305.

Morel, A., and Prieur, L. (1977). Analysis of Variations in Ocean Color. *Limnology Oceanography, 22*, 709–722.

Morrison, J. R. (2003). *In situ* determination of the quantum yield of phytoplankton chlorophyll a fluorescence: A simple algorithm, observations, and a model. *Limnology and Oceanography, 48*, 618–631.

Neville, R. A., and Gower, J. F. R. (1977). Passive remote sensing of phytoplankton via chlorophyll α fluorescence. *Journal of Geophysical Research (1896-1977), 82*, 3487–3493.

Oxborough, K. (2021). LabSTAF and RunSTAF Handbook: 2408-014-HB | Issue E. West Molesey, UK, Chelsea Technologies Ltd. 116pp. (Doc No. 2408-014-HB | Issue E). http://dx.doi.org/10.25607/OBP-1029.3

Oxborough, K., Moore, C. M., Suggett, D. J., Lawson, T., Chan, H. G., and Geider, R. J. (2012). Direct estimation of functional PSII reaction center concentration and PSII electron flux on a volume basis: a new approach to the analysis of Fast Repetition Rate fluorometry (FRRf) data. *Limnology Oceanography: Methods, 10*, 142–154.

Platt, T., and Gallegos, C. L. (1980). "Modelling Primary Production," in *Primary Productivity in the Sea,* ed. P.G. Falkowski. (Boston, MA: Springer US), 339–362.

Platt, T., and Jassby, A.D. (1976). The Relationship between Photosynthesis and Light for Natural Assemblages of Coastal Marine Phytoplankton. *Journal of Phycology, 12*, 421–430.

Ryan-Keogh, T. J., and Robinson, C. M. (2021). Phytoplankton Photophysiology Utilities: A Python Toolbox for the Standardization of Processing Active Chlorophyll aFluorescence Data. *Frontiers in Marine Science,* 8.

Schreiber, U., Schliwa, U., and Bilger, W. (1986). Continuous recording of photochemical and non-photochemical chlorophyll fluorescence quenching with a new type of modulation fluorometer. *Photosynthesis Research, 10*, 51–62.

Schuback, N., Schallenberg, C., Duckham, C., Maldonado, M. T., and Tortell, P. D. (2015). Interacting effects of light and iron availability on the coupling of photosynthetic electron transport and CO2-assimilation in marine phytoplankton. *PloS One,* 10:e0133235. https://doi.org/10.1371/journal.pone.0133235

Schuback, N., Hoppe, C. J. M., Tremblay, J. É, Maldonado, M. T., and Tortell, P. D. (2017). Primary productivity and the coupling of photosynthetic electron transport and carbon fixation in the Arctic Ocean. *Limnol. Oceanogr*., *62*, 898–921. https://doi.org/10.1002/lno.10475

Schuback, N., Tortell, P.D., Berman-Frank, I., Campbell, D.A., Ciotti, A., Courtecuisse, E., Erickson, Z.K., Fujiki, T., Halsey, K., Hickman, A.E., Huot, Y., Gorbunov, M.Y., Hughes, D.J., Kolber, Z.S., Moore, C.M., Oxborough, K., Prášil, O., Robinson, C.M., Ryan-Keogh, T.J., Silsbe, G., Simis, S., Suggett, D.J., Thomalla, S., and Varkey, D.R. (2021). Single-Turnover Variable Chlorophyll Fluorescence as a Tool for Assessing Phytoplankton Photosynthesis and Primary Productivity: Opportunities, Caveats and Recommendations. *Frontiers in Marine Science*, 8, 895.

SCOR Working Group (2022). "A User Guide for the Application of Single Turnover Active Chlorophyll Fluorescence for Phytoplankton Productivity Measurements. Version 1." (Baltimore, MD: Scientific Committee on Oceanic Research Working Group 156). https://repository.oceanbestpractices.org/handle/11329/1585

Silsbe, G. M., and Malkin, S. Y. (2015). Phytotools: Phytoplankton production tools. R package Version 1.0. https://CRAN.R-project.org/package=phytotools

Silsbe, G. M., Oxborough, K., Suggett, D.J., Forster, R. M., Ihnken, S., Komárek, O., Lawrenz, E., Prášil, O., Röttgers, R., Šicner, M., Simis, S. G. H., Van Dijk, M. A., and Kromkamp, J.C. (2015). Toward autonomous measurements of photosynthetic electron transport rates: An evaluation of active fluorescence-based measurements of photochemistry. *Limnology and Oceanography: Methods, 13*, 138–155.

Suggett, D. J., Prášil, O., & Borowitzka, M. A. (2010). *Chlorophyll a fluorescence in aquatic sciences: methods and applications* (Vol. 4). Dordrecht: Springer.

Thomalla, S. J., Moutier, W., Ryan-Keogh, T. J., Gregor, L., and Schütt, J. (2018). An optimized method for correcting fluorescence quenching using optical backscattering on autonomous platforms. *Limnology and Oceanography: Methods, 16*, 132–144.

Zhu, Y., Ishizaka, J., Tripathy, S.C., Wang, S., Sukigara, C., Goes, J., Matsuno, T., and Suggett, D.J. (2017). Relationship between light, community composition and the electron requirement for carbon fixation in natural phytoplankton. *Marine Ecology Progress Series, 580*, 83–100.

10. Autonomous Platforms

David P. Nicholson[1], Andrea J. Fassbender[2], Magdalena M. Carranza[3], Ivona Cetinić[4,5]

[1]*Marine Chemistry and Geochemistry Department, Woods Hole Oceanographic Institution, Massachusetts, USA*
[2]*NOAA Pacific Marine Environmental Laboratory, Washington, USA*
[3]*Monterey Bay Aquarium Research Institute, California, USA*
[4]*Morgan State University, Maryland, USA*
[5]*NASA Goddard Space Flight Center, Maryland, USA*

10.1. Introduction

In recent decades, advances in underwater robotics and biogeochemical sensors have greatly expanded the ability of oceanographers to observe ocean processes using autonomous systems (Lee et al., 2017). These tools have enabled new approaches for quantifying ocean productivity and hold the promise to vastly improve the spatial and temporal coverage of *in situ* primary productivity and net community productivity estimates. In the last several years, multiple methods relying on measures of biogeochemical properties such as oxygen, carbon, nitrogen, chlorophyll fluorescence, optical backscatter, irradiance, etc. have been used to estimate productivity rates in the upper ocean. These emerging applications for autonomous observations complement existing satellite remote sensing and ship-based approaches. Autonomous platforms profile the subsurface water column capturing the vertical structure, such as the deep chlorophyll maximum, often missed by ocean color satellites. However, in the open ocean, these applications are still relatively new and vary widely in the type of productivity (net, gross, etc.) captured and methodological assumptions required. Here, we summarize the current state of autonomous platform-based productivity estimates, best practices, and potential for future growth with a focus on routinely deployed chemical and optical sensors and open ocean applications.

Depending on the approach, autonomous estimates of productivity approximate either net community production (NCP), net primary production (NPP), or gross primary production (GPP) and quantify these rates in carbon, oxygen, or nitrogen-based units (Fig. 10.1). Some approaches also quantify heterotrophic rates such as community respiration (CR), which is the sum of respiration by autotrophs (R_A) and heterotrophs (R_H). Here, we outline more widespread methodologies used to quantify these metabolic rates, recognizing that these approaches continue to evolve, mature, and expand. First, NCP methods based on mass balance approaches to estimating NCP are described, followed by NPP and GPP methods based on optical algorithms and diel budgets, respectively.

10.1.1. Platforms, sensors, and calibration

Advancements in autonomous sensors and platforms over the past few decades are transforming our ability to observe ocean biogeochemical changes persistently and over a wide range of time scales (Sauzède et al., 2016, Bushinsky et al., 2019, Chai et al., 2020, Bisson et al., 2021). Moorings (Körtzinger et al., 2008; Emerson and Stump, 2010; Weeding and Trull, 2014; Fassbender et al. 2016, 2017), wave gliders (Wilson et al., 2014; Chavez et al. 2017; Nicholson et al., 2022), subsurface gliders (Rudnick, 2016), floats (D'Asaro, 2003; Yang et al. 2017; Williams et al., 2018; Bushinsky et al., 2018; Arteaga et al., 2020; Claustre et al., 2020), and

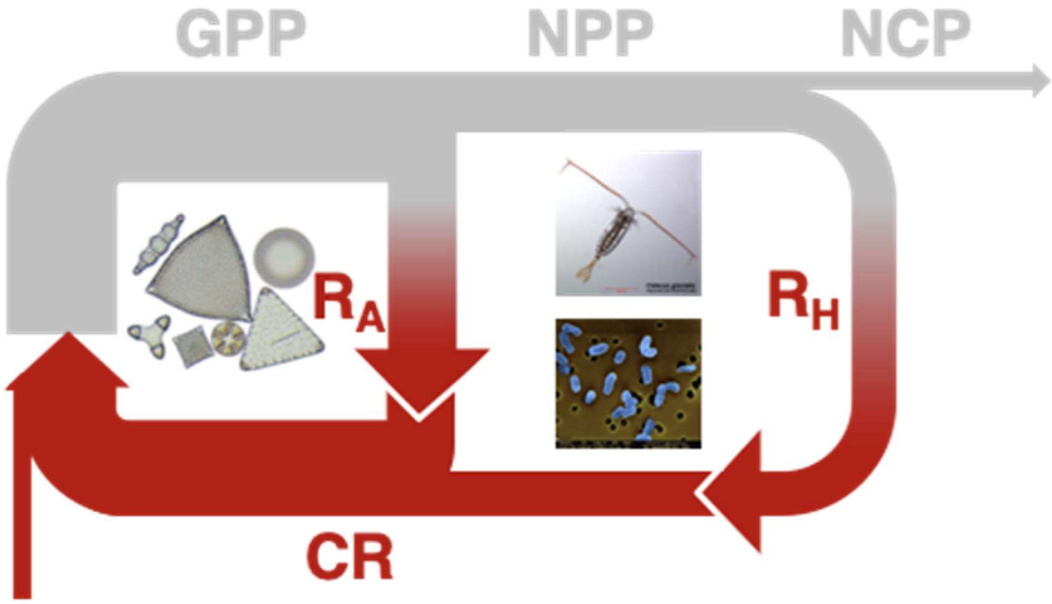

Fig. 10.1. Diagram of metabolic rates of in the surface ocean.

Wirewalkers (Lucas et al., 2013; Omand et al., 2017) are becoming more commonly used to evaluate upper ocean metabolic balances, study the magnitude and phenology of biological processes, and quantify the biological pump. The most mature and widespread chemical and optical sensors used to quantify primary productivity are shown in Table 10.1. These sensors are suitable for long-term deployment based on their robustness and power requirements.

Long-term deployments of biogeochemical sensors aboard autonomous platforms and moorings (Chai et al., 2020) allow for unprecedented insights into the variability of oceanic productivity. Yet, despite recent advances in sensor technology, biogeochemical sensors require careful calibration and evaluation. So far, no biogeochemical sensors should be considered to have sufficient accuracy and stability for quantitative estimates of biogeochemical rates without careful calibration and validation. Biogeochemical sensors are subject to a range of factors that can reduce accuracy and bias primary productivity estimates. These include aging/degradation of sensor components (both before and during deployment) caused by, for example, reduced intensity of LED light sources with time, biofouling of optical windows, dynamic errors due to finite sensor response times, sensor drift, and inadequate sensor characterization or factory calibration. Best practices for calibration of each sensor type have been documented through several efforts by NASA, SCOR, IOCCG, Argo, and GEOTRACES-led groups who have produced detailed protocols outlining proper calibration procedures and best deployment practices (e.g., Owens and Wong, 2009; Boss et al., 2015, 2019, 2020; Bittig et al., 2019).

Once deployed, various techniques are used to improve calibration. Often these approaches involve comparing the sensor to known or calculated reference values. For example, for optical sensors, deep values can be assumed to be below detection limits for downwelling irradiance, chlorophyll, and optical backscatter. These reference values can be used to adjust factory-calibrated dark values. For oxygen, measurements can be compared against climatological values

at deep reference levels (Takeshita et al., 2013). Some platforms are capable of in-air measurement of a known atmospheric oxygen partial pressure. This air-calibration approach is applied to profiling floats (Bushinsky et al., 2016; Johnson et al., 2015; Bittig and Körtzinger, 2015, 2017) and gliders (Nicholson et al. 2017). Statistical models are also commonly used to predict inorganic carbon and nitrate concentrations at depth (Williams et al., 2016; Carter et. al. 2018; Bittig et al., 2018) as a means of sensor performance calibration/validation. Overall, calibration approaches are nuanced and depend significantly on the platform and sensor model.

High-quality discrete measurements taken from research vessels are the ultimate standard for biogeochemical sensors. In many cases, there is a direct correspondence between sensor and shipboard measurements. For example, oxygen optodes are calibrated against shipboard Winkler oxygen titrations. Other sensors measure a property more removed from the quantity of biogeochemical interest. For example, optical backscatter sensors, which measure the intensity of light scattered back to the sensor, are used to estimate particulate organic carbon (POC). Making such connections requires what is termed "proxy building," where shipboard biogeochemical (BGC) measurements of the desired variable (e.g., POC) are statistically compared to the related sensor measurement (e.g., optical backscatter). Such proxy relationships can vary regionally and temporally as a function of a wide range of factors, including, for example, phytoplankton community composition and mineral deposition. Similarly, Chlorophyll *a* concentrations are obtained from float fluorescence data that have been corrected for non-photochemical quenching (NPQ) effects and, in some cases, calibrated against HPLC measurements of Chlorophyll *a* concentration from two near-surface water samples obtained during float deployments (Johnson et al., 2017a; Haëntjens et al., 2017). Regional, temporal, and depth dependences of the fluorescence to chlorophyll relationship are another challenge for interpreting sensor data used for proxy estimation (Roesler et al., 2017; Long et al., 2021).

Sensor data quality challenges often depend on the platform on which sensors are deployed. Moored instruments and instrumentation that spend substantial time in the euphotic zone are more susceptible to biofouling. In both cases, post-deployment calibration (some platforms are not recoverable), sensor redundancy on the same platform (hard due to the power/weight limitations of the platforms), or intercalibration with other *in situ* platforms or ocean color satellites can help with long-term drift correction. Profiling floats spend most of the time at great depths, and the transition to faster communication systems (Iridium) has substantially decreased the amount of time floats spend at the surface for data transmission (~20'), significantly reducing bio-fouling effects (Roemmich et al., 2019).

In addition to individual sensor calibration, sensors that are part of a sensor array require intercalibration to provide consistency between each sensor unit. For example, NAB08 (Briggs et al., 2011) and EXPORTS (Siegel et al., 2021) took the approach of a "gold standard" well-characterized and calibrated sensor, usually deployed aboard a ship's CTD (Boss et al., 2015) that is then used for intercalibration via ship-board calibration casts and vicarious intercalibration opportunities. For large-scale programs such as Biogeochemical Argo, ship-based programs such as GO-SHIP and databases such as SOCAT (Bakker et al., 2016) serve as validation datasets.

Table 10.1

Biogeochemical properties routinely measured aboard autonomous platforms that can be used for productivity estimates. Modified from Chai et al. (2020).

Property	Symbol	Sensor	Platform	PP Measurement
Dissolved oxygen	O_2	Luminescence lifetime optode	All autonomous platforms	NCP/GPP
Partial pressure of carbon dioxide	pCO_2	NDIR/Equilibration based infrared analyzer	Unmanned Surface Vehicles	NCP
Nitrate	NO_3^-	Ultraviolet spectrophotometer	Profiling floats, gliders	NCP
pH	pH	Ion sensitive field-effect transistor	All autonomous platforms	NCP/GPP
Particulate organic carbon	b_{bp}	Optical backscatter	All autonomous platforms	GPP/NPP
Particulate organic carbon	c_p	Optical attenuation	Floats	
Chlorophyll a	Chl / ChlF	Fluorometer	All autonomous platforms	NPP
Downwelling irradiance and PAR	PAR	Radiometer	Profiling floats, gliders	NPP

10.2. Net Community Production

Net community production (NCP) is equal to the gross photosynthesis (GPP) minus the combined autotrophic and heterotrophic respiration (i.e., CR), reflecting the net ecosystem metabolism of both dissolved and particulate organic material (see Section 2.2). While this definition is straight-forward, multiple approaches have been used to quantify NCP, providing complementary but often dissimilar information about upper ocean carbon cycling. The general approach is to look at the change over time in the depth-integrated concentration (stock) of a biologically active parameter. When evaluated over a sufficient time period (commonly 1 year), NCP is equivalent to the amount of carbon exported from the depth (or density) horizon evaluated, assuming that the system is in steady state (i.e., there is no time-rate-of-change in the property used to assess NCP) (Emerson, 2014).

The current state of autonomous sensor technology makes it possible to estimate NCP from oxygen (O2) (Alkire et al., 2014; Bushinsky and Emerson, 2015; Haskell et al. 2019; Huang et al., 2018; Nicholson et al., 2008; Thomalla et al., 2015; Yang et al., 2017), nitrate (NO3) (Bif et al., 2019; Haskell et al., 2020; Johnson, 2010; Johnson et al., 2017; Plant et al., 2016; Williams et al., 2018), DIC (Fassbender et al., 2016, 2017; Johnson, 2010; Körtzinger et al., 2008; Williams et al., 2018) and total alkalinity (TA) (Fassbender et al., 2016, 2017; Williams et al., 2018). Chemical sensors are capable of measuring O_2 and NO_3^- directly. However, TA is commonly derived from regional TA-salinity relationships or global algorithms (Bittig et al., 2018, Carter et al., 2016, Carter et al., 2018, Lee et al., 2006), while DIC is often computed from TA estimates and measurements of pCO_2 or pH but can also be directly estimated from empirical algorithms (e.g., Bittig et al., 2018). Changes in the stock of a parameter over time, within a specific depth or density interval, reflect the various processes occurring within or influencing that layer of

water, some of which are biological in nature. By quantifying all physical fluxes, the residual term reflects the biological contributions in addition to computational errors.

10.2.1. Underlying equations

Chemical tracer budgets must account for all upper-ocean fluxes that influence the tracer over the observing period, including physical (Phys), freshwater (FW), and biological (Bio) fluxes. Additionally, DIC and O_2 budgets must account for air-sea exchange processes (Gas). An example equation for the changes in tracer stock over time (t), expressed for DIC, is

$$\frac{\partial DIC}{\partial t} = \frac{\partial DIC}{\partial t}\Big|_{Gas} + \frac{\partial DIC}{\partial t}\Big|_{Phys} + \frac{\partial DIC}{\partial t}\Big|_{FW} + \frac{\partial DIC}{\partial t}\Big|_{Bio}. \tag{10.1}$$

The Gas term accounts for bulk air-sea gas exchange and is parameterized as the difference between observed (obs) and saturated (sat) concentrations (with respect to the atmosphere) of the molecule of interest multiplied by the gas transfer velocity (k), which scales as a function of wind speed (Wanninkhof, 2014).

$$\frac{\partial DIC}{\partial t}\Big|_{Gas} = k([CO_2]_{obs} - [CO_2]_{sat}) \tag{10.2}$$

Observed and saturated concentrations are often calculated from gas partial pressures (e.g., pCO_2 and pO_2) measured in seawater and the atmospheric boundary layer (corrected to the water-vapor-saturated gas partial pressures (Dickson et al., 2007), and the respective solubility constants (Garcia and Gordon, 1992; Weiss, 1974). Note that the flux direction is determined by the difference in gas partial pressures between the ocean and atmosphere, and the sign convention of Eq. 10.2 is such that positive flux is into the ocean. When *in situ*, local observations are unavailable, so the wind speed, atmospheric surface pressure, and relative humidity data are retrieved by interpolating reanalysis data to the autonomous asset location. Additionally, the dry air mixing ratio of atmospheric CO_2 can be obtained from NOAA's Marine Boundary Layer dataset (Wanninkhof et al., 2019), while the dry air mixing ratio of atmospheric O_2 can be assumed constant, surface pO_2 changes due to sea level pressure and water vapor pressure variations, as described in Bittig and Körtzinger (2015).

Unlike CO_2 (which is more soluble), the air-sea exchange of O_2 must also account for bubble-mediated flux (F_B), which can significantly increase mixed layer O_2 concentrations and leave a lasting (~1 month) signature on the water column (see Emerson and Bushinsky 2016 and citations therein).

$$\frac{\partial O_2}{\partial t}\Big|_{Gas} = k([O_2]_{obs} - [O_2]_{sat}) + F_B \tag{10.3}$$

The FW budget term accounts for evaporation and precipitation effects on tracer concentrations based on salinity (Sal) observations, expressed here for DIC

$$\left.\frac{\partial DIC}{\partial t}\right|_{FW} = \left(\frac{\partial Sal}{\partial t} - \left.\frac{\partial Sal}{\partial t}\right|_{Phys}\right) \times \left.\frac{DIC}{Sal}\right|_{t=0}, \tag{10.4}$$

where t = 0 is the DIC to salinity ratio at time zero in the budget integration. The Phys term accounts for tracer supply or removal due to vertical advection, entrainment (i.e., changes in the mixed layer depth) and turbulent mixing, expressed here for DIC

$$\left.\frac{\partial DIC}{\partial t}\right|_{Phys} = -\left(w + \frac{\partial h}{\partial t}\right)\frac{(DIC_{ML} - DIC_h)}{h} - \frac{1}{h}\left(K_z \frac{\partial DIC}{\partial z}\right)\Big|_h, \tag{10.5}$$

where DIC_{ML} is DIC the averaged concentration in a mixed layer of depth h, and w, DIC_h, K_Z, and $\delta DIC/\delta z$ are the vertical velocity, DIC concentration, eddy diffusivity, and vertical concentration gradient evaluated at the depth of the mixed layer. Horizontal advection and diffusion processes are often omitted, particularly in annual NCP budgets, due to poor constraint on lateral gradients and the dominance of vertical processes on seasonal timescales (see discussion below).

After accounting for Gas, FW, and Phys, the residual Bio term (which includes all errors) can be solved by rearranging Eq. 10.1. For the DIC and TA budgets, the residual biological term reflects both NCP and net calcium carbonate ($CaCO_3$) production.

$$\left.\frac{\partial DIC}{\partial t}\right|_{Bio} = \left.\frac{\partial DIC}{\partial t}\right|_{NCP} + \left.\frac{\partial DIC}{\partial t}\right|_{CaCO_3} \tag{10.6}$$

To differentiate these terms, one must leverage the fact that biological processes influence DIC and TA at well-known stoichiometric ratios. For example, each mole of $CaCO_3$ produced results in a reduction of one mole of DIC and two moles of TA. Additionally, for organic matter production, one mole of hydrogen phosphate, 18 moles of H^+ and 117 moles of CO_2 are consumed, resulting in a TA increase of 17 moles (Wolf-Gladrow et al., 2007; Anderson and Sarmiento, 1994; Brewer and Goldman, 1976). Using these relationships and rearranging Eq. 10.5 and 10.6, one can solve for the DIC and TA budget NCP and $CaCO_3$ terms (Fassbender et al., 2016).

$$\left.\frac{\partial DIC}{\partial t}\right|_{NCP} = \frac{\left.\frac{\partial TA}{\partial t}\right|_{Bio} - 2\left.\frac{\partial DIC}{\partial t}\right|_{Bio}}{-2 + (-17/117)} \tag{10.7}$$

$$\left.\frac{\partial DIC}{\partial t}\right|_{CaCO_3} = \left.\frac{\partial DIC}{\partial t}\right|_{Bio} - \left.\frac{\partial DIC}{\partial t}\right|_{NCP} \tag{10.8}$$

The inclusion of $CaCO_3$ cycling in tracer budget evaluations remains rare (Fassbender et al., 2016, 2017; Williams et al., 2018; Haskell et al., 2020) and provides an integrated (rather than *in situ*) view of $CaCO_3$ production because TA is presently estimated from parameters that are not

instantaneously influenced by $CaCO_3$ production (often salinity and temperature). Still, the separation of carbon pools can bring new insight to the role of calcium carbonate minerals in the biological carbon pump (e.g., Marañón et al., 2016).

When networks of chemical sensors are deployed, even more information can be gleaned from tracer budgets (e.g., Johnson, 2010; Haskell et al., 2020). For example, by assuming a C:O organic matter conversion ratio of 1.4 (Laws, 1991), C:N stoichiometry of 16:117 (Anderson and Sarmiento, 1994), and a TA:N stoichiometry of -17:16 (Brewer and Goldman, 1976, Wolf-Gladrow et al., 2007), the budgets can be solved in multiple ways to independently deconvolve the $CaCO_3$ and NCP terms. For example, DIC_{NCP} can be determined using the C:O or C:N ratio, which can be subtracted from the overall DIC_{Bio} term to solve for DIC_{CaCO3},

$$DIC_{CaCO_3} = DIC_{Bio} - (R_{C:O} \times O_{2Bio}) = DIC_{Bio} - (R_{C:N} \times NO^{-}_{3Bio}). \quad (10.9)$$

Alternatively, TA_{NCP} can be determined using the TA:N ratio to solve for TA_{CaCO3} and DIC_{CaCO3},

$$TA_{CaCO_3} = 2 \times DIC_{CaCO_3} = TA_{Bio} - (R_{TA:N} \times NO^{-}_{3Bio}). \quad (10.10)$$

Redundant closing of budgets with different tracer pairings can thus provide quantitative information about potential systematic biases in the tracer methods, which each have different strengths and weaknesses.

10.2.2. Net community production uncertainties

10.2.2.1. Elemental stoichiometries

A key uncertainty in tracer budget approaches is the use of fixed and often unknown elemental stoichiometries (i.e., $R_{C:O}$, $R_{C:N}$, etc.) for bulk net community production and respiration. With sensor networks, different ratios can be used to convert biological production terms to other elemental quantities, providing some bounds on the error associated with these conversions. For example, the $O_{2\,Bio}$ and $NO_{3^-\,Bio}$ terms provide estimates of net organic matter production that can be converted to units of DIC and compared. Alternatively, the DIC_{NCP} term derived from $O_{2\,Bio}$ can be used with the $NO_{3^-\,NCP}$ term to estimate the C:N ratio of net community metabolism. The recent advent and widespread use of autonomous pH sensors (Martz et al., 2010, Johnson et al., 2016) now make it possible to estimate DIC from pH observations and TA estimates rather than through the C:O (or C:N) conversion and look at changes in DIC_{NCP} and $NO_{3^-\,NCP}$ (or $O_{2\,NCP}$) simultaneously to evaluate variability in the C:N (or C:O) ratio over time (Haskell et al., 2020). This is useful because most tracer budgets assume a C:N stoichiometry near ~6.6 (Redfield et al., 1963) even though dissolved organic carbon (DOC) production also contributes to NCP and can have a C:N ratio that differs significantly (e.g., DOC $R_{C:N}$ ~10) from Redfield (e.g., Letscher and Moore, 2015).

With more comprehensive sensor networks now being deployed on autonomous platforms (e.g., Johnson et al., 2017), upper ocean tracer budgets are becoming more complex and comprehensive. Some investigators are now attempting to differentiate the particulate organic carbon (POC) and dissolved organic carbon (DOC) phases of NCP using solely *in situ* observations on autonomous platforms (Fig. 10.2). For example, Alkire et al. (2012) quantified

NCP using oxygen and nitrate observations from a Lagrangian profiling float (D'Asaro, 2003) in the North Atlantic Ocean. Considering differing elemental stoichiometries for POC and DOC, they estimated the POC and DOC components of NCP. They were then able to subtract the standing stock of POC, derived from float backscattering measurements, from NCP_{POC} term to determine how much of the NCP_{POC} had been exported from the upper ocean during the 1.5-month study period. Similarly, Haskell et al. (2020) used nitrate, DIC, and TA budgets to solve for POC, DOC, and $CaCO_3$ production and export for > 10 years of biogeochemical profiling float and mooring observations in the North Pacific Ocean. Building on this work, Huang et al. (2022) applied chemical and optical tracer budget approaches to observations from a single biogeochemical profiling float in the North Pacific Ocean to partition all biogenic carbon pools. A key advancement in this study came from combining the integrated POC production information provided by chemical tracer budgets with the instantaneous POC stock information provided by the optical tracer budget. This allowed Huang et al. (2022) to determine the *in situ* POC sinking flux, which was combined with float-based NPP estimates to quantify the *in situ* carbon export ratio. The recent combination of nitrate, oxygen, pH, and optical sensors on biogeochemical profiling floats (Johnson et al., 2017), and ongoing efforts with subsurface gliders (Takeshita et al., 2021; Saba et al., 2019), will provide new opportunities to further advance tracer budget methodologies enabling more comprehensive upper ocean carbon cycling studies. In particular, the quantification of all biogenic carbon pools represents a step forward in autonomous carbon cycle analyses that will yield a more nuanced understanding of marine ecosystem responses to ocean warming and acidification.

10.2.2.2. Integration time scales and steady state assumptions

The timescale of integration will determine the dominant physical processes to evaluate or sources of uncertainty in the physical flux estimates if relevant processes are not quantifiable due to a lack of appropriate observations. On the shortest scales (~hours-diurnal), wave dynamics, inertial responses to high-frequency atmospheric forcing, convective-driven mixing, and coherent vortices from wave-wind interactions (i.e., Langmuir Circulation) play a dominant role. Atmospheric weather phenomena (on synoptic scales, O(100–1000 km)) and sub-mesoscale ocean dynamics (O(1–10 km) (e.g., Levy et al., 2018; Estapa et al., 2015) will introduce variability on scales of a few days. These short-term events can introduce significant variability in physical fluxes and biogeochemical tracers and, if undersampled, produce aliasing effects on long-term means (Monteiro et al., 2015; Whitt et al., 2019). For instance, storm events can lead to short-term deepening of the mixed layer, entraining additional carbon or nutrients into the mixed layer. Such short-term events cannot be estimated from monthly data or averages. The ten-day profiling frequency of most floats will also miss this short-term variability (Xing et al., 2020; Nicholson et al., 2022).

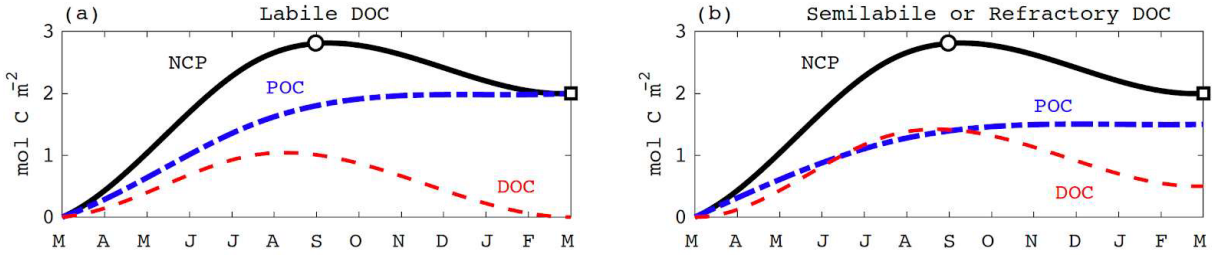

Fig 10.2. Schematic of mixed layer NCP over the course of one year (black line) at a hypothetical location. The blue line shows the POC component of NCP, and the red line shows the DOC component of NCP. In the left panel, labile DOC is produced and consumed over the course of the year. In the right panel, a fraction of the DOC produced is recalcitrant and is not remineralized within the year. NCP evaluated from March to September provides a consistent seasonal NCP estimate between scenarios. However, due to heterotrophic respiration of DOC in the latter portion of the year, seasonal NCP is not an accurate estimate of annual NCP, which is commonly assumed to be equivalent to the annual export. If the recalcitrant DOC is eventually respired in the upper ocean, it will not contribute to carbon export. Seasonal integration time scales and the assumption of steady state are just two challenges associated with omitting DOC cycling in upper ocean carbon budgets, short integration time scales, and the assumption of steady state.

The ocean mesoscale (with spatial scales of O(10–100 km)) introduces variability on sub-seasonal scales of weeks to months. Though mesoscale eddies and the associated geostrophic currents can be estimated from satellite altimetry (i.e., sea surface height anomalies), biogeochemical tracer distributions on these temporal scales are not yet possible from observations at a global scale. Gliders, on the other hand, can return nearly vertical profiles at much higher temporal resolution (~1 hour) and capture both the high-frequency internal ocean dynamics from submesoscale to mesoscale eddies, as well as influences of atmospheric weather, though glider missions typically only last a few months (i.e., ~3–6 months; Rudnick, 2016). Eddies and fronts become a source of uncertainty for physical flux estimates in float-based tracer budgets; they can be particularly important during springtime restratification in the mid-latitude subtropical gyres (Johnson et al., 2016) or regions with strong horizontal gradients such as western boundary currents. On seasonal to annual scales, seasonal changes in insolation, air-sea buoyancy fluxes, and wind forcing (depending on the region) will tend to dominate but horizontal advection can also be regionally important (e.g., in the Southern Ocean; Rosso et al., 2017).

Practically, to use the time-rate of change terms in Eq.10.1–1.07 it is desirable to conduct work in a Lagrangian reference frame (Alkire et al., 2012; Siegel et al., 2021). Otherwise, difficult-to-resolve lateral advective fluxes and spatial variability can obscure the temporal evolution. When the time rate of change cannot be determined, a steady-state assumption is often employed by assuming a zero rate of change. Such steady-state estimates can contain significant biases and are most useful when averaged over significant space and time. On annual and longer timescales, the time rate of change term tends to be very small compared to NCP.

10.2.2.3. The choice of integration depth

The depth or density horizon to which upper ocean tracer budgets are integrated often varies depending on the research question of interest. The most common integration depths include the seasonally varying mixed layer (ML), a fixed light level (often the euphotic depth or 1% light level), and the local maximum winter mixed layer. Seasonal ML budgets are often used when observations are limited to the near-surface (e.g., moorings) and provide information about the

processes influencing air-sea exchange. However, ML budgets do not account for NCP that occurs below the ML in regions of clear waters with deep euphotic zones (e.g., in the subtropical gyres), which can cause an underestimation of total NCP. Additionally, ML budgets do not account for the fall/winter re-entrainment of biologically respired carbon that may have escaped the warm season mixed layer as particles before being metabolized. This re-entrained carbon would be interpreted as a physical process, which can lead to an overestimation of NCP. While these two biases are compensating, it is not clear that they balance.

Euphotic zone budgets more accurately capture the total net production of biomass in the upper ocean (Buesseler et al., 2020), which provides a constraint on how much carbon is available for export to support mesopelagic food webs. However, quantifying physical contributions to these budgets can be more challenging due to the decoupling of the euphotic depth with the ML depth, which is a physically meaningful horizon at which it is easier to estimate turbulent fluxes. The euphotic depth is also often decoupled from the air-sea exchange interface (i.e., ML) during the warm season, making it more difficult to quantify the biological influence on air-sea gas exchange. Additionally, this horizon is sensitive to biases caused by seasonal re-entrainment of biologically respired carbon, which can lead to an overestimate of NCP.

The local maximum winter ML is another common depth horizon, often preferred in studies targeting questions related to carbon export (Palevsky and Doney, 2018). Integrating over this depth horizon accounts for all production and respiration above the export depth. However, the production estimate will be lower than the maximum NCP due to the inclusion of deeper depths where net heterotrophy occurs. This approach, therefore, provides a lower bound estimate on annual NCP but a realistic estimate of the amount of carbon exported from the upper ocean annually and thus available for mesopelagic food webs.

The depth horizon of integration will also determine the subtleties and uncertainties in the calculation of physical flux terms. Integrating to a fixed depth implies an estimation of vertical and horizontal advection and turbulent fluxes. An integration to the base of the mixed-layer depth (MLD) should incorporate an assessment of entrainment fluxes due to temporal changes in the MLD, in addition to vertical turbulent diffusion, as well as horizontal advection across a sloping ML (e.g., Levy et al., 2013; Emerson et al., 2008). A depth horizon away from the influence of the seasonally varying surface forcing will minimize errors from vertical diffusion or entrainment. Integration to an isopycnal layer involves estimates of isopycnal and diapycnal fluxes, which can deviate from horizontal and vertical fluxes in regions where isopycnals outcrop to the surface, e.g., near fronts or eddies.

Due to important differences in the type of information gleaned from tracer budgets evaluated to different integration depths, it is recommended that investigators are very clear about these nuances of their study, justify the choice of integration depth, and document associated uncertainties.

10.2.2.4. Air-sea exchange parameterizations

A key source of uncertainty in tracer budgets that include a gaseous component (e.g., O_2 and DIC) comes from the parametrization of air-sea fluxes using a global bulk equation (Wanninkhof, 2014). Oxygen can be particularly challenging, as the air-sea fluxes induced by bubbles and solubility are generally equivalent to or larger than the flux induced by biological

activity, particularly during winter and spring due to larger uncertainty in bubble flux parameterizations at high windspeeds (Emerson and Stump, 2010; Emerson and Bushinsky, 2016). Deconvolving the changes in oxygen caused by physical and biological processes is therefore highly sensitive to the accuracy of the oxygen measurements (Takeshita et al., 2013; Johnson et al., 2015) and the gas exchange computation (Emerson and Bushinksy, 2016; Plant et al., 2016, Fig. 10.3). CO_2, on the other hand, is a more soluble gas for which it is generally not necessary to directly parameterize bubbles (Broecker and Peng, 1974). However, a different challenge associated with all air-sea flux calculations was recently pointed out by Ho et al. (2020), who identified the potential for significant biases when observations below the sea surface don't capture near-surface phenomena such as rain events. This bias was found in underway ship observations and may be more challenging to identify from one autonomous platform. However, profiling floats with O_2 air calibration capability currently collect O_2 observations all the way to the sea surface, which will make it possible to further probe this issue. Floats without air calibration may not sample the near-surface and may have lower accuracy as they are calibrated against deep O_2 climatology.

The recent development and commercialization of robust pH sensors for application on autonomous ocean platforms make it possible to use pH observations and TA estimates to calculate sea surface pCO_2 values with ~3% uncertainty (Williams et al., 2018) and, thus, quantify air-sea CO_2 fluxes. This is now enabling DIC budgets to be constrained on platforms that do not measure pCO_2 directly (e.g., Fassbender et al., 2016, 2017). Additionally, this method has important potential for filling gaps in the global carbon budget (Gray et al., 2018; Bushinsky et al., 2019) and significant effort is being made to validate the methodology in numerous ocean regions (Fay et al., 2018; Takeshita et al., 2019).

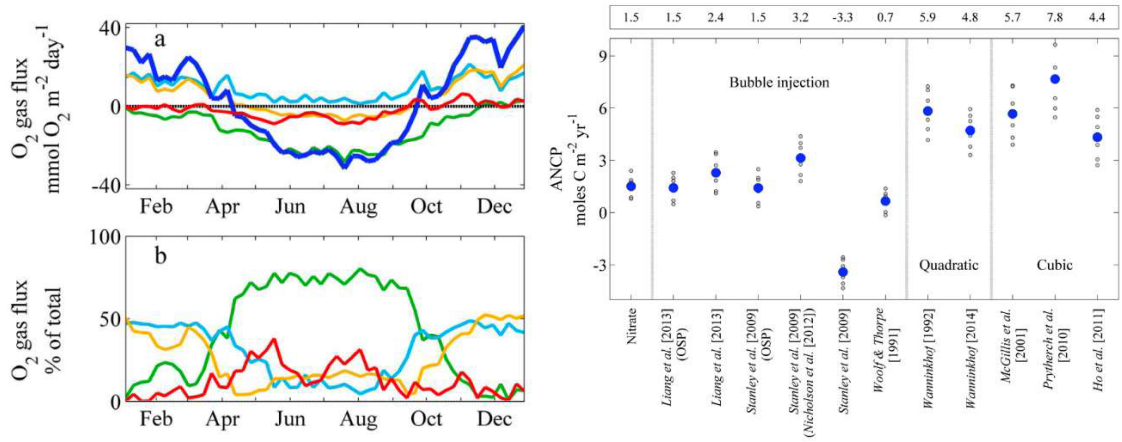

Fig. 10.3. From Plant et al. (2016). Left panel, their Fig.9 caption: "(a) Average annual oxygen flux across the air sea boundary using the optimized gas exchange model from Liang et al. [2013]: net (heavy blue), diffusive flux (green), completely dissolving bubble flux (light blue), partially dissolving bubble flux (orange), and oxygen flux due to biology (red). A positive flux is into the ocean. (b) The same as Fig. 9 a above but plotted as a percent of the total absolute magnitude." Right panel, their Fig. 8 caption: "Model-derived estimates of ANCP for all years integrated to 35 m depth. Estimates based on nitrate measurements are compared to oxygen-based estimates using various gas flux parameterizations grouped by model type. Individual years are grey. Average of all years is blue and in the top row of values. Parentheses indicate different tunings for the Liang et al. [2013] or Stanley et al. [2009] formulations in this work (OSP) and by Nicholson et al. [2012]."

10.2.2.5. The impact of ocean physics on NCP estimates

The estimation of physical fluxes requires consideration of the spatio-temporal variability captured by the different types of platforms and frames of reference. Moorings measure ocean variability passing through a fixed location (i.e., from a Eulerian frame of reference). Lagrangian floats are designed to be neutrally buoyant and follow the 3D movement of water parcels (D'Asaro, 2003), providing an ideal frame of reference for tracer budget calculations (Alkire et al., 2012), but they remain specialized platforms that are not widely available. Profiling floats provide quasi-Lagrangian measurements, as they are ballasted to drift along constant pressure rather than isopycnals during their park phase before profiling. Profile data from floats fully capture vertical structure on many scales, but individual floats do not resolve timescales of variability shorter than twice their profile sampling period (~10 days), temporal variability on shorter scales can be assessed statistically on regional/basin to global scales using arrays of floats (e.g., Gille, 2012; Carranza et al. 2018; Johnson and Bif, 2021). Gliders, like floats, are buoyancy-driven but can slowly travel laterally because they have wings. The slow survey speed of gliders (~20 km per day) provides information about spatial variability, but it can be difficult to disentangle variations in time versus space unless a coordinated fleet of gliders is deployed (Leonard et al., 2010).

Regardless of integration depth (or density) horizon, any tracer budget analysis requires an assessment of advective and turbulent fluxes in/out of the control volume.

10.2.2.6. Advective fluxes

Though it is possible to estimate large-scale currents, both geostrophic and wind-driven components, from satellite altimetry (i.e., sea surface height) and wind data (e.g., from the Ocean Surface Current Analyses Real-time (OSCAR) product; Dohan, 2017), estimation of horizontal advective fluxes for biogeochemical tracers is hindered by the lack of information on horizontal gradients in tracer data. Furthermore, the overground speed of gliders is only approximately 20 km per day, and a single glider cannot survey quickly enough to capture a synoptic view of ocean variability. Thus, physical advective terms are often neglected from tracer budgets. Horizontal advection can be significant even on short temporal and spatial scales ($\leq$ 1 month, 20 km; Alkire et al., 2014). The role of horizontal advection by geostrophic currents will be important near strong surface currents (e.g., western boundary currents, e.g., Dong and Kelly, 2004). Ekman advection, however, can dominate the seasonal cycle of horizontal advection in open ocean areas subject to strong wind forcing (e.g., in the Southern Ocean; Dong et al., 2007). Vertical advection due to wind-driven convergences/divergences in the surface Ekman transport (i.e., Ekman pumping) can be quantified from satellite wind stress curl fields (e.g., Risien and Chelton, 2008). Horizontal Ekman advection is typically limited to a fraction of the mixed layer (though in summer, the Ekman depth can be deeper than the MLD), and its effects should be considered if the depth of integration chosen for tracer budget analysis is shallower than the seasonally varying MLD. Ekman pumping effects, however, can be influential below the mixed layer.

10.2.2.7. Turbulent fluxes

In contrast to lateral gradients, vertical gradients in biogeochemical tracers are often well constrained by vertical profiles, and uncertainty largely stems from estimating the vertical (or diapycnal) eddy diffusivity coefficient (K_z). Turbulent fluxes are often parameterized as the

product of the eddy diffusivity coefficient and vertical tracer gradient (i.e., in analogy to down-gradient molecular diffusion). Turbulence homogenizes properties and momentum cascading energy from large to small eddies. Turbulent billows span scales of order 10 m to mm scales, where they dissipate energy. The most accurate Kz estimates rely on measurements of turbulent dissipation rates, which require microstructure observations.

Microstructure observations are acquired using very specialized sensors capable of resolving cm-scale fluctuations of shear or temperature variance, which are typically deployed on free-falling profilers from ships, and require high expertise. Though microstructure sensor technology is evolving, and reliable estimates are possible from autonomous platforms (e.g., Lien et al., 2016; Nagai et al., 2020; Fer et al., 2014), satellite data transmission remains a challenge, and instrument recovery for data acquisition is still necessary. Thus, diapycnal diffusivities from microstructure measurements remain very sparse in the global oceans, and parameterizations will be required for years to come (e.g., Frajka-Williams et al., 2022).

Indirect methods to estimate dissipation rates have leveraged CTD measurements sampled at relatively high vertical resolution (i.e., ~1 m). These so-called fine-scale parameterizations, though more uncertain, allow for estimates of vertical eddy diffusivities and their spatial and seasonal patterns on regional to global scales (Kunze, 2006; Wu et al., 2011; Whalen et al., 2012). These parameterizations either relate 10–100m scale strain and shear variance from the internal wave field to the associated turbulence dissipation rates (i.e., from breaking internal waves due to shear and convective instabilities) or estimate dissipation rates from the largest scales of turbulent overturns (i.e., Thorpe scales, from m-scale density inversions; Alford and Pinkel, 2000; Thompson et al., 2007; Frants et al., 2013). A major shortcoming of any of these dissipation-rate-based estimates is that diapycnal eddy diffusivities are related to dissipation rates through the mean stratification indirectly (i.e., $K_\rho = \Gamma\varepsilon/N^2$, Osborn 1972), and thus the relationship breaks in regions of weak stratification or steep pycnoclines. This implies that estimates of diffusivities in or around the mixed layer, where primary productivity occurs, are more challenging. A promising indirect method based on similarity theory (i.e., the so-called Large Eddy Method) has proven successful in inferring eddy diffusivities in low stratification conditions using glider's CTD data, but the requirement of a calibration coefficient and its impact on dissipation rate estimates remains unknown (Frajka-Williams et al., 2022).

Approaches to estimating turbulent fluxes across the integration horizon, in order of likely accuracy, include (1) direct measurement of turbulence via microstructure or other measurements; (2) quantitative estimates of temporally/seasonally varying K_z, for example, based on heat and salt budgets (Cronin et al., 2015; Pelland et al., 2017); and (3) use of a constant, canonical value, or values for K_z, such as 10^{-5} m^2 s^{-1} (Bushinsky and Emerson, 2015). However, direct measurements or seasonal estimates of diffusivity may not always be feasible. In many cases, the uncertainty associated with vertical diffusive flux is smaller than from other sources, such as air-sea gas exchange. Uncertainty from these estimates should be propagated through the mass balance equation using a Monte Carlo approach to estimate overall uncertainty in NCP.

Horizontal turbulent fluxes of biogeochemical tracers are difficult to quantify. Though estimates of horizontal eddy diffusivities, K_H , are available at the surface from satellite altimetry (Klocker and Abernathy, 2014), surface drifters (Zhurbas et al., 2014), and even for the subsurface from Argo floats (Cole et al., 2015), as well as from combinations of different platforms globally (Roach et al., 2018); the estimation of turbulent horizontal fluxes of

biogeochemical parameters is challenging due to the lack of biogeochemical tracer distributions at the appropriate temporal and spatial scales.

Another method for estimating physical flux terms is the use of a physical ocean model forced by atmospheric reanalysis data collocated in space and time with float profiles (Plant et al., 2016). This approach requires model optimization (i.e., tuning of model parameters) for the site to properly capture physical processes. An assessment of the modeled physics can be performed leveraging temperature and salinity data from the CTD sensors on the floats.

10.3. GPP and NPP Rate Estimates

An emerging approach for calculating ocean primary productivity is to use biogeochemical sensor output from platforms such as floats, moorings, or gliders to estimate rates of photosynthetic carbon fixation. Approaches have been applied that estimate either Gross Primary Productivity (GPP), the total rate of photosynthetic carbon fixation, or Net Primary Productivity (NPP), the remaining photosynthetic production of organic carbon by autotrophs once autotrophic respiratory losses are removed.

Various approaches have been published in recent years which broadly can be classified into methods that depend on diel dynamics and methods that depend on photosynthetic algorithms. The diel methods rely on changes in the stock of carbon, oxygen, or nitrogen over the diel period. In this sense, they can be considered analogous to the traditional light/dark bottle incubation approach (see Chapter 5). In contrast, the algorithmic methods employ models of photosynthesis normalized to carbon or chlorophyll, and thus are much more akin to satellite ocean color productivity models (Behrenfeld and Falkowski, 1997; Westberry et al., 2008).

10.3.1. Diel productivity approaches

10.3.1.1. Platforms and sensors for diel productivity

Diel PP measurements have been achieved using a range of platforms, including gliders, profiling floats, surface drifters, and shipboard flow-through systems. For oxygen-based estimates, optode-type sensors are preferable due to their proven stability. Slower response optodes are a good match for this application as they are less noisy than fast-response optodes and still have sufficient time to equilibrate with the homogenous mixed layer. The exception would be in a region with very shallow mixed layer depths and a strong oxygen gradient below. For bio-optics, diel cycles have been observed in both particulate beam attenuation (c_p) or b_{bp}. Diel cycles generally are more robust in c_p. Transmissometers, however, are less frequently used on autonomous systems than optical backscatter. Thus, measuring c_p is recommended when possible, but b_{bp} can be considered an alternative.

The primary requirement for observing diel cycles is sufficient temporal sampling resolution to resolve the diel cycle. In theory, because the phasing of the 24-hour cycle is known, a priori, the minimum sampling frequency would be twice per day if measurement timing corresponded to near dawn and dusk. However, this minimal cycling frequency leaves no free degrees of measurement freedom to evaluate the quality of the diel cycle fit or if physical fluxes may have biased an estimate. In general, the 5–8 daily profiles of an open-ocean glider are a more useful minimum sampling frequency. Platforms with higher frequency sampling, such as profiling moorings, Wirewalkers, or surface drifters can improve the resolution of diel cycles and potentially resolve sub-daily variations, such as morning intensified photosynthetic rates. Alternatively, networks of sensors on platforms with offset profiling times could be used to

capture regional diel cycles in locations where spatial heterogeneity does not dominate the signal.

10.3.1.2. Diel productivity: Underlying equations and assumptions

The use of diel signals to estimate primary productivity has a long history in aquatic sciences, appearing in the literature as early as the 1930s (Butcher et al., 1930) and was formalized by Odum (1956). These early applications in rivers were based on large diel changes observed in shallow riverine systems. Only recently, these approaches have been applied to open-ocean systems, which often are characterized by small diel amplitudes and are not traditionally samples on diel timescales from research vessels. Such an approach has been demonstrated (Tijssen, 1979) using Winkler titrations, yet it proved too laborious for common application. The advent of robust sensors on autonomous platforms (Johnson et al., 2009) has greatly expanded the possibility of widespread productivity estimates.

In recent years, autonomous platforms have been used to obtain productivity estimates based on diel signals using oxygen (Barone et al., 2019; Briggs et al., 2018; Nicholson et al., 2015; Johnson and Bif, 2021) and bio-optical estimates of particulate organic carbon (Briggs et al., 2018, Loisel et al., 2011, White et al., 2017). These approaches are based on measuring changes over the diel period in the surface mixed layer and estimate the volumetric primary productivity (GPP_v) averaged over the surface mixed layer. While in theory, the method should be extensible below the mixed layer but still within the euphotic zone, lower rates and higher physical variability in the deep euphotic layer make it difficult to extract a diel productivity signal. Both approaches estimate GPP_v based on the relationship that the net change in either dissolved oxygen or organic carbon due to biological processes depends on the balance of gross photosynthesis (GPP) and community respiration (CR).

$$\frac{dC}{dt} = GPP(t) + CR(t) \tag{10.11}$$

If one assumes that CR proceeds at an unchanged throughout the 24-hour day, then

$$GPP_v = \frac{t^{day}}{24}\frac{dC}{dt}^{day} - \frac{dC}{dt}^{night}, \tag{10.12}$$

where *tday* is the length of daylight in hours, *dCdtday* represents the rate (per hour) of increase in oxygen or POC during the day due to photosynthetic production, *dCdtnight* is the rate of change due to nighttime respiration. When the photoperiod is close to 12 hours, GPP_v can be approximated as the rate of daytime increase plus twice the rate of nighttime decrease. Integrated mixed layer GPP (GPP_{ml}) can then be calculated as the product of GPP_v and mixed layer depth. In

practice, approaches to calculate oxygen and carbon-based productivity differ and are outlined in detail below.

10.3.1.3. Diel productivity: oxygen-based approaches

For dissolved oxygen, several physical processes can also influence dissolved oxygen concentrations, including advective fluxes (F_{adv}), air-sea exchange (F_{Gas}), and vertical entrainment and mixing (F_v). Eq 10.11 thus can be revised as

$$\frac{dO_2}{dt} = GPP(t) + CR(t) + F_{Gas} + F_{Phys}. \tag{10.13}$$

Generally, air-sea flux can be estimated directly using an air-sea flux parameterization that includes bubble dynamics (Liang et al., 2013; Nicholson et al., 2016), as described in Section 10.2.2.4. In general, diel GPP and CR estimates are much less sensitive to air-sea flux estimates than NCP because the daily GPP and CR rates are much higher than air-sea fluxes (Fig. 10.4). Advective and turbulent fluxes are more difficult to estimate (see Section 10.2.2.5). The approach to observationally constraining GPP and CR has been to integrate the above equation over the course of a day such that

$$\frac{dO_2}{dt} = GPP(t) + CR(t) + F_{Gas} + F_{Phys}O_2(t) = \int_{t_o}^{t_1} GPP + CR(t_1 - t_o) + \int_{t_o}^{t_1} F_{Gas} + C, \tag{10.14}$$

where C is a constant of integration. If the functional form of GPP is assumed (for example, to be linearly related to PAR), then the theoretical shape of a diel O_2 curve can be statistically fit to observations to estimate the magnitude of GPP and CR as well as the uncertainty of each daily estimate (Barone et al., 2019). A statistical significance test to each daily estimate can help to filter out estimates contaminated by physical O_2 fluxes.

Complementary to oxygen-based approaches, diel rates can also be determined from nitrate and DIC (by measuring pCO_2 or pH and assuming alkalinity). This approach has been demonstrated in Monterey Bay (Johnson, 2010).

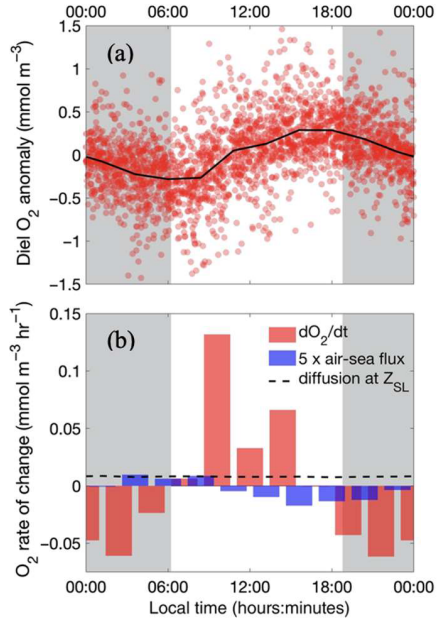

Fig. 10.4. Adapted from Barone et al. (2019). These figures represent the aggregate observations from four glider missions. (a) Observed (red dots) and average (black line) O_2 anomaly with respect to the average concentration calculated daily in the surface layer (SL). (b) The average rate of change in O_2 (red bars) and the sea surface flux divided by ZSL (multiplied by 5 to make it visible, blue bars); the dashed line depicts diapycnal O_2 fluxes divided by ZSL assuming $K_z = 10^{-4} m^2 s^{-1}$. The gray background represents the time of day between the average sunset time and the average sunrise time.

10.3.1.4. Diel productivity: optics-based approaches

Diel changes in POC have also been used to calculate GPP using autonomous sensors (Fig. 10.5). The most successful applications have used beam transmission rather than backscatter (Briggs et al., 2018; Loisel et al., 2011; White et al., 2017). The first step in this approach is to convert measured beam attenuation to carbon units using a locally appropriate relationship (Section 10.1.2 above). Once in carbon units, GPP can be estimated using Eq. 10.12 above.

In the interpretation of diel c_p or b_{bp} measurements, several considerations and potential sources of error have been identified. One source of uncertainty is in the conversion of c_p or b_{bp} to carbon concentration. Each responds more sensitively to different particle size ranges more efficiently, and empirical relationships between and c_p or b_{bp} and POC can vary significantly on factors such as community composition, particle size, shape, mineral and chemical composition, etc. (Cetinić et al., 2012; Rasse et al., 2017). While POC-based approaches do not have an air-sea exchange term to contend with, there can be a loss of POC from the mixed layer due to sinking flux. This loss term would lead to a positive bias in the magnitude of CR.

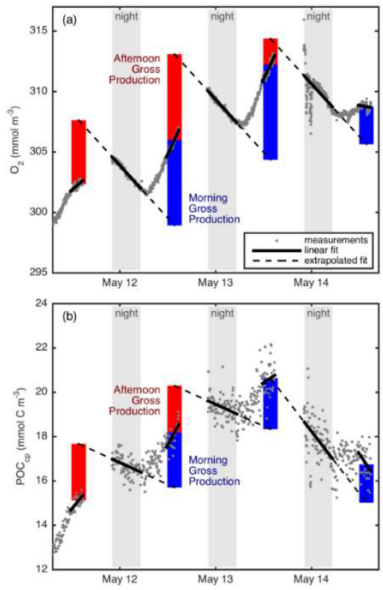

Fig. 10.5. (a) Diel O_2 measurements compared to (b) diel POC (derived from c_p) measurements. Reproduced from Briggs et al. (2018). Observations are from the 2008 North Atlantic Bloom Experiment.

10.3.1.5. Sources of error in diel productivity estimates

Stoichiometry

When estimating GPP from diel O_2, a photosynthetic quotient (PQ) is required to convert to carbon units. Given that GPP is generally much larger than NCP, an O:C ratio for recycled production, such as 1.1 is more appropriate for converting from GPP_{O2} to GPP_C (Laws, 1991). Also of note, is diel O_2 methodologies are not sensitive to light dependent reactions such as the Mehler cycle which are "water-water" reactions with no net oxygen evolution. Thus, a GPP estimate from diel O_2 estimates should be expected to be lower than isotopic approaches (e.g., triple O_2 isotopes, Chapter 7).

Fluxes due to ocean physics for diel productivity approaches

The diel approach is subject to biases that are introduced by any unresolved fluxes that vary significantly throughout a day. A common example is if the platform crosses a front which results in a large advective flux. Physical processes with a diurnal timescale of less than a day can also interfere with extracting GPP and CR information. For example, mixing can vary on the diel scale due to daily surface heating, cooling, and wind speed variations (Briggs et al., 2018; Nicholson et al., 2015) or surface wave effects. Another physical process that can confound GPP and CR estimates is internal, near-inertial oscillations driven by wind bursts that occur at a frequency near the inertial period, which can be close to the diurnal period (Gordon et al., 2020), depending on latitude. The Coriolis frequency is 24 hours at 30°N and 30°S and care should be taken when observations are near these latitudes or towards higher latitudes as the inertial period decreases.

Air-sea gas exchange is also a potential source of bias for O_2-based diel cycles. The rate of air-sea flux is generally small compared to GPP and CR. However, over the timescale of a day,

the flux is often consistently in one direction depending on if the water is supersaturated or undersaturated. The air-sea flux term in Eq. 10.14 thus can introduce a bias towards GPP or CR. A comparison between GPP and CR requires careful accounting of the air-sea flux.

10.3.2. Float-based photosynthetic production models

Photosynthetic production algorithms offer an alternative approach to estimating rates of ocean productivity. Such approaches are based on photosynthesis versus irradiance relationships and generally have been translated from ocean color remote sensing community and have applied algorithms designed for ocean color remote sensing measurements (Behrenfeld et al., 2005; Behrenfeld and Falkowski, 1997; Westberry et al., 2008) and later translated for application with *in situ*, sensor-based measurements. Compared to ocean color remote sensing, autonomous platforms have the advantage of resolving the vertical structure of parameters including chlF, b_{bp}, and PAR. Rather than inferring the vertical structure of these parameters from surface properties like satellite algorithms, profiles of relevant properties can be directly measured. This can result in a simplified application of remote algorithms in which equations to infer vertical structure are replaced by direct observations. These remote sensing approaches predict net primary productivity using quasi-empirical algorithms developed based on laboratory and field observations of phytoplankton physiology. These can be broadly divided into chlorophyll-based algorithms, such as VGPM, and carbon-based algorithms, such CbPM.

10.3.2.1. Chlorophyll-based NPP

A chlorophyll-based NPP algorithm fundamentally quantifies net photosynthetic production as the product of chlorophyll concentration and chlorophyll-specific photosynthetic rate, which is parameterized as a function of environmental conditions, including irradiance €, temperature (*T*), and day length (t_{day}). For example, the VGPM model seeks to integrate the following equation from the surface to the base of the euphotic zone

$$NPP = \int_0^{z_{eu}} \left(Chl(z) \times P^b_{opt}(z) \times t_{day}\right) dz. \tag{10.15}$$

But it is limited to surface properties as inputs available via remote sensing

$$NPP = Chl_{(z=0)} P^b_{opt_{(z=0)}} \times t_{day} \times f(PAR) \times z_{eu}, \tag{10.16}$$

where f(PAR) is the fractional relationship between integrated NPP and maximum NPP if optimal rates (P^b_{opt}) were achieved from surface to euphotic zone depth (z_{eu}). The P^b_{opt} term is a function of temperature and accounts both for direct temperature dependencies of metabolic rates and nutrient stress that correlate with higher sea surface temperature. f(PAR) is an empirical function of surface PAR, while z_{eu} is based on an empirical relationship to surface chlorophyll (Morel and Berthon 1989).

A profiling autonomous system with optical sensors for chlorophyll and PAR can, in theory, directly quantify the parameters needed to use Eq. 10.15 and avoid the assumptions and empirical equations required to arrive at Eq. 10.16 because chlorophyll profiles and z_{eu} can be measured directly and thus potentially improve upon uncertainties inherent to remote sensing algorithms (Jacox et al., 2015). For example, a chlorophyll-based *in situ* model was used to

estimate NPP from a Seaglider using vertical profiles of irradiance and chlorophyll (Hemsley et al., 2015).

10.3.2.2. Carbon-based NPP

Carbon-based algorithms, particularly CbPM (Behrenfeld et al., 2005; Westberry et al., 2008), have been applied to estimate NPP from profiling floats (Estapa et al., 2019; Arteaga et al., 2020; Long et al., 2021; Yang et al., 2021). Carbon based algorithms are dependent on equating NPP to the product of phytoplankton carbon stock (C_{phyto}) and specific growth rate (μ)

$$NPP(z) = C_{phyto}(z) \times \mu(z), \text{ where } \mu = f(Chl, C_{phyto}, I, T, t_{day}, \dots). \quad (10.17)$$

10.3.2.3. Challenges for float-based photosynthetic production models

Accurately applying float-based optical productivity approaches requires attention to several potential pitfalls. The first is the quality of chlorophyll and irradiance measurements. For chlorophyll, fluorometers measure chlorophyll fluorescence, often excited at 470 nm. There is significant variability in converting chlorophyll fluorescence to chlorophyll *a* concentration based on phytoplankton community structure and physiology (Roesler et al., 2017). Furthermore, non-photochemical quenching lowers quantum yield and contaminates observations during daytime in the upper tens of meters (Xing et al., 2018). Accurately measuring downwelling irradiance and/or PAR is also a challenge on a platform such as a glider, and measurements must be corrected for sensor orientation while profiling. Profiles often are not coordinated to local noon, so adjustments for time of day are also necessary. Standards on which discrete downwelling irradiance bands are measured are still emerging, while hyperspectral irradiance sensors show promise but are not yet widely deployed on floats and gliders.

Float-based CbPM NPP estimates are somewhat simpler than the full remote sensing algorithm because directly measured profiles of chlorophyll and C_{phyto} and irradiance are used. However, most applications on autonomous platforms have been on systems that do not include direct measurements of downwelling irradiance (I). In such cases, surface irradiance from remote sensing products, together with chlorophyll-dependent models of diffuse attenuation coefficient (K_d) are used to calculate irradiance at depth (Estapa et al., 2019; Morel and Maritorena, 2001). Validation of Argo float-based NPP against ^{14}C PP incubations in the North Atlantic indicate promising yet mixed results, suggesting the potential for future improvement in *in situ* NPP algorithms (Yang et al., 2021).

10.4. Recommendations and Future Outlook

Primary productivity estimation approaches using biogeochemical sensor observations from autonomous platforms are rapidly developing. A range of methods from mass balances of carbon, oxygen, and nitrogen to diel fitting and bio-optical algorithms target a range of metabolic rates, including GPP, NPP, and NCP. Due to the diversity of sensors, platforms, and strategies used to estimate these rates, we provide generalized recommendations for investigators should keep in mind.

(1) Robust results require taking the utmost care to calibrate and continuously validate sensor performance over the deployment lifetime by following platform-specific quality control (QC) best practices. When feasible, this may require collection of discrete samples (POC, O_2, HPLC, etc.) to calibrate and validate sensor accuracy.

(2) When applying any of the outlined methods, it is critical to consider the specific study setting and identify the most significant sources of uncertainty. For mass balance approaches, this may include, for example, air-sea flux or lateral advection. For optical approaches, relationships for the conversion of optical properties measured to more ecologically relevant quantities such as C_{phyto} and Chlorophyll *a* involve inherent uncertainties. Total uncertainty should be reported using Monte Carlo simulation or other methods.

(3) Governing equations and any assumptions should be clearly documented, including whether any mass balance terms were assumed to be zero (e.g., steady-state assumption or neglecting physical flux terms).

(4) Because methods are not standardized, we recommend archiving and sharing both raw observational datasets and code to provide reproducible workflows.

We anticipate that quantification of primary productivity from in situ sensor-based observations will continue to mature and methodologies will become more standardized. Growing observing systems such as Biogeochemical Argo and other multiplatform observing systems have the potential to quantify rates of productivity in situ, on regional to global scales. The merging of in situ observations with remotely sensed ocean color (Bisson et al., 2021, Sauzède et al., 2016) and numerical biogeochemistry and ecosystem models (Wang et al., 2020) could fuel a new generation of global-scale ocean primary productivity products.

10.5. References

Alford, M. H., & Pinkel, R. (2000). Observations of Overturning in the Thermocline: The Context of Ocean Mixing. *Journal of Physical Oceanography*, *30*(5), 805–832. https://doi.org/10.1175/1520-0485(2000)030<0805:OOOITT>2.0.CO;2

Alkire, M. B., D'Asaro, E., Lee, C., Jane Perry, M., Gray, A., Cetinić, I., et al. (2012). Estimates of net community production and export using high-resolution, Lagrangian measurements of O2, NO3−, and POC through the evolution of a spring diatom bloom in the North Atlantic. *Deep Sea Research Part I: Oceanographic Research Papers*, *64*, 157–174. https://doi.org/10.1016/j.dsr.2012.01.012

Alkire, M. B., Lee, C., D'Asaro, E., Perry, M. J., Briggs, N., Cetinić, I., & Gray, A. (2014). Net community production and export from Seaglider measurements in the North Atlantic after the spring bloom. *Journal of Geophysical Research: Oceans*, *119*(9), 6121–6139. https://doi.org/10.1002/2014JC010105

Anderson, L. A., & Sarmiento, J. L. (1994). Redfield ratios of remineralization determined by nutrient data analysis. *Global Biogeochemical Cycles*, *8*(1), 65–80. https://doi.org/10.1029/93GB03318

Arteaga, L. A., Boss, E., Behrenfeld, M. J., Westberry, T. K., & Sarmiento, J. L. (2020). Seasonal modulation of phytoplankton biomass in the Southern Ocean. *Nature Communications*, *11*(1), 5364. https://doi.org/10.1038/s41467-020-19157-2

Bakker, D. C. E., Pfeil, B., Landa, C. S., Metzl, N., O'Brien, K. M., Olsen, A., et al. (2016). A multi-decade record of high-quality fCO_2 data in version 3 of the Surface Ocean CO_2 Atlas (SOCAT). *Earth System Science Data*, *8*(2), 383–413. https://doi.org/10.5194/essd-8-383-2016

Barone, B., Nicholson, D., Ferrón, S., Firing, E., & Karl, D. (2019). The estimation of gross oxygen production and community respiration from autonomous time-series measurements in the oligotrophic ocean. *Limnology and Oceanography: Methods*, *17*(12), 650–664. https://doi.org/10.1002/lom3.10340

Behrenfeld, M. J., & Falkowski, P. G. (1997). Photosynthetic rates derived from satellite-based chlorophyll concentration. *Limnology and Oceanography*, *42*(1), 1–20. https://doi.org/10.2307/2838857

Behrenfeld, M. J., Boss, E., Siegel, D. A., & Shea, D. M. (2005). Carbon-based ocean productivity and phytoplankton physiology from space. *Global Biogeochemical Cycles*, *19*(1), GB1006. https://doi.org/10.1029/2004GB002299

Bif, M. B., Siqueira, L., & Hansell, D. A. (2019). Warm Events Induce Loss of Resilience in Organic Carbon Production in the Northeast Pacific Ocean. *Global Biogeochemical Cycles*, *33*(9), 1174–1186. https://doi.org/10.1029/2019GB006327

Bisson, K. M., Boss, E., Werdell, P. J., Ibrahim, A., & Behrenfeld, M. J. (2021). Particulate Backscattering in the Global Ocean: A Comparison of Independent Assessments. *Geophysical Research Letters*, *48*(2), e2020GL090909. https://doi.org/10.1029/2020GL090909

Bittig, H. C., & Körtzinger, A. (2017). Technical note: Update on response times, in-air measurements, and in situ drift for oxygen optodes on profiling platforms. *Ocean Sci.*, *13*(1), 1–11. https://doi.org/10.5194/os-13-1-2017

Bittig, Henry C., & Körtzinger, A. (2015). Tackling Oxygen Optode Drift: Near-Surface and In-Air Oxygen Optode Measurements on a Float Provide an Accurate in Situ Reference. *Journal of Atmospheric and Oceanic Technology*, *32*(8), 1536–1543. https://doi.org/10.1175/JTECH-D-14-00162.1

Bittig, Henry C., Steinhoff, T., Claustre, H., Fiedler, B., Williams, N. L., Sauzède, R., et al. (2018). An Alternative to Static Climatologies: Robust Estimation of Open Ocean CO2 Variables and Nutrient Concentrations From T, S, and O2 Data Using Bayesian Neural Networks. *Frontiers in Marine Science*, *5*. https://doi.org/10.3389/fmars.2018.00328

Bittig, Henry C., Maurer, T. L., Plant, J. N., Schmechtig, C., Wong, A. P. S., Claustre, H., et al. (2019). A BGC-Argo Guide: Planning, Deployment, Data Handling and Usage. *Frontiers in Marine Science*, *6*, 502. https://doi.org/10.3389/fmars.2019.00502

Boss, E., Guidi, L., Richardson, M. J., Stemmann, L., Gardner, W., Bishop, J. K. B., et al. (2015). Optical techniques for remote and in-situ characterization of particles pertinent to GEOTRACES. *Progress in Oceanography*, *133*, 43–54. https://doi.org/10.1016/j.pocean.2014.09.007

Boss, E., Haëntjens, N., Ackleson, S. G., Balch, B., Chase, A., Dall'Olmo, G., et al. (2019, November). IOCCG Ocean Optics and Biogeochemistry Protocols for Satellite Ocean Colour Sensor Validation Inherent Optical Property Measurements and Protocols: Best Practices for the Collection and Processing of Ship-Based Underway Flow-Through Optical Data (v4.0) [Miscellaneous]. https://doi.org/10.25607/OBP-664

Boss, E., Waite, A. M., Uitz, J., Acinas, S. G., Sosik, H. M., Fennel, K., et al. (2020). Recommendations for plankton measurements on the GO-SHIP program with relevance to other sea-going expeditions. SCOR Working Group 154 GO-SHIP Report. (Report). Scientific Committee on Oceanic Research (SCOR). Retrieved from https://repository.oceanbestpractices.org/handle/11329/1201

Brewer, P. G., & Goldman, J. C. (1976). Alkalinity changes generated by phytoplankton growth1. *Limnology and Oceanography*, *21*(1), 108–117. https://doi.org/10.4319/lo.1976.21.1.0108

Briggs, N., Perry, M. J., Cetinić, I., Lee, C., D'Asaro, E., Gray, A. M., & Rehm, E. (2011). High-resolution observations of aggregate flux during a sub-polar North Atlantic spring bloom. *Deep Sea Research Part I: Oceanographic Research Papers*, *58*(10), 1031–1039. https://doi.org/10.1016/j.dsr.2011.07.007

Briggs, N., Guðmundsson, K., Cetinić, I., D'Asaro, E., Rehm, E., Lee, C., & Perry, M. J. (2018). A multi-method autonomous assessment of primary productivity and export efficiency in the springtime North Atlantic. *Biogeosciences*, *15*(14), 4515–4532. https://doi.org/10.5194/bg-15-4515-2018

Buesseler, K. O., Boyd, P. W., Black, E. E., & Siegel, D. A. (2020). Metrics that matter for assessing the ocean biological carbon pump. *Proceedings of the National Academy of Sciences*, *117*(18), 9679–9687. https://doi.org/10.1073/pnas.1918114117

Bushinsky, S. M., & Emerson, S. (2015). Marine biological production from *in situ* oxygen measurements on a profiling float in the subarctic Pacific Ocean. *Global Biogeochemical Cycles*, *29*(12), 2050–2060. https://doi.org/10.1002/2015GB005251

Bushinsky, S. M., & Emerson, S. R. (2018). Biological and physical controls on the oxygen cycle in the Kuroshio Extension from an array of profiling floats. *Deep Sea Research Part I: Oceanographic Research Papers*, *141*, 51–70. https://doi.org/10.1016/j.dsr.2018.09.005

Bushinsky, S. M., Takeshita, Y., & Williams, N. L. (2019). Observing Changes in Ocean Carbonate Chemistry: Our Autonomous Future. *Current Climate Change Reports*, *5*(3), 207–220. https://doi.org/10.1007/s40641-019-00129-8

Butcher, B. W., Pentelow, F. T. K., & Woodley, J. W. A. (1930). Variations in Composition of River Waters. *Internationale Revue Der Gesamten Hydrobiologie Und Hydrographie*, *24*(1–2), 47–80. https://doi.org/10.1002/iroh.19300240104

Carranza, M. M., Gille, S. T., Franks, P. J. S., Johnson, K. S., Pinkel, R., & Girton, J. B. (2018). When Mixed Layers Are Not Mixed. Storm-Driven Mixing and Bio-optical Vertical Gradients in Mixed Layers of the Southern Ocean. *Journal of Geophysical Research: Oceans*, *123*(10), 7264–7289. https://doi.org/10.1029/2018JC014416

Carter, B. R., Williams, N. L., Gray, A. R., & Feely, R. A. (2016). Locally interpolated alkalinity regression for global alkalinity estimation. *Limnology and Oceanography: Methods*, *14*(4), 268–277. https://doi.org/10.1002/lom3.10087

Carter, B. R., Feely, R. A., Williams, N. L., Dickson, A. G., Fong, M. B., & Takeshita, Y. (2018). Updated methods for global locally interpolated estimation of alkalinity, pH, and nitrate: LIR: Global alkalinity, pH, and nitrate estimates. *Limnology and Oceanography: Methods*, *16*(2), 119–131. https://doi.org/10.1002/lom3.10232

Cetinić, I., Perry, M. J., Briggs, N. T., Kallin, E., D'Asaro, E. A., & Lee, C. M. (2012). Particulate organic carbon and inherent optical properties during 2008 North Atlantic Bloom Experiment. *Journal of Geophysical Research: Oceans*, *117*(C6), C06028. https://doi.org/10.1029/2011JC007771

Chai, F., Johnson, K. S., Claustre, H., Xing, X., Wang, Y., Boss, E., et al. (2020). Monitoring ocean biogeochemistry with autonomous platforms. *Nature Reviews Earth & Environment*, *1*(6), 315–326. https://doi.org/10.1038/s43017-020-0053-y

Chavez, F. P., Sevadjian, J., Wahl, C., Friederich, J., & Friederich, G. E. (2017). Measurements of pCO2 and pH from an autonomous surface vehicle in a coastal upwelling system. *Deep Sea Research Part II: Topical Studies in Oceanography*. https://doi.org/10.1016/j.dsr2.2017.01.001

Claustre, H., Johnson, K. S., & Takeshita, Y. (2020). Observing the Global Ocean with Biogeochemical-Argo. *Annual Review of Marine Science*, *12*(1), 23–48. https://doi.org/10.1146/annurev-marine-010419-010956

Cole, S. T., Wortham, C., Kunze, E., & Owens, W. B. (2015). Eddy stirring and horizontal diffusivity from Argo float observations: Geographic and depth variability. *Geophysical Research Letters*, *42*(10), 3989–3997. https://doi.org/10.1002/2015GL063827

Cronin, M. F., Pelland, N. A., Emerson, S. R., & Crawford, W. R. (2015). Estimating diffusivity from the mixed layer heat and salt balances in the North Pacific. *Journal of Geophysical Research: Oceans*, *120*(11), 7346–7362. https://doi.org/10.1002/2015JC011010

D'Asaro, E. A. (2003). Performance of Autonomous Lagrangian Floats. *Journal of Atmospheric and Oceanic Technology*, *20*(6), 896–911. https://doi.org/10.1175/1520-0426(2003)020<0896:POALF>2.0.CO;2

Dickson, A. G., Sabine, C. L., & Christian, J. R. (2007). *Guide to Best Practices for Ocean CO2 Measurements.* (Report). North Pacific Marine Science Organization. Retrieved from http://www.oceandatapractices.net/handle/11329/249

Dohan, K. (2017). Ocean surface currents from satellite data. *Journal of Geophysical Research: Oceans*, *122*(4), 2647–2651. https://doi.org/10.1002/2017JC012961

Dong, S., & Kelly, K. A. (2004). Heat Budget in the Gulf Stream Region: The Importance of Heat Storage and Advection. *Journal of Physical Oceanography*, *34*(5), 1214–1231. https://doi.org/10.1175/1520-0485(2004)034<1214:HBITGS>2.0.CO;2

Dong, S., Gille, S. T., & Sprintall, J. (2007). An Assessment of the Southern Ocean Mixed Layer Heat Budget. *Journal of Climate*, *20*(17), 4425–4442. https://doi.org/10.1175/JCLI4259.1

Emerson, S. (2014). Annual net community production and the biological carbon flux in the ocean. *Global Biogeochemical Cycles*, *28*(1), 2013GB004680. https://doi.org/10.1002/2013GB004680

Emerson, S., & Bushinsky, S. (2016). The role of bubbles during air-sea gas exchange. *Journal of Geophysical Research: Oceans*. https://doi.org/10.1002/2016JC011744

Emerson, S., & Stump, C. (2010). Net biological oxygen production in the ocean—II: Remote in situ measurements of O2 and N2 in subarctic pacific surface waters. *Deep Sea Research Part I: Oceanographic Research Papers*, *57*(10), 1255–1265. https://doi.org/10.1016/j.dsr.2010.06.001

Emerson, S., Stump, C., & Nicholson, D. (2008). Net biological oxygen production in the ocean: Remote in situ measurements of O2 and N2 in surface waters. *Global Biogeochemical Cycles*, *22*(3). https://doi.org/10.1029/2007GB003095

Estapa, M. L., Siegel, D. A., Buesseler, K. O., Stanley, R. H. R., Lomas, M. W., & Nelson, N. B. (2015). Decoupling of net community and export production on submesoscales in the Sargasso Sea. *Global Biogeochemical Cycles*, *29*(8), 2014GB004913. https://doi.org/10.1002/2014GB004913

Estapa, M. L., Feen, M. L., & Breves, E. (2019). Direct Observations of Biological Carbon Export From Profiling Floats in the Subtropical North Atlantic. *Global Biogeochemical Cycles*, *33*(3), 282–300. https://doi.org/10.1029/2018GB006098

Fassbender, A. J., Sabine, C. L., & Cronin, M. F. (2016). Net community production and calcification from 7 years of NOAA Station Papa Mooring measurements. *Global Biogeochemical Cycles*, *30*(2), 250–267. https://doi.org/10.1002/2015GB005205

Fassbender, A. J., Sabine, C. L., Cronin, M. F., & Sutton, A. J. (2017). Mixed-layer carbon cycling at the Kuroshio Extension Observatory. *Global Biogeochemical Cycles*, *31*(2), 272–288. https://doi.org/10.1002/2016GB005547

Fay, A. R., Lovenduski, N. S., McKinley, G. A., Munro, D. R., Sweeney, C., Gray, A. R., et al. (2018). Utilizing the Drake Passage Time-series to understand variability and change in subpolar Southern Ocean pCO_2. *Biogeosciences*, *15*(12), 3841–3855. https://doi.org/10.5194/bg-15-3841-2018

Fer, I., Peterson, A. K., & Ullgren, J. E. (2014). Microstructure Measurements from an Underwater Glider in the Turbulent Faroe Bank Channel Overflow. *Journal of Atmospheric and Oceanic Technology*, *31*(5), 1128–1150. https://doi.org/10.1175/JTECH-D-13-00221.1

Frajka-Williams, E., Brearley, J. A., Nash, J. D., & Whalen, C. B. (2022). Chapter 14 - New technological frontiers in ocean mixing. In M. Meredith & A. Naveira Garabato (Eds.), *Ocean Mixing* (pp. 345–361). Elsevier. https://doi.org/10.1016/B978-0-12-821512-8.00021-9

Frants, M., Damerell, G. M., Gille, S. T., Heywood, K. J., MacKinnon, J., & Sprintall, J. (2013). An Assessment of Density-Based Finescale Methods for Estimating Diapycnal Diffusivity in the Southern Ocean. *Journal of Atmospheric and Oceanic Technology*, *30*(11), 2647–2661. https://doi.org/10.1175/JTECH-D-12-00241.1

Garcia, H. E., & Gordon, L. I. (1992). Oxygen solubility in seawater: Better fitting equations. *Limnology and Oceanography*, *37*(6), 1307–1312. https://doi.org/10.4319/lo.1992.37.6.1307

Gille, S. T. (2012). Diurnal variability of upper ocean temperatures from microwave satellite measurements and Argo profiles. *Journal of Geophysical Research: Oceans*, *117*(C11). https://doi.org/10.1029/2012JC007883

Gray, A. R., Johnson, K. S., Bushinsky, S. M., Riser, S. C., Russell, J. L., Talley, L. D., et al. (2018). Autonomous Biogeochemical Floats Detect Significant Carbon Dioxide Outgassing in the High-Latitude Southern Ocean. *Geophysical Research Letters*, *45*(17), 9049–9057. https://doi.org/10.1029/2018GL078013

Haëntjens, N., Boss, E., & Talley, L. D. (2017). Revisiting Ocean Color algorithms for chlorophyll a and particulate organic carbon in the Southern Ocean using biogeochemical floats. *Journal of Geophysical Research: Oceans*, *122*(8), 6583–6593. https://doi.org/10.1002/2017JC012844

Haskell, W. Z., Hammond, D. E., Prokopenko, M. G., Teel, E. N., Seegers, B. N., Ragan, M. A., et al. (2019). Net Community Production in a Productive Coastal Ocean From an Autonomous Buoyancy-Driven Glider. *Journal of Geophysical Research: Oceans*, *124*(6), 4188–4207. https://doi.org/10.1029/2019JC015048

Haskell, W. Z., Fassbender, A. J., Long, J. S., & Plant, J. N. (2020). Annual Net Community Production of Particulate and Dissolved Organic Carbon From a Decade of Biogeochemical Profiling Float Observations in the Northeast Pacific. *Global Biogeochemical Cycles*, *34*(10), e2020GB006599. https://doi.org/10.1029/2020GB006599

Hemsley, V. S., Smyth, T. J., Martin, A. P., Frajka-Williams, E., Thompson, A. F., Damerell, G., & Painter, S. C. (2015). Estimating Oceanic Primary Production Using Vertical Irradiance and Chlorophyll Profiles from Ocean Gliders in the North Atlantic. *Environmental Science & Technology*, *49*(19), 11612–11621. https://doi.org/10.1021/acs.est.5b00608

Ho, D. T., & Schanze, J. J. (2020). Precipitation-Induced Reduction in Surface Ocean pCO2: Observations From the Eastern Tropical Pacific Ocean. *Geophysical Research Letters*, *47*(15), e2020GL088252. https://doi.org/10.1029/2020GL088252

Huang, Y., Yang, B., Chen, B., Qiu, G., Wang, H., & Huang, B. (2018). Net community production in the South China Sea Basin estimated from in situ O2 measurements on an Argo profiling float. *Deep Sea Research Part I: Oceanographic Research Papers*, *131*, 54–61. https://doi.org/10.1016/j.dsr.2017.11.002

Jacox, M. G., Edwards, C. A., Kahru, M., Rudnick, D. L., & Kudela, R. M. (2015). The potential for improving remote primary productivity estimates through subsurface chlorophyll and irradiance measurement. *Deep Sea Research Part II: Topical Studies in Oceanography*, *112*, 107–116. https://doi.org/10.1016/j.dsr2.2013.12.008

Johnson, K. S. (2010). Simultaneous measurements of nitrate, oxygen, and carbon dioxide on oceanographic moorings: Observing the Redfield ratio in real time. *Limnology and Oceanography*, *55*(2), 615–627. https://doi.org/10.4319/lo.2010.55.2.0615

Johnson, K. S, Berelson, W. M., Boss, E. S., Chase, Z., Claustre, H., Emerson, S. R., et al. (2009). Observing biogeochemical cycles at global scales with profiling floats and gliders: Prospects for a global array, *22*(3).

Johnson, Kenneth S., Plant, J. N., Riser, S. C., & Gilbert, D. (2015). Air Oxygen Calibration of Oxygen Optodes on a Profiling Float Array. *Journal of Atmospheric and Oceanic Technology*, *32*(11), 2160–2172. https://doi.org/10.1175/JTECH-D-15-0101.1

Johnson, Kenneth S., Plant, J. N., Dunne, J. P., Talley, L. D., & Sarmiento, J. L. (2017). Annual nitrate drawdown observed by SOCCOM profiling floats and the relationship to annual net community production. *Journal of Geophysical Research: Oceans*, *122*(8), 6668–6683. https://doi.org/10.1002/2017JC012839

Johnson, Kenneth S., Plant, J. N., Coletti, L. J., Jannasch, H. W., Sakamoto, C. M., Riser, S. C., et al. (2017). Biogeochemical sensor performance in the SOCCOM profiling float array. *Journal of Geophysical Research: Oceans*, *122*(8), 6416–6436. https://doi.org/10.1002/2017JC012838

Johnson, L., Lee, C. M., & D'Asaro, E. A. (2016). Global Estimates of Lateral Springtime Restratification. *Journal of Physical Oceanography*, *46*(5), 1555–1573. https://doi.org/10.1175/JPO-D-15-0163.1

Klocker, A., & Abernathey, R. (2014). Global Patterns of Mesoscale Eddy Properties and Diffusivities. *Journal of Physical Oceanography*, *44*(3), 1030–1046. https://doi.org/10.1175/JPO-D-13-0159.1

Körtzinger, A., Send, U., Lampitt, R. S., Hartman, S., Wallace, D. W. R., Karstensen, J., et al. (2008). The seasonal pCO_2 cycle at 49°N/16.5°W in the northeastern Atlantic Ocean and what it tells us about biological productivity. *Journal of Geophysical Research: Oceans*, *113*(C4), C04020. https://doi.org/10.1029/2007JC004347

Kunze, E., Firing, E., Hummon, J. M., Chereskin, T. K., & Thurnherr, A. M. (2006). Global Abyssal Mixing Inferred from Lowered ADCP Shear and CTD Strain Profiles. *Journal of Physical Oceanography*, *36*(8), 1553–1576. https://doi.org/10.1175/JPO2926.1

Laws, E. A. (1991). Photosynthetic quotients, new production and net community production in the open ocean. *Deep-Sea Res*, *38*(1), 143–167.

Lee, C., Paluszkiewicz, T., Rudnick, D., Omand, M., & Todd, R. (2017). Autonomous Instruments Significantly Expand Ocean Observing: An Introduction to the Special Issue. *Oceanography*, *30*(2), 15–17. https://doi.org/10.5670/oceanog.2017.211

Lee, K., Tong, L. T., Millero, F. J., Sabine, C. L., Dickson, A. G., Goyet, C., et al. (2006). Global relationships of total alkalinity with salinity and temperature in surface waters of the world's oceans. *Geophysical Research Letters*, *33*(19). https://doi.org/10.1029/2006GL027207

Leonard, N. E., Paley, D. A., Davis, R. E., Fratantoni, D. M., Lekien, F., & Zhang, F. (2010). Coordinated control of an underwater glider fleet in an adaptive ocean sampling field experiment in Monterey Bay. *Journal of Field Robotics*, *27*(6), 718–740. https://doi.org/10.1002/rob.20366

Letscher, R. T., & Moore, J. K. (2015). Preferential remineralization of dissolved organic phosphorus and non-Redfield DOM dynamics in the global ocean: Impacts on marine productivity, nitrogen fixation, and carbon export. *Global Biogeochemical Cycles*, *29*(3), 325–340. https://doi.org/10.1002/2014GB004904

Levy, M., Bopp, L., Karleskind, P., Resplandy, L., Ethe, C., & Pinsard, F. (2013). Physical pathways for carbon transfers between the surface mixed layer and the ocean interior. *Global Biogeochemical Cycles*, *27*(4), 1001–1012. https://doi.org/10.1002/gbc.20092

Lévy, M., Franks, P. J. S., & Smith, K. S. (2018). The role of submesoscale currents in structuring marine ecosystems. *Nature Communications*, *9*(1), 4758. https://doi.org/10.1038/s41467-018-07059-3

Liang, J.-H., Deutsch, C., McWilliams, J. C., Baschek, B., Sullivan, P. P., & Chiba, D. (2013). Parameterizing bubble-mediated air-sea gas exchange and its effect on ocean ventilation. *Global Biogeochemical Cycles*, *27*(3), 894–905. https://doi.org/10.1002/gbc.20080

Lien, R.-C., Sanford, T. B., Carlson, J. A., & Dunlap, J. H. (2016). Autonomous microstructure EM-APEX floats. *Methods in Oceanography*, *17*, 282–295. https://doi.org/10.1016/j.mio.2016.09.003

Loisel, H., Vantrepotte, V., Norkvist, K., Mériaux, X., Kheireddine, M., Ras, J., et al. (2011). Characterization of the bio-optical anomaly and diurnal variability of particulate matter, as seen from scattering and backscattering coefficients, in ultra-oligotrophic eddies of the Mediterranean Sea. *Biogeosciences*, *8*(11), 3295–3317. https://doi.org/10.5194/bg-8-3295-2011

Lucas, A. J., Pitcher, G. C., Probyn, T. A., & Kudela, R. M. (2014). The influence of diurnal winds on phytoplankton dynamics in a coastal upwelling system off southwestern Africa. *Deep Sea Research Part II: Topical Studies in Oceanography*, *101*, 50–62. https://doi.org/10.1016/j.dsr2.2013.01.016

Marañón, E., Balch, W. M., Cermeño, P., González, N., Sobrino, C., Fernández, A., et al. (2016). Coccolithophore calcification is independent of carbonate chemistry in the tropical ocean. *Limnology and Oceanography*, *61*(4), 1345–1357. https://doi.org/10.1002/lno.10295

Monteiro, P. M. S., Gregor, L., Lévy, M., Maenner, S., Sabine, C. L., & Swart, S. (2015). Intraseasonal variability linked to sampling alias in air-sea CO2 fluxes in the Southern Ocean. *Geophysical Research Letters*, *42*(20), 8507–8514. https://doi.org/10.1002/2015GL066009

Morel, A., & Berthon, J.-F. (1989). Surface pigments, algal biomass profiles, and potential production of the euphotic layer: Relationships reinvestigated in view of remote-sensing applications. *Limnology and Oceanography*, *34*(8), 1545–1562. https://doi.org/10.4319/lo.1989.34.8.1545

Morel, A., & Maritorena, S. (2001). Bio-optical properties of oceanic waters: A reappraisal. *Journal of Geophysical Research: Oceans*, *106*(C4), 7163–7180. https://doi.org/10.1029/2000JC000319

Nagai, T., Rosales Quintana, G. M., Durán Gómez, G. S., Hashihama, F., & Komatsu, K. (2021). Elevated turbulent and double-diffusive nutrient flux in the Kuroshio over the Izu Ridge and in the Kuroshio Extension. *Journal of Oceanography*, *77*(1), 55–74. https://doi.org/10.1007/s10872-020-00582-2

Nicholson, D., Emerson, S., & Eriksen, C. C. (2008). Net community production in the deep euphotic zone of the subtropical North Pacific gyre from glider surveys. *Limnology and Oceanography*, *53*(5part2), 2226–2236. https://doi.org/10.4319/lo.2008.53.5_part_2.2226

Nicholson, D., Stanley, R. H. R., Barkan, E., Karl, D. M., Luz, B., Quay, P. D., & Doney, S. C. (2012). Evaluating triple oxygen isotope estimates of gross primary production at the Hawaii Ocean Time-series and Bermuda Atlantic Time-series Study sites. *Journal of Geophysical Research-Oceans*. https://doi.org/10.1029/2010JC006856

Nicholson, D. P., Khatiwala, S., & Heimbach, P. (2016). Noble gas tracers of ventilation during deep-water formation in the Weddell Sea. *IOP Conference Series: Earth and Environmental Science*, *35*(1), 012019. https://doi.org/10.1088/1755-1315/35/1/012019

Nicholson, David P., & Feen, M. (2017). Air calibration of an oxygen optode on an underwater glider. *Limnology and Oceanography: Methods*. https://doi.org/10.1002/lom3.10177

Nicholson, David P., Wilson, S. T., Doney, S. C., & Karl, D. M. (2015). Quantifying subtropical North Pacific gyre mixed layer primary productivity from Seaglider observations of diel oxygen cycles. *Geophysical Research Letters*, *42*(10), 2015GL063065. https://doi.org/10.1002/2015GL063065

Nicholson, S.-A., Whitt, D. B., Fer, I., du Plessis, M. D., Lebéhot, A. D., Swart, S., et al. (2022). Storms drive outgassing of CO2 in the subpolar Southern Ocean. *Nature Communications*, *13*(1), 158. https://doi.org/10.1038/s41467-021-27780-w

Odum, H. T. (1956). Primary production in flowing waters. *Limnology and Oceanography*, *1*(2), 102–117.

Omand, M., Cetinić, I., & Lucas, A. (2017). Using Bio-Optics to Reveal Phytoplankton Physiology from a Wirewalker Autonomous Platform. *Oceanography*, *30*(2), 128–131. https://doi.org/10.5670/oceanog.2017.233

Osborn, T. R., & Cox, C. S. (1972). Oceanic fine structure. *Geophysical Fluid Dynamics*, *3*(4), 321–345. https://doi.org/10.1080/03091927208236085

Owens, W. B., & Wong, A. P. S. (2009). An improved calibration method for the drift of the conductivity sensor on autonomous CTD profiling floats by θ–S climatology. *Deep Sea Research Part I: Oceanographic Research Papers*, *56*(3), 450–457. https://doi.org/10.1016/j.dsr.2008.09.008

Palevsky, H. I., & Doney, S. C. (2018). How Choice of Depth Horizon Influences the Estimated Spatial Patterns and Global Magnitude of Ocean Carbon Export Flux. *Geophysical Research Letters*, *45*(9), 4171–4179. https://doi.org/10.1029/2017GL076498

Pelland, N. A., Eriksen, C. C., & Cronin, M. F. (2017). Seaglider surveys at Ocean Station Papa: Diagnosis of upper-ocean heat and salt balances using least squares with inequality constraints. *Journal of Geophysical Research: Oceans*, *122*(6), 5140–5168. https://doi.org/10.1002/2017JC012821

Plant, J. N., Johnson, K. S., Sakamoto, C. M., Jannasch, H. W., Coletti, L. J., Riser, S. C., & Swift, D. D. (2016). Net community production at Ocean Station Papa observed with nitrate and oxygen sensors on profiling floats. *Global Biogeochemical Cycles*, *30*(6), 2015GB005349. https://doi.org/10.1002/2015GB005349

Rasse, R., Dall'Olmo, G., Graff, J., Westberry, T. K., van Dongen-Vogels, V., & Behrenfeld, M. J. (2017). Evaluating Optical Proxies of Particulate Organic Carbon across the Surface Atlantic Ocean. *Frontiers in Marine Science*, *4*. https://doi.org/10.3389/fmars.2017.00367

Redfield, A. C., Ketchum, B. H., & Richards, F. A. (1963). The influence of organisms on the composition of seawater. *The Sea*, *2*, 26–77.

Risien, C. M., & Chelton, D. B. (2008). A Global Climatology of Surface Wind and Wind Stress Fields from Eight Years of QuikSCAT Scatterometer Data. *Journal of Physical Oceanography*, *38*(11), 2379–2413. https://doi.org/10.1175/2008JPO3881.1

Roach, C. J., Balwada, D., & Speer, K. (2018). Global Observations of Horizontal Mixing from Argo Float and Surface Drifter Trajectories. *Journal of Geophysical Research: Oceans*, *123*(7), 4560–4575. https://doi.org/10.1029/2018JC013750

Roemmich, D., Alford, M. H., Claustre, H., Johnson, K., King, B., Moum, J., et al. (2019). On the Future of Argo: A Global, Full-Depth, Multi-Disciplinary Array. *Frontiers in Marine Science*, *6*. https://doi.org/10.3389/fmars.2019.00439

Roesler, C., Uitz, J., Claustre, H., Boss, E., Xing, X., Organelli, E., et al. (2017). Recommendations for obtaining unbiased chlorophyll estimates from in situ chlorophyll fluorometers: A global analysis of WET Labs ECO sensors. *Limnology and Oceanography: Methods*, *15*(6), 572–585. https://doi.org/10.1002/lom3.10185

Rosso, I., Mazloff, M. R., Verdy, A., & Talley, L. D. (2017). Space and time variability of the Southern Ocean carbon budget. *Journal of Geophysical Research: Oceans*, *122*(9), 7407–7432. https://doi.org/10.1002/2016JC012646

Rudnick, D. L. (2016). Ocean Research Enabled by Underwater Gliders. *Annual Review of Marine Science*, *8*(1), 519–541. https://doi.org/10.1146/annurev-marine-122414-033913

Sauzède, R., Claustre, H., Uitz, J., Jamet, C., Dall'Olmo, G., D'Ortenzio, F., et al. (2016). A neural network-based method for merging ocean color and Argo data to extend surface bio-optical properties to depth: Retrieval of the particulate backscattering coefficient. *Journal of Geophysical Research: Oceans*, *121*(4), 2552–2571. https://doi.org/10.1002/2015JC011408

Siegel, D. A., Cetinić, I., Graff, J. R., Lee, C. M., Nelson, N., Perry, M. J., et al. (2021). An operational overview of the EXport Processes in the Ocean from RemoTe Sensing (EXPORTS) Northeast Pacific field deployment. *Elementa: Science of the Anthropocene*, *9*(1). https://doi.org/10.1525/elementa.2020.00107

Stanley, R. H. R., Jenkins, W. J., Lott, D. E., & Doney, S. C. (2009). Noble gas constraints on air-sea gas exchange and bubble fluxes. *Journal of Geophysical Research Oceans*, *114*, C11020. https://doi.org/10.1029/2009JC005396

Takeshita, Y., Martz, T. R., Johnson, K. S., Plant, J. N., Gilbert, D., Riser, S. C., et al. (2013). A climatology-based quality control procedure for profiling float oxygen data. *Journal of Geophysical Research: Oceans*, *118*(10), 5640–5650. https://doi.org/10.1002/jgrc.20399

Thomalla, S. J., Racault, M.-F., Swart, S., & Monteiro, P. M. S. (2015). High-resolution view of the spring bloom initiation and net community production in the Subantarctic Southern Ocean using glider data. *ICES Journal of Marine Science*, *72*(6), 1999–2020. https://doi.org/10.1093/icesjms/fsv105

Thompson, A. F., Gille, S. T., MacKinnon, J. A., & Sprintall, J. (2007). Spatial and Temporal Patterns of Small-Scale Mixing in Drake Passage. *Journal of Physical Oceanography*, *37*(3), 572–592. https://doi.org/10.1175/JPO3021.1

Tijssen, S. B. (1979). Diurnal oxygen rhythm and primary production in the mixed layer of the Atlantic Ocean at 20°N. *Netherlands Journal of Sea Research*, *13*(1), 79–84. https://doi.org/10.1016/0077-7579(79)90034-6

Wang, B., Fennel, K., Yu, L., & Gordon, C. (2020). Assessing the value of biogeochemical Argo profiles versus ocean color observations for biogeochemical model optimization in the Gulf of Mexico. *Biogeosciences*, *17*(15), 4059–4074. https://doi.org/10.5194/bg-17-4059-2020

Wanninkhof, R. (2014). Relationship between wind speed and gas exchange over the ocean revisited. *Limnology and Oceanography: Methods*, *12*(6), 351–362. https://doi.org/10.4319/lom.2014.12.351

Wanninkhof, R., Asher, W. E., Ho, D. T., Sweeney, C., & McGillis, W. R. (2009). Advances in Quantifying Air-Sea Gas Exchange and Environmental Forcing. *Annual Review of Marine Science*, *1*(1), 213–244. https://doi.org/10.1146/annurev.marine.010908.163742

Wanninkhof, R., Pickers, P. A., Omar, A. M., Sutton, A., Murata, A., Olsen, A., et al. (2019). A Surface Ocean CO2 Reference Network, SOCONET and Associated Marine Boundary Layer CO2 Measurements. *Frontiers in Marine Science*, *6*. https://doi.org/10.3389/fmars.2019.00400

Weeding, B., & Trull, T. W. (2014). Hourly oxygen and total gas tension measurements at the Southern Ocean Time Series site reveal winter ventilation and spring net community production. *Journal of Geophysical Research: Oceans*, *119*(1), 348–358. https://doi.org/10.1002/2013JC009302

Weiss, R. F. (1974). Carbon dioxide in water and seawater: the solubility of a non-ideal gas. *Marine Chemistry*, *2*(3), 203–215. https://doi.org/10.1016/0304-4203(74)90015-2

Westberry, T., Behrenfeld, M. J., Siegel, D. A., & Boss, E. (2008). Carbon-based primary productivity modeling with vertically resolved photoacclimation. *Global Biogeochemical Cycles*, *22*(2), GB2024. https://doi.org/10.1029/2007GB003078

Whalen, C. B., Talley, L. D., & MacKinnon, J. A. (2012). Spatial and temporal variability of global ocean mixing inferred from Argo profiles. *Geophysical Research Letters*, *39*(18). https://doi.org/10.1029/2012GL053196

White, A. E., Barone, B., Letelier, R. M., & Karl, D. M. (2017). Productivity Diagnosed from the Diel Cycle of Particulate Carbon in the North Pacific Subtropical Gyre. *Geophysical Research Letters*, 2016GL071607. https://doi.org/10.1002/2016GL071607

Whitt, D. B., Nicholson, S. A., & Carranza, M. M. (2019). Global Impacts of Subseasonal (<60 Day) Wind Variability on Ocean Surface Stress, Buoyancy Flux, and Mixed Layer Depth. *Journal of Geophysical Research: Oceans*, *124*(12), 8798–8831. https://doi.org/10.1029/2019JC015166

Williams, N. L., Juranek, L. W., Johnson, K. S., Feely, R. A., Riser, S. C., Talley, L. D., et al. (2016). Empirical algorithms to estimate water column pH in the Southern Ocean. *Geophysical Research Letters*, *43*(7), 3415–3422. https://doi.org/10.1002/2016GL068539

Williams, N. L., Juranek, L. W., Feely, R. A., Russell, J. L., Johnson, K. S., & Hales, B. (2018). Assessment of the Carbonate Chemistry Seasonal Cycles in the Southern Ocean From Persistent Observational Platforms. *Journal of Geophysical Research: Oceans*, *123*(7), 4833–4852. https://doi.org/10.1029/2017JC012917

Wolf-Gladrow, D. A., Zeebe, R. E., Klaas, C., Körtzinger, A., & Dickson, A. G. (2007). Total alkalinity: The explicit conservative expression and its application to biogeochemical processes. *Marine Chemistry*, *106*(1), 287–300. https://doi.org/10.1016/j.marchem.2007.01.006

Wu, L., Jing, Z., Riser, S., & Visbeck, M. (2011). Seasonal and spatial variations of Southern Ocean diapycnal mixing from Argo profiling floats. *Nature Geoscience*, *4*(6), 363–366. https://doi.org/10.1038/ngeo1156

Xing, X., Briggs, N., Boss, E., & Claustre, H. (2018). Improved correction for non-photochemical quenching of in situ chlorophyll fluorescence based on a synchronous irradiance profile. *Optics Express*, *26*(19), 24734–24751. https://doi.org/10.1364/OE.26.024734